Perylenes Bearing Multiple H-Bonding Donor and Acceptor Groups for Photonic Applications

Seyedeh Melika Mostafanejad

Submitted to the
Institute of Graduate Studies and Research
in partial fulfillment of the requirements for the degree of

Doctor of Philosophy
in
Chemistry

Eastern Mediterranean University
July 2018
Gazimağusa, North Cyprus

Approval of the Institute of Graduate Studies and Research

Assoc. Prof. Dr. Ali Hakan Ulusoy
Acting Director

I certify that this thesis satisfies all the requirements as a thesis for the degree of Doctor of Philosophy in Chemistry.

Prof. Dr. Izzet Sakallı
Chair, Department of Chemistry

We certify that we have read this thesis and that in our opinion it is fully adequate in scope and quality as a thesis for the degree of Doctor of Philosophy in Chemistry.

Prof. Dr. Saim Özkar
Co-Supervisor

Prof. Dr. Huriye Icil
Supervisor

Examining Committee

1. Prof. Dr. Huriye Icil
2. Prof. Dr. Sermet Koyuncu
3. Prof. Dr. Şefik Süzer
4. Assoc. Prof. Dr. Nur P. Aydınlık
5. Asst. prof. Dr. Rene M. Williams

ABSTRACT

Construction of supra-molecular self-assembled building blocks due to their relevance in organic, inorganic, polymeric compounds as well as biological systems has attracted many attentions and various well-defined supra complexes with different sizes and shapes in the range of 1-100 nm dimensions have been prepared. Modification of perylene dye at imides or bay positions leads to high solubility of the product along with wide range of absorption expands to near infrared region. In the present study, Three different perylene diimide which two of them were symmetrical (*N*,*N'*-bis-[2-(5-carboxamidyl-3-cyano-4-methyl)-thienyl]-3,4,9,10-perylene bis (dicarboximide) TPDI and *N*,*N'*-bis-[3-((2-methyl-5-pyrimidinyl) methyl)-5-(2-hydroxyethyl)-4-methylthiazolium] perylene-3,4:9,10-tetracarboxylic diimide TCPDI and one was highly soluble asymmetrical (*N*-(dehydroabietyl)-*N'*-[3-((2-methyl-5-pyrimidinyl) methyl)-5-(2-hydroxyethyl)-4-methylthiazolium] perylene-3,4,9,10-tetracarboxylic diimide TAPDI with donor-acceptor-donor (DAD systems) building block have been synthesized, in order to change the photophysical and photochemical properties of the diimides, 1,7-symmetrically substituted perylenebis (dicarboximide) dyes (*N*,*N'*-di((s)-1-phenylethyl)-1,7-di(3,5-diamino-pyrimidoxyl) perylene-3,4,9,10-tetracarboxy diimide BPY-PPDI, *N*,*N'*-bis-[3-((2-methyl-5-pyrimidinyl) methyl)-5-(2-hydroxyethyl)-4-methylthiazolium]-1,7-di-(2-[3[(4-amino-2-methylpyrimidin-5-yl) methyl]-4-methyl-1,3-thiazol-3-ium-5yl] ethoxy-perylene-3,4:9,10-tetracarboxylic diimide BTC-TCPDI and *N*,*N'*-bis-(dehydroabietyl)-1,7-di-(2-[3[(4-amino-2-methylpyrimidin-5-yl) methyl]-4-methyl-1,3-thiazol-3-ium-5-yl] ethoxyperylene-3,4:9,10-tetracarboxylic diimide TC-APDI

with electron donating groups have been synthesized in good amount of product under mild conditions, The products have been purified and optical, thermal and electrochemical properties of them were measured and characterized carefully.

Keywords: Perylene, thiophene, vitamin, bay-substitution, hydrogen bonding.

ÖZ

Günümüzde organik, inorganik, polimerik bileşiklerin ve biyolojik sistemlerdeki önemi nedeniyle kendiliğinden düzenlenme özelliğine sahip supramoleküler madde sentezi çok dikkat çekmekte ve 1-100 nm aralığında farklı boyut ve şekillerde çeşitli iyi tanımlanmış supra kompleks maddeler hazırlanmaktadır. Perilen boyalarının imid ve körfez pozisyonlarındaki yer değiştermesi ürünün çözünürlüğünün arttırmasıyla birlikte absorbsiyonun kızılötesi bölgesine kadar genişlemesine öncülük etmektedir. Bu çalışmada, ikisi simetrik (*N,N'*-bis-[2-(5-karboksiamidil-3-siyano-4-metil) -tiyenil]-3,4,9,10-perilenbis(dikarboksimid) TPDI ve *N,N'*-bis-[3-((2-metil-5-pirimidinil) metil) -5- (2-hidroksietil) -4-metilthiazoliumklorür] perilen-3,4:9,10-tetrakarboksilik diimid TC-PDI ve biri büyük ölçüde çözünür olan asimetrik (*N*-dehidroabiyetil-*N'*-[3-((2-metil-5-pirimidinil) metil) -5-(2-hidroksietil) -4-metilthiazoliumklorür] perilen-3,4,9,10-tetrakarboksilik diimid TAPDI üç farklı perilendiimid donör-akseptör-donör (D-A-D sistemi) yapı taşı ile sentezlenmiştir. Bu diimidlerin fotofiziksel ve fotokimyasal özelliklerini değiştirmek için, 1 ve 7 pozisyonundan simetrik olarak yer değiştirilen perilen bis(dikarboksiimid) boyaları (*N,N'*-di((S)-1-feniletil)-1,7-di(3,5-diamino-pirimidoksilperilen-3,4:9,10-tetrakarbosilik diimid BPY-PPDI, *N,N'*-bis-[3- ((2-metil-5-pirimidinil)metil)-5- (2-hidroksietil) -4-metilthiazoliumklorür]-1,7-di-(2-[3[(4-amino-2-metilpirimidin-5-il) metil]-4-metil-1,3-tiyazol-3-yum-5-il] etoksi perilen-3,4:9,10-tetrakarboksilik diimid BTC-TCPD ve *N,N'*-bis-(dehidroabiyetil)-1,7-ditiyazolyum klorür perilen-3,4:9,10-tetrakarboksilik diimid TC-APDI elektron verici gruplarla birlikte ılımlı koşullarda iyi miktarda ürün sentezlenmiştir. Sentezlenen ürünler

saflandırılmış ve optik, termal ve elektrokimyasal özellikleri ölçülmüş ve dikkatlice tanımlanmıştır.

Anahtar kelimeler: Perilen, tiyofen, vitamin, bay-substitution, hidrojen bağı.

DEDICATION

To My Parents Ashraf, Mehdi,

Batool and Abbas

To My Husband Bahador

ACKNOWLEDGEMENT

Firstly, I would like to express my most humble gratitude to my supervisor **Prof. Dr. Huriye Icil**, for all the support through my study and research, for her motivation, and maternal kindness that I received continuously during many restless days and sleepless nights. And also I would like to state my gratitude to **Prof. Dr. Saim Ozkar**, my co-supervisor whose guidance helped me in all the time of research.

A special thank to **Dr. Duygu Uzun** for her round the clock support. I thank my fellow lab mates who never let me down and we shared many hours of hardships together.

Last but not least my parents, **Ashraf** and **Mehdi**, who gave me whatever I have and boundless love, their presence gives me confidence and my husband, my soulmate and my best friend **Bahador**.

TABLE OF CONTENTS

ABSTRACT iii

ÖZ v

DEDICATION vii

ACKNOWLEDGEMENT viii

LIST OF TABLES xiv

LIST OF FIGURES xviii

LIST OF ILLUSTRATIONS xxviii

LIST OF SYMBOLS AND ABBREVIATIONS xxix

1 INTRODUCTION 1

1.1 Overview of Supra-molecular Structures 1

1.1.1 The Notion of Hydrogen Bond 2

1.1.2 The Nature of π- π Stacking 4

1.2 Perylene Dyes as a Back Bone for Supramolecular Structural Design 5

1.2.1 Bay-Substituted Perylene Dyes 5

2 THEORETICAL 13

2.1 Photochemistry 13

2.1.1 Absorption 14

2.1.2 Fluorescence 15

2.1.3 Photo-Induced Electron Transfer (PET) 16

2.1.4 Excimers and Exciplexes Formation 17

2.1.5 Energy Transfer 18

2.2 Aggregation 20

2.3 Organic Solar-Cells 21

3 EXPERIMENTAL 24
3.1 Chemicals and Reagents 24
3.2 Instrumental Part 24
3.3 Synthetic Route 25
3.3.1 Schematic Illustration of Synthesis of Perylene Diimides 26
3.3.2 Schematic Illustration of Synthesis of Bay Substituted Perylene Diimides 27
3.4 Synthetic Procedure of *N*,*N*′-bis-[2-(5-carboxamidyl-3-cyano-4-methyl)-thienyl]-3,4,9,10-perylenebis(dicarboximide) (TPDI) 30
3.5 Synthetic Procedure of *N*,*N*′-bis-[3-((2-methylpyrimidinyl) methyl)-5-(2-hydroxyethyl)-4-methylthiazolium] perylene-3,4:9,10-tetracarboxylic diimide (TCPDI) 32
3.6 Synthetic Procedure of *N*-(dehydroabietyl)-*N*′-[3-((2-methyl-5-pyrimidinyl) methyl)-5-(2-hydroxyethyl)-4-methylthiazolium] 34
perylene- 3,4,9,10-tetracarboxylic diimide (TAPDI) 34
3.6.1 Perylene-3,4,9,10-tetracarboxylicacid monoanhydride monopotassium carboxcylate (K-salt) Preparation 35
3.6.2 *N*-[3-((2-methyl-5-pyrimidinyl) methyl)-5-(2-hydroxyethyl)-4-methyl thia zolium]-3,4,9,10-tetracarboxylicacid monoanhydride monoimide Preparation (TCPMI) 35
3.6.3 Synthesis of *N*-(dehydroabietyl)-*N*′-[3-((2-methyl-5-pyrimidinyl) methyl)-5-(2-hydroxyethyl)-4-methylthiazolium] perylene-3,4,9,10-tetracarboxylic diimide (TAPDI) 37
3.7 Synthetic Procedure of *N*,*N*′-di((s)-1-phenylethyl)-1,7-di(3,5-diamino-pyrimidoxyl) perylene-3,4,9,10-tetracarboxy diimide (BPY-PPDI) 39

3.7.1 Bromination of Perylene tetracarboxylic dianhydride (Br-PDA)..... 40

3.7.2 Synthesis of 1,7-di(3,5-diamino-pyrimidoxyl perylene-3,4,9,10-tetracarboxy dianhydride (BPY-PDA) 41

3.7.3 Synthesis of *N,N'*-di((s)-1-phenylethyl)-1,7-di(3,5-diamino-pyrimidoxyl perylene-3,4,9,10-tetracarboxy diimide (BPY-PPDI) 42

3.8 Synthetic Procedure of *N,N'*-bis-[3-((2-methyl-5-pyrimidinyl) methyl)-5-(2-hydroxyethyl)-4-methylthiazolium]-1,7-di-(2-[3[(4-amino-2-methylpyrimidin-5-yl)methyl]-4-methyl-1,3-thiazol-3-ium-5-yl]) ethoxyperylene-3,4:9,10-tetracarboxylic diimide (BTC-TCPDI) 44

3.8.1 Synthesis of 1,7-di-(2-[3[(4-amino-2-methylpyrimidin-5-yl) methyl]-4-methyl-1,3-thiazol-3-ium-5-yl]) ethoxyperylene-3,4:9,10-tetracarboxylic dianhydride (BTC-PDA) 45

3.8.2 Synthesis of *N,N'*-bis-[3-((2-methyl-5-pyrimidinyl)methyl)-5-(2-hydroxy ethyl)-4-methylthiazolium chloride]- 1,7-di-(2-[3[(4-amino-2-methylpyrimidin-5-yl) methyl]-4-methyl-1,3-thiazol-3-ium-5-yl]) ethoxyperylene-3,4:9,10-tetracarboxylic diimide (BTC-TCPDI)..... 46

3.9 Synthetic Procedure of *N,N'*-bis-(dehydroabietyl)- 1,7-di-(2-[3[(4-amino-2-methylpyrimidin-5-yl) methyl]-4-methyl-1,3-thiazol-3-ium-5-yl]) ethoxyperylene-3,4:9,10-tetracarboxylic diimide (BTC-APDI) 48

3.9.1 Synthesis of *N,N'*-bis-(dehydroabietyl)- 1,7-di-(2-[3[(4-amino-2-methyl pyrimidin-5-yl) methyl]-4-methyl-1,3-thiazol-3-ium-5-yl]) ethoxyperylene-3,4,9,10 –tetracarboxylic diimide (BTC-APDI)..... 49

4 DATA AND CALCULATIONS 52

4.1 Electrochemical Data and Calculations..... 52

4.1.1 Redox Potentials And Half-Wave Potentials ($E_{1/2}$)..... 52

4.1.2 LUMO and HOMO Energy Level 54
4.1.3 Optical Band-Gap Energies (Eg) 55
4.1.4 HOMO Energy Level 56
4.2 Optical Parameters Calculations 59
4.2.1 Maximum Molar Extinction Coefficient 59
4.2.2 Fluorescence Quantum Yields (Φ_f) 63
4.2.3 Half-width of The Selected Absorption ($\Delta\tilde{\upsilon}_{1/2}$) 67
4.2.4 Theoretical Radiative Lifetimes (τ_0) 70
4.2.5 Theoretical Fluorescence Lifetime (τ_f) 73
4.2.6 Theoretical Fluorescence Rate Constant (K_f) 75
4.2.7 Radiation-less Deactivation Rate-Constants (K_d) 76
4.2.8 Oscillator Strength (f) 78
4.2.9 Singlet-Energies (E_s) 79
4.3 Förster/Fluorescence Resonance Energy Transfer (FRET) 84
4.3.1 Intra-Molecular Critical Transfer Distance of TPDI in NMP 85
4.4.2 Rate Constants for Bimolecular Fluorescence Quenching (K_q) 86
5 RESULTS AND DISCUSSION 174
5.1 Synthesis of Symmetrical and Asymmetrical Perylene Diimide (PDI) 174
5.2 Synthesis of Bay-Substituted Perylene Diimide 175
5.3 Solubility of the Perylene Diimides 177
5.4 Solubility of the Bay Substituted PDI 179
5.5 Analyses of NMR and Mass Spectra 182
5.6 Analysis of UV-vis and Emission Spectroscopic Measurements 190
5.6.1 UV-vis and Emission Spectra of TPDI 190

5.6.2 Intramolecular Fluorescence Quenching of *N,N'*-bis-[2-(5-carboxamidyl-3-cyano-4-methyl)-thienyl]-3,4,9,10-perylenebis(dicarboximide) (TPDI) 193
5.6.3 UV-Vis and Emission Spectra of TCPDI 194
5.6.4 UV-Vis and Emission Spectra of TAPDI 196
5.6.4 UV-Vis and Emission Spectra of BPY-PDA 198
5.6.5 UV-vis and Emission Spectra of BPY-PPDI 200
5.6.6 UV-Vis and Emission Spectra of BTC-PDA 202
5.6.7 UV-Vis and Emission Spectra of BTC-PPDI 204
5.6.8 UV-Vis and Emission Spectra of BTC-APDI 206
5.7 Analysis of Intra-Molecular Fluorescence-Quenching in TPDI 208
5.8 Electro-Chemical Information and Analysis of *N,N'*-bis-[2-(5-Carboxamidyl-3-cyano-4-methyl)-thienyl]-3,4,9,10-perylenebis- (dicarboximide) (TPDI) 209
5.9 Thermal Properties of the Compounds 211
6 CONCLUSION 213
REFERENCES 215

LIST OF TABLES

Table 4.1: Electrochemical data of TPDI.....58

Table 4.2: Concentration with their absorbance of TPDI in DMF.....59

Table 4.3: Molar absorption coefficient of TPDI in the selected solvents.....60

Table 4.4: Maximum molar absorption coefficient of TCPDI in selected solvents.....61

Table4.5: Maximum molar absorption coefficient of TAPDI in selected solvents.....62

Table 4.6: Maximum molar absorption coefficient of BPY-PDA in selected solvents 62

Table 4.7: Maximum molar absorption coefficient of BPY-PPDI in selected solvent 62

Table 4.8: Maximum molar absorption coefficient of BTC-PDA in selected solvents 62

Table 4.9: Maximum molar absorption coefficient of BTC-TCPDI in selected solvents.....63

Table 4.10: Maximum molar absorption coefficient of BTC-APDI in selected solvents.....63

Table 4.11: Fluorescence quantum yield (Φ_f) of TPDI, TCPDI and TAPDI in various solvents.....66

Table 4.12: Fluorescence quantum yield (Φ_f) of BPY-PDA and BPY-PPDI in various solvents.....66

Table 4.13: Fluorescence quantum yield (Φ_f) of BTC-PDA, BTC-TCPDI and BTC-

APDI in various solvents.....66

Table 4.14: FWHM of TPDI, TCPDI and TAPDI in cm^{-1}.....70

Table 4.15: FWHM of BPY-PDA and BPY-PPDI in cm^{-1}.....70

Table 4.16: FWHM of BTC-PDA, BTC-TCPDI and BTC-APDI in cm^{-1}.....70

Table 4.17: Theoretical radiative life time of TPDI in selected solvents.....71

Table 4.18: Theoretical radiative life time of TC-PDI in selected solvents.....72

Table 4.19: Theoretical radiative life time of TA-PDI in selected solvents.....72

Table 4.20: Theoretical radiative life time of BPY-PDA in selected solvents.....72

Table 4.21: Theoretical radiative life time of BPY-PPDI in selected solvents.....72

Table 4.22: Theoretical radiative life time of BTC-PDA in selected solvents.....73

Table 4.23: Theoretical radiative life time of BTC-TCPDI in selected solvents.....73

Table 4.24: Theoretical radiative life time of BTC-APDI in selected solvents.....73

Table 4.25: Theoretical Fluorescence Lifetime of TPDI, TC-PDI and TA-PDI.....74

Table 4.26: Theoretical Fluorescence Lifetime of BPY-PDA and BPY-PPDI.....74

Table 4.27: Theoretical Fluorescence Lifetime of BTC-PDA, BBTC-TCPDI and BTC-APDI.....75

Table 4.28: Theoretical fluorescence rate constant of TPDI, TC-PDI and TAPDI.....76

Table 4.29: Theoretical fluorescence rate constant of BPY-PDA and BPY-PPDI.....76

Table 4.30: Theoretical fluorescence rate constant of BTC-PDA, BTC-TCPDI and BPY-PPDI.....76

Table 4.31: Radiation-less deactivation rate constants of TPDI, TC-PDI and TA-PDI.....77

Table 4.32: Radiation-less deactivation rate constants of BPY-PDA and BPY-

PPDI.....78

Table 4.33: Radiation-less deactivation rate constants of BTC-PDA, BTC-TCPDI and BTC-APDI.....78

Table 4.34: Oscillator strength of TPDI, TCPDI and TAPDI.....79

Table 4.35: Oscillator strength of BPY-PDA and BPY-PPDI.....79

Table 4.36: Oscillator strength of BTC-PDA, BTC-TCPDI and BTC-APDI.....79

Table 4.37: Singlet energy values of TPDI, TC-PDI and TA-PDI.....80

Table 4.38: Singlet energy values of BPY-PDA and BPY-PPDI.....80

Table 4.39: Singlet energy values of BTC-PDA, BTC-TCPDI and BTC-APDI.....81

Table 4.40: Maximum wavelength of the absorption λ_{max} (nm), molar extinction coefficient ε_{max} ($M^{-1}cm^{-1}$), oscillator strength f, fluorescence quantum-yield Φ_f (λ_{exc}= 485 nm), radiative life time τ_0 (ns), fluorescence life time τ_f (ns), fluorescence rate-constant k_f (s^{-1}), rate-constant of radiation-less deactivation k_d (s^{-1}), and singlet-energy Es (kcal mole -1) data of TPDI, TCPDI and TAPDI.....82

Table 4.41: Maximum wavelength of the absorption λ_{max} (nm), molar extinction coefficient ε_{max} ($M^{-1}cm^{-1}$), oscillator strength f, fluorescence quantum-yield Φ_f (λ_{exc}= 485 nm), radiative life time τ_0 (ns), fluorescence life time τ_f (ns), fluorescence rate-constant k_f (s^{-1}), rate-constant of radiationless deactivation k_d (s^{-1}), and singlet-energy E_s (kcal mole $^{-1}$) data of BPY-PDA, BPY-PPDI,BTC-PDA, BTC-TCPDI and BTC-APDI.....83

Table 5.1: Qualitative solubility of TPDI.....182

Table 5.2: Qualitative solubility of TCPDI.....182

Table 5.3: Qualitative solubility of APDI.....183

Table 5.4: Qualitative solubility of BPY-PDA and BPY-PPDI.....184

Table 5.5: Qualitative solubility of BTC-PDA, BTC-TCPDI and BTC-APDI.....185

Table 5.6: Ratio of absorption intensities of TPDI in various solvents.....195

Table 5.7: Ratio of absorption intensities of TCPDI in various solvents.....200

Table 5.8: Ratio of absorption intensities of TAPDI in various solvents.....201

Table 5.9: Ratio of absorption intensities of BPY-PDA in various solvents.....203

Table 5.10: Ratio of absorption intensities of BPY-PPDI in various solvents.....205

Table 5.11: Ratio of absorption intensities of BTC-PDA in various solvents.....207

Table 5.12: Ratio of absorption intensities of BTC-TCPDI in various solvents.....208

Table 5.13: Ratio of absorption intensities of BTC-APDI in various solvents.....211

LIST OF FIGURES

Figure 1.1: Scheme of the major hydrogen bond geometries.....3

Figure 1.2: Representative geometries of quadruple moments of aromatic π-interactions (blue is positive and pink is negative).....4

Figure 1.3: Chemical structure of perylene.....6

Figure1.4: Schematic structure of *N,N′*-bis-[2-(5-carboxamidyl-3-cyano-4-methyl) thienyl]-3,4,9,10-perylenebis(dicarboximide) (TPDI).....8

Figure 1.5: Schematic structure of *N,N′*-bis-[3-((2-methyl-5-pyrimidinyl) methyl)-5-(2-hydroxyethyl)-4-methylthiazolium] perylene-3,4:9,10-tetracarboxylic diimide (TCPDI).....8

Figure 1.6: Chemical structure of *N*-(dehydroabietyl)-*N′*-[3-((2-methyl-5-pyrimidinyl) methyl)-5-(2-hydroxyethyl)-4-methylthiazolium] perylene-3,4:9,10-tetracarboxylic diimide (TAPDI).....8

Figure 1.7: Chemical structure of 1,7-di(3,5-diamino-pyrimidoxylperylene-3,4,9,10-tetracarboxy dianhydride (BPY-PDA).....9

Figure 1.8: Chemical structure of *N,N′*-Di((s)-1-phenylethyl)-1,7-di(3,5-diamino-pyrimidoxyl) perylene-3,4,9,10-tetracarboxy diimide (BPY-PPDI).....9

Figure 1.9: Schematic structure of 1,7-Di-(2-[3[(4-amino-2-methylpyrimidin-5-yl)methyl]-4-methyl-1,3-thiazol-3-ium-5-yl] ethoxy perylene-3,4:9,10-tetracarboxylic dianhydride (BTC-PDA).....10

Figure 1.10: Schematic structure of *N,N′*-bis-[3-((2-methyl-5-pyrimidinyl) methyl)-5-(2-hydroxyethyl)-4-methylthiazolium chloride]- 1,7-Di-(2-[3[(4-amino-2-methylpyrimidin-5-yl) methyl]-4-methyl-1,3-thiazol-3-ium-5-yl] ethoxy perylene-3,4:9,10-

tetracarboxylic diimide (BTC-TCPDI).....11

Figure 1.11: Schematic structure of *N,N'*-bis-(dehydroabietyl)- 1,7-Di-(2-[3[(4-amino-2-methylpyrimidin-5-yl) methyl]-4-methyl-1,3-thiazol-3-ium-5-yl]) ethoxylperylene-3,4,9,10-tetracarboxylic diimide (TCAPDI)……...……12

Figure 2.1: The route of photo-chemical processes.....15

Figure 2.2: Electron-transfer processes.....16

Figure 2.3: Reductive electron transfer.....17

Figure 2.4: Oxidative electron transfer.....17

Figure 2.5: Energy level scheme of donor and acceptor molecules.....20

Figure 2.6: Scheme of principle solar-cell.....22

Figure 3.1: *N,N'*-bis-[2-(5-carboxamidyl-3-cyano-4-methyl) thienyl] 3,4,9,10-perylene bis (dicarboximide) (TPDI).....31

Figure 3.2: *N,N'*-bis-[3-((2-methyl-5-pyrimidinyl)methyl)-5-(2-hydroxyethyl)-4-methylthiazolium] perylene-3,4:9,10-tetracarboxylic diimide (TCPDI).....33

Figure 3.3: K-salt.....35

Figure 3.4: *N*-[3-((2-methyl-5-pyrimidinyl) methyl)-5-(2-hydroxyethyl)-4-methyl thiazolium]-3,4:9,10-tetracarboxylic acid monoanhydride monoimide preparation (TCPMI).....36

Figure 3.5: *N*-(dehydroabietyl)-*N'*-[3-((2-methyl-5-pyrimidinyl) methyl)-5-(2-hydroxyethyl)-4-methylthiazolium] perylene-3,4:9,10-tetracarboxylic diimide (TAPDI).....37

Figure 3.6: 1,7-Dibromoperylene dianhydride (Br-PDA).....40

Figure 3.7: 1,7-Di(3,5-diamino-pyrimidoxyl) perylene-3,4,9,10-tetracarboxy dianhydride (BPY-PDA).....41

Figure 3.8: *N,N'*-Di((s)-1-phenylethyl)-1,7-di(3,5-diamino-pyrimidoxyl) perylene-

3,4, 9,10-tetracarboxy diimide (BPY-PPDI).....43
Figure 3.9: 1,7-Di-(2-[3[(4-amino-2-methylpyrimidin-5-yl) methyl]-4-methyl-1,3-thiazol-3-ium-5-yl]) ethoxylperylene-3,4:9,10-tetracarboxylic dianhydride (BTC-PDA).....45
Figure 3.10: *N,N'*-bis-[3-((2-methyl-5-pyrimidinyl) methyl)-5-(2-hydroxyethyl)-4-methylthiazolium chloride]- 1,7-Di-(2-[3[(4-amino-2-methylpyrimidin-5-yl) methyl]-4-methyl-1,3-thiazol-3-ium-5-yl]) ethoxylperylene-3,4:9,10-tetracarboxylic diimide (BTC-TCPDI).....47
Figure 3.11: *N,N'*-bis-(dehydroabietyl)-1,7-Di-(2-[3[(4-amino-2-methylpyrimidin-yl) methyl]-4-methyl-1,3-thiazol-3-ium-5-yl]) ethoxylperylene-3,4:9,10-tetra carboxylic diimide (BTC-APDI).....50
Figure 4.1: Absorption spectrum of TPDI in DMF.....56
Figure 4.2: Concentration dependent measurement of TPDI in DMF.....60
Figure 4.3: Chart of absorbance versus concentration of TPDI in DMF.....61
Figure 4.4: The ideal spectrum at a single wavelength.....67
Figure 4.5: Gaussian-like spectrum…….....67
Figure 4.6: Demonstration of the determination of Half-width.....68
Figure 4.7: Illustration of the determination of half-width of TPDI in DMF.....69
Figure 4.8: Normalized fluorescence spectrum of donor (Thiophene) in absence of acceptor.....85
Figure 4.9: TPDI in DMF solution (supporting electrolyte: 0.1 M $NaBF_4$); the left figure demonstrates scan rate dependent cyclic voltammograms (inset shows the CV at 100 mVs^{-1} for clarity); the right figure shows frequency dependent squarewave voltammograms.....87
Figure 4.10: Stern-Volmer plots of donor in different concentration.....88

Figure 4.11: The left figure shows scan rate dependent cyclic voltammograms of TPDI in NMP solution (supporting electrolyte: 0.05 M $NaBF_4$); the right figure demonstrates cyclic voltammogram at 100 mVs^{-1} (inset shows the enlarged CV of TPDI part for clarity).....89

Figure 4.12: The left figure shows scan rate dependent cyclic voltammograms of TPDI in DMAC solution (supporting electrolyte: 0.05 M $NaBF_4$), the right figure demonstrates cyclic voltammograms at 100 and 50 mVs^{-1} with the anodic region...90

Figure 4.13: The left figure shows Squarewave voltammograms of TPDI in NMP and the right figure demonstrates DMAC solutions (supporting electrolyte: 0.05 M $NaBF_4$).....91

Figure 4.14: TPDI in solid-state (supporting electrolyte: 1 M HCl); the left figure demonstrates cyclic voltammogram in the cathodic region (from –1.05 V to –0.825 V); the right figure shows cyclic voltammogram in the cathodic region (from –0.625 V to +0.125 V).....92

Figure 4.15: TPDI in solid-state (supporting electrolyte: 1 M HCl); cyclic voltammogram in the anodic region (from +0.1 V to +0.9 V); scan rate dependent complete cyclic voltammograms from cathodic to anodic region (from –1.00 V to +1.00 V; and the inset shows the CV at 100 mVs^{-1} for clarity).....93

Figure 4.16: (a) Scan rate dependent cyclic voltammograms of TH in DMAC; (b) Squarewave voltammograms of TH in DMAC; (c) Cyclic voltammograms of TH in NMP; (d) Squarewave voltammograms of TH in NMP solutions (supporting electrolyte: 0.05 M $NaBF_4$).....94

Figure 4.17: Infrared spectrum of perylene tetracarboxylic dianhydride (PDA), KBr pellet.....95

Figure 4.18: Infrared spectrum of TPDI, KBr pellet.....96

Figure 4.19: Infrared spectrum of TC-PDI, KBr pellet.....97

Figure 4.20: Infrared spectrum of TCPMI, KBr pellet.....98

Figure 4.21: Infrared spectrum of TAPDI, KBr pellet.....99

Figure 4.22: Infrared spectrum of Br-PDA, KBr pellet.....100

Figure 4.23: Infrared spectrum of BPY-PDA, KBr pellet.....101

Figure 4.24: Infrared spectrum of BPY-PPDI, KBr pellet.....102

Figure 4.25: Infrared spectrum of BTC-PDA, KBr pellet.....103

Figure 4.26: Infrared spectrum of BTC-TCPDI, KBr pellet.....104

Figure 4.27: Infrared spectrum of BTC-APDI, KBr pellet.....105

Figure 4.28: (a) Absorption spectra of TPDI in different solvents; (b) Emission spectra of TPDI in different solvents at excitation wavelength of 485 nm.....106

Figure 2.29: (a) Absorption spectra of TH in NMP; (b) Emission spectra of TH in NMP at excitation wavelength of 310 nm.....107

Figure 4.30: Concentration dependent UV measurements of TPDI in (a)DMF, (b) MeOH and (c) NMP.....108

Figure 4.31: Concentration dependent UV spectra of TPDI in (a) DCM, (b) EtOH and (c) DMAC.....109

Figure 4.32: Concentration dependent emission spectra of TPDI in (a) DMF, (b) MeOH and (d) NMP at excitation wavelength of 485 nm.....110

Figure 4.33: Concentration dependent emission spectra of TPDI in (a) DCM, (b) EtOH and (d) DMAC at excitation wavelength of 485 nm.....111

Figure 4.34: Concentration dependent emission spectra of TPDI in (a) DMF, (b) MeOH and (d) NMP at excitation wavelength of 315 nm.....112

Figure 4.35: Concentration dependent emission spectra of TPDI in (a) DCM,(b) EtOH and (d) DMAC at excitation wavelength of 315 nm.....113

Figure 4.36: Solid-state absorption spectrum of TPDI is shown by black color, absorption spectrum of TPDI in NMP is shown by red color, inset shows absorption spectrum with wavelengths.....114
Figure 4.37: (a) TC-PDI, UV spectra in different solvents. (b) Excitation spectra at emission wavelength of 620 nm in different solvents.....115
Figure 4.38: Emission spectra of TC-PDI at (a) Excitation wavelength of 485 nm (b) Excitation wavelength of 315 nm.....116
Figure 4.39: (a) Absorption spectra of Vitamin and (b) Emission spectra of Vitamin at excitation wavelength of 310 nm.....117
Figure: 4.40: Concentration dependent UV spectra of TC-PDI in (a) NMP, (b) DMF and (c) DMAC.....118
Figure 4.41: Concentration dependent emission spectra of TC-PDI in (a) NMP, (b) DMF and (d) DMAC at excitation wavelength of 485 nm.....119
Figure 4.42: Concentration dependent emission spectra of TC-PDI in (a) NMP, (b) DMF and (d) DMAC at excitation wavelength of 315 nm.....120
Figure 4.43: (a) TA-PDI, UV spectra in different solvents. (b) Excitation spectra at emission wavelength of 620 nm in different solvents.....121
Figure 4.44: Emission spectra of TA-PDI at (a) Excitation wavelength of 485 nm (b) Excitation wavelength of 315 nm.....122
Figure 4.45: Concentration dependent UV spectra of TA-PDI in (a) CHL, (b) Isopropanol and (c) DMAC.....123
Figure 4.46: Concentration dependent emission spectra of TA-PDI in (a) CHL, (b) Isopropanol and (c) DMAC at excitation wavelength of 485 nm.....124
Figure 4.47: Concentration dependent emission spectra of TA-PDI in (a) CHL, (b) Isopropanol and (c) DMAC at excitation wavelength of 315 nm.....125

Figure 4.48: (a) UV spectra of BPY-PDA and (b) Emission spectra at excitation wavelength of 485 nm in different solvents.....126
Figure 4.49: (a) UV spectra of Pyrimidine and (b) Emission spectra at excitation wavelength of 310 nm in different solvents.....127
Figure 4.50: Concentration dependent UV spectra of BPY-PDA in (a) NMP, (b) DMF and (c) DMAC.....128
Figure 4.51: Concentration dependent emission spectra of BPY-PDA in(a) NMP, (b) DMF and (c) DMAC at excitation wavelength of 485 nm.....129
Figure 4.52: Concentration dependent emission spectra of BPY-PDA in (a) NMP, (b) DMF and (c) DMAC at excitation wavelength of 315 nm.....130
Figure 4.53: (a) UV spectra of BPY-PPDI and (b) emission spectra at excitation wavelength of 485 nm in different solvents.....131
Figure 4.54: Concentration dependent UV spectra of BPY-PPDI in(a) NMP, (b) DMF and (c) DMAC.....132
Figure 4.55: Concentration dependent emission spectra of BPY-PPDI in(a) NMP, (b) DMF and (c) DMAC at excitation wavelength of 485 nm.....133
Figure 4.56: Concentration dependent emission spectra of BPY-PPDI in (a) NMP, (b) DMF and (c) DMAC at excitation wavelength of 315 nm.....134
Figure 4.57: (a) UV spectra of BTC-PDA and (b) excitation spectra at emission wavelength of 620 nm.....135
Figure 4.58: Emission spectra of BTC-PDA (a) at excitation wavelength of 485nm and (b) 315 nm.....136
Figure 4.59: Concentration dependent UV spectra of BTC-PDA in (a) NMP, (b) DMAC and (c) DMF.....137
Figure 4.60: Concentration dependent emission spectra of BTC-PDA in(a) NMP, (b)

DMAC and (c) DMF at excitation wavelength of 485 nm.....138
Figure 4.61: Concentration dependent emission spectra of BTC-PDA in (a) NMP, (b) DMAC and (c) DMF at excitation wavelength of 315 nm.....139
Figure 4.62: (a) UV spectra of BTC-TCPDI and (b) excitation spectra at emission wavelength of 620 nm.....140
Figure 4.63: Emission spectra of BTC-TCPDI(a) at excitation wavelength of 485 nm and (b) 315 nm.....141
Figure 4.64: Concentration dependent UV spectra of BTC-TCPDI in (a) NMP, (b) DMAC and (c) DMF.....142
Figure 4.65: Concentration dependent emission spectra of BTC-TCPDI in (a) NMP, (b) DMAC and (c) DMF at excitation wavelength of 485 nm.....143
Figure 4.66: Concentration dependent emission spectra of BTC-TCPDI in (a) NMP, (b) DMAC and (c) DMF at excitation wavelength of 315 nm.....144
Figure 4.67: (a) UV spectra of BTC-APDI and (b) excitation spectra at emission wavelength of 620 nm.....145
Figure 4.68: Emission spectra of BTC-APDI at excitation wavelength of (a) 485 nm (b) 315 nm.....146
Figure 4.69: Concentration dependent UV spectra of BTC-APDI in (a) CHL,(b) THF and (c) DMAC.....147
Figure 4.70: Concentration dependent emission spectra of BTC-APDI in (a) CHL, (b) THF and (c) DMAC at excitation wavelength of 485 nm.....148
Figure 4.71: Concentration dependent emission spectra of BTC-APDI in (a) CHL, (b) THF and (c) DMAC at excitation wavelength of 315 nm.....149
Figure 4.72: H-NMR spectrum of TPDI in TFAc:CHL.....150
Figure 4.73: C-NMR spectrum of TPDI in TFAc:CHL at low ppm.....151

Figure 4.74: C-NMR spectrum of TPDI in TFAc:CHL at high ppm.....152

Figure 4.75: H-NMR spectrum of TA-PDI in CHL at low ppm.....153

Figure 4.76: H-NMR spectrum of TA-PDI in CHL at high ppm.....154

Figure 4.77: H-NMR spectrum of BTC-APDI in CHL.....155

Figure 4.78: H-NMR spectrum of BTC-APDI in CHL at low ppm.....156

Figure 4.79: H-NMR spectrum of BTC-APDI in CHL at high ppm.....157

Figure 4.80: Mass-spectrum of TPDI in DMF.....158

Figure 4.81: Mass-spectrum of TC-PDI in DMF.....159

Figure 4.82: Mass-spectrum of in TC-PDI in DMF zoomed in.....160

Figure 4.83: Mass-spectrum of in TC-PDI in DMF zoomed in.....161

Figure 4.84: Mass-spectrum of APDI in CHL.....162

Figure 4.85: Mass-spectrum of BPY-PDA in DMF.....163

Figure 4.86: Mass-spectrum of BTC-APDI in CHL.....164

Figure 4.87: Mass-spectrum of BTC-APDI in CHL.....165

Figure 4.88: (a) DSC thermogram; (b) TGA curves of TPDI at a heating rate of 10 ^{o}C min^{-1}.....166

Figure 4.89: (a) DSC thermogram; (b) TGA curves of TC-PDI at a heating rate of 10 ^{o}C min^{-1}.....167

Figure 4.90: (a) DSC thermogram; (b) TGA curves of TA-PDI at a heating rate of 10 ^{o}C min^{-1}.....168

Figure 4.91: (a) DSC thermogram; (b) TGA curves of BPY-PDA at a heating rate of 10 ^{o}C min^{-1}.....169

Figure 4.92: (a) DSC thermogram; (b) TGA curves of BPY-PPDI at a heating rate of 10 ^{o} C min^{-1}.....170

Figure 4.93: (a) DSC thermogram; (b) TGA curves of BTC-PDA at a heating rate of

10 ^{o}C min^{-1}.....171

Figure 4.94: (a) DSC thermogram; (b) TGA curves of BTC-TCPDI at a heating rate of 10 ^{o}C min^{-1}.....172

Figure 4.95: (a) DSC thermogram; (b) TGA curves of BTC-APDI at a heating rate of 10 ^{o}C min^{-1}.....173

LIST OF ILLUSTRATIONS

Scheme 3.1: Synthesis of symmetrical and unsymmetrical perylene diimides.....26

Scheme 3.2: Synthesis of brominated perylene dianhydride.....27

Scheme 3.3: Synthesis of bay substituted perylene dianhydride.....28

Scheme 3.4: Synthesis of bay substituted perylene diimide.....29

Scheme 3.5: Synthesis of *N,N'*-bis-[2-(5-carboxamidyl-3-cyano-4-methyl)-thienyl]-3,4,9,10-perylenebis(dicarboximide) (TPDI).....30

Scheme 3.6: Synthesis of *N,N'*-bis-[3-((2-methyl-5-pyrimidinyl) methyl)-5-(2 hydroxyethyl)-4-methylthiazolium] perylene-3,4:9,10-tetracarboxylic diimide (TCPDI).....32

Scheme 3.7: Synthesis of *N*-(dehydroabietyl)-*N'*-[3-((2-methyl-5-pyrimidinyl) methyl)-5-(2-hydroxyethyl)-4-methylthiazolium chloride] perylene-3,4:9,10-tetracarboxylic diimide (TAPDI).....34

Scheme 3.8: Synthesis of *N,N'*-Di((s)-1-phenylethyl)-1,7-di(3,5-diamino-pyrimidoxylperylene-3,4,9,10-tetracarboxy diimide (BPY-PPDI).....39

Scheme 3.9: Synthesis of *N,N'*-bis-[3-((2-methyl-5-pyrimidinyl) methyl)-5-(2-hydroxyethyl)-4-methylthiazolium]-1,7-di-thiazolium chloride perylene-3,4:9,10-tetracarboxylic diimide (BTC-TCPDI).....44

Scheme 3.10: Synthesis of *N,N'*-bis-(dehydroabietyl)-1,7-di-thiazolium chloride perylene-3,4:9,10-tetracarboxylic diimide (BTC-APDI).....48

Scheme 5.1: (a)-(d) Representative 3D molecular structure of TPDIin different energy levels. (all rendered using Marvin by Chem Axon).....192

LIST OF SYMBOLS AND ABBREVIATIONS

Å	Angstrom
A	Absorption
A	Electron Acceptor
Anal.	Analytical
AU	Arbitrary unit
Avg.	Average
BPY-PDA	1,7-di(3,5-diamino-pyrimidoxyl perylene-3,4,9,10-tetracarboxy dianhydride
BPY-PPDI	*N*,*N'*-Di((s)-1-phenylethyl)-1,7-di(3,5-diamino-pyrimidoxyl perylene-3,4,9,10-tetracarboxy diimide
BTC-APDI	*N*,*N'*-bis-(dehydroabietyl)-1,7-Di-(2-[3[(4-amino-2-methylpyrimidin-5-yl) methyl]-4-methyl-1,3-thiazol-3-ium-5-yl] perylene-3,4:9,10-tetracarboxylic diimide
BTC-PDA	1,7-Di-(2-[3[(4-amino-2-methylpyrimidin-5-yl) methyl]-4-methyl-1,3-thiazol-3-ium-5-yl] perylene-3,4:9,10-tetracarboxylic dianhydride
BTC-TCPDI	*N*,*N'*-bis-[3-((2-methyl-5-pyrimidinyl) methyl)-5-(2-hydroxyethyl)-4-methylthiazolium chloride]- 1,7-Di-(2-[3[(4-amino-2-methylpyrimidin-5-yl) methyl]-4-methyl-1,3-thiazol-3-ium-5-yl] perylene-3,4:9,10-tetracarboxylic diimide
C	Concentration
calcd.	Calculated
^{13}C NMR	Carbon-13 nuclear magnetic resonance spectroscopy

cm	Centimeter
$CDCl_3$	Deutero-Chloroform
$CHCl_3$	Chloroform
CV	Cyclic Voltammetry
^oC	Degree Celsius
δ	Chemical shift (ppm)
D	Electron donor
DC	Dielectric constant
DCM	Dichloromethane
DMF	*N,N'*-dimethylformamide
DMSO	Dimethyl sulfoxide
DSC	Differential scanning calorimetry
DSSC	Dye sensitized solar cell
ε	Extinction coefficient
ε_{max}	Maximum extinction coefficient(Molar absorptivity)
eV	Electron volt
$E_{1/2}$	Half-wave potential
E_g	Band gap energy
E_{ox}	Oxidation potential
E_p	Separation of peak potentials
E_{pa}	Anodic peak potential
E_{pc}	Cathodic peak potential
E_{red}	Reduction potential
E_s	Singlet state
f	Oscillator strength

Fc	Ferrocene
Fig.	Figure
FRET	Fluorescence resonance energy transfer
FT-IR	Fourier transform infrared spectroscopy
h	Hour
hν	Irradiation
Hz	Hertz
^{1}H NMR	Proton nuclear magnetic resonance spectroscopy
HOMO	Highest occupied molecular orbital
i_p	Peak current
i_{pa}	Anodic peak current
i_{pc}	Cathodic peak current
IR	Infrared spectrum/spectroscopy
J	Coupling constant
kcal	Kilocalorie
k_d	Rate constant of radiationless deactivation
k_f	Fluorescence rate constant
l	Path length
KBr	Potassium bromide
KOH	Potassium hydroxide
LED	Light emitting diode
LUMO	Lowest unoccupied molecular orbital
M	Molar concentration
M^+	Molecular ion peak
M_w	Weight average molecular weight

MHz	Megahertz
min	Minimum
mmol	Millimole
mol	Mole
MS	Mass spectrometry
n	Refractive index
n	Number of electrons (in the reduction process)
NMP	*N*-methylpyrrolidinone
NMR	Nuclear magnetic resonance spectroscopy
nm	Nanometer
$NaBF_4$	Sodium tetrafluoroborate
Φ_f	Fluorescence quantum yield
PDA	Perlyene 3,4,9,10-tetracarboxylic dianhydride
PDI	Perlylene diimide
PET	Photoinduced electron transfer
ppm	Parts per million
PV	Photovoltaic
RT	Room temperature
SC	Solar cell
Std.	Standard
SWV	Square Wave Voltammetry
τ_o	Theoretical radiative lifetime
τ_f	Fluorescence lifetime
t	Time
$TBAPF_6$	Tetrabutylammoniumhexafluorophosphate

TGA	Thermogravimetric analysis
TFAc	Trifluoroacetic acid
TAPDI	*N*-(dehydroabietyl)-*N′*-[3-((2-methyl-5-pyrimidinyl) methyl)-5-(2-hydroxyethyl)-4-methylthiazolium chloride] perylene-3,4:9,10-tetracarboxylic diimide
TCPDI	*N*,*N′*-bis-[3-((2-methyl-5-pyrimidinyl) methyl)-5-(2-hydroxyethyl)-4-methylthiazolium chloride] perylene-3,4:9,10-tetracarboxylic diimide
TC-PMI	*N*-[3-((2-methyl-5-pyrimidinyl) methyl)-5-(2-hydroxyethyl) -4-methylthiazolium]-3,4:9,10-tetracarboxylic acid monoanhydride monoimide
TPDI	*N*,*N′*-bis-[2-(5-carboxamidyl-3-cyano-4-methyl)-thienyl]-3,4,9,10-perylenebis(dicarboximide)
u	Unknown
μ	Micro
UV	Ultraviolet
UV-vis	Ultraviolet visible light absorption
ν	Scan rate
ν	Wavenumber
$\Delta\tilde{\upsilon}_{1/2}$	Half-width of the selected absorption
V	Volt
vs.	Versus
λ	Wavelength
λ_{exc}	Excitation wavelength
λ_{em}	Emission wavelength

Chapter 1

INTRODUCTION

1.1 Overview of Supra-molecular Structures

In the recent decades as can be seen by great number of publications the synthesis of supra molecular structures has attracted much attentions and various well-defined supra complexes with different sizes and shapes in the range of 1-100 nm dimension have been prepared [1-7]. The main goal of supra-molecular electronics is that particularly designated π-conjugated compounds self-assemble subjected to proper conditions into well-ordered linear arrangements, in such a way that the overlap of the π-orbitals permits the transmission of electron-holes and excitons co-linear with the sense of stacking direction. In comparison with molecular structures which are based on covalently bonded atoms, supra-molecular structures are formed by spontaneous intermolecular interactions of chemically similar or dissimilar molecules. The assembly of the compounds in supra structures can be achieved by different weak secondary interactions like hydrogen bonding, π-π stacking, hydrophobic hydrophilic effects, metal cations coordination, etc. The afore mentioned processes is called “bottom up” method in nanostructure construction [8-9]. Among various bottom up interactions, the hydrogen bonds play a key role in supra-molecular association, hence learning of non-covalent bonds (secondary interactions) is critical to identify assembly processes in supra-molecular chemistry of organic, inorganic, polymeric compounds as well as biological systems.

1.1.1 The Notion of Hydrogen Bond

According to the definition proposed by Linus Pauling at 1940,"It had been known that a hydrogen atom can be attracted by two atoms more willingly than simply one, so it might be considered as a bond between them" [10].

Since then, many non-covalent bonds in structural chemistry have been sorted as hydrogen bonds that made difficulty in description of what exactly constitutes a hydrogen bond. Peter Atkin at 1989 tried to explain this phenomenon as follows "A H-bond is a connection produced by hydrogen atom between two strongly electronegative atoms" [11]. Many varieties of H-bonding are available including different geometries and bond energies that mostly hydrogen is shared between hydrogen donor (D) and the acceptor (A) which is a molecule with none shared electrons. The hydrogen donation can be intensified by increasing the acidity and the acceptor character can be strengthened when the basicity increases. The interaction also can involve multiple H-bonding in which the donation takes place to more than one acceptor [12-13]. Figure 1.1 depicts the role of H-bond in biomaterials, dyes and pigment, ionic conductor and organic semiconductors. In the centre the structures of H-bonds are demonstrated schematically. In the top left corner the presence of hydrogen bond in protein and DNA base pairs (Guanine-Cytosine) can be seen whilst at the top right side the intra-molecular hydrogen bonding in dyes such as Indigo, Alizarin and Tyrian purple are shown. In bottom right and left the intermolecular H-bondings are presented [14,15].

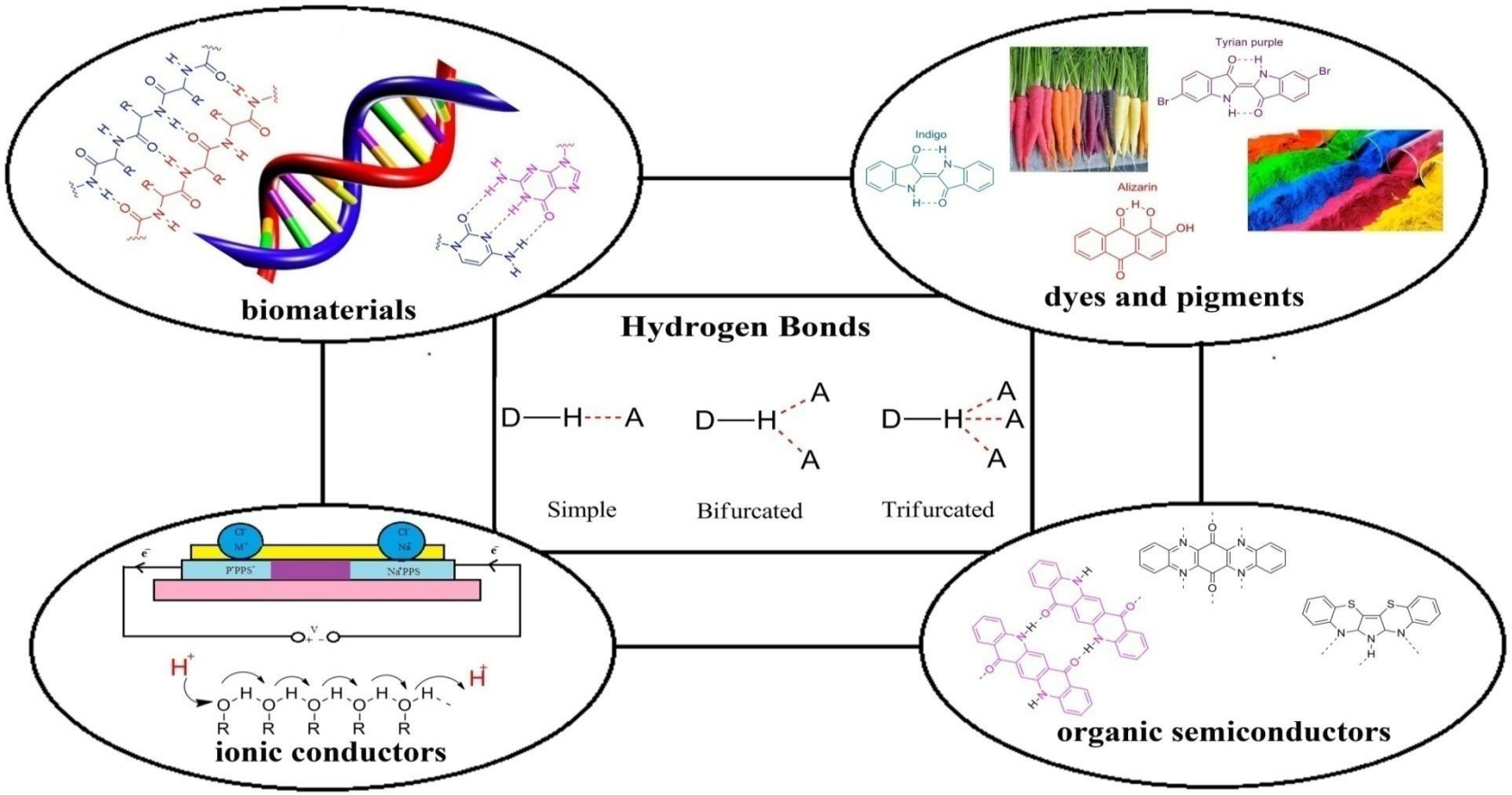

Figure 1.1: Scheme of the major hydrogen bond geometries

1.1.2 The Nature of π- π Stacking

Another type of secondary interactions that can be mostly perceived in self-assembled systems is π effects. This general expression refers to another type of non-covalent interaction including a π-electron rich component with a cation, an anion, or an alternative π-system [12]. The last one is called π-π interaction or π-stacking. The typical π-π system can be benzene rings with three favoured stacking arrangements including face-to-face, edge-to-face and T-shaped that can be seen in figure 1.2. The stability of these conformers can be interpreted by the arrangement of the quadrupole- moments related with the π-rings.

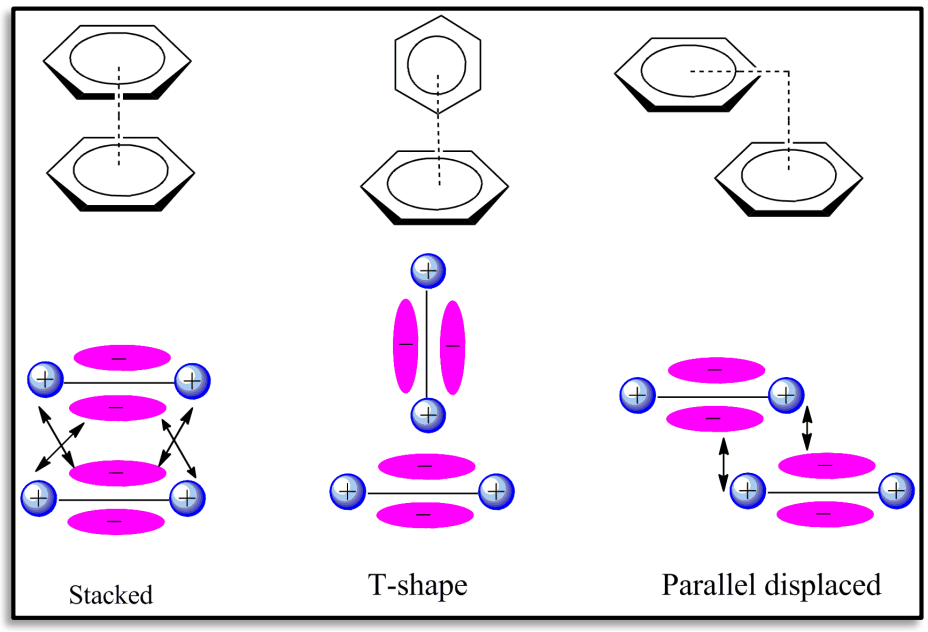

Figure 1.2: Representative geometries of quadrupole moments of aromatic π-interactions (blue is positive and pink is negative)

As can be seen above in those arrangements the π-orbitals have formed a partially negative charge above and below the aromatic plane and partially positive charge at the edge of the π-ring accordingly the T-shape and parallel-displaced conformers are constructive interactions in contrast to least favourable typically stacked structures [16].

1.2 Perylene Dyes as a Back Bone for Supramolecular Structural Design

Perylene tetracarboxylic acid bisimide or shortly PDI have received extensive consideration in area such as academic research lab and industry. They are interesting group of flourophores with elevated thermal, photo-chemical strength inorganic solvents and quantum yield of nearly one [17]. Recently it has been found that these dyes have wide range of utilities in electronic materials as the best semiconductors. Solubility, uv-visible and fluorescence behaviour of them can be properly changed by functionalising at imide or core position with different groups such as electron-withdrawing, electron- donating and hydrophobic, hydrophilic substitutes [18]. The electrochemical measurements of PDI have shown that they can be easily reduced rather than oxidized because of their electron deficiency [19-20]. For designing supra-complexes of perylene dyes using directional secondary forces such as H-bonding and metal ligandation have been developed. In addition to that, non-covalent interactions in these supra-architectures could have controlled the stacking (π-π interaction) behaviour of the perylene dyes. For instance the π-π interaction in the backbone of the supra-structures can widely change the properties of the molecules such as absorption-emission and also the favourable property like charge transfer (CT) can be facilitated which is applicable in electronic productions (solar cells as well as field-effect transistor and etc.).

1.2.1 Bay-Substituted Perylene Dyes

Working with PDI derivatives that have been substituted at imide position have had two main challenges [21]. First, planar configuration of these dyes that enhance the formation of π-π aggregates reduces the solubility of these dyes. Second, because of nodes at the HOMO-LUMO orbitals in imide position, the photochemical and

photophysical behaviour of them can't be affected by changing the substituents at nitrogen atoms [17]. Because of the above reasons the modification of a perylene core in the bay-position (Figure 1.3) have been started at 1997 by Böhmn [22] that could change the properties of the dye and make them cover the broad area of visible (400–760 nm) and near infrared (760–1200 nm) absorption [23-27] that this enlargement of the PDI core can be initially obtained by functionalisation with halogen group.

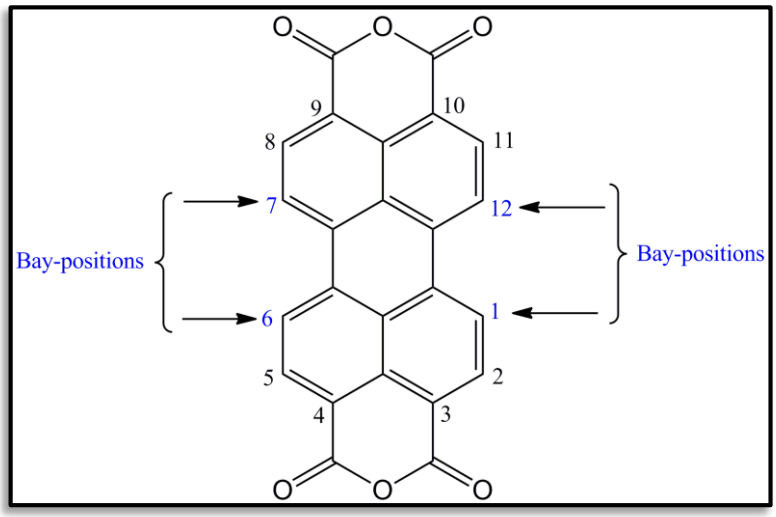

Figure 1.3: Chemical structure of perylene

In the present study, three different perylene diimides two of which were symmetrical (**TPDI** and **TCPDI**) and one was highly soluble asymmetrical (**TAPDI**) have been synthesized. In order to change the photophysical and photochemical properties of the diimides, 1,7-symmetrically substituted perylene bis (dicarboximide) dyes (**BTC-TCPDI**, **BPY-PPDI** and **BTC-APDI**) with electron donating groups have been synthesized in good amount of product under mild conditions, to achieve this purpose, at first brominated PDA or shortly (Br-PDA) was prepared in accordance with the literature procedure and then modification of perylene core at bay position was done by using different alcoholic substituents, and

at the end the synthesis was completed by functionalisation of imide positions. The products have been purified and thermal, optical and electrochemical indices of them were measured and characterized carefully. In most of the above mentioned synthetic compounds (**TPDI**, **TCPDI**, **APDI**, **BTC-TCPDI**, **BTC-PDA**, **BTC-APDI**) the reactions are done by using thiazolium hydrochloride (Vitamin B_1) as an electron donating group either at imide or bay positions, based on literature it was reported that the resonance energy transfers generally takes place over distances similar to most biological macromolecules i.e. ranging from 10 to 100 A˚, The energy transfer rate is extremely dependent on how close are the gaps between excited and ground states of donor-acceptor system. It can be a great method for studying conformation and activity of biological molecules such as DNA, protein etc., which play an important role in maintenance of human-body healthiness [28]. Since vitamine B_1 is one of the crucial biological molecules and a vital nutritional compound in the human diet with water solubility it has been used as a substituent for modification of perylene properties in the present research.

The structures of all the synthesized compounds are shown in the following pages (8-13).

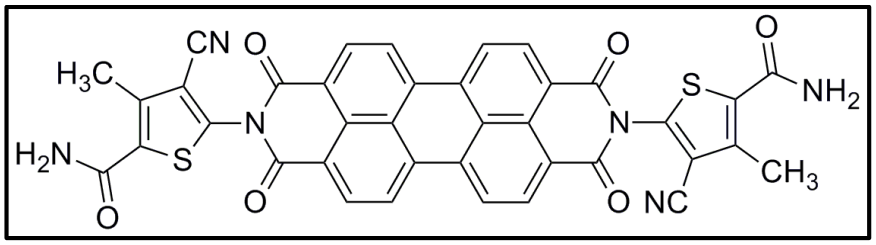

Figure 1.4: Schematic structure of *N,N'*-bis-[2-(5-carboxamidyl-3-cyano-4-methyl)-thienyl]-3,4,9,10-perylenebis(dicarboximide) (**TPDI**)

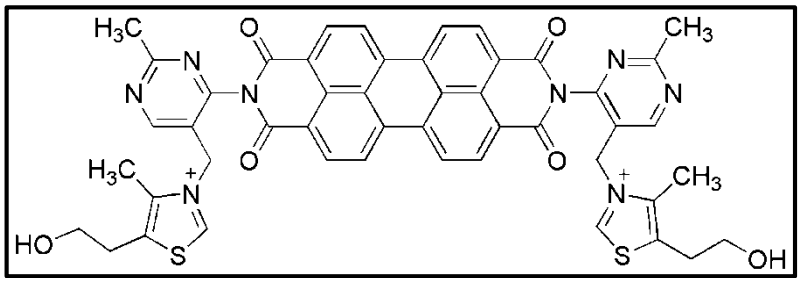

Figure 1.5: Schematic structure of *N*,*N'*-bis-[3-((2-methyl-5-pyrimidinyl) methyl)-5-(2-hydroxyethyl)-4-methylthiazolium] perylene-3,4:9,10-tetracarboxylic diimide (**TCPDI**)

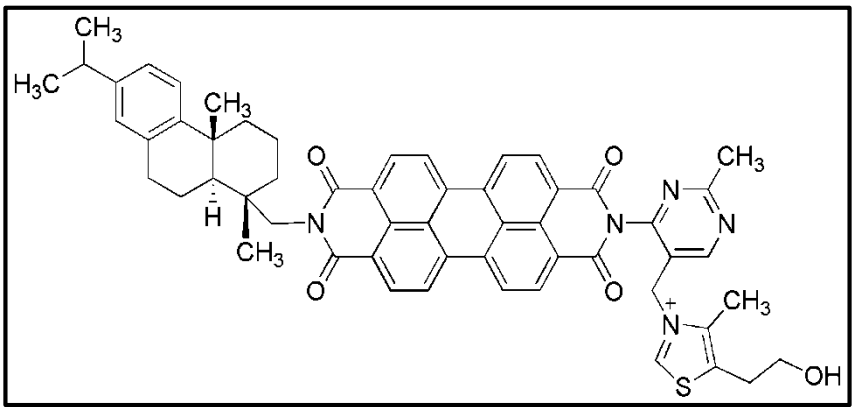

Figure 1.6: Chemical structure of *N*-(dehydroabietyl)-*N'*-[3-((2-methyl-5-pyrimidinyl) methyl)-5-(2-hydroxyethyl)-4-methylthiazolium] perylene-3,4:9,10-tetracarboxylic diimide (**TAPDI**)

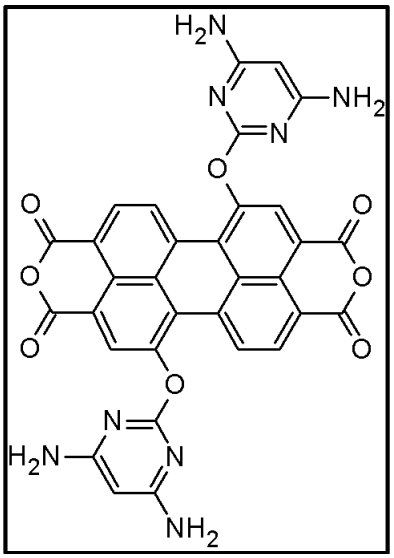

Figure 1.7: Chemical structure of 1,7-di(3,5-diamino-pyrimidoxylperylene-3,4,9,10-tetracarboxy dianhydride (**BPY-PDA**)

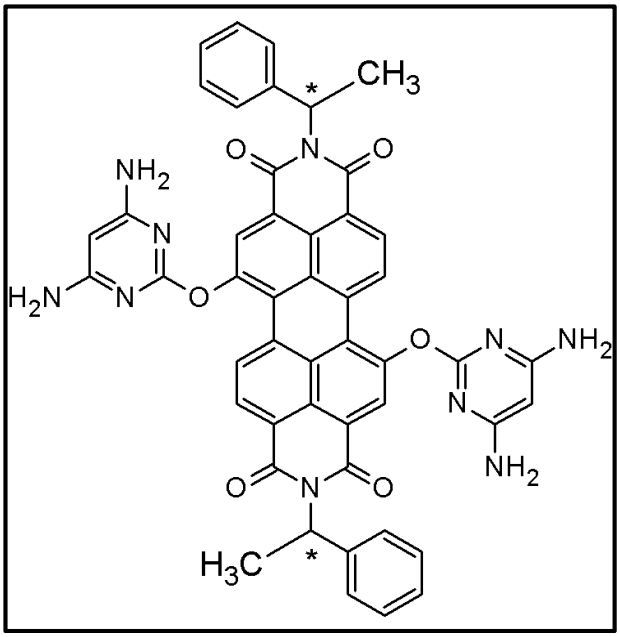

Figure 1.8: Chemical structure of *N*,*N'*-di((s)-1-phenylethyl)-1,7-di(3,5-diamino-pyrimidoxylperylene-3,4,9,10-tetracarboxy diimide (**BPY-PPDI**)

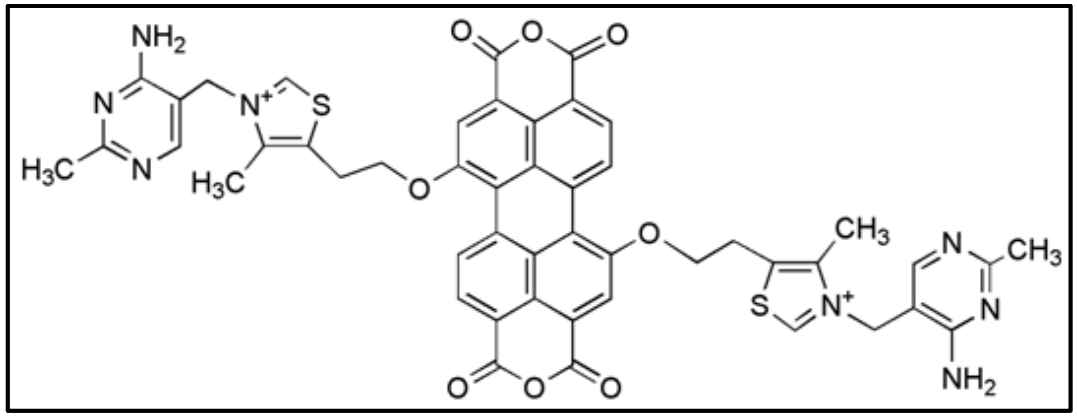

Figure 1.9: Schematic structure of 1,7-di-(2-[3[(4-amino-2-methylpyrimidin-5-yl) methyl]-4-methyl-1,3-thiazol-3-ium-5-yl] ethoxy perylene-3,4:9,10-tetracarboxylic dianhydride (**BTC-PDA**)

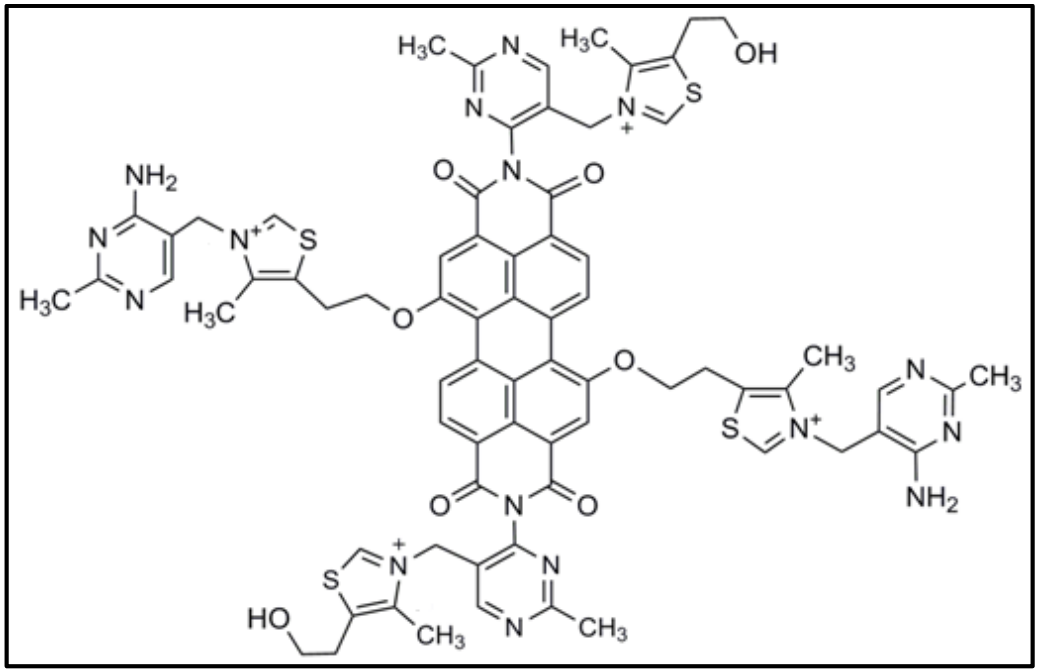

Figure 1.10: Schematic structure of *N,N'*-bis-[3-((2-methyl-5-pyrimidinyl) methyl)-5-(2-hydroxyethyl)-4-methylthiazolium chloride]- 1,7-di-(2-[3[(4-amino-2-methylpyrimidin-5-yl) methyl]-4-methyl-1,3-thiazol-3-ium-5-yl] ethoxy perylene-3,4:9,10-tetracarboxylic diimide (**BTC-TCPD**)

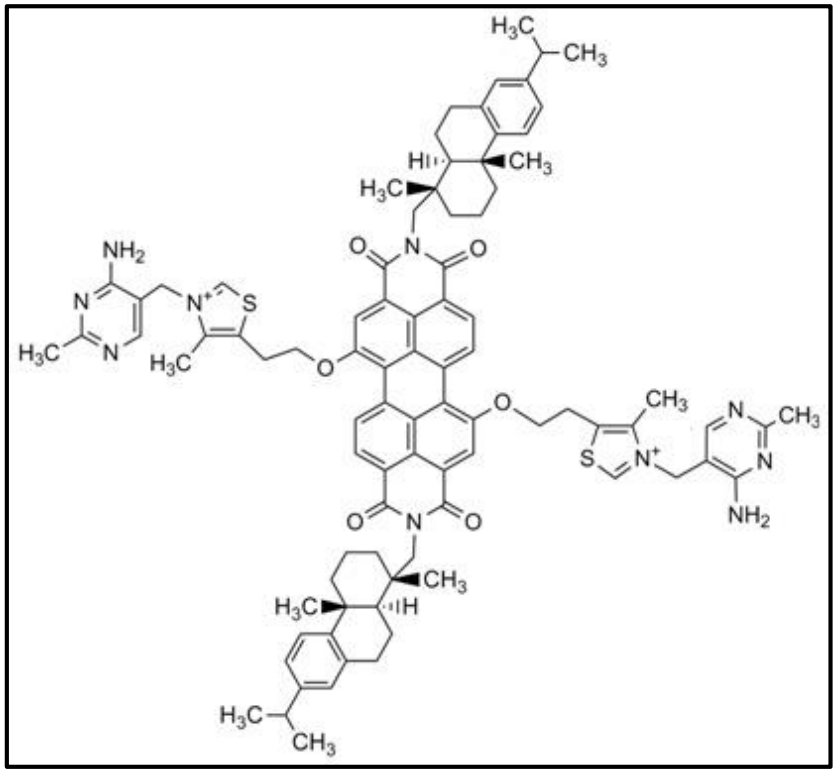

Figure 1.11: Schematic structure of *N,N'*-bis-(dehydroabietyl)- 1,7-di-(2-[3[(4-amino-2-methylpyrimidin-5-yl) methyl]-4-methyl-1,3-thiazol-3-ium-5-yl] ethoxy perylene-3,4:9,10-tetracarboxylic diimide (**TC-APDI)**

Chapter 2

THEORETICAL

2.1 Photochemistry

Photochemistry is the fundamental mechanism which is at the junction of chemistry, physics and biology and at the crossing point between matter and light in other words photochemistry is the study of some types of reactions in chemistry, isomerizations and physical behaviour that may occur under the influence of UV-Vis light. When the absorption of light takes place in a molecule, electronic structure changes and different reaction with other molecules. The absorbed energy of light produces photochemical changes in the molecule, or in a nearby molecule (e.g., photosensitization). The energy can also be released as heat, or as a light with lower energy (fluorescence or phosphorescence) for relaxation of the molecule to its ground state. To release the energy of absorbed photon of light molecules depending on their structures have their own preferences of relaxation mechanism, e.g., some prefer fluorescence over chemical reaction [29]. The researcher's interest and curiosity moved from intra-molecular photochemical reactions to intermolecular electron or energy transfer processes, proceeding among excited states molecules and appropriate reaction partners. In recent years studying the artificial assemblies of multi molecular components (photochemistry of supra-structures) became popular to elaborate the photo-biological processes and design of functional artificial system [30].

The first and second law of photo chemistry:

1- Light should be absorbed by molecules (Law of Grotthuss-Draper)
2- Radiation energy and energy difference of ground and excited state should be well matched (Stark-Einstein Law)

2.1.1 Absorption

When a molecule absorbs light the electron configuration will be altered. In accordance with Franck-Condon principle the positions of heavy nucleus in atom doesn't change. This causes the initial geometry of the excited state to be at higher energy level compared with ground state. In excitation the spin of electron doesn't change (by quantum mechanics inversion of electron's spin during excitation is not allowed). From UV-absorption spectra taken with various concentrations of the compound, the molar extinction coefficients of all peaks can be calculated, either for the peak with low or high absorption intensity. Quickly after finishing the excitation few processes can take place. 1) Vibronic relaxation takes back the molecule right to an entirely new minimum energy level of the excited state. Energy will be given to the solvent. 2) Intersystem crossing is the other type of relaxation that leads to triplet energy level along with inversion of the electron spin 3) Energy of the excited molecule can be released as light while relaxation (fluorescence, phosphorescence). 4) Energy can be transferred to another molecule to quench the excited molecule. 5) In thermal relaxation molecules turn back to zero vibrational level (ground state) by radiation-less deactivation (Figure 2.1) and the energy will be released to the solvent or surroundings of molecule [31-37].

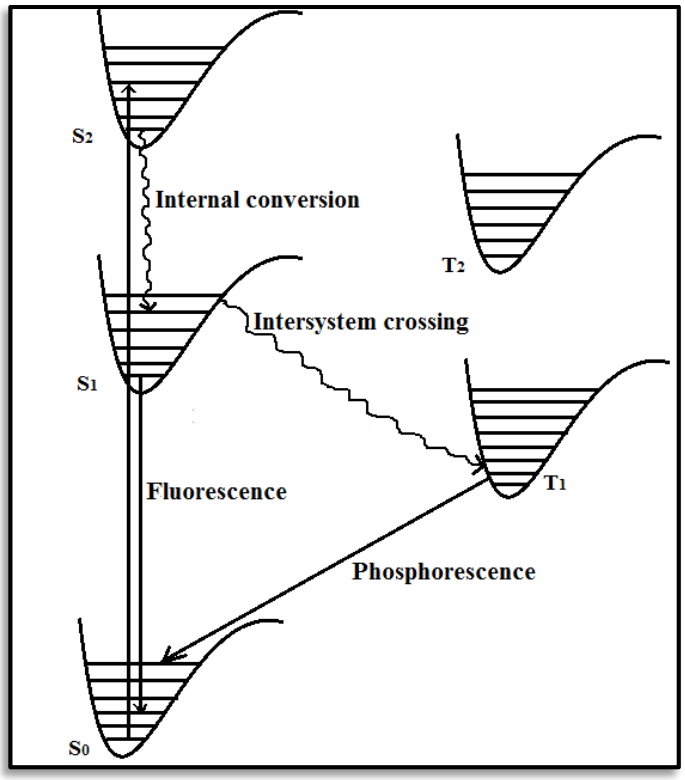

Figure 2.1: The route of photo-chemical processes

2.1.2 Fluorescence

Deactivation of excited molecule by changing S_1 to S_0 companied by emission of photon is called fluorescence. Caused by the energy that is lost by vibrational de-activation at excited state the fluorescence bands will be placed on higher wavelengths (lower energy) compared with the absorption bands (Based on the Stokes Rule). Yet in majority of instances, the absorption and fluorescence bands can be partially overlapped, i.e. a portion of emitted light is at shorter wavelengths. Companied by emission of light for the process of relaxation many other competitive processes for de-activation are probable (as has been discussed in part 2.1.1) if they occur on a period analogous with the time at which the excited molecule remains in the excitation level. The fluorescence bands, quantum yield and the fluorescence duration (life-time) that can be influenced by any other process at excitation level including interactions of the molecule that has been excited with its neighbouring

atmosphere can give data of molecular environment at micro scale. It has to be recalled that some processes at excitation level like conformational change, electron-transfer, energy-transfer, excimer or exciplex formation can cause a fluorescent generations with emitting spectrum that may cover up that radiation of the molecule which had been originally excited. These types of emissions shall be differentiated from the "major" fluorescence emerge from molecule of excitation state. Since fluorescence de-activation can be strongly affected by the neighbouring environment, fluorescent species recently has been utilized as probes for the physic-chemical, bio-chemical etc. explorations [38].

2.1.3 Photo-Induced Electron Transfer (PET)

This is well known that fluorescence gets quenched due to photo-induced electron transfer (PET) and is present in variety of photochemical organic reactions by playing a vital part in converting solar energy by photo-induced charge separation. By studying fluorescence quenching a better understanding of the electron transfer procedures can be achieved. It is notable that the property of oxidative-reductive of molecules may be improved in the excitation level. Figure 2.3 and 2.4 are depicting the mechanism of oxidative-reductive electron transfer processes based on the given reaction below [38].

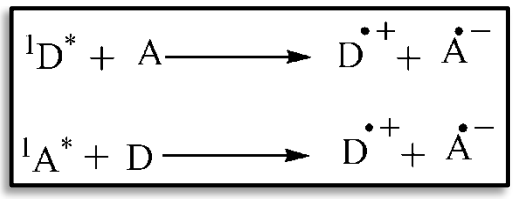

Figure 2.2: Electron-transfer processes

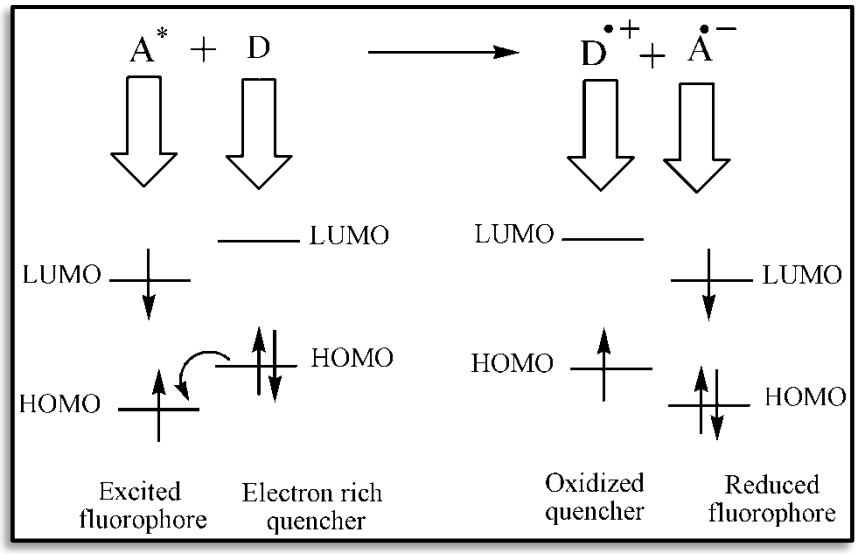

Figure 2.3: Reductive electron transfer

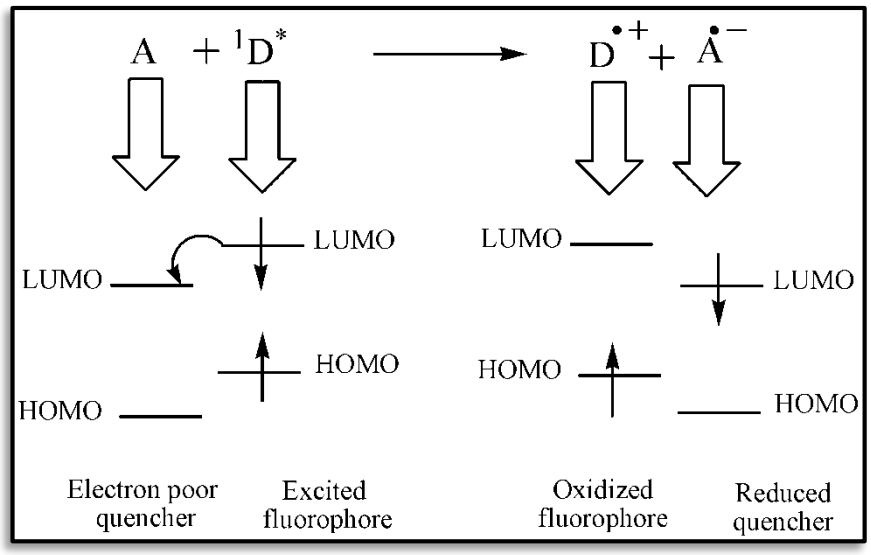

Figure 2.4: Oxidative electron transfer

2.1.4 Excimers and Exciplexes Formation

If an excited molecule collides with exactly the same but unexcited molecule excimers will be resulted. They are in fact excited state of dimmers as given below:

$$^1M^* + {}^1M \longrightarrow {}^1(MM)^*$$

The (MM)* represents that the delocalization of excitation energy took place on two moieties. Furthermore, if a molecule at excitation state collides with a different and unexcited molecule, exciplex will be resulted. These excited and unexcited molecules might be either electron donor or acceptor.

$$^1D^* + A \rightleftharpoons {}^1(AD)^*$$

$$D + {}^1A^* \rightleftharpoons {}^1(AD)^*$$

Many aromatic compounds for example naphthalene or perylene can have excimer type fluorescence. The excimer spectrum is placed at longer wavelengths compared with the single molecule which has a broad emission peak and undistinguishable vibronic transition bands [38].

2.1.5 Energy Transfer

When the energy is transferred from a donor excited molecule to an acceptor with different chemical structure in accordance to the following reaction.

$$D^* + A \longrightarrow D + A^*$$

The process is called hetero transfer and this will be probable when the donor's Fluorescence bands partly overlap the absorption bands of the acceptor. If the donor specie and acceptor are equal, the process is said to be homo transfer [38,39].

$$D^* + D \longrightarrow D + D^*$$

Radiative Energy-Transfer

This process is including two different steps: The emitted photon of D can be absorbed by the acceptor which has different structure (A) or totally the same (D).

$$D^* \longrightarrow D + h\upsilon$$

$$A + h\upsilon \longrightarrow A^* \quad \text{or} \quad D + h\upsilon \longrightarrow D^*$$

Although the given process is known as slight transfer due to its simple mechanism but the actual concept is sophisticated since it is highly depended to the size of the molecule and its configuration [38].

Radiationless Energy Transfer

When the donor emission bands are overlapping the absorption bands of acceptor, radiation-less transition may take place, in this case some of the transitions in the donor have identical energy as the transitions in the acceptor this transition is known as resonance energy transfer.

As can be seen in the following figure (2.5), the schematic energy level of donor and acceptor molecules demonstrates the resonance transitions whence the vibrational deactivation happens quicker than energy-transfer (slight coupling). The overlapped spectrums of donor emission and acceptor absorbance were shown schematically in the mentioned figure [38].

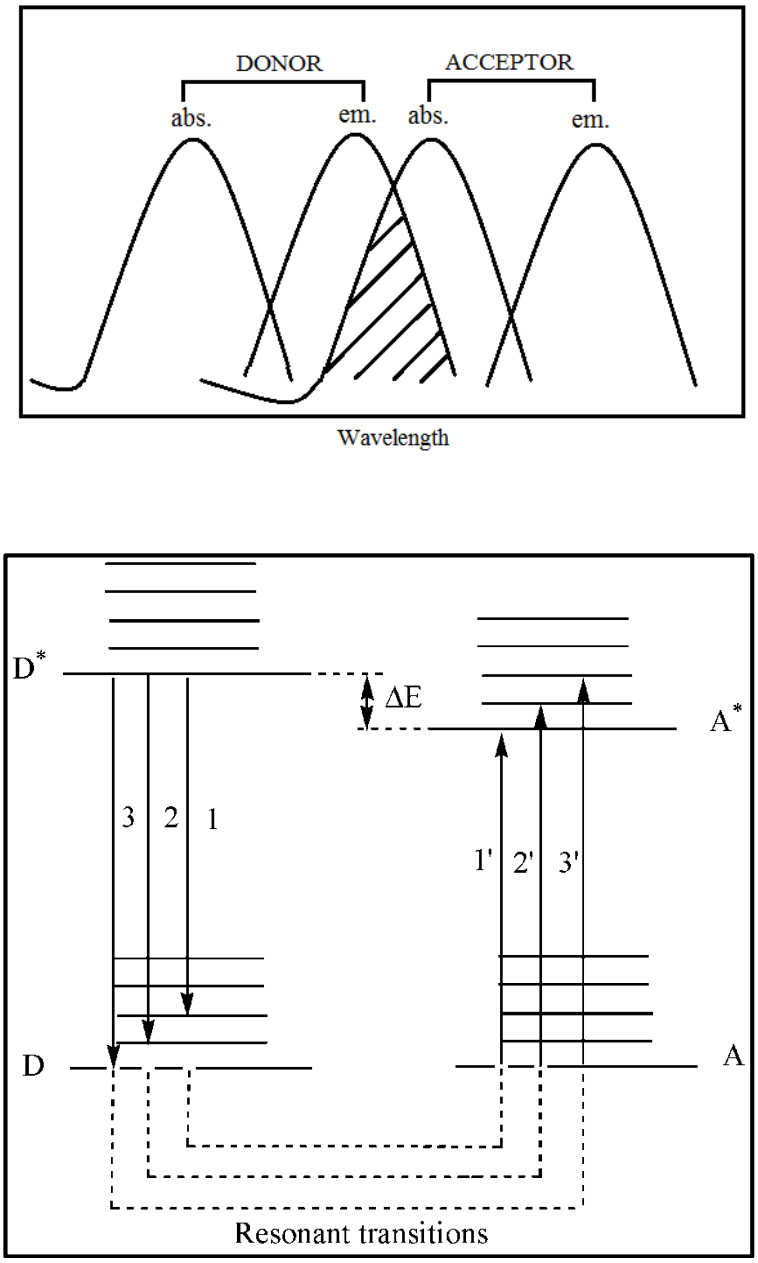

Figure 2.5: Energy level scheme of donor and acceptor molecules

2.2 Aggregation

The self-organization of molecules via intermolecular forces in solution or at the interface of solid-liquid is a commonly reason of aggregation in chemistry of dye molecules [40-48]. This process, effects on photo-physical properties of the molecule and thus it can be considered as distinctive behaviours [49]. The aggregation of molecules in solution reveals different absorption spectrum in comparison with non-

aggregated molecule, in solution it can be divided in to two different types of H or J-aggregation due to the shifting of the wavelength. If the spectrum is shifted to the higher or lower wavelength as a result of aggregation it is known as H-and J-aggregation respectively. Even though dyes have distinctive structure and, definitely different behaviours, due to the aggregation, wide range of regulations have been generally reputed for them as follows:

1- Aggregation may increase by increasing the concentration of the dye or ionic strengths
2- It can reduce by increasing temperature or having additional solvents.

Because of sensitivity of spectroscopic methods, the concentration dependent UV-Vis spectroscopy can be one of the best appropriate techniques for investigating on aggregation behaviour of dyes [50].

It's worthy to mention that aggregation of dyes serves a crucial function in both scientific and industrial purposes, optical memory, organic solar-cells and organic light-emitting diodes [51-53].

2.3 Organic Solar-Cells

Organic photovoltaic solar-cells (OPVs) are primarily composed of carbon-based semi-conducting materials for conversion of incident light to electricity. To have a profitable organic solar-cell, optimization of five processes is required:

1. Light absorption and excitons creation.
2. Exciton diffusion to dynamic interface.
3. Charge separation.
4. Charge transportation.

5. Charge assortment.

For creation of applicable solar-cell, the two photoactive compounds are pack in between two electrodes for collection of the charges that have been generated by incident photon it should be noted that the when the charges are separated they have to be carried to the electrodes for entering to the external circuit without recombination. In figure 2.6 the schematic principle mechanism of the cell is demonstrated.

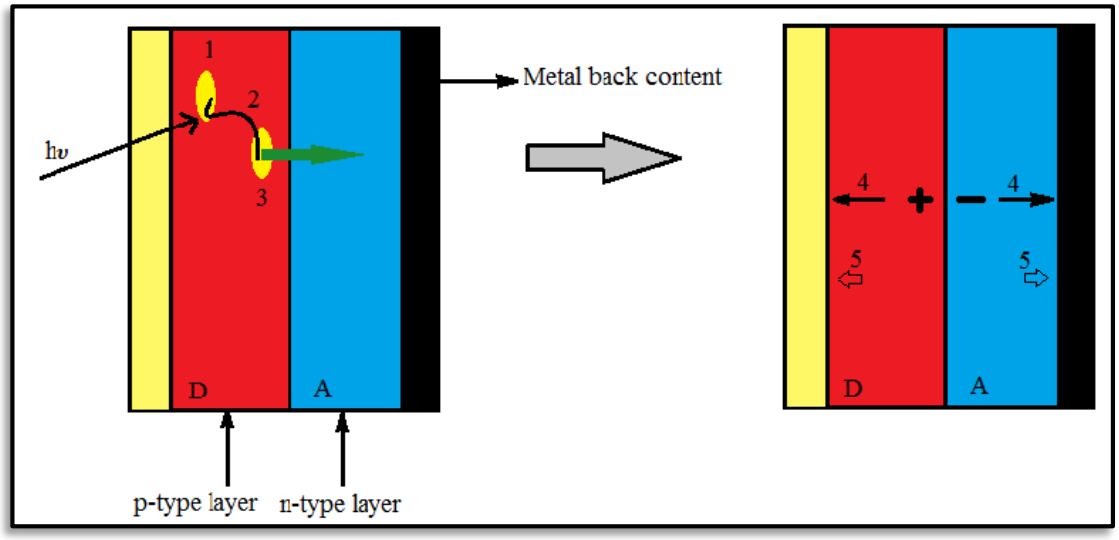

Figure 2.6: Scheme of principle solar-cell

As can been seen above after formation of excition in photo-active donor layer (red colour) (1), the diffusion of exciton has been done (2) to the boundary of donor-acceptor (blue colour) layer, the charge is transferred to the acceptor ($A^{\cdot -}$), and the donor textile will be left by hole ($D^{\cdot +}$**)** (3). The photo-generated charges (4) will be transferred to the opposite electrodes (5).

In dye sensitised solar-cell, an organic dye with ability of light absorption is attached to an inorganic layer with wide band gap, and the exciton will be transported to the conduction band of inorganic semi-conducting layer of the cell. Since the demand for progressing an affordable photo-voltaic generator raised dramatically in the recent decade the subject of organic-solar cells has become a very hot topic.

Chapter 3

EXPERIMENTAL

3.1 Chemicals and Reagents

Apart from solvents distillation using standard procedures [54], all other materials have been used as received from commercial sources. Perylene-3,4,9,10-tetracarboxylic dianhydride, 5-amino-4-cyano-3-methylthiophene-2-carboxamide, 2,4-diamino-6-hydroxypyrimidine, (S)-(-)-1-phenyl-ethylamine, thiamine hydrochloride (Vitamin B_1), dehydroabietylamine, zinc acetate, iodine, bromine, potassium carbonate were all purchased from Aldrich.

3.2 Instrumental Part

Reactions progresses were controlled by Thin-Layer Chromatography (TLC) on Merk silica gel aluminium coated films and observed under UV irradiated lamp. Infrared spectra were recorded with Mattson (USA) satellite FT-IR spectrometer by making KBr pellets. Mass spectrometric measurements were carried out with Finnigan MAT 311A instrument and the results have been represented in *m*/*z* (%) values. UV spectra in solid-state and solutions were obtained on a Varian-Cary 100 spectrometer. Fluorescence, excitation spectra and absolute Φ_f values were taken on a Varian-Cary Eclipse spectrophotometer in a quartz cell. ^{1}H and ^{13}C NMR spectra were measured with 400MHz Buker spectrometer utilizing tetramethylsilane (TMS) as an internal reference. To determine the contents of carbon, nitrogen, hydrogen and sulfur, elemental analysis was done over a Carlo-Erba-1106 analyser. Differential scanning calorimetry (DSC) and thermo-gravimetric analysis (TGA) methods were

applied for determination of thermal properties and were documented on a Perkin-Elmer/Pyris1 at a heating rate of 10°C min^{-1} with the samples weight of 10 mg, under nitrogen and oxygen atmosphere respectively. Electrochemical properties were analyzed once in solution and once in solid-state by cyclic voltammetry (CV) and squarewave voltammetry (SQWV). The measurement was carried out under argon atmosphere with a REFERENCE 600 computer-controlled Potentiostat/Galvanostat/ZRA utilizing three electrodes and single electrochemical cell. The glassy carbon working electrode was polished by 0.05 µm BUEHLER alumina, the Ag/AgCl electrode and Pt wire have been used as a reference electrode and counter electrode respectively which were immersed in 0.1 M Sodium tetrafluoroborate ($NaBF_4$) serving like a supporting electrolyte. Ferrocene redox couple (Fc/Fc^+) was employed as an internal reference.

3.3 Synthetic Route

In this part, initially synthetic methods of two new symmetrical and one asymmetrical perylene diimides have been explained in details. Additionally synthetic routs, purification steps and analysis results of two different bay substituted perylene dianhydrides and their three bay substituted perylene diimide derivatives are presented. It's noteworthy to mention that all the promising synthesised compounds have novelty in their structures, high stability, color tenability, wide range of absorption spectra and intermolecular donor-acceptor hydrogen bonding ability.

3.3.1 Schematic Illustration of Synthesis of Perylene Diimides

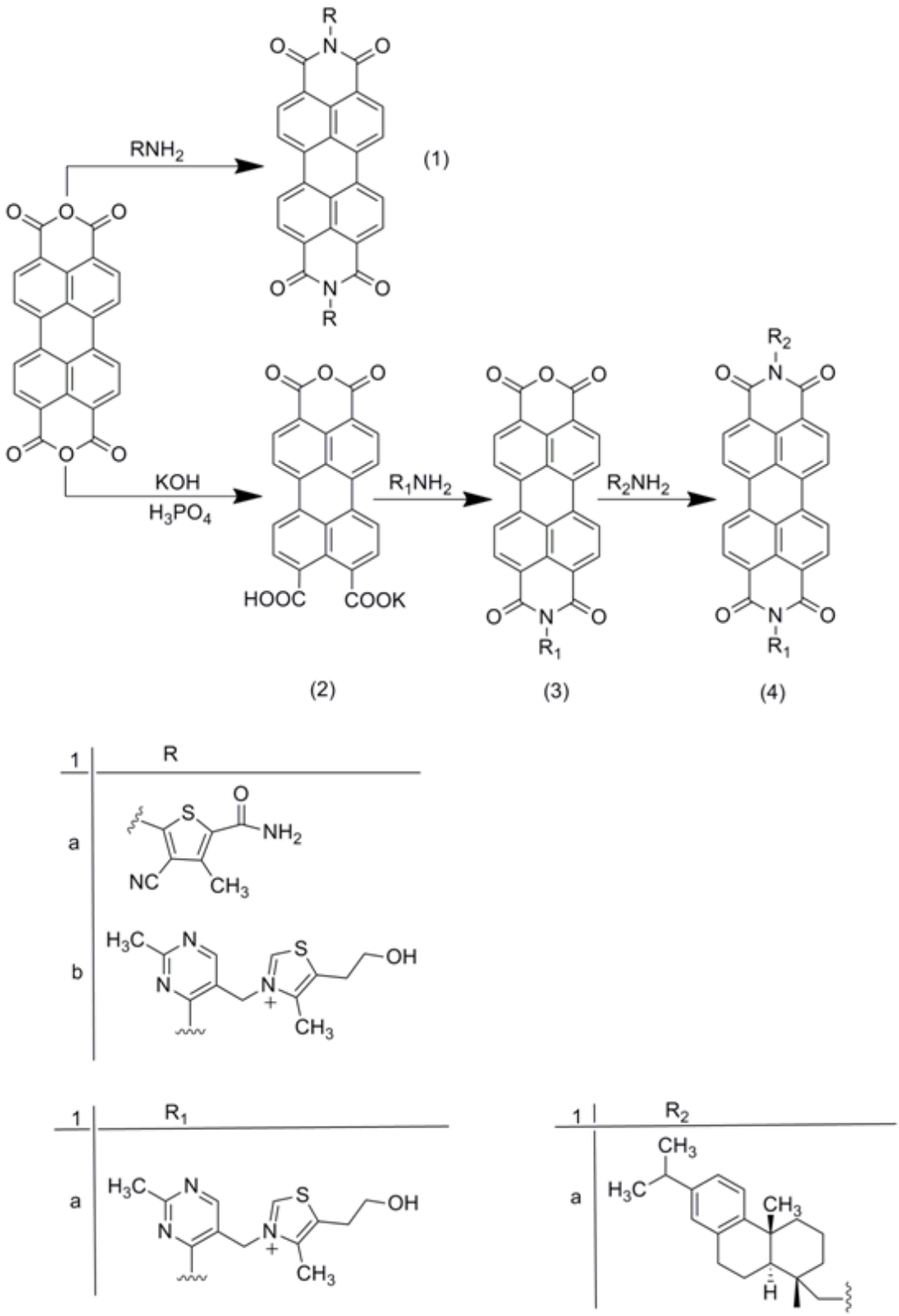

Scheme 3.1: Synthesis of symmetrical and unsymmetrical perylene diimides

Symmetrical and asymmetrical perylene diimides was produced by the methods reported earlier [55].

3.3.2 Schematic Illustration of Synthesis of Bay Substituted Perylene Diimides

The synthesis has been done within three different steps of first bromination, second bay substitution and third imidization that the general scheme of each step is shown below.

Step 1:

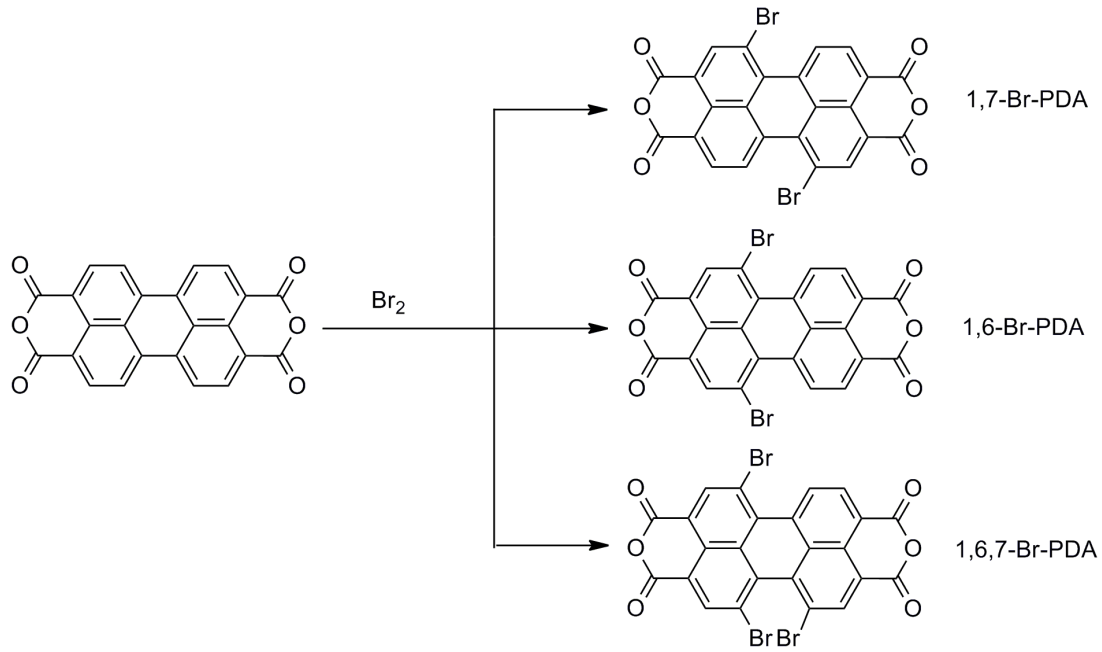

Scheme 3.2: Synthesis of brominated perylene dianhydride

Bromination reaction of perylene tetracarboxylic dianhydride was performed according to the article procedure [56] and the crude product was regioisomeric mixture of 1,6- and 1,7-dibrominated perylene bis anhydride together with a little amount of 1,6,7-trisubstituted regioisomer.

Step 2:

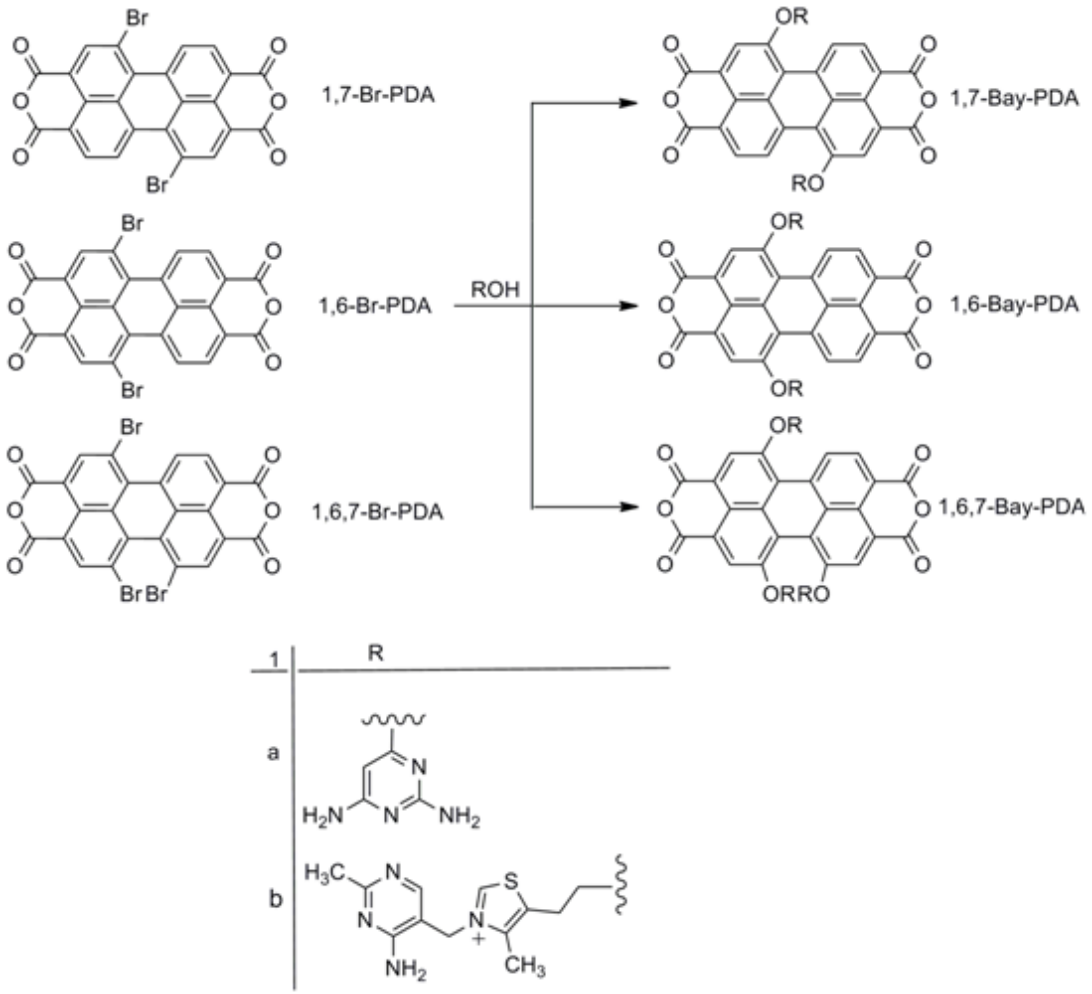

Scheme 3.3: Synthesis of bay substituted perylene dianhydride

As a result of insoluble products (brominated perylene dianhydride) in common organic solvents, the crude product has been undergone the subsequent bay substitution reaction without isomerically separation of the mixture, according to the synthetic procedure proposed by [57].

Step 3:

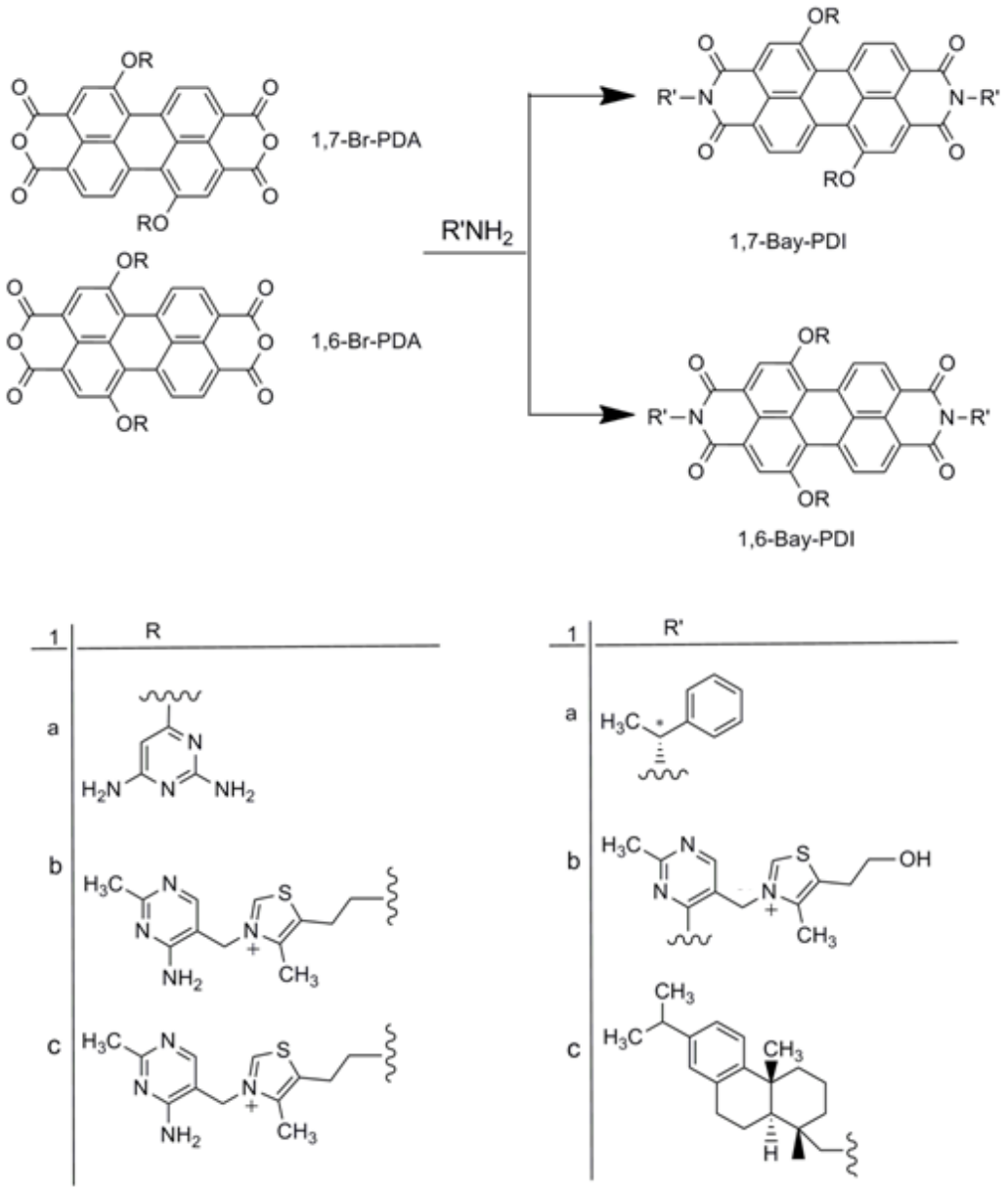

Scheme 3.4: Synthesis of bay substituted perylene diimide

Successive imidization of bay substituted perylene dianhydrides with different amine groups were done according to the literature [55]. Due to increasing solubility of the products at this step, the separation of 1,6,7-trisubstituted regioisomer has been done in accordance to the proposed procedure [56]. Consequently 1,7-disubstituted was collected at much higher yield compared with 1,6-disubstituted regioisomer.

3.4 Synthetic Procedure of *N,N′*-bis-[2-(5-carboxamidyl-3-cyano-4-methyl)-thienyl]-3,4,9,10-perylenebis(dicarboximide) (TPDI)

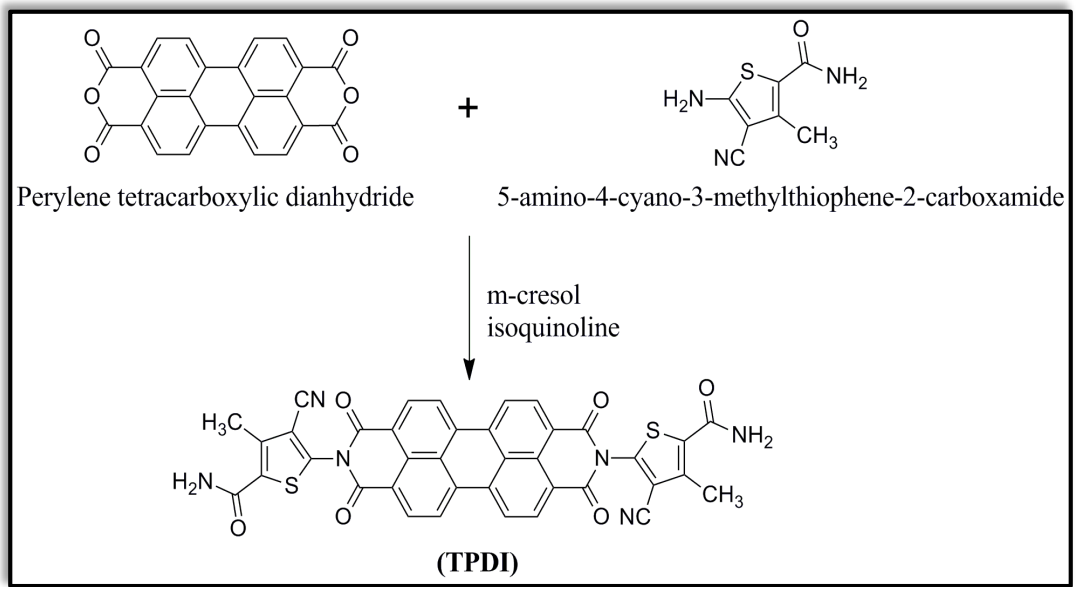

Scheme 3.5: Synthesis of *N,N′*-bis-[2-(5-carboxamidyl-3-cyano-4-methyl)-thienyl]-3,4,9,10-perylenebis(dicarboximide) (TPDI)

Perylene- 3,4,9,10-tetracarboxylic dianhydride (0.2 g, 0.45 mmol), 5-amino-4-cyano-3-methylthiophene-2-carboxamide (0.2 g, 1.10 mmol) and $Zn(OAc)_2.2H_2O$ (0.1 g, 0.45 mmol) were mixed with well-dried solvent mix (50 mL m-cresol and 8 mL isoquinoline) into a 100 mL three necked flask connected to argon input and was heated at 120 °C for 4 hours, 160 °C for 4 hours, and at 200 °C for 2 hours. After cooling down the mixture to room temperature it was poured into 100 mL cold methanol. The crude product was then filtered off, exposed to Methanol in soxhlet set up for 1day to get rid of excess starting materials and solvents. After all, purple color product was placed in vacuum oven at 120 °C for 24 hours.

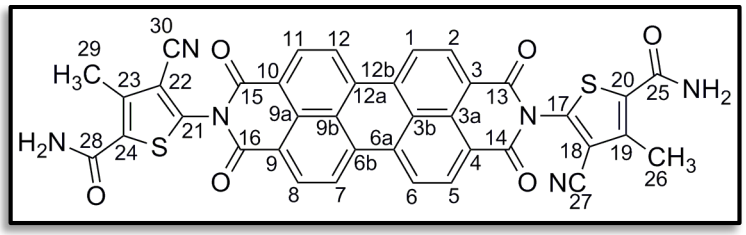

Figure 3.1: *N*,*N'*-bis-[2-(5-carboxamidyl-3-cyano-4-methyl)-thienyl]-3,4,9,10-perylenebis(dicarboximide) (TPDI)

Yield: 93% (0.33 g); **Color:** Purple powder.

FTIR (KBr, cm^{-1}): υ: 3341 and 3179 (amide N-H stretch), 2970 (aromatic C-H stretch), 2913 (aliphatic C-H stretch), 2222 (aromatic C≡N stretch), 1715 and 1683 (imide C=O stretch), 1658, 1652 and 1580 (overlapped amide C=O and aromatic C=C stretch), 1508 (N-H bend), 1408 (C-S-C stretch), 1330 (imide C-N stretch), 1065 (amide C-N stretch) and 1034 (C-C stretch), 814 and 737 (aromatic C-H bend).

UV-Vis (DMF, λ_{max} nm): 528, 491, 463.

UV-Vis (solid state, λ_{max} nm): 478, 509, 552.

Fluorescence (DMF, λ_{max} nm): 545,583,637. Φ_f = 50%

Anal. Calcd for ($C_{38}H_{18}N_6O_6S_2$) (M_w, 718.72)**:** C, 63.50%; H, 2.52%; N, 11.69%. Found: C, 63.21%; H, 2.61%; N, 11.47%.

^{1}H NMR, (δ_H ppm, 400 MHz, $CDCl_3$): 8.53-8.49 (m, Ar-H, H-C(1), H-C(2), H-C(5), H-C(6), H-C(7), H-C(8), H-C(11), H-C(12)), 8.14 (s, 2H, NH), 7.94 (s, 2H, NH), 2.26 (s, 1CH_3, H_3-C (29)), 2.39(s, 1CH_3, H_3-C (26)).

^{13}C NMR, (δ_c ppm, 400 MHz, $CDCl_3$): 164.13 (6 C=O, C(13), C(14), C(15), C(16), C(25), C(28)), 145.94 (4 ArC, C(17), C(20), C(21), C(24)), 133.90 (4 ArC, C(3), C(4), C(9), C(10)), 131.27 (4 ArC, C(6a), C(6b), C(12a), C(12b)), 127.57 (4 ArC, C(3a),C(9a), C(3b), C(9b)), 124.68 (4 ArC, C(2), C(5), C(8), C(11)), 121.65 (4 ArC, C(1), C(6), C(7), C(12)), 120.20 (2 CN, C(27), C(30)), 108.55 (4(C), C(18), C(19), C(22), C(23)), 53.42 (2 CH_3, C(26), C(29)).

MS (EI, m/z): (Mw, 718), 552.8, 524.8, 509, 109.8.

3.5 Synthetic Procedure of *N,N'*-bis-[3-((2-methylpyrimidinyl) methyl)-5-(2-hydroxyethyl)-4-methylthiazolium] perylene-3,4:9,10-tetracarboxylic diimide (TCPDI)

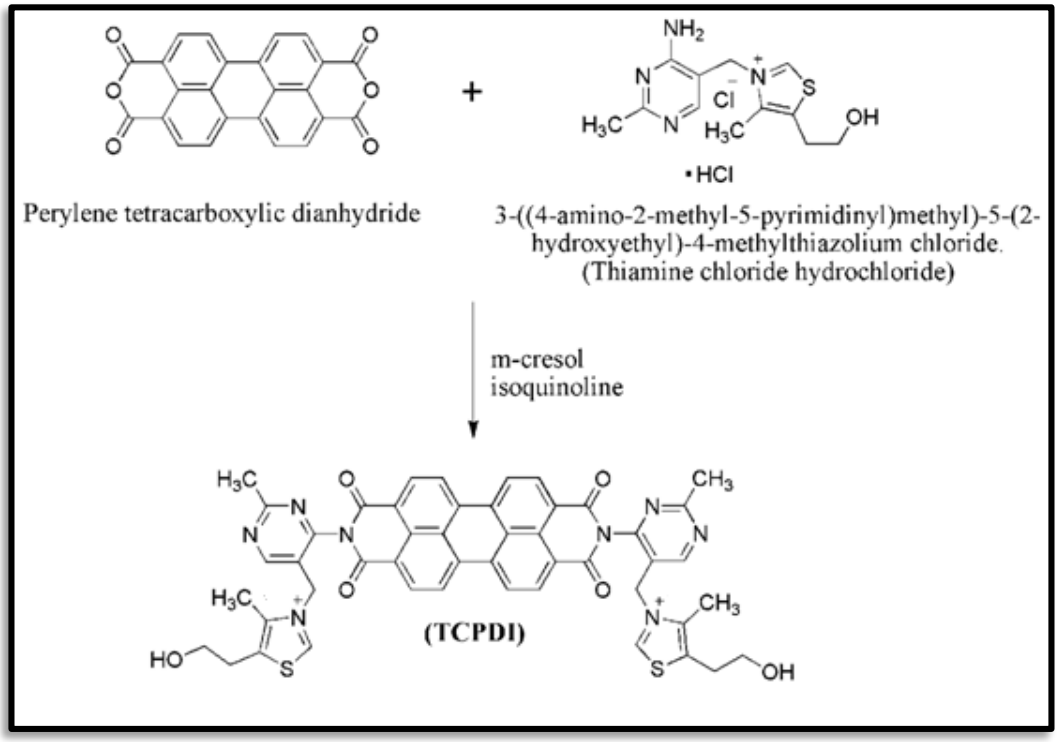

Scheme 3.6: Synthesis of *N,N'*-bis-[3-((2-methyl-5-pyrimidinyl) methyl)-5-(2-hydroxyethyl)-4-methylthiazolium] perylene-3,4:9,10-tetracarboxylic diimide (TCPDI)

The mixture of Perylene- 3,4,9,10-tetracarboxylic dianhydride (1 g, 2.55 mmol), thiamine chloride hydrochloride (3.4 g, 10.2 mmol) and zincacetate dihydrate (0.56 g, 2.55 mmol) were stirred in dry isoquinoline and m-cresol (40:20 mL) under argon atmosphere at 100 °C for 6 hours, 150 °C for 10 hours and 190 °C for 48 hours. IR detection indicated the disappearance of anhydride peaks. When the mixture was cooled down to room temperature, it was poured in to 250 mL cold acetone and the crude product was filtered by vacuum filtration. To get rid of excess amine and other

impurities the product was wrapped in filter paper and treated by water soxhlet for 2days, methanol for 1day and acetone for 4days. The collected black product was dried in vacuum oven for 48 h at 120 °C.

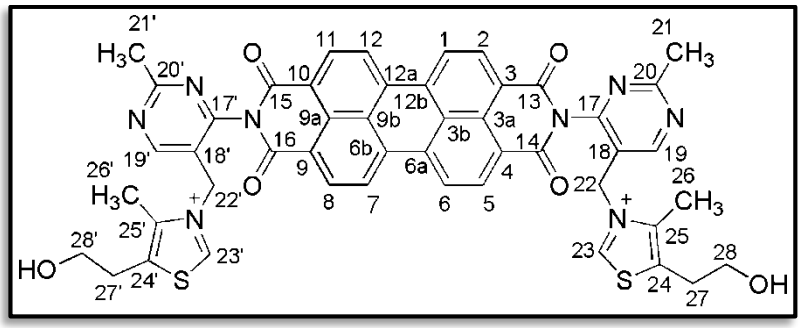

Figure 3.2: *N,N'*-bis-[3-((2-methyl-5-pyrimidinyl) methyl)-5-(2-hydroxyethyl)-4-methylthiazolium] perylene-3,4:9,10-tetracarboxylic diimide (TCPDI)

Yield: 90.2% (2.16 g); **Color:** black powder.

FTIR (KBr, cm^{-1}): υ: 3338 (O-H str.), 3046 (aromatic C-H), 2850 (aliphatic C-H), 1695 and 1584 (imide C=O), 1569 (aromatic C=C), 1353 (C-N), 1109 (C-O str.), 810 (C-H bend).

UV-Vis (DCM, λ_{max} nm): 523, 488, 456.

Fluorescence (DCM, λ_{max} nm): 533,574,622. Φ_f = 31%

Anal. Calcd for ($C_{48}H_{38}N_8O_6S_2$) (M_w, 886.994)**:** C, 65 %; H, 4.32 %; N, 12.63 %. Found: C, 63.6%; H, 3.97%; N, 10.3%.

^{1}H NMR and **^{13}C NMR** of this compound due to the low solubility couldn't be detected.

MS (EI, m/z): (Mw, 886.994), 777.5, 674.57, 122.05.

3.6 Synthetic Procedure of *N*-(dehydroabietyl)-*N′*-[3-((2-methyl-5-pyrimidinyl) methyl)-5-(2-hydroxyethyl)-4-methylthiazolium] perylene- 3,4,9,10-tetracarboxylic diimide (TAPDI)

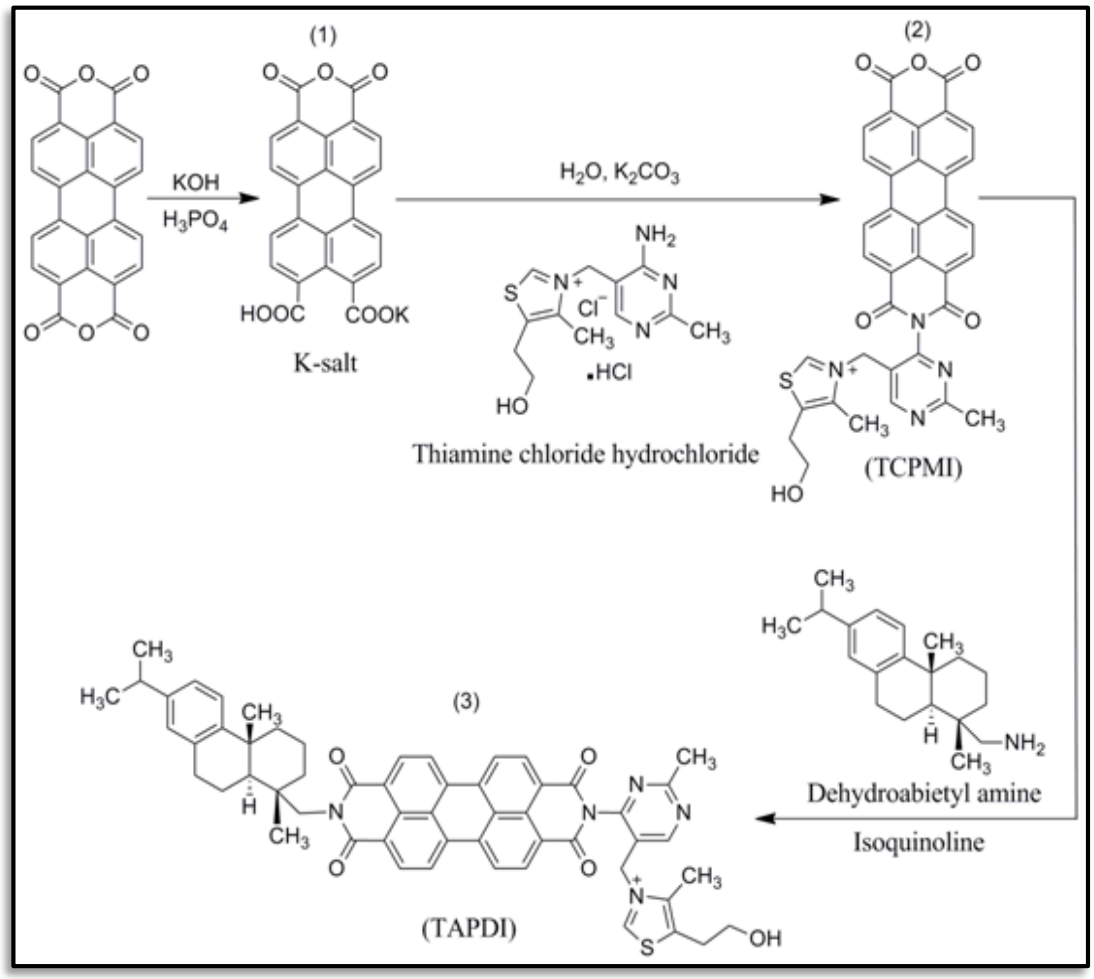

Scheme 3.7: Synthesis of *N*-(dehydroabietyl)-*N′*-[3-((2-methyl-5-pyrimidinyl) methyl)-5-(2-hydroxyethyl)-4-methylthiazolium] perylene-3,4:9,10-tetracarboxylic diimide (TAPDI)

The reaction had been done via three different steps:

1- K-salt preparation

2- Monoimide mono anhydride preparation.

3- Asymmetric perylene diimide preparation.

3.6.1 Perylene-3,4,9,10-tetracarboxylicacid monoanhydride monopotassium carboxcylate (K-salt) Preparation

According to the procedure from literature [55] the (3 g, 7.647 mmol) 3,4,9,10-perylene tetracarboxylic dianhydride was dissolved in (5%, 51.4 mL) KOH solution and refluxed at 90 °C for 6 hours. When the mixture reached to room temperature, H_3PO_4 (10%, 19.5 mL) was added into the reaction. Subsequently the solution was refluxed at 90 °C for 1 hour and rested to cool and filtered off. Afterwards the dark red product was washed few times with water and treated by acetone in soxhlet for 3 days and dried at 120 °C under vacuum.

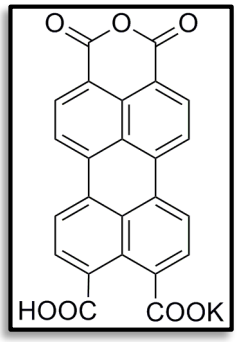

Figure 3.3: K-salt

Yield: 77% (2.4 g); **Color:** Red powder.

FTIR (KBr, cm^{-1}): υ: 3442 (acid O-H stretch), 3094 and 3065 (aromatic C-H stretch), 1768 and 1725 (overlapped C=O of anhydride and acid stretch), 1594 and 1508 (salt C=O stretch), 1315 (C-O anhydride stretch), 944 (acid O-H bend).

3.6.2 *N*-[3-((2-methyl-5-pyrimidinyl) methyl)-5-(2-hydroxyethyl)-4-methyl thia zolium]-3,4,9,10-tetracarboxylicacid monoanhydride monoimide Preparation (TCPMI)

Followed by literature procedure [55] the (1 g, 2.2 mmol) of Perylene-3,4:9,10-tetracarboxylic acid monoanhydride monopotassium carboxcylate was mixed with

thiamine chloride hydrochloride (3.7 g, 11 mmol), water (50 mL), and the solution was stirred at 0-5 °C for 83 hours. Then the mixture was heated at 90 °C for 2 hours, potassium carbonate (25%, 12.5 mL) was poured drop wise and stirred for an additional hour at 90 °C. The collected precipitate by vacuum filtration was washed by potassium carbonate (2%) and dissolved in KOH (3.5%, 100 mL). The obtained solution was heated to 90 °C for about 5 min and then filtered when it was hot. Acidification was done by hydrochloric acid (10%), and the precipitate had been gathered by vacuum filtration. The product was wrapped in filter paper and washed in water soxhlet for 2 days and well-dried in vacuum oven at 120 °C.

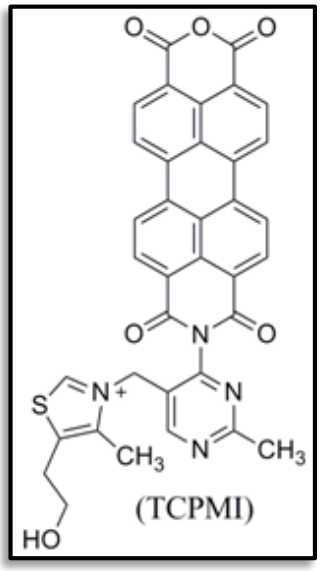

Figure 3.4: *N*-[3-((2-methyl-5-pyrimidinyl) methyl)-5-(2-hydroxyethyl)-4-methylthiazolium]-3,4:9,10-tetracarboxylic acid monoanhydride monoimide preparation (TCPMI)

Yield: 35.22% (0.55 g); **Color:** Red powder.

FTIR (KBr, cm^{-1}): υ: 3420 (alcohol C-H), 3088(Aromatic C-H), 2927(aliphatic C-H), 1762 and 1720(anhydride C=O), 1593(aromatic C=C), 1380 (C-N), 1005(alcohol C-O), 802(C-H bend).

3.6.3 Synthesis of *N*-(dehydroabietyl)-*N'*-[3-((2-methyl-5-pyrimidinyl) methyl)-5-(2-hydroxyethyl)-4-methylthiazolium] perylene-3,4,9,10-tetracarboxylic diimide (TAPDI)

Imidization of monoimide mono anhydride had been done by the procedure proposed by [55]. Accordingly (0.5 g, 0.7 mmol) of N-[3-((2-methyl-5-pyrimidinyl)methyl)-5-(2-hydroxyethyl)-4-methylthiazolium chloride]-3,4:9,10-tetracarboxylic acid monoanhydride monoimide(TCPMI) was blended with (0.4 g, 1.4 mmol) of dehydroabietyl amine, zinc acetate dehydrate (0.15 g, 0.7 mmol) in carefully dried isoquinoline (15 mL) as a solvent and the resulted mixture was stirred under argon atmosphere at 110 °C for 20 hours, 180 °C for 6 hours and 1 hour at 200 °C and the progress was monitored by Infrared spectrometer and TLC. When cooled downthe reaction solution was poured into 100 mL methanol and the precipitate was collected over vacuum filtration. The crude product was stirred in NaOH (5%) solution for 30 min at room temperature and after filtration it was washed by water soxhlet for two weeks and dried in vacuum oven. Then the red product powder was re-crystallized 3 times by chloroform-hexane and separated from mother solution by filtration.

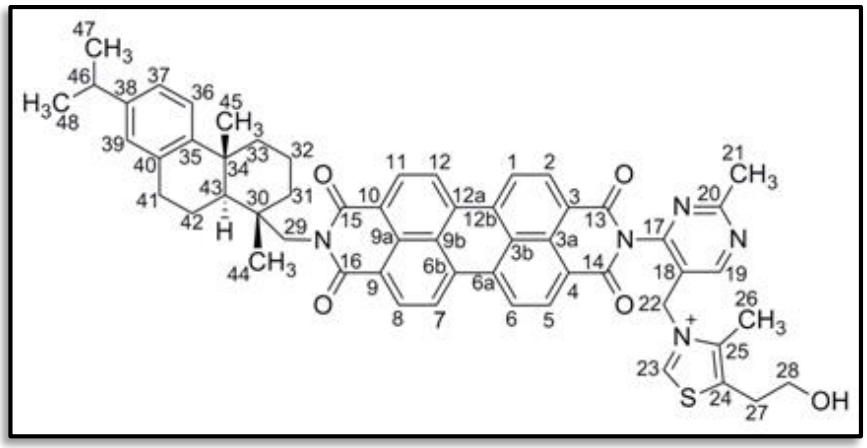

Figure 3.5: *N*-(dehydroabietyl)-*N'*-[3-((2-methyl-5-pyrimidinyl) methyl)-5-(2-hydroxyethyl)-4-methylthiazolium] perylene-3,4,9,10-tetracarboxylic diimide (TAPDI)

Yield: 54.2% (0.705 g); **Color:** red powder.

FTIR (KBr, cm^{-1}): υ: 2919 (C-H aliphatic), 1703, 1652 (imide C=O), 1592 (aromatic C=C), 1329 (C-N), 819 and 751 (C-H bend).

UV-Vis (THF, λ_{max} nm): 522, 486, 455, 430.

Fluorescence (THF, λ_{max} nm): 529, 571. Φ_f= 77%

Anal. Calcd for ($C_{56}H_{52}N_5O_5S$) (M_w, 907.107)**:** C, 74.15 %; H, 5.78 %; N, 7.72 %. Found: C, 79.6 %; H, 6.84 %; N, 3.09 %.

^{1}H NMR, (δ_H ppm, 400 MHz, $CDCl_3$): 8.53-8.43 (m, 8H, H-C(1), H-C(2), H-C(5), H-C(6), H-C(7), H-C(8), H-C(11), H-C(12)), 7.50 (s, 2H, H-C(19), H-C(23)), 7.09-7.02 (m, 3H, H-C(36), H-C(37), H-C(39)), 5.19 (m, 1H, O-H), 4.19 (m, 2H, H-C(29), 2.77 (s, 2H, H-C(22), 2.37 (m, 2H, H-C(28), 2.6 (m, 1H, H-C(46), 1.5 (d, J=12.5, 6H, H_3-C(48), H_3-C(47)), 1.17-1.14 (m, 13H, H_2-C(27), H_2-C(31), H_2-C(32), H_2-C(33), H_2-C(41), H_2-C(42), H-C(43)), 0.92 (br, s, 6H, H_3-C(21), H_3-C(26)), 0.8 (s, 6H, H_3-C(44), H_3-C(45)).

MS (EI, m/z): (Mw, 907.107), 904.67, 741.42, 727.33, 670.6, 329.018.

3.7 Synthetic Procedure of *N,N'*-di((s)-1-phenylethyl)-1,7-di(3,5-diamino-pyrimidoxyl) perylene-3,4,9,10-tetracarboxy diimide (BPY-PPDI)

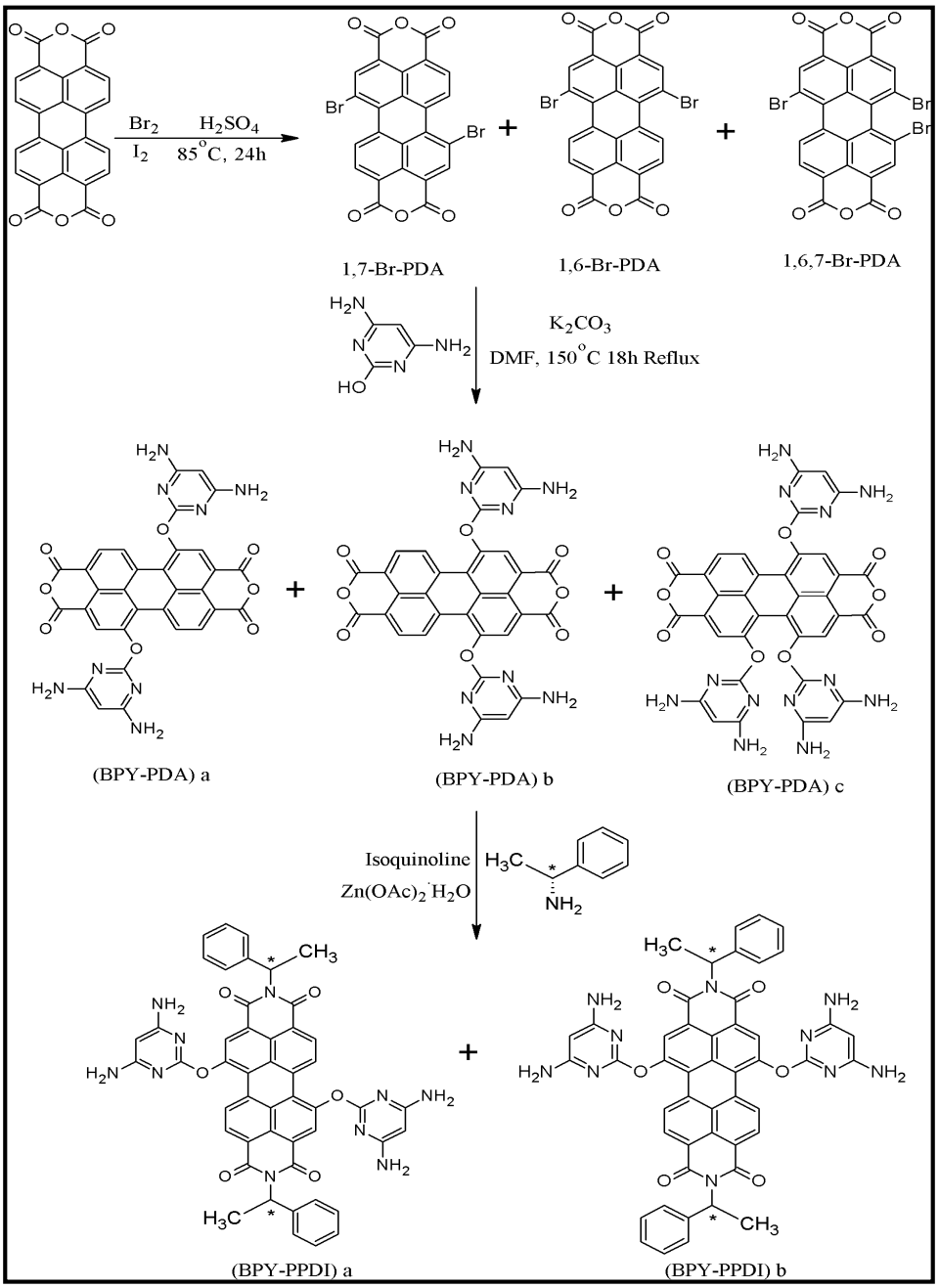

Scheme 3.8: Synthesis of *N,N'*-di((s)-1-phenylethyl)-1,7-di(3,5-diamino-pyrimidoxyl) perylene-3,4,9,10-tetracarboxy diimide (BPY-PPDI)

The reaction had been done within three different steps:

1- Bromination of perylene dianhydride.

2- Synthesis of bay substituted perylene dianhydride.

3- Imidization of bay substituted perylene dianhydride.

3.7.1 Bromination of Perylene tetracarboxylic dianhydride (Br-PDA)

The reaction was done in accordance to the article procedure [56], (2 g, 5.10 mmol) of perylene dianhydride was mixed with 30 mL of H_2SO_4 (95-97 %) and stirred for 6 hours at room temperature and 24 hours at 60 °C. Then the mixture was cooled down to room temperature for idonide (0.06 g, 0.236 mmol) to be added as a catalyst and stirred for 2 h, and additional 5 hours at 55 °C. When the reaction was cooled down to 25 °C Br_2 (0.8 mL, 15.61 mmol) was added in 1 h with stirring for 2 h at room temperature, 24 h at 85 °C and 2 h at 100 °C. Extra Br_2 was evacuated with argon gas stream. 20 mL of water was added dropwise to settle down the product as a precipitate which was collected later on by vacuum filtration. The product was next washed with water in soxhlet apparatus for 24 h and was dried in oven under vacuum at 120 °C.

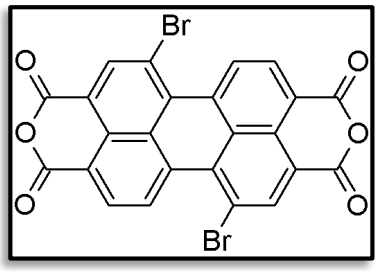

Figure 3.6: 1,7-dibromoperylene dianhydride (Br-PDA)

Yield: 86 % (2.4 g); **Color:** Reddish-brown powder.

FTIR (KBr, cm^{-1}): υ:3054 (aromatic C-H stretch), 1774, 1725 (anhydride C=O stretch), (conjugated C=C stretch), 1025 (anhydride C-O-C stretch), 735, 815 (C-H bend), 690 (C-Br stretch).

3.7.2 Synthesis of 1,7-di(3,5-diamino-pyrimidoxyl perylene-3,4,9,10-tetracarboxy dianhydride (BPY-PDA)

Bay substitution reaction of brominated PDA was performed according to the article procedure [57]. A mixture of Br-PDA (1 g, 1.82 mmol), K_2CO_3 (0.622 g, 4.50 mmol), 2,4-diamino-6-hydroxypyrimidine (0.8 g, 5.45 mmol) and dried DMF (67mL) were stirred at 150 °C for 18 hours under argon atmosphere. The progress was monitored by IR spectroscopy. When the reaction was completed, the solution was added to a mixture of water: acetic acid (1:1 ratio) and allowed to cool at 0 °C over night. The day after the crude product was filtered off by vacuum filtration and purifiedin soxhlet apparatus with water for 3 days. The dark purple product was dried in vacuum oven at 120 °C.

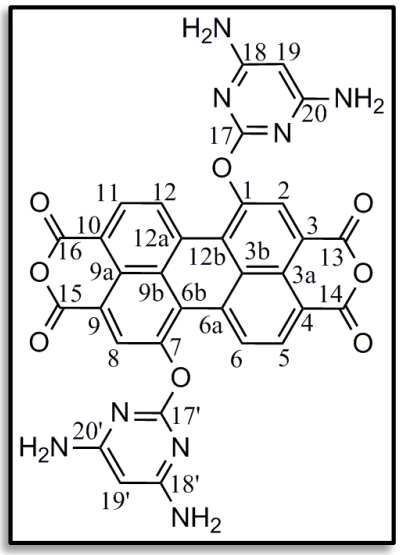

Figure 3.7: 1,7-di(3,5-diamino-pyrimidoxylperylene-3,4,9,10-tetracarboxy dianhydride (BPY-PDA)

Yield: 65% (0.78 g); **Color:** dark purple powder.

FTIR (KBr, cm^{-1}): υ: 3410, 3216 (amine N-H stretch), 1773, 1712 (anhydride C=O stretch), 1589 (conjugated C=C stretch), 1352(amine C-N stretch), 1254 (ether C-O-C stretch), 1025 (anhydride C-O-C stretch); 735(C-H bend)

UV-Vis (Pyridine, λ_{max} nm): 517, 484.

Fluorescence (Pyridine, λ_{max} nm):552, 576. Φ_f = 31%

Anal. Calcd for ($C_{32}H_{16}N_8O_8$)(M_w, 644.5)**:** C, 59.63 %; H, 3.13 %; N, 17.38 %. Found: C, 58.81 %; H, 2.94 %; N, 27.72 %.

^{1}H NMR and **^{14}C NMR** of this compound couldn't be detected due to the low solubility of the compound.

MS (EI, m/z): (Mw, 642.53), 627.3, 611.3, 511.6.

3.7.3 Synthesis of *N,N'*-di((s)-1-phenylethyl)-1,7-di(3,5-diamino-pyrimidoxyl perylene-3,4,9,10-tetracarboxy diimide (BPY-PPDI)

The reaction was done by using the literature procedure [58], BPY-PDA (0.5 g, 0.788 mmol), S-(-)-1-phenylethylamine (0.25 mL, 1.97 mmol) and zinc acetate (0.17 g, 0.788 mmol) are mixed in dried isoquinoline (30 mL) and the mixture has been stirred under argon atmosphere 5 hours at 80 °C, 7 hours at 100 °C, 11 hours at 150 °C and 2 hours at 200 °C. After cooling the reaction to room temperature, themixture was added in 100 mL cold methanol and the precipitate was gathered via filtration. To purify the product the black precipitate was wrapped in filter paper and washed by acetone in soxhlet apparatus for 2 days. To gain BPY-PPDI (figure 3.8) re-crystallization had been done and the product was dried at 120 °C in vacuum oven.

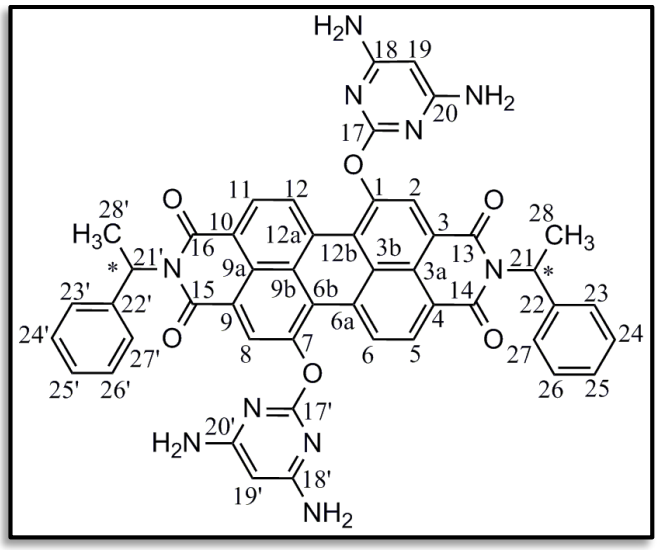

Figure 3.8: *N,N'*-di((s)-1-phenylethyl)-1,7-di(3,5-diamino-pyrimidoxyl) perylene-3,4,9,10-tetracarboxy diimide (BPY-PPDI)

Yield: 88% (0.60 g); **Color:** black powder.

FTIR (KBr, cm^{-1}): υ: 3321, 3163 (amine N-H stretch), 3058 (aromatic C-H stretch), 2935 (aliphatic C-H stretch), 1694, 1660 (imides C=O stretch), 1589 (conjugatedC=C stretch), 1342(amine or imide C-N stretch), 1254 (ether C-O-C stretch).

UV-Vis (Pyridine, λ_{max} nm): 526, 471.

Fluorescence (Pyridine, λ_{max} nm): 541, 576. Φ_f = 10%

Anal. Calcd for ($C_{48}H_{34}N_{10}O_6$)(M_w, 846.84)**:** C, 68.08 %; H, 4.05 %; N, 16.54 %. Found: C, 65.14 %; H, 3.40 %; N, 11.62 %.

^{1}H NMR and **^{13}C NMR** of this compound couldn't be detected due to the low solubility of the compound.

3.8 Synthetic Procedure of *N,N′*-bis-[3-((2-methyl-5-pyrimidinyl) methyl)-5-(2-hydroxyethyl)-4-methylthiazolium]-1,7-di-(2-[3[(4-amino-2-methylpyrimidin-5-yl)methyl]-4-methyl-1,3-thiazol-3-ium-5-yl]) ethoxyperylene-3,4:9,10-tetracarboxylic diimide (BTC-TCPDI)

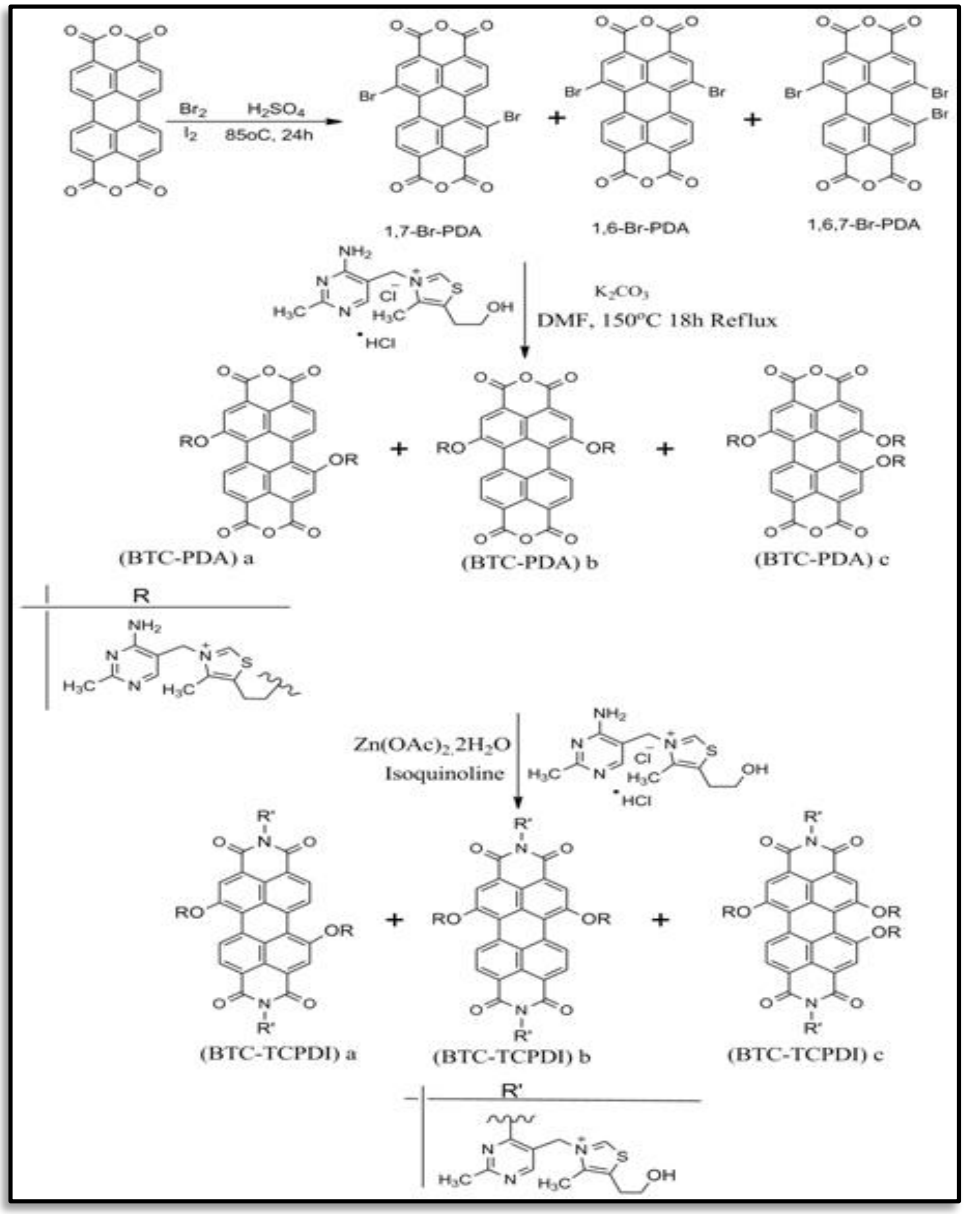

Scheme 3.9: Synthesis of *N,N′*-bis-[3-((2-methyl-5-pyrimidinyl) methyl)-5-(2-hydroxyethyl)-4-methylthiazolium]- 1,7-di-(2-[3[(4-amino-2-methylpyrimidin-5-yl) methyl]-4-methyl-1,3-thiazol-3-ium-5-yl]) ethoxyperylene-3,4:9,10-tetracarboxylic diimide (BTC-TCPDI)

The reaction had been done via three different steps that have been mentioned in previous session (3.7).

3.8.1 Synthesis of 1,7-di-(2-[3[(4-amino-2-methylpyrimidin-5-yl) methyl]-4-methyl-1,3-thiazol-3-ium-5-yl]) ethoxyperylene-3,4:9,10-tetracarboxylic dianhydride (BTC-PDA)

Via article procedure [57], a mixture of Br-PDA (1 g, 1.82 mmol), K_2CO_3 (0.63 g, 4.60 mmol), thiamine chloride hydrochloride (1.8 g, 5.4 mmol) and dried DMF (38 mL) were stirred at 150 °C for 18 hours under argon atmosphere. The progress was monitored by IR spectroscopy. When the reaction was completed, the solution was added into a mixture of water: acetic acid (1:1 ratio) and allowed to cool at 0 °C over night. The day after the crude product was filtered off by vacuum filtration and purified in soxhlet set up with water for 14 days. The b product was dried in vacuum oven at 120 °C.

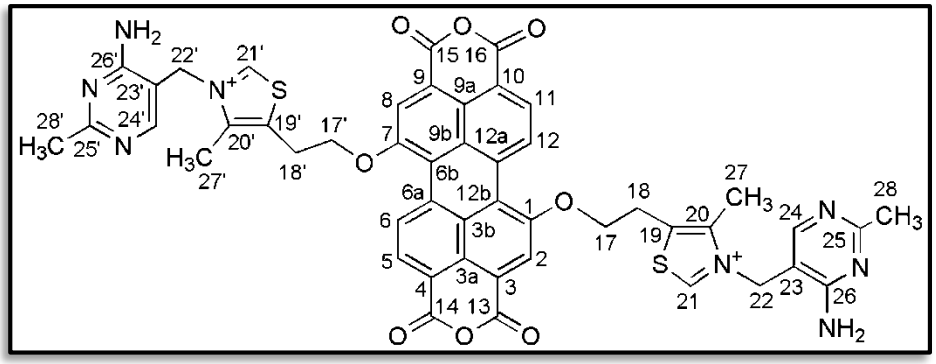

Figure 3.9: 1,7-di-(2-[3[(4-amino-2-methylpyrimidin-5-yl) methyl]-4-methyl-1,3-thiazol-3-ium-5-yl]) ethoxyperylene-3,4:9,10-tetracarboxylic dianhydride (BTC-PDA)

Yield: 64 % (1.21 g); **Color:** black powder.

FTIR (KBr, cm^{-1}): υ: 3445 and 3335 (amine N-H), 3063 (aromatic C-H), 2910 (aliphatic C-H), 1721 and 1753 (anhydride C=O), 1584 (aromatic C=C), 1236 (C-O-C ether), 1014(C-O-C anhydride), 734 (C-H bend).

UV-Vis (Pyridine, λ_{max} nm): 523, 487, 455, 421.

Fluorescence (Pyridine, λ_{max} nm):536, 575. Φ_f = 30%

^{1}H NMR and **^{13}C NMR** of this compound couldn't be detected due to the low solubility of the compound.

3.8.2 Synthesis of *N,N'*-bis-[3-((2-methyl-5-pyrimidinyl)methyl)-5-(2-hydroxy ethyl)-4-methylthiazolium chloride]- 1,7-di-(2-[3[(4-amino-2-methylpyrimidin-5-yl) methyl]-4-methyl-1,3-thiazol-3-ium-5-yl]) ethoxyperylene-3,4:9,10-tetracarboxylic diimide (BTC-TCPDI)

The mixture of 1,7-Di-thiazolium chloride perylene-3,4:9,10-tetracarboxylic dianhydride (BTC-PDA) (1 g, 0.93 mmol), thiamine chloride hydrochloride (1.26 g, 3.70 mmol) and zincacetate dihydrate (0.20 g, 0.93 mmol) were stirred in dried isoquinoline and m-cresol (20:20 mL) in argon atmosphere at 110 °C for 7 hours, 140 °C for 7 hours and 180 °C for 16 hours. IR detection indicated the disappearance of anhydride peaks. When cooled down to room temperature, the mixture was added in to 250 mL cold acetone and the crude product was filtered by vacuum filtration. To get rid of excess amine and other impurities the product was wrapped in filter paper and treated by water soxhlet for 3days, acetone for 6day and chloroform for 1day. The collected black product was dried in vacuum oven for 48 h at 120 °C.

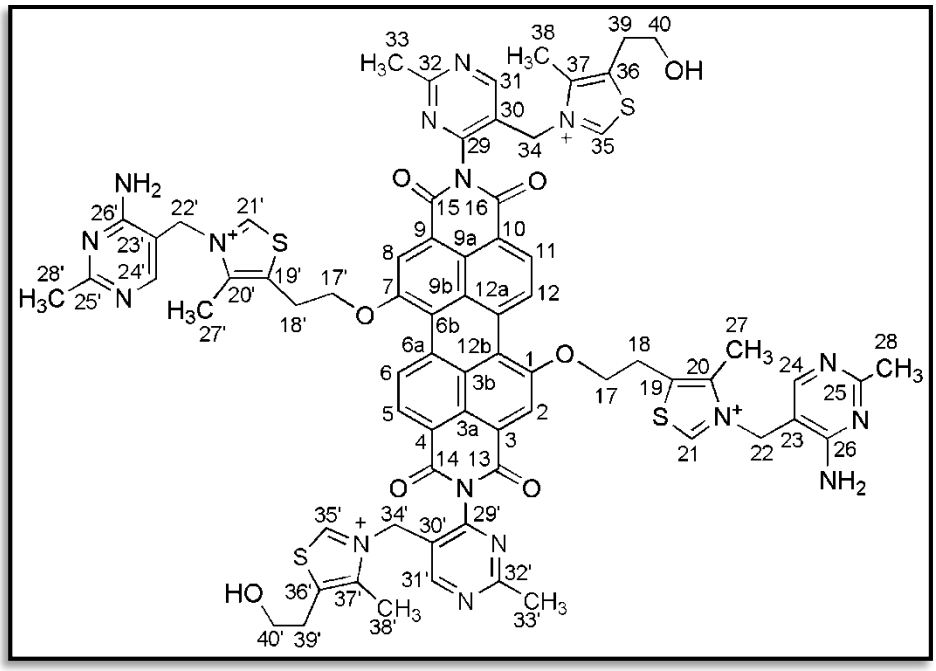

Figure 3.10: *N,N'*-bis-[3-((2-methyl-5-pyrimidinyl) methyl)-5-(2-hydroxyethyl)-4-methylthiazolium chloride]-1,7-1,7-di-(2-[3[(4-amino-2-methylpyrimidin-5-yl) methyl]-4-methyl-1,3-thiazol-3-ium-5-yl]ethoxy perylene-3,4:9,10-tetracarboxylic diimide (BTC-TCPDI),4:9,10-tetracarboxylic dianhydride (BTC-TCPDI)

Yield: 55 % (0.795 g); **Color:** black powder.

FTIR (KBr, cm^{-1}): υ: 3335 and 3165 (amine N-H), 3045 (aromatic C-H), 2927 (aliphatic C-H), 1660 and 1694 (imide C=O), 1584 (aromatic C=C), 1252 (C-O-C ether), 1014 (alcohol C-O), 810 and 734 (C-H bend).

UV-Vis (Pyridine, λ_{max} nm): 551, 526.

Fluorescence (Pyridine, λ_{max} nm): 537, 578. Φ_f = 10%

Anal. Calcd for ($C_{72}H_{68}N_{16}O_8S_4$) (M_w, 1413.67)**:** C, 61.17 %; H, 4.85 %; N, 15.85 %. Found: C, 58.56 %; H, 4.00 %; N, 10.42 %.

^{1}H NMR and **^{14}C NMR** of this compound couldn't be detected due to the low solubility of the compound.

MS (EI, m/z) spectrum of this compound couldn't be detected due to the low solubility of the compound organic solvents.

3.9 Synthetic Procedure of *N,N′*-bis-(dehydroabietyl)- 1,7-di-(2-[3[(4-amino-2-methylpyrimidin-5-yl) methyl]-4-methyl-1,3-thiazol-3-ium-5-yl]) ethoxyperylene-3,4:9,10-tetracarboxylic diimide (BTC-APDI)

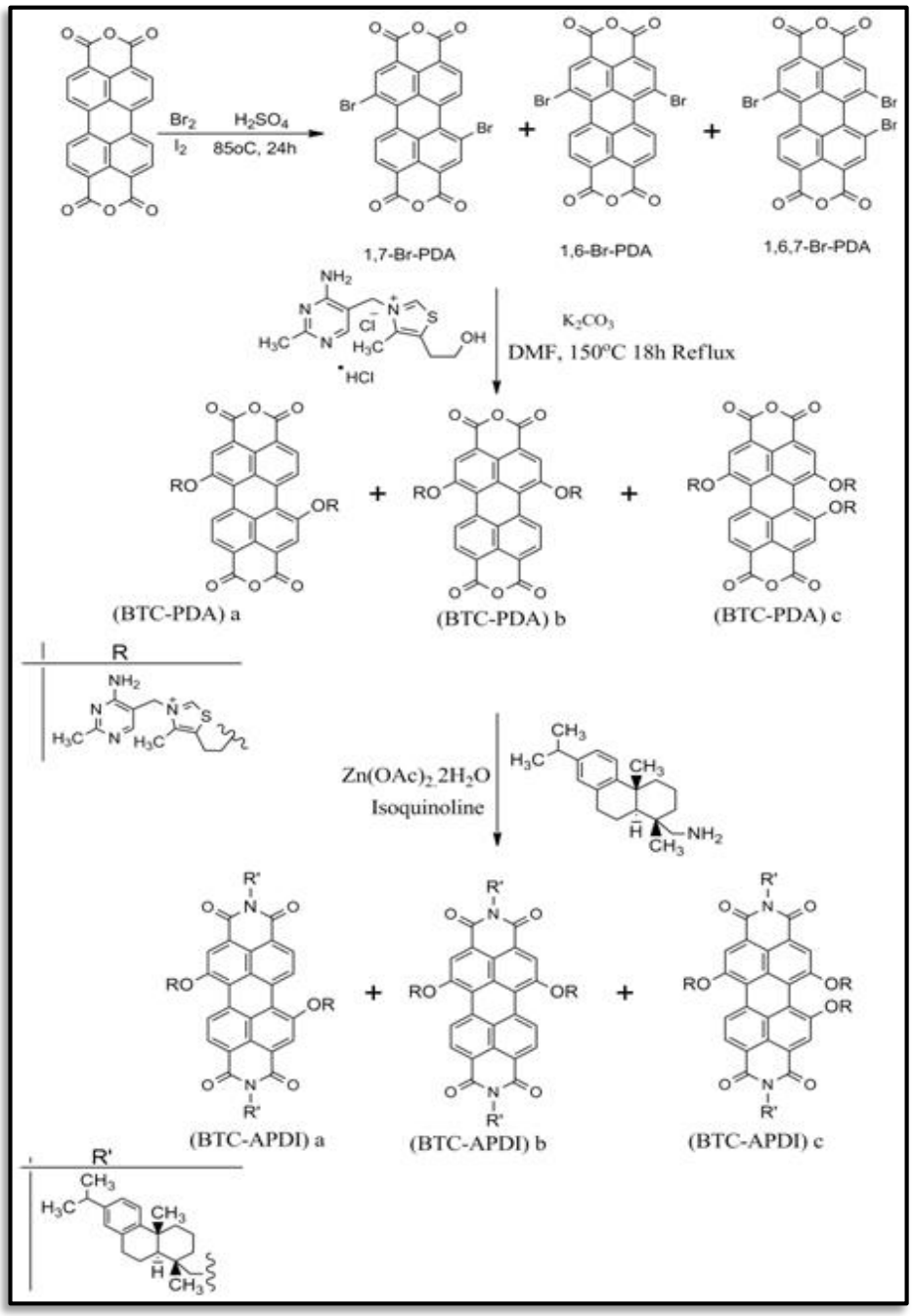

Scheme 3.10: Synthesis of *N,N′*-bis-(dehydroabietyl)- 1,7-di-(2-[3[(4-amino-2-methylpyrimidin-5-yl) methyl]-4-methyl-1,3-thiazol-3-ium-5-yl]) ethoxyperylene-3,4:9,10-tetracarboxylic diimide (BTC-APDI)

3.9.1 Synthesis of *N,N'*-bis-(dehydroabietyl)- 1,7-di-(2-[3[(4-amino-2-methyl pyrimidin-5-yl) methyl]-4-methyl-1,3-thiazol-3-ium-5-yl]) ethoxyperylene-3,4,9,10 –tetracarboxylic diimide (BTC-APDI)

Following the literature procedure [58],the mixture of 1,7-Di-thiazolium chloride perylene-3,4:9,10-tetracarboxylic dianhydride (BTC-PDA) (0.9 g, 0.91 mmol), dehydroabietyle (0.78g, 2.27 mmol) and zincacetate dihydrate (0.20 g, 0.91 mmol) were stirred in 30 mL dry isoquinoline subjected to argon atmosphere at 110 °C for 20 h, 180 °C for 6 h and 1 h at 200 °C. IR detection indicated the disappearance of anhydride peaks. When cooled down to room temperature, the mixture was transfered in to 250 mL cold acetone and the crude product was filtered by vacuum filtration. To get rid of excess amine and other impurities the product was wrapped in filter paper and treated by acetone soxhlet for 6day. At the end re-crystallization had been done by chloroform hexan and the collected black product was dried in vacuum oven for 48 h at 120 °C.

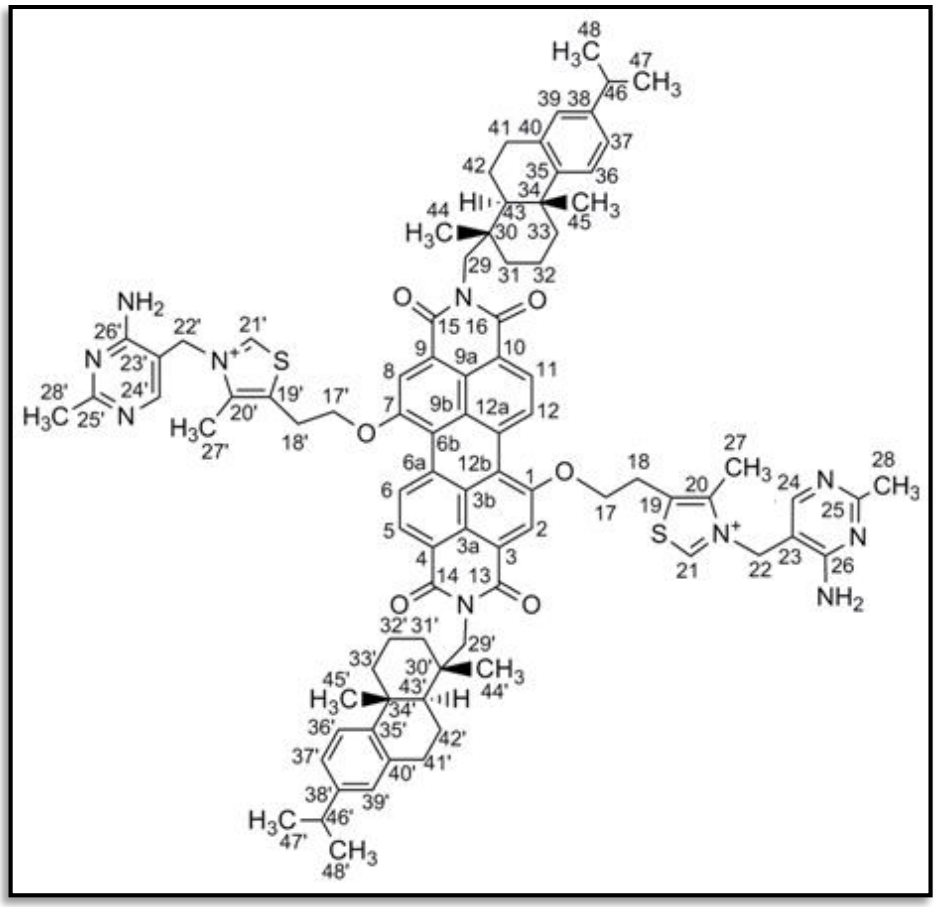

Figure 3.11: *N,N'*-bis-(dehydroabietyl)- 1,7-di-(2-[3[(4-amino-2-methylpyrimidin-5-yl) methyl]-4-methyl-1,3-thiazol-3-ium-5-yl]) ethoxyperylene-3,4:9,10-tetracarboxylic diimide (BTC-APDI)

Yield: 50% (1.04g); **Color:** black powder.

FTIR (KBr, cm^{-1}): υ: 3326 (amine N-H), 3054 (aromatic C-H), 2918 (aliphatic C-H), 1695 and 1660 (imide C=O), 1593 (aromatic C=C), 1337 (C-N), 1252 (C-O-C ether), 819 and 750 (C-H bend).

UV-Vis (CHL, λ_{max} nm): 525, 488, 460.

Fluorescence (CHL, λ_{max} nm): 535, 576, 621.Φ_f = 40 %

Anal. Calcd for ($C_{88}H_{96}N_{10}O_6S_2$) (M_w: 1453.896)**:** C, 72.70 %; H, 6.66 %; N, 9.63 %. Found: C, 67.07%; H, 5.45%; N, 6.93%.

^{1}H NMR, (δ_H ppm, 400 MHz, $CDCl_3$): 8.42 (m, 4H, H-C(11), H-C(12), H-C(6), H-C(5)), 7.89(m, 1H, H-C(24)), 7.71(m, 1H, H-C(24')), 7.51 (br, s, 2H, H-C(2), H-

C(8)), 7.33 (m, 1H, H-C(39)), 7.25 (m, 1H, H-C(39')), 7.03-7.9 (m, 4H, H-C(36), H-C(36'), H-C(37), H-C(37')), 3.68(s, 2H, H-C(21), H-C(21')), 2.49(s, 4H, H_2C-(24), H_2C-(24')), 1.78(s,4H, H_2C-(29), H_2C-(29')), 1.61(s,6H, H_3C-(27), H_3C-(27')), 1.52(m,4H, H_2C-(18), H_2C-(18'), 1.35(m,2H, H-C(46), H-C(46')), 1.25(m, 8H, H_2C-(41), H_2C-(41'), H_2C-(42), H_2C-(42')), 1.14-1.31(m, 12H, H_2C-(31), H_2C-(31'), H_2C-(32), H_2C-(32'), H_2C-(33), H_2C-(33')), 1.16(m,12H, H_3C-(47), H_3C-(47'), H_3C-(48), H_3C-(48')), 1.01(s, br, 6H, H_3C-(28), H_3C-(28')), 0.89(m, 4H, H_2C-(43), H_2C-(43')), 0.78(s, 12H, H_3C-(44), H_3C-(44'), H_3C-(45), H_3C-(45')).

MS (EI, m/z): (Mw, 1453.896), 1422.7, 1391.6, 1312, 1303.43, 886.4.

Chapter 4

DATA AND CALCULATIONS

4.1 Electrochemical Data and Calculations

Electrochemistry of the synthesized TPDI and separately 5-amino-4-cyano-3-methylthiophene-2-carboxamide were investigated by cyclic-voltammetry (CV) and squarewave-voltammetry (SWV) techniques in solution (DMF, NMP and DMAC containing supporting electrolyte: 0.05 M $NaBF_4$) and solid state in 1 M HCl solution. Similar measurements had been done for BPY-PPDI in DMF as a solvent and 0.05 M $NaBF_4$ supporting electrolyte along with solid state measurement in 1 M HCl solution all the electrochemical measurements were performed in several scan rates to approve the reproducibility of the redox waves.

4.1.1 Redox Potentials And Half-Wave Potentials ($E_{1/2}$)

Using cyclic-voltammograms of the compounds, the half-wave or mid-point potentials ($E_{1/2}$) can be obtained by calculating the average value of anodic and cathodic potentials measured approximately at half height of the anodic and cathodic peaks equation (4.1) [59].

$$\boldsymbol{E_{1/2}} = \frac{\boldsymbol{E_{pc} + E_{pa}}}{\boldsymbol{2}} \qquad \textbf{(4.1)}$$

$\boldsymbol{E_{1/2}}$: Mid-point / Half-wave potentional (V)

$\boldsymbol{E_{pc}}$ **:** Potential of cathodic peak (V)

$\boldsymbol{E_{pa}}$**:** Potential of anodic peak (V)

Redox Potential of TPDI

The cyclic-voltammograms of TPDI in DMF (Figure 4.9) illustrated two reversible reduction waves, in solid state TPDI showed a different electrochemical behaviour in comparison with solution electrochemistry. The redox potentials in solutions are calculated to the reference electrode below.

$$\boldsymbol{E_{red1,1/2}\ vs.Ag/AgCl = \frac{E_{pc}+E_{pa}}{2} = \frac{-0.496-0.388}{2} = -0.422\ V}$$

$$\boldsymbol{E_{red2,1/2}\ vs.Ag/AgCl = \frac{E_{pc}+E_{pa}}{2} = \frac{-0.269-0.181}{2} = -0.225\ V}$$

Where $E_{red1,1/2}$ and $E_{red2,1/2}$ show the first and second reduction potentials.

Using the same anodic and cathodic peak potentials the peak separations for both redox processes can be calculated with the equation shown below which demonstrates the number of electrons transferred.

$$\Delta E = \boldsymbol{E_{pa} - E_{pc} = \frac{0.059}{n}\ V} \qquad \textbf{(4.2)}$$

Peak Potential separations of TPDI.

$$\Delta E = \boldsymbol{E_{pa} - E_{pc}}$$

$\Delta E_{P,1}$ = -0.388+0.496= 0.108 V= 108 mV

$\Delta E_{P,2}$ =-0.181+0.269=0.088 V= 88 mV

The oxidation potential of Ferrocene as an internal reference was calculated 0.509 V. Therefore, E_{ox}= 0.509 V. Accordingly the redox potentials can be estimated proportionate to internal reference, Ferrocene (Fc).

$$E_{red1/2} \textit{ vs. } \mathbf{Fc} = (E_{red1/2} \textit{ vs.} \mathbf{Ag/AgCl} - E_{Ox} \textit{ vs.} \mathbf{Ag/AgCl})$$

$E_{red1,1/2}$ ***vs.*** **Fc =** (-0.422)-(0.509)=-0.951

$E_{red1,1/2}$ ***vs.*** **Fc =** (-0.225)-(0.509)=-0.734

With the similar method, the redox potential of TPDI, 5-amino-4-cyano-3-methylthiophene-2-carboxamide and BPY-PPDI in solution and solid-state were computed, and the obtained data are given in Table 4.1.

4.1.2 LUMO and HOMO Energy Level

In the part related to semi-conductive organic materials, HOMO is defined as the energy which is demanded to obtain an electron from a molecule that can be called as an oxidation process and LUMO is the energy needed to project an electron to a molecule, thus has been known as a reduction process. These properties can be obtained utilizing cyclic-voltammetry method by measuring the redox potentials E_{red} and E_{ox}. Ferrocence is known to be a reference for calculating the HOMO-LUMO energy levels [60].

$$E_{LUMO} = -(4.8 + E_{1/2}) \quad (4.3)$$

E_{LUMO}**:** Energy level of LUMO (eV)

$E_{1/2}$**:** Mid-point potential ($E_{red1/2}$ *vs.* Fc)

E_{LUMO} of TPDI

$$E_{LUMO} = -(4.8 + E_{1/2})$$

$$E_{LUMO} = -(4.8 + (-0.734)) = -4.07 \text{ eV}$$

The LUMO energy values of TPDI in different solvents are calculated with the same way explained above and the results are presented in Table 4.1.

4.1.3 Optical Band-Gap Energies (Eg)

The band-gap is defined as the difference of energy between the valence-band and the conduction-band. Electrons are generally able to jump from one band to another as long as least amount of energy for the transition (the band-gap energy) is provided. The optical band-gap can be computed utilizing absorption spectrum of the compound at absorption edge value (extrapolation of maximum absorption to zero absorption) and replacing the wavelength in following equation.

$$E_g = \frac{1240\ eV\ nm}{\lambda} \quad (4.4)$$

E_g**:** Energy of band gap

λ**:** Cut-off wavelength of the absorption band in nm

Band gap energy of TPDI in DMF:

The absorption spectrum of TPDI in DMF and the extrapolation of maximum to zero absorbance were shown below (Figure 4.1) and the wavelength was found 641 nm.

$$E_g = \frac{1240\ eV\ nm}{\lambda}$$

$$E_g = \frac{1240\ eV\ nm}{779} = 1.59\ \text{eV}$$

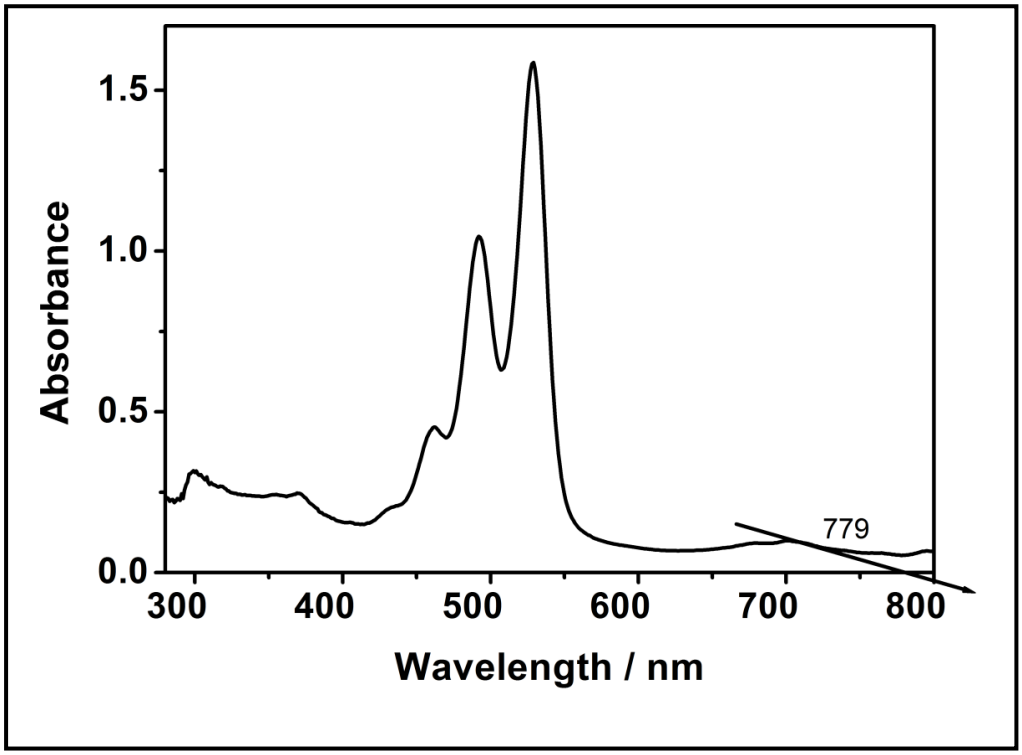

Figure 4.1: Absorption spectrum of TPDI in DMF

4.1.4 HOMO Energy Level

The HOMO energy level can be determined by using the LUMO and band gap energies with the following equation.

$$E_{HOMO} = E_{LUMO} - E_g \quad (4.5)$$

E_{HOMO}: Energy of HOMO level in eV

E_{LUMO}: Energy of LUMO level in eV

E_g: Band-gap energy

HOMO Energy Level of TPDI

$E_{HOMO} = E_{LUMO} - E_g$

$E_{HOMO} = -4.07 - 1.59 = -5.66$ eV

Table 4.1: Electrochemical data of TPDI

TPDI	Scan rate (mVs^{-1})	E_{pc}[a] (V)	E_{pa}[b] (V)	ΔE_p[c] (mV)	$E_{1/2}$[d] *vs.* Ag/AgCl (V)	E_{Fc}[e] *vs.* Ag/AgCl (V)	$E_{1/2}$ *vs.* Fc (V)	LUMO[f] (eV)	E_g[g] (eV)	HOMO[i] (eV)
DMF	100	−0.269	−0.181	88	−0.225	0.509	−0.734	−4.07	1.59	−5.66
		−0.496	−0.388	108	−0.442	0.509	−0.951			
NMP	100	−0.244	−0.153	91	−0.199	0.592	−0.791	−4.01	1.62	−5.63
		−0.475	−0.384	91	−0.430	0.592	−1.022			
DMAc	100	−0.239	−0.152	87	−0.196	0.583	−0.779	−4.07	1.63	−5.70
		−0.479	−0.385	94	−0.432	0.583	−1.015			
Solid-state	100	−0.021	−0.467	446	−0.244	0.320	−0.564	−4.24	1.93	−6.17
		0.342	0.705	363	+0.524	0.320	+0.204			

[a]E_{pc}: cathodic potential.
[b]E_{pa}: anodic potential.
[c]ΔE_p: peak potential separations.
[d]$E_{1/2}$: half wave potential.
[e]E_{Fc} : oxidation potential of ferrocene (internal reference).
[f]LUMO: lowest unoccupied molecular orbital.
[g]E_g: energy gap calculated by optical data.
[i]HOMO: highest occupied molecular orbital calculated by optical data.

4.2 Optical Parameters Calculations

4.2.1 Maximum Molar Extinction Coefficient

The molar extinction-coefficient (ε) shows how strongly a molecule absorbs light at a specific wavelength. Molar extinction-coefficient values are distinctive for each molecule and wavelength and have units M^{-1} cm^{-1}. It can be determined by Beer-Lambert's Law.

$$\varepsilon_{max} = \frac{A}{cl} \quad \textbf{(4.6)}$$

A: absorbance

ε_{max}: maximum molar extinction-coefficient (M^{-1} cm^{-1})

c: concentration (mol L^{-1})

l: pathwaylength (cm)

ε_{max} calculation of TPDI:

To compute ε_{max} , five different concentrations of the compound have been made and their absorbance were measured, the graph of maximum absorbance versus concentrations had given a line which the slope was maximum extinction co-efficient.

Table 4.2: Concentration with their absorbances of TPDI in DMF

Concentration	λ_{max}	Absorbance
2×10^{-5}	529	2.1
1.5×10^{-5}	529	1.6
1×10^{-5}	528	1.07
5×10^{-6}	528	0.56
1×10^{-6}	528	0.19

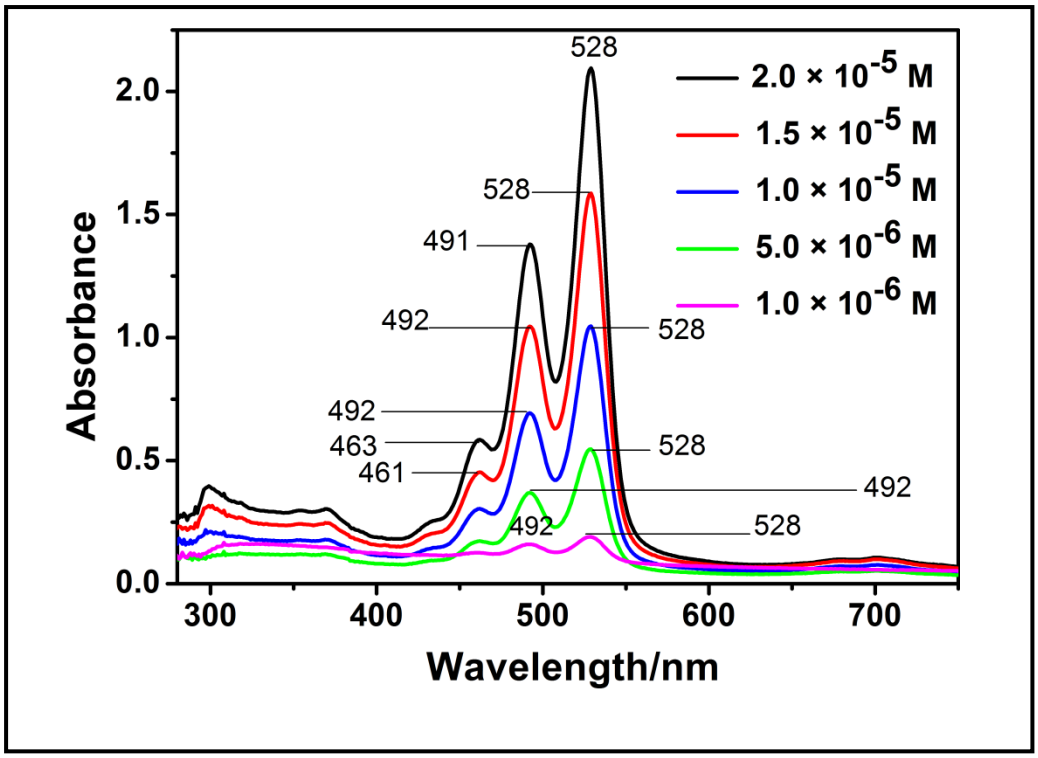

Figure 4.2: Concentration dependent measurement of TPDI in DMF

Table 4.3: Molar absorption coefficient of TPDI in selected solvents

Solvent	**TPDI**					
	$\lambda_{max(1)}$	$\varepsilon_{max(1)}$	$\lambda_{max(2)}$	$\varepsilon_{max(1)}$	$\lambda_{max(3)}$	$\varepsilon_{max(1)}$
TCE	533	8885	495	6063	464	3277
DCM	528	9785	491	6348	461	2900
NMP	528	50583	492	33581	462	15081
MeOH	523	1805	488	1300	457	795
DMF	528	101325	491	69125	463	25953
DMAC	527	74693	491	49601	461	20324
DMSO	531	84315	495	55624	464	23328

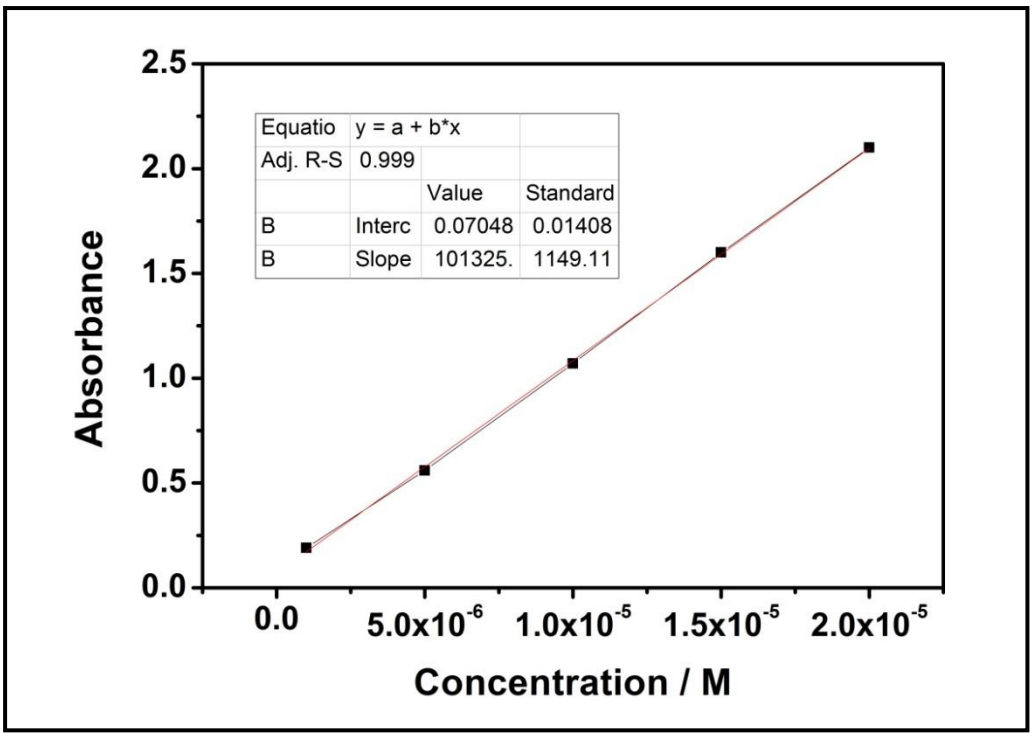

Figure 4.3: Chart of absorbance versus concentration of TPDI in DMF

The slope of the graph, ε_{max}, was found 101325 M^{-1} cm^{-1},With the same way, ε_{max} of other compounds were calculated in different solvents, and the results were shown in Tables 4.4-4.10.

Table 4.4: Maximum molar absorption coefficient of TCPDI in selected solvents

Solvent	**TCPDI**	
	λ_{max}	$\varepsilon_{max}(M^{-1}cm^{-1})$
NMP	528	30892.4
DMF	523	4719.2
DMAC	523	33333.3

Table 4.5: Maximum molar absorption coefficient of TAPDI in selected solvents

Solvents	TAPDI	
	λ_{max}	$\varepsilon_{max}(M^{-1}cm^{-1})$
CHL	525	102951.0
THF	520	10800.0
Isopropanol	522	21926.2
MeOH	516	74385.3
DMAC	525	37600.0

Table 4.6:Maximum molar absorption coefficient of BPY-PDA in selected solvents

Solvents	BPY-PDA	
	λ_{max}	$\varepsilon_{max}(M^{-1}cm^{-1})$
NMP	520	9305.0
DMF	514	8229.3
DMAC	511	6612.1
DMSO	515	10267.0

Table 4.7:Maximum molar absorption coefficient of BPY-PPDI in selected solvents

Solvents	BPY-PPDI	
	λ_{max}	$\varepsilon_{max}(M^{-1}cm^{-1})$
NMP	518	15600.0
DMF	514	11777.0
DMAC	511	16663.7
DMSO	522	16200.0

Table 4.8:Maximum molar absorption coefficient of TC-PDA in selected solvents

Solvents	TC-PDA	
	λ_{max}	$\varepsilon_{max}(M^{-1}cm^{-1})$
NMP	519	31201.0
DMF	518	25483.0
DMAC	516	34000.0

Table 4.9:Maximum molar absorption coefficient of BTC-TCPDI in selected solvents

Solvents	BTC-TCPDI	
	λ_{max}	$\varepsilon_{max}(M^{-1}cm^{-1})$
NMP	546	30266.0
DMF	544	33000.0
DMAC	543	39600.0

Table 4.10:Maximum molar absorption coefficient of BTC-APDI in selected solvents

Solvents	BTC-APDI	
	λ_{max}	$\varepsilon_{max}(M^{-1}cm^{-1})$
CHL	525	33904.1
THF	520	35033.0
DMAC	525	43802.0

4.2.2 Fluorescence Quantum Yields (Φ_f)

The fluorescence quantum-yield is a fundamental character of chromophore and is a great magnitude for the characterization of newly investigated chromophores and it can be defined as fraction of absorbed photons to fluorescence emitted photons. Single-point and comparative method are two different ways for measurements of relative quantum yield: In single point technique the quantum-yield is computed by the integrated emission intensities of a single sample and reference couple, separately in same dilution. Whilst these techniques are faster and easier, it is not always trustworthy as a result of the inexact measurement of the chromophor's absorbance. In the comparative method [61] multiple references with known fluorescence quantum yields will be used. Integrating fluorescence intensity a plot was constructed by drawing intensity versus the absorption of various concentrations, the slope of the line is obtained and used for the quantum yield calculation based on

following equation. Although this method is time consuming but gives more accurate result.

$$\emptyset_f = \emptyset_R \left(\frac{m}{m_R}\right)\left(\frac{n}{n_R}\right)^2 \quad \textbf{(4.7)}$$

$\emptyset_f$: Fluorescence quantum-yield of unknown

$\emptyset_R$: Fluorescence quantum-yield of reference

m: Slope of the line of the integrated fluorescence intensity vs. Absorbance of unknown

m_R: Slope of the line of the integrated fluorescence intensity vs. Absorbance of reference

n : Refractive-index of unknown sample solvent

n_R: Refractive index of reference solvent

In contrast to comparative technique, single-point analysis for determination of the fluorescence quantum-yield has the benefit of gaining results more rapidly. In the single point method, the quantum-yield of the compound is calculated based on the following equation:

$$\emptyset_f = \frac{A_R}{A_u}\left(\frac{S_u}{S_R}\right)\left(\frac{n_u}{n_R}\right)^2 \emptyset_R \quad \textbf{(4.8)}$$

$\emptyset_f$: Fluorescence quantum-yield of unknown

$\emptyset_R$: Fluorescence quantum-yield of reference

n_u : Refractive index of unknown sample solvent

n_R: Refractive index of reference solvent

A_R: Absorbance of the reference at the excitation wavelength

A_u: Absorbance of the unknown sample at the excitation wavelength

S_R: The integrated emission area of the reference

S_u: The integrated emission area of the unknown sample

The *N,N'*-bis(dodecyl)-3,4,9,10-perylenebis(dicarboximide) in chloroform (Φ_f =1) [62] had been used as reference for Φ_f computation of the synthesized compounds with the excitation wavelength of 485 nm.

Φ_f calculation of TPDI in DMF:

$\emptyset_R = 1$ With chloroform as a solvent

$A_R = 0.1003$

$A_u = 0.1007$

$S_R = 3099$ counts / (cm.sec)

S_u= 1339 counts / (cm.sec)

$n_{CHL} = 1.4458$

$n_{DMF} = 1.4305$

$$\emptyset_f\,(TPDI) = \frac{0.1003}{0.1007}\left(\frac{3099}{1339}\right)\left(\frac{1.4305}{1.4458}\right)^2 1 = 0.50$$

The Φ_f values of other synthesized compounds were calculated in different solvents with the same way and the results are tabulated below (Tables 4.11- 4.13).

Table 4.11: Fluorescence quantum-yield (Φ_f) of TPDI, TCPDI and TAPDI in various solvents

Solvents	TPDI	TCPDI	TAPDI
	Φ_f	Φ_f	Φ_f
CHL	-	-	0.73
THF	-	-	0.77
TCE	0.30	0.20	0.74
DCM	0.25	0.31	-
NMP	0.30	0.25	0.40
MeOH	0.10	-	0.21
DMF	0.50	0.24	0.63
DMAC	0.25	0.30	0.64
DMSO	0.10	0.10	0.33

Table 4.12: Fluorescence quantum-yield (Φ_f) of BPY-PDA, BPY-PPDI and TA-PDI in various solvents

Solvents	BPY-PDA	BPY-PPDI
	Φ_f	Φ_f
Pyridine	0.31	0.104
NMP	0.01	0.087
MeOH	0.10	-
DMF	0.30	0.077
DMAC	0.02	0.096
DMSO	0.15	0.1

Table 4.13: Fluorescence quantum-yield (Φ_f) of BTC-PDA, BTC-TCPDI and BTC-APDI in various solvents

Solvents	BTC-PDA	BTC-TCPDI	BTC-APDI
	Φ_f	Φ_f	Φ_f
CHL	-	-	0.40
THF	-	-	0.30
TCE	-	-	0.24
Pyridine	0.30	0.10	-
NMP	0.11	0.05	-
DMF	0.23	0.074	0.33
DMAC	0.10	0.068	0.21
DMSO	0.04	0.03	0.16

4.2.3 Half-width of The Selected Absorption ($\Delta\bar{\upsilon}_{1/2}$)

The terms band-pass and resolution are proven to express the ability of a spectrometer to separate light into distinct wavelength and resolve closely spaced peaks. For an instrument, the band-pass of the spectrometer describes which fraction of the spectrum can be isolated by the spectrometer in a single wavelength form and ideally the spectrum would appear as a single line (Fig.4.4).

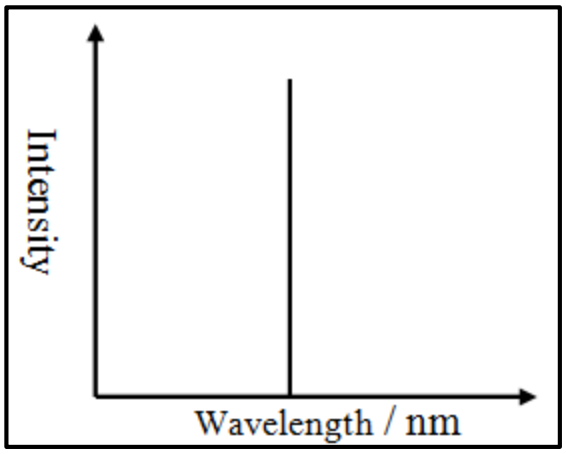

Figure 4.4: The ideal spectrum at a single wavelength

When an aforementioned spectrum is measured via a typical spectrometer, a broad Gaussian-like (bell-shape) curve spectrum as shown in (Figure 4.5) is yielded.

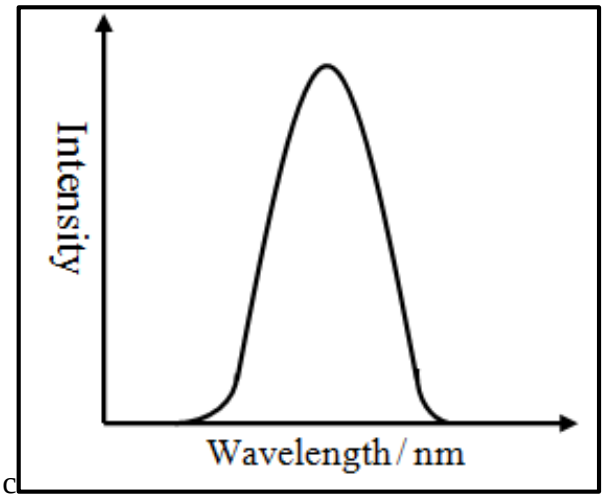

c

Figure 4.5: Gaussian-like spectrum

For any kind of instrument the valid band-pass can be determined by computing the full-width at half-maximum (FWHM) of the bell-shaped spectrum. Therefore in the case of band depicted in (Figure 4.5) the FWHM can be obtained by calculating the wavelength corresponding to the maximum intensity. Then the bandwidth corresponding to the half of obtained height is measured as demonstrated in Figure 4.6.

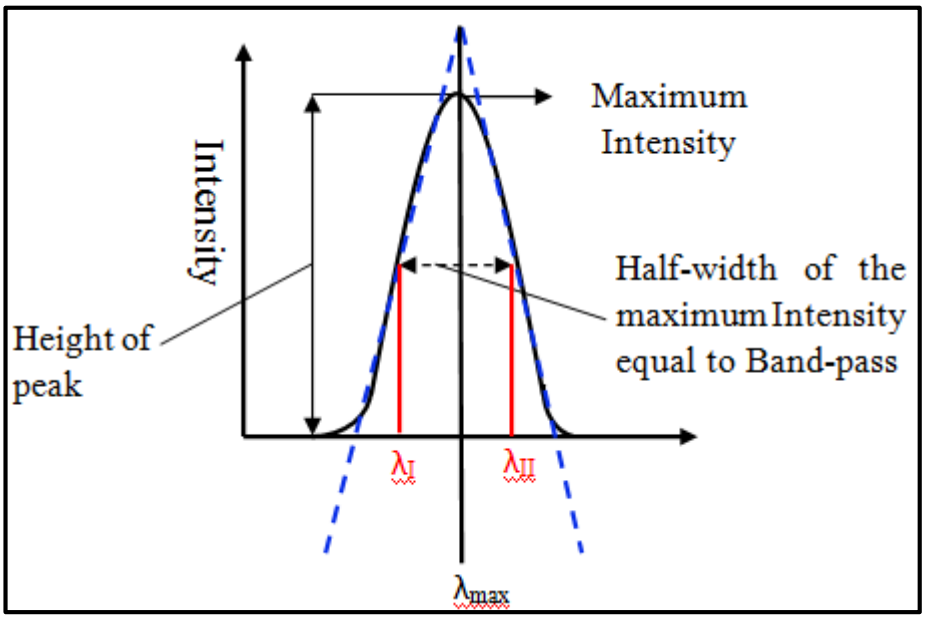

Figure 4.6: Demonstration of the determination of Half-width

$$\Delta\bar{\upsilon}_{1/2} = \bar{\upsilon}_I - \bar{\upsilon}_{II} \qquad (4.9)$$

$\bar{\upsilon}_I - \bar{\upsilon}_{II}$: The frequencies from absorption spectrum in cm^{-1}.

$\Delta\bar{\upsilon}_{1/2}$: Half-width of the selected maximum absorption in cm^{-1}

Calculating the $\Delta\bar{\upsilon}_{1/2}$ for TPDI in DMF.

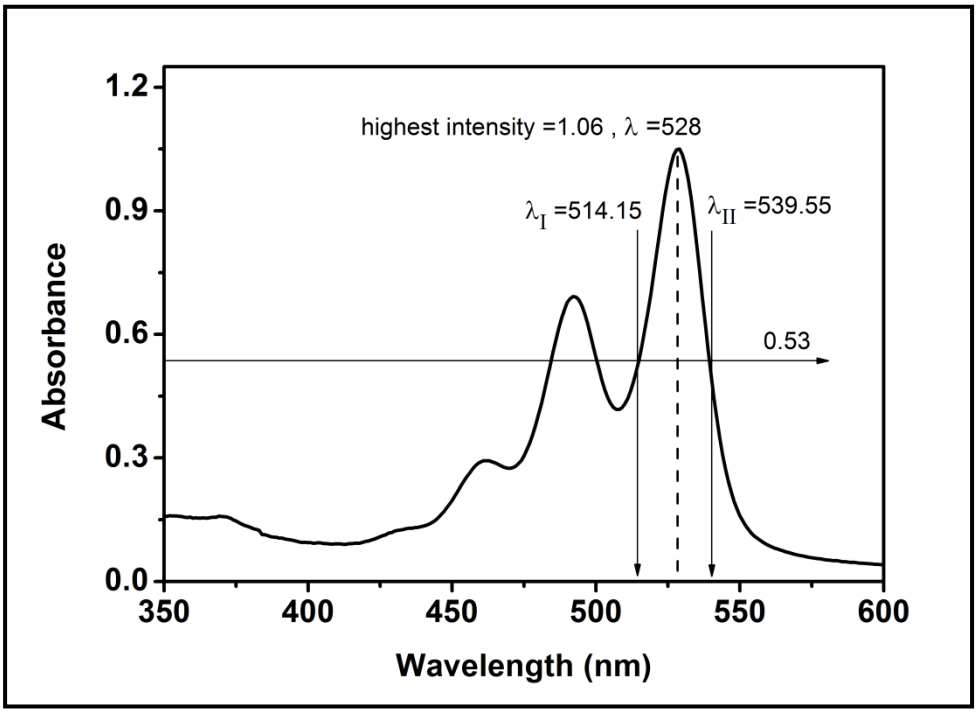

Figure 4.7: Illustration of the determination of Half-width of TPDI in DMF

λ_{max} = 528 nm

λ_I = 514.15 nm

$$\lambda_{max} = 514.15\, nm \times \frac{1m}{10^9} \times \frac{100cm}{1m} = 5.1415 \times 10^{-5} cm$$

$$\bar{\upsilon}_I = \frac{1}{5.1415 \times 10^{-5}} = 19449.57\ cm^{-1}$$

λ_{II} = 539.55 nm

$$\lambda_{max} = 539.55\, nm \times \frac{1m}{10^9} \times \frac{100cm}{1m} = 5.3955 \times 10^{-5} cm$$

$$\bar{\upsilon}_I = \frac{1}{5.3955 \times 10^{-5}} = 18533.96$$

$\Delta\bar{\upsilon}_{1/2} = \bar{\upsilon}_I - \bar{\upsilon}_{II}$ = 19449.57-18533.96=915.61 cm^{-1}

Table 4.14: FWHM of TPDI,TCPDI and TAPDI in cm^{-1}

Solvents	TPDI	TCPDI	TAPDI
	$\Delta\bar{\upsilon}_{1/2}$	$\Delta\bar{\upsilon}_{1/2}$	$\Delta\bar{\upsilon}_{1/2}$
CHL	-	-	766
THF	-	-	853
TCE	1230	1509	758
DCM	683	1441	-
Isopropanol	-	-	1228
NMP	974	1693	1352
MeOH	1259	-	1313
DMF	916	1686	877
DMAC	1055	1699	986
DMSO	930	2324	1210

Table 4.15: FWHM of BPY-PDA and BPY-PPDI in cm^{-1}

Solvents	BPY-PDA	BPY-PPDI
	$\Delta\bar{\upsilon}_{1/2}$	$\Delta\bar{\upsilon}_{1/2}$
NMP	2296	3178
DMF	2534	3940
DMAC	2151	2669
DMSO	2669	3687

Table 4.16: FWHM of BTC-PDA, BTC-TCPDI and BTC-APDI in cm^{-1}

Solvents	BTC-PDA	BTC-TCPDI	BTC-APDI
	$\Delta\bar{\upsilon}_{1/2}$	$\Delta\bar{\upsilon}_{1/2}$	$\Delta\bar{\upsilon}_{1/2}$
CHL	-	-	1414
THF	-	-	1504
NMP	1725	3366	-
DMF	1909	3142	-
DMAC	1481	3053	1712

4.2.4 Theoretical Radiative Lifetimes (τ_0)

The theoretical radiative life time can be defined as the life time of a molecule at excited stated without radiation-less transitions and it can be calculated via the following equation.

$$\boldsymbol{\tau_0 = \frac{3.5\times10^8}{\bar{\upsilon}^2_{max}\varepsilon_{max}\Delta\bar{\upsilon}_{1/2}}} \quad \textbf{(4.10)}$$

τ_0 : Theoretical radiative lifetimes (ns)

$\bar{\upsilon}^2_{max}$: Wavenumber (cm^{-1})

ε_{max} : The maximum molar absorption-coefficient at the maximum wavelength

$\boldsymbol{\Delta\bar{\upsilon}_{1/2}}$: Full width at half maximum (cm^{-1})

Theoretical radiative life time of TPDI in DMF:

$$\tau_0 = \frac{3.5 \times 10^8}{\bar{\upsilon}^2_{max}\varepsilon_{max}\Delta\bar{\upsilon}_{1/2}}$$

$$\tau_0 = \frac{3.5 \times 10^8}{(18939)^2 \times 101325 \times 916} = 1.05 \times 10^{-8} s$$

$$\boxed{\tau_0 = 1.05 \times 10^{-8}\ \text{s} \times \frac{10^9 \text{ns}}{1\text{s}} = 10.5\text{ns}}$$

With the same way the theoretical radiative life time of other compounds have been calculated and tabulated below.

Table 4.17: Theoretical radiative lifetime of TPDI in selected solvents

Solvents	**TPDI**				
	$\boldsymbol{\lambda_{max}}$	$\varepsilon_{max}(M^{-1}cm^{-1})$	$\bar{\upsilon}^2_{max}$	$\boldsymbol{\Delta\bar{\upsilon}_{1/2}}$	τ_0
TCE	533	8885	3.52×10^8	1230	91.0
DCM	528	9785	3.59×10^8	683	146.0
NMP	528	50583	3.59×10^8	974	19.8
MeOH	523	1805	3.65×10^8	1259	422.0
DMF	528	101325	3.59×10^8	916	10.5
DMAC	527	74693	3.60×10^8	1055	12.3
DMSO	531	84315	3.55×10^8	930	12.6

Table 4.18: Theoretical radiative lifetime of TCPDI in selected solvents

Solvents	TCPDI				
	λ_{max}	$\varepsilon_{max}(M^{-1}cm^{-1})$	$\bar{\upsilon}^2_{max}$	$\Delta\bar{\upsilon}_{1/2}$	τ_0
NMP	520	9305.0	3.69×10^8	1693	60.2
DMF	514	8220.3	3.79×10^8	1686	66.5
DMAC	511	6612.1	3.83×10^8	1699	81.3
DMSO	515	10267.0	3.77×10^8	2324	38.9

Table 4.19: Theoretical radiative lifetime of TAPDI in selected solvents

Solvents	TAPDI				
	λ_{max}	$\varepsilon_{max}(M^{-1}cm^{-1})$	$\bar{\upsilon}^2_{max}$	$\Delta\bar{\upsilon}_{1/2}$	τ_0
CHL	525	102951.0	3.62×10^8	766	12.3
THF	520	10800.0	3.69×10^8	853	103.0
Isopropanol	522	21926.2	3.67×10^8	1228	35.4
MeOH	516	74385.3	3.76×10^8	1313	18.8
DMAC	525	37600.0	3.62×10^8	986	26.0

Table 4.20: Theoretical radiative lifetime of BPY-PDA in selected solvents

Solvents	BPY-PDA				
	λ_{max}	$\varepsilon_{max}(M^{-1}cm^{-1})$	$\bar{\upsilon}^2_{max}$	$\Delta\bar{\upsilon}_{1/2}$	τ_0
NMP	518	9305.0	3.73×10^8	2296	26.2
DMAF	524	8229.3	3.79×10^8	2534	30.9
DMAC	511	6612.1	3.83×10^8	2151	25.5
DMSO	522	10267.0	3.67×10^8	2669	22.1

Table 4.21: Theoretical radiative lifetime of BPY-PPDI in selected solvents

Solvents	BPY-PPDI				
	λ_{max}	$\varepsilon_{max}(M^{-1}cm^{-1})$	$\bar{\upsilon}^2_{max}$	$\Delta\bar{\upsilon}_{1/2}$	τ_0
NMP	528	15600.0	3.59×10^8	3178	19.7
DMAF	523	11777.0	3.65×10^8	3940	20.6
DMAC	523	16663.7	3.65×10^8	2669	21.6
DMSO	522	16200.0	3.67×10^8	3687	15.9

Table 4.22: Theoretical radiative lifetime of BTC-PDA in selected solvents

Solvents	BTC-PDA				
	λ_{max}	$\varepsilon_{max}(M^{-1}cm^{-1})$	$\bar{\upsilon}^2_{max}$	$\Delta\bar{\upsilon}_{1/2}$	τ_0
NMP	519	31201.1	3.71×10^8	1725	17.5
DMF	518	25483.0	3.73×10^8	1909	19.1
DMAC	516	34000.0	3.76×10^8	1481	18.5

Table 4.23: Theoretical radiative lifetime of BTC-TCPDI in selected solvents

Solvents	BTC-TCPDI				
	λ_{max}	$\varepsilon_{max}(M^{-1}cm^{-1})$	$\bar{\upsilon}^2_{max}$	$\Delta\bar{\upsilon}_{1/2}$	τ_0
NMP	546	30266	3.35×10^8	3366	10.2
DMF	544	33000	3.38×10^8	3142	10.0
DMAC	543	39600	3.39×10^8	3053	8.50

Table 4.24: Theoretical radiative lifetime of BTC-APDI in selected solvents

Solvents	BTC-APDI				
	λ_{max}	$\varepsilon_{max}(M^{-1}cm^{-1})$	$\bar{\upsilon}^2_{max}$	$\Delta\bar{\upsilon}_{1/2}$	τ_0
CHL	525	33904.1	3.62×10^8	1414	20
THF	520	35033.0	3.69×10^8	1504	18
DMAC	525	43802.0	3.62×10^8	1712	13

4.2.5 Theoretical Fluorescence Lifetime (τ_f)

The theoretical fluorescence lifetime is described as the average time that a molecule stays at excited state rather than relaxation and having fluorescence.

Fluorescence lifetime was calculated with the following equation:

$$\tau_f = \tau_0 \times \emptyset_f \qquad (4.11)$$

τ_f: Theoretical Fluorescence Lifetime (ns)

τ_0: Theoretical radiative lifetime (ns)

$\emptyset_f$: Fluorescence quantum-yield

Theoretical Fluorescence Lifetime of TPDI in DMF

With the data of fluorescence quantum-yield and theoretical radiative lifetime of TPDI in DMF computed above fluorescence lifetime can be determined as follow:

$$\tau_f = \tau_0 \times \emptyset_f$$

$$\tau_f = 10.5 \times 0.50 = 5.25 \text{ ns}$$

The Theoretical Fluorescence Lifetime of other synthesized compounds were calculated via same way and tabulated below in Table 4.25- 2-27.

Table 4.25: Theoretical Fluorescence Lifetime of TPDI, TCPDI and TAPDI

Solvents	TPDI	TCPDI	TAPDI
	τ_f	τ_f	τ_f
CHL	-	-	9.0
THF	-	-	79.3
TCE	27.3	-	-
DCM	36.5	-	-
NMP	5.94	15.1	-
MeOH	40	-	3.95
DMF	5.25	16.0	-
DMAC	3.08	24.4	16.6
DMSO	1.26	3.89	-

Table 4.26: Theoretical Fluorescence Lifetime of BPY-PDA and BPY-PPDI

Solvents	BPY-PDA	BPY-PPDI
	τ_f	τ_f
NMP	0.262	1.71
DMF	9.27	1.59
DMAC	0.51	2.07
DMSO	3.32	1.59

Table 4.27: Theoretical Fluorescence Lifetime of BTC-PDA, BTC-TCPDI and BTC-APDI

Solvents	BTC-PDA	BTC-TCPDI	BTC-APDI
	τ_f	τ_f	τ_f
CHL	-	-	0.400
THF	-	-	0.300
NMP	1.93	0.510	-
DMF	4.39	0.740	-
DMAC	1.85	0.578	0.210

4.2.6 Theoretical Fluorescence Rate Constant (K_f)

The theoretical fluorescence rate constant can be determined via following equation and defined as the speed of emission radiation of a molecule.

$$K_f = 1/\tau_0 \quad \textbf{(4.12)}$$

K_f : Fluorescence Rate Constant (s^{-1})

τ_0 : Theoretical radiative lifetime (s)

Theoretical Fluorescence Rate Constant of TPDI in DMF

The K_f value for TPDI can be determined by τ_0 of TPDI calculated above.

$$K_f = 1/\tau_0 = \frac{1}{(1.05\times10-8)\ s} = 9.5\times10^7\ s^{-1}$$

Table 4.28: Theoretical Fluorescence Rate Constant ofTPDI, TCPDI and TAPDI

Solvents	TPDI	TCPDI	TAPDI
	$K_f(s^{-1})$	$K_f(s^{-1})$	$K_f(s^{-1})$
CHL	-	-	0.81×10^8
THF	-	-	0.10×10^8
TCE	0.11×10^8	-	-
DCM	0.07×10^8	-	-
NMP	0.51×10^8	0.17×10^8	-
MeOH	0.03×10^8	0.15×10^8	0.53×10^8
DMF	0.95×10^8	0.12×10^8	-
DMAC	0.81×10^8	0.26×10^8	0.38×10^8
DMSO	0.79×10^8	-	-

Table 4.29: Theoretical Fluorescence Rate Constant of BPY-PDA and BPY-PPDI

Solvents	BPY-PDA	BPY-PPDI
	$K_f(s^{-1})$	$K_f(s^{-1})$
NMP	0.38×10^8	0.51×10^8
DMF	0.32×10^8	0.49×10^8
DMAC	0.39×10^8	0.46×10^8
DMSO	0.45×10^8	0.63×10^8

Table 4.30: Theoretical Fluorescence Rate Constant of BTC-PDA, BTC-TCPDI and BTC-APDI

Solvents	BTC-PDA	BTC-TCPDI	BTC-APDI
	$K_f(s^{-1})$	$K_f(s^{-1})$	$K_f(s^{-1})$
CHL	-	-	0.5×10^8
THF	-	-	0.55×10^8
NMP	0.57×10^8	0.98×10^8	-
DMF	0.52×10^8	1.0×10^8	-
DMAC	0.54×10^8	1.2×10^8	0.77×10^8

4.2.7 Radiation-less Deactivation Rate-Constants (K_d)

The radiation-less deactivation rate-constant is determined via the following equation:

$$\mathbf{K_d} = \left(\frac{\mathbf{K_f}}{\emptyset_f}\right) - \mathbf{K_f} \qquad \textbf{(4.13)}$$

$\mathbf{K_d}$: Radiation-less Deactivation Rate-Constants (s^{-1})

$\mathbf{K_f}$: Fluorescence Rate Constant (s^{-1})

$\emptyset_f$: Fluorescence quantum yield

Radiation-less deactivation rate-constants of TPDI in DMF:

The value can be calculated by fluorescence quantum yield and fluorescence rate constant of TPDI in DMF that were determined before.

$K_d = \left(\frac{K_f}{\emptyset_f}\right) - K_f$

$$K_d = \left(\frac{K_f}{\emptyset_f}\right) - K_f = \frac{(9.5\times10^7)}{0.50} - 9.5\times10^7 = 9.5\times10^7$$

Table 4.31: Radiation-less Deactivation Rate-Constants of TPDI, TCPDI and TAPDI

Solvents	TPDI	TCPDI	TAPDI
	$K_d(s^{-1})$	$K_d(s^{-1})$	$K_d(s^{-1})$
CHL	-	-	0.30×10^8
THF	-	-	0.03×10^8
TCE	0.26×10^8	-	-
DCM	0.20×10^8	-	-
NMP	1.20×10^8	0.51×10^8	-
MeOH	0.23×10^8	-	2.0×10^8
DMF	0.95×10^8	0.47×10^8	-
DMAC	2.40×10^8	0.28×10^8	0.21×10^8
DMSO	7.10×10^8	2.3×10^8	-

Table 4.32: Radiation-less Deactivation Rate-Constants of BPY-PDA and BPY-PPDI

Solvents	BPY-PDA	BPY-PPDI
	$K_d(s^{-1})$	$K_d(s^{-1})$
NMP	3.8×10^8	5.4×10^8
DMF	0.75×10^8	5.9×10^8
DMAC	19×10^8	4.3×10^8
DMSO	2.6×10^8	5.7×10^8

Table 4.33: Radiation-less Deactivation Rate-Constants of BTC-PDA, BTC-TCPDI and BTC-APDI

Solvents	BTC-PDA	BTC-TCPDI	BTC-APDI
	$K_d(s^{-1})$	$K_d(s^{-1})$	$K_d(s^{-1})$
CHL	-	-	0.75×10^8
THF	-	-	1.3×10^8
NMP	4.6×10^8	19×10^8	-
DMF	1.7×10^8	13×10^8	-
DMAC	4.9×10^8	16×10^8	2.9×10^8

4.2.8 Oscillator Strength (*f*)

Oscillator strength is a quantity without dimension and based on definition is the strength of and electronic transition and can be computed from equation 4.14.

$$f = 4.32 \times 10^{-9} \Delta\bar{\upsilon}_{1/2} \varepsilon_{max} \qquad (4.14)$$

f: Oscillator Strength

$\Delta\bar{\upsilon}_{1/2}$: Half-width of the selected absorption (cm^{-1})

ε_{max} : maximum absorption-coefficient in $M^{-1}\ cm^{-1}$

Oscillator Strength of TPDI in DMF

$$f = 4.32 \times 10^{-9} \Delta\bar{\upsilon}_{1/2} \varepsilon_{max}$$

$$\boxed{f = 4.32 \times 10^{-9}(916)101325 = 0.40}$$

Table 4.34: Oscillator Strength of TPDI, TCPDI and TAPDI

Solvents	TPDI	TCPDI	TAPDI
	f	*f*	*f*
CHL	-	-	0.34
THF	-	-	0.04
TCE	0.05	-	-
DCM	0.03	-	-
NMP	0.21	0.23	-
MeOH	0.01	-	0.46
DMF	0.40	0.03	-
DMAC	0.34	0.24	0.16
DMSO	0.34	-	-

Table 4.35: Oscillator Strength of BPY-PDA and BPY-PPDI

Solvents	BPY-PDA	BPY-PPDI
	f	*f*
NMP	0.092	0.210
DMF	0.90	0.200
DMAC	0.061	0.192
DMSO	0.118	0.258

Table 4.36: Oscillator Strength of BTC-PDA, BTC-TCPDI and BTC-APDI

Solvents	BTC-PDA	BTC-TCPDI	BTC-APDI
	f	*f*	*f*
CHL	-	-	0.207
THF	-	-	0.228
NMP	0.233	0.440	-
DMF	0.210	0.447	-
DMAC	0.218	0.522	0.324

4.2.9 Singlet-Energies (E_s)

Singlet-energy is defined as the least amount of energy needed for excitation of a fluorophore or chromophore from ground singlet (S_0) to the first excited (S_1) energy level.

$$\mathbf{E_s = \frac{2.86\times10^5}{\lambda_{max}}} \qquad \textbf{(4.15)}$$

E_s: Singlet-energy (kcal mol^{-1})

λ_{max}: Highest absorption wavelength (A°)

Singlet energies of TPDI in DMF

λ_{max} = 528 nm × $\frac{10\ A^0}{1\ nm} = 5280\ A^0$

$E_s = \frac{2.86\times10^5}{5280}$ = 54.2 kcal mol^{-1}

Table 4.37: Singlet Energies of TPDI, TCPDI and TAPDI

Solvents	TPDI	TCPDI	TAPDI
	E_s	E_s	E_s
CHL	-	-	54.48
THF	-	-	55.00
TCE	53.65	-	-
DCM	54.17	-	-
NMP	54.17	55.00	-
MeOH	54.68	-	55.43
DMF	54.17	55.64	-
DMAC	54.27	55.97	54.48
DMSO	53.86	55.86	-

Table 4.38: Singlet Energies of BPY-PDA and BPY-PPDI

Solvents	BPY-PDA	BPY-PPDI
	E_s	E_s
NMP	55.21	54.17
DMF	55.64	54.68
DMAC	55.97	54.68
DMSO	54.79	-

Table 4.39: Singlet Energies of BTC-PDA, BTC-TCPDI and BTC-APDI

Solvents	BTC-PDA	BTC-TCPDI	BTC-APDI
	E_s	E_s	E_s
CHL	-	-	54.48
THF	-	-	55.00
NMP	55.11	52.38	-
DMF	55.21	52.57	-
DMAC	55.43	52.67	54.48

Table 4.40: Maximum wavelength of the absorption λ_{max} (nm), molar extinction coefficient ε_{max} ($M^{-1}cm^{-1}$), oscillator strength f, fluorescence quantum-yield Φ_f (λ_{exc}= 485 nm), radiative life time τ_0 (ns), fluorescence life time τ_f (ns), Fluorescenc Rate constant k_f (s^{-1}),rate-constant of radiation-less deactivation k_d (s^{-1}), and singlet-energy E_s (kcal mole $^{-1}$) data of **TPDI, TCPDI** and **TAPDI**

Solvents	**TPDI**								
	λ_{max}	ε_{max}	f	Φ_f	τ_0	τ_f	k_f	k_d	E_s
TCE	533	8885	0.05	0.3	91	27.3	0.11×10^8	0.26×10^8	53.65
DCM	528	9785	0.03	0.25	146	36.5	0.07×10^8	0.20×10^8	54.17
NMP	528	50583	0.21	0.3	19.8	5.94	0.51×10^8	1.20×10^8	54.17
MeOH	523	1805	0.09	0.1	422	40.0	0.03×10^8	0.23×10^8	54.68
DMF	528	101325	0.40	0.5	10.5	5.25	0.95×10^8	0.95×10^8	54.17
DMAC	527	74693	0.34	0.25	12.3	3.08	0.81×10^8	2.40×10^8	54.27
DMSO	531	84315	0.34	0.1	12.6	1.26	0.79×10^8	7.10×10^8	53.86
	TCPDI								
NMP	520	30892.4	0.23	0.25	60.2	15.1	0.17×10^8	0.50×10^8	55.00
DMF	514	4719.2	0.03	0.24	55.6	16.0	0.15×10^8	0.47×10^8	55.64
DMAC	511	33333.3	0.24	0.3	81.3	24.4	0.12×10^8	0.28×10^8	55.97
DMSO	512	-	-	0.1	38.9	3.89	0.26×10^8	2.30×10^8	55.86
	TAPDI								
CHL	525	102951	0.34	0.73	12.3	8.98	0.81×10^8	0.29×10^8	54.48
THF	520	10800	0.04	0.77	103	79.3	0.10×10^8	0.03×10^8	55.00
Isopropanol	522	21926	0.12	-	35.4	-	0.28×10^8	-	-
MeOH	516	74385	0.46	0.21	18.8	3.95	0.53×10^8	1.9×10^8	55.43
DMAC	525	37600	0.16	0.64	26	16.6	0.38×10^8	0.21×10^8	54.48

Table 4.41: Maximum wavelength of the absorption λ_{max} (nm), molar extinction coefficient ε_{max} ($M^{-1}cm^{-1}$), oscillator strength f, fluorescence quantum-yield Φ_f (λ_{exc}= 485 nm), radiative life time τ_0 (ns), fluorescence life time τ_f (ns), fluorescence rate constant k_f (s^{-1}), rate-constant of radiationless deactivation k_d (s^{-1}), and singlet-energy E_s (kcal mole $^{-1}$) data of **BPY-PDA, BPY-PPDI, BTC-PDA, BTC-TCPDI** and **BTC-APDI**

Solvents	λ_{max}	ε_{max}	f	Φ_f	τ_0	τ_f	k_f	k_d	E_s
				BPY-PDA					
NMP	518	9305	0.092	0.01	26.2	0.262	0.38×10^8	38.0×10^8	55.21
DMF	514	8229	0.090	0.30	30.9	9.270	0.32×10^8	0.75×10^8	55.64
DMAC	511	6612	0.061	0.02	25.5	0.510	0.39×10^8	19.0×10^8	55.97
DMSO	522	10267	0.118	0.15	22.1	3.315	0.45×10^8	2.60×10^8	54.79
				BPY-PPDI					
NMP	528	15600	0.210	0.09	19.7	1.710	0.51×10^8	5.4×10^8	54.17
DMF	523	11777	0.200	0.08	20.6	1.586	0.49×10^8	5.9×10^8	54.68
DMAC	523	16664	0.190	0.09	21.6	2.074	0.46×10^8	4.3×10^8	54.68
DMSO	522	16200	0.260	0.10	15.9	1.590	0.63×10^8	5.7×10^8	-
				BTC-PDA					
NMP	519	31201	0.233	0.11	17.5	1.925	0.57×10^8	4.6×10^8	55.11
DMF	518	25483	0.210	0.23	19.1	4.390	0.52×10^8	1.7×10^8	55.21
DMAC	516	34000	0.218	0.10	18.9	1.85	0.54×10^8	4.9×10^8	55.43
				BTC-TCPDI					
NMP	546	30266	0.440	0.05	10.2	0.510	0.98×10^8	19×10^8	52.38
DMF	544	33000	0.447	0.07	10.0	0.740	1.0×10^8	13×10^8	52.57
DMAC	543	39600	0.522	0.07	8.50	0.578	1.2×10^8	16×10^8	52.67
				BTC-APDI					
CHL	525	33904	0.207	0.40	20.0	8.00	0.50×10^8	0.75×10^8	54.48
THF	520	35033	0.228	0.30	18.0	5.40	0.55×10^8	1.3×10^8	55.00
DMAC	525	43802	0.324	0.21	13.0	2.73	0.77×10^8	2.9×10^8	54.48

4.3 Förster/Fluorescence Resonance Energy Transfer (FRET)

A mechanism which defines transferred energy among two chromophors is called Förster resonance energy transfer A.K.A. FRET. This energy is transferred nonradiatively from donor to acceptor molecule, which the donor is fluorophore that nonradiatively transfers absorbed energy of a photon to the acceptor.

Based on Förster the critical transfer distance (R_0), which is the distance limit that the transfer takes place throughout the excitation lifetime, can be computed from the following equation.

$$\boldsymbol{R_0^6 = \frac{8.785\times10^{-5}K^2\emptyset_f J}{n^4}} \qquad \textbf{(4.16)}$$

$$\boldsymbol{J = \int_0^\infty F_D(\lambda)\varepsilon_A(\lambda)\lambda^4 d\lambda}$$

K^2: Orientation factor ($K^2 = 0.67$ for normally distributed molecules)

$\emptyset_f$: Fluorescence quantum-yield of donor.

J: The integral between the overlapped fluorescence spectrum of donor and the molar absorption spectrum of acceptor.

n: Refractive index of solvent

$F_D(\lambda)$: Peak-normalized fluorescence spectrum of the donor.

$\varepsilon_A(\lambda)$: Extinction co-efficient of acceptor in M^{-1} cm^{-1} at the max wavelength

λ : Maximum wavelength of acceptor in nm

R_0: Critical transfer distance in A°

4.3.1 Intra-Molecular Critical Transfer Distance of TPDI in NMP

In the study of intra-molecular energy transfer in TPDI molecule, the thiophene is considered as a donor and perylene core as an acceptor. The measurements of UV and Emission had been done separately for Thiophene and TPDI in NMP.

From the fluorescence spectrum of the donor/Thiophene (Figure 4.8), the normalized Area $F_D(\lambda)$ = 126.47

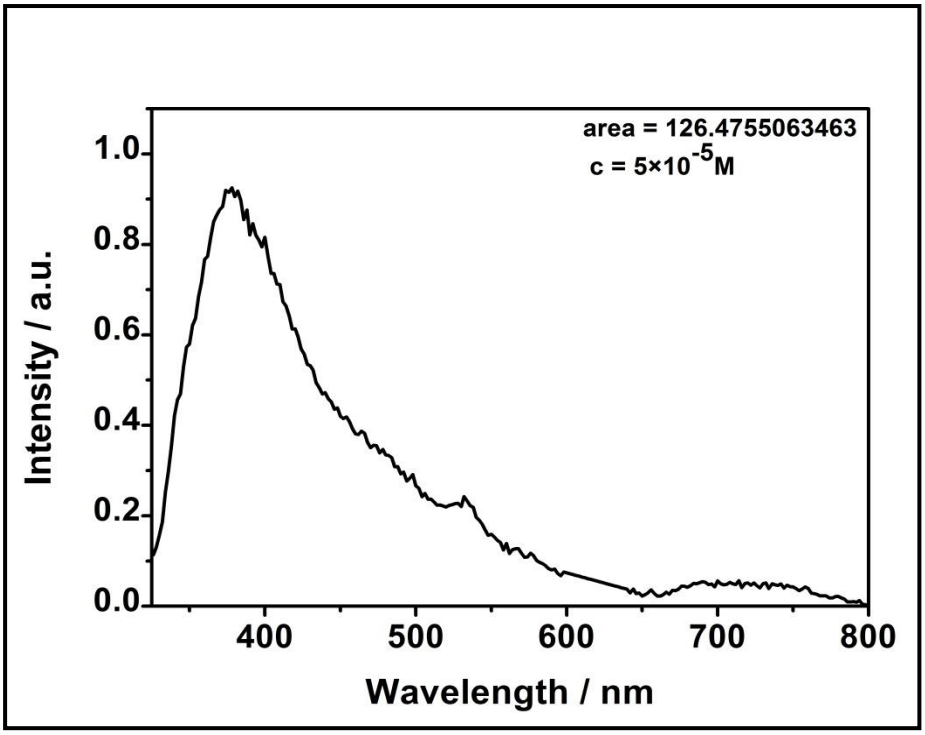

Figure 4.8: Normalized fluorescence spectrum of donor (Thiophene) in absence of acceptor

From the absorption spectrum of acceptor in NMP the molar absorptivity $\varepsilon_A(\lambda) = 50583$ at wavelength of 528 nm was found (Table 4.3).

$$\mathbf{J} = \int_{\mathbf{0}}^{\infty} \mathbf{F_D(\lambda)\varepsilon_A(\lambda)\lambda^4 d\lambda}$$

$J = 126.47 \times 50583 \times (528)^4 = 4.97 \times 10^{17}$

$R_0^6 = \frac{8.785\times10^{-5}\times0.67\times4.97\times10^{17}\times0.30}{(1.4700)^4} = 1.76 \times 10^{12}$ $R_0 = 109.88$ A°

4.4.2 Rate Constants for Bimolecular Fluorescence Quenching (K_q)

The rate-constant (K_q) was calculated utilizing Stern-Volmer plot and via following equation.

$$\frac{\mathbf{I_0}}{\mathbf{I}} = \mathbf{1} + \mathbf{K_q\tau_0[Q]} \qquad \textbf{(4.17)}$$

$\frac{I_0}{I}$: Intensity of relative fluorescence

I: Intensities of donor emission in absence of acceptor

I_0: Intensities of donor emission in the presence of acceptor at different concentrations

K_q: Rate-constant for bi-molecular fluorescence quenching

τ_0: Theoretical radiative-lifetime of donor on the absence of quencher.

Using emission spectrum of TPDI in NMP (Figure 4.34-d) the relative fluorescence intensities were approximately calculated (in variant concentrations) and plotted vs. Concentration of quencher (Figure 4.10).

Obtained from first order regression the slop of the line is $\mathbf{K_q\tau_0 = 10647}$

$$\mathbf{Kq} = \frac{\mathbf{10647}}{\mathbf{19.1\times10^{-9}}} = \mathbf{5.6 \times 10^{11} M^{-1}s^{-1}}$$

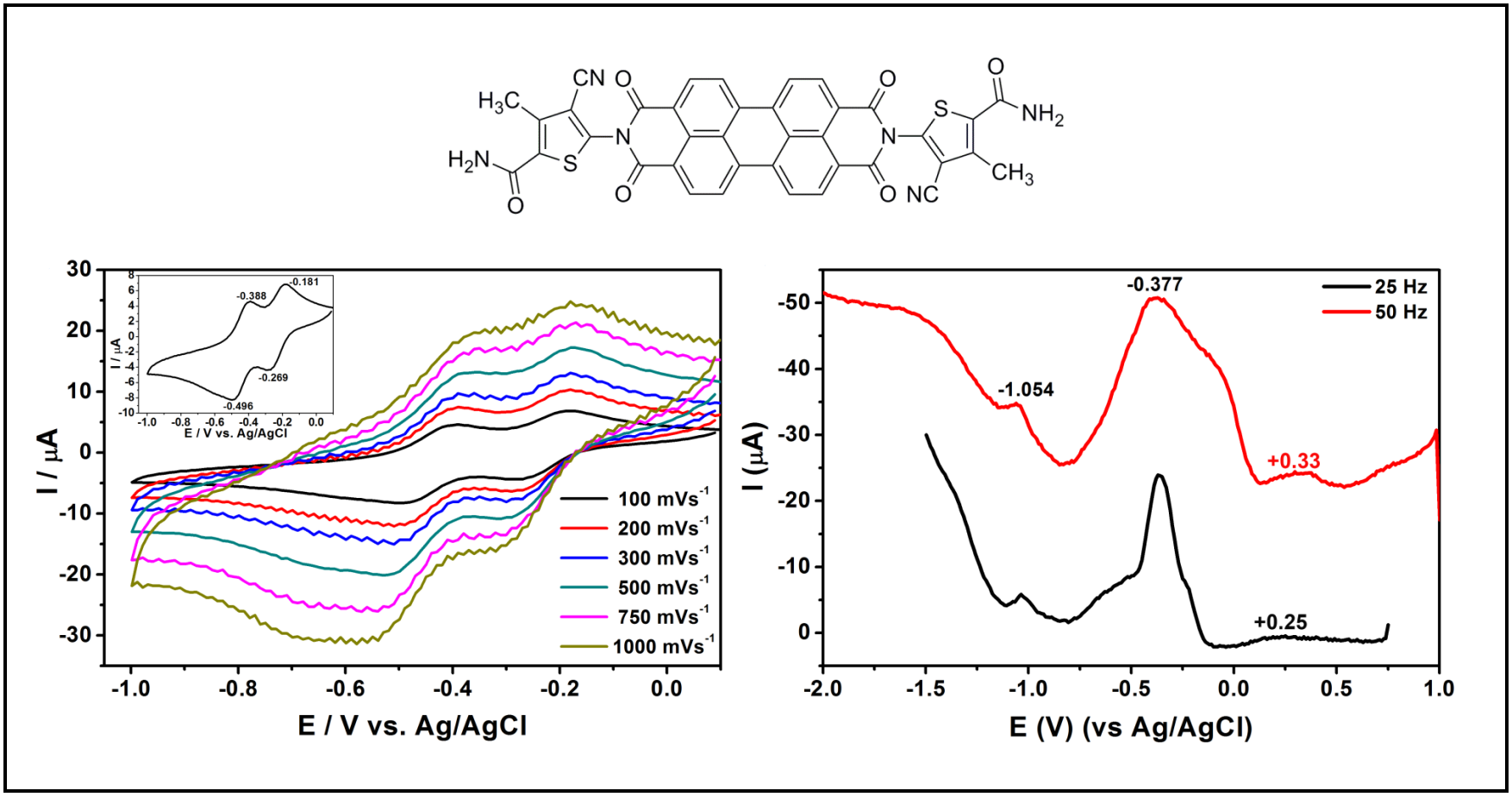

Figure 4.9: **TPDI** in DMF solution (supporting electrolyte: 0.1 M $NaBF_4$); the left figure demonstrates scan rate dependent cyclic voltammograms (inset shows the CV at 100 mVs^{-1} for clarity); the right figure shows frequency dependent squarewave voltammograms

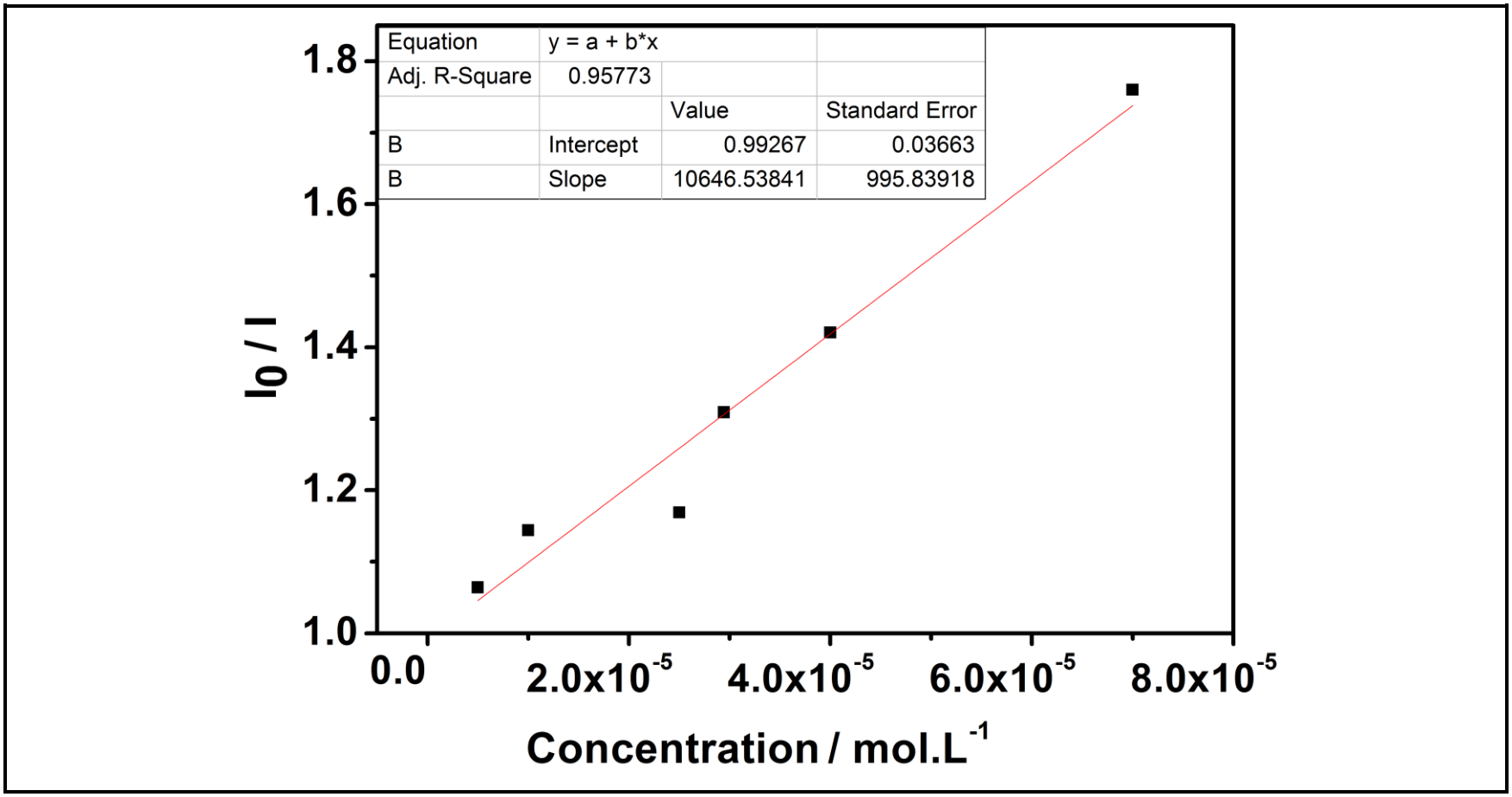

Figure 4.10: Stern-Volmer plots of donor in different concentration

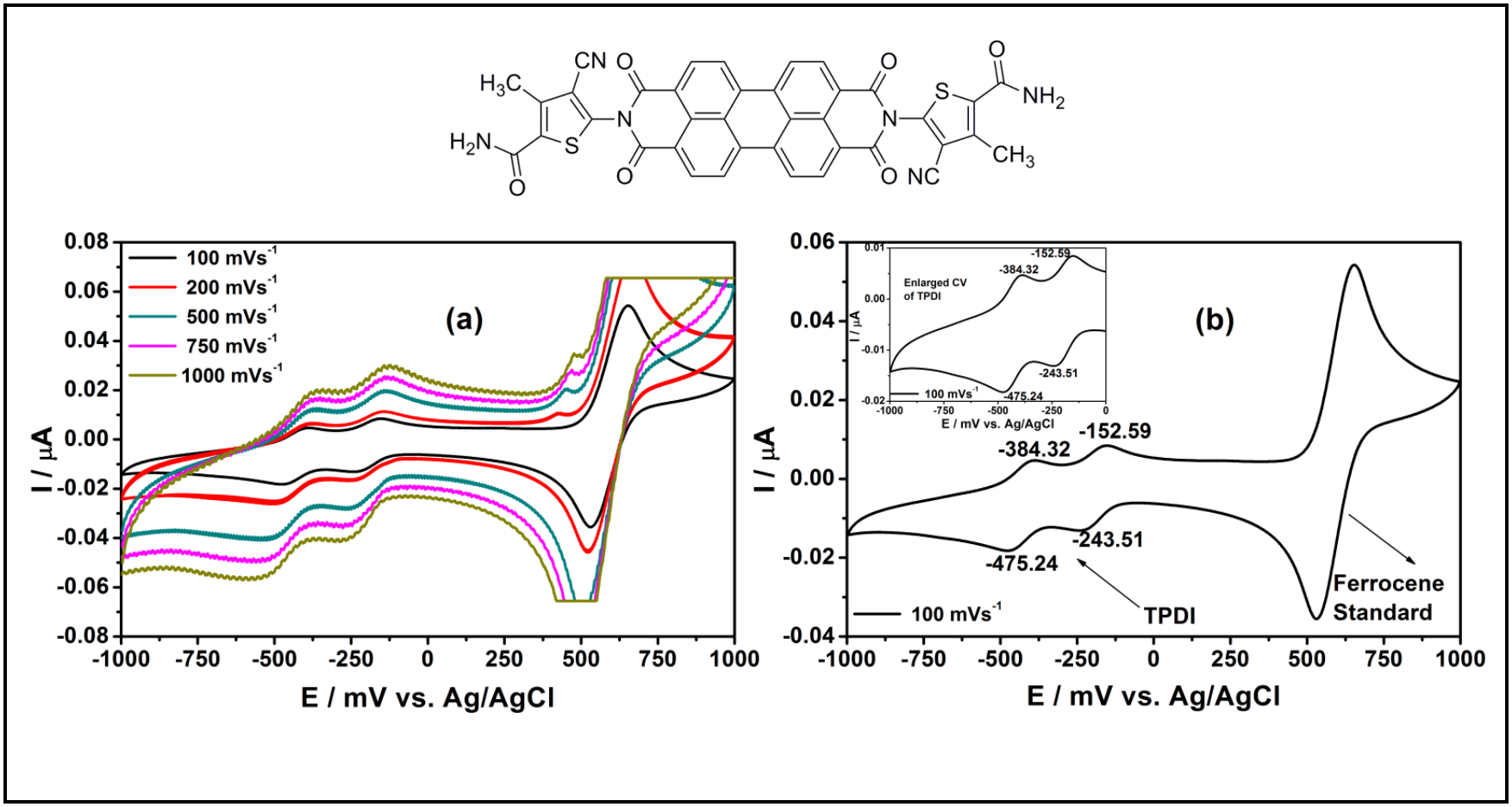

Figure 4.11: The left figure shows scan rate dependent cyclic voltammograms of **TPDI** in NMP solution (supporting electrolyte: 0.05 M $NaBF_4$); the right figure demonstrates cyclic voltammogram at 100 mVs^{-1} (inset shows the enlarged CV of **TPDI** part for clarity)

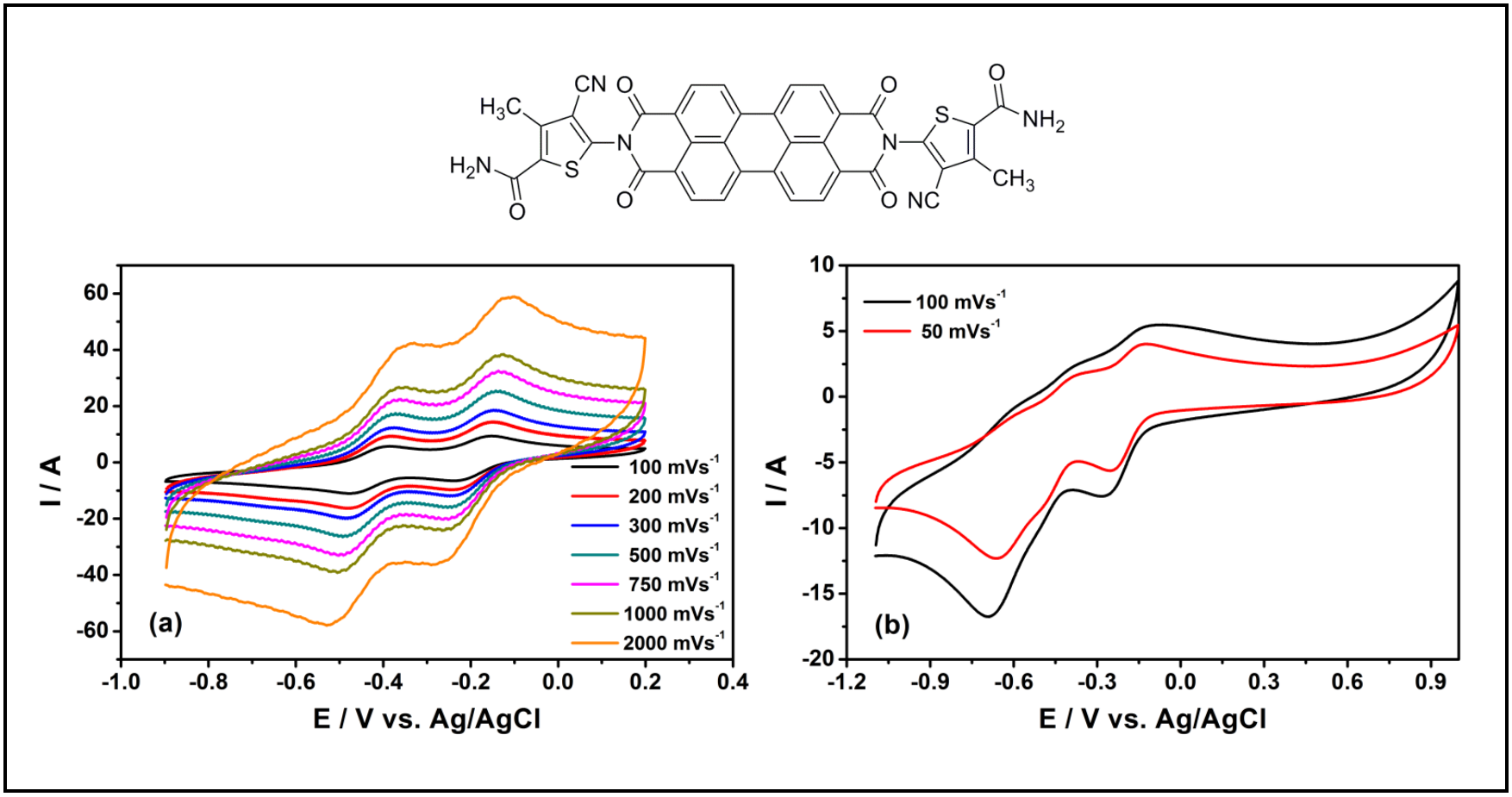

Figure 4.12: The left figure shows scan rate dependent cyclic voltammograms of **TPDI** in DMAC solution (supporting electrolyte: 0.05 M $NaBF_4$), the right figure demonstrates cyclic voltammograms at 100 and 50 mVs^{-1} with the anodic region

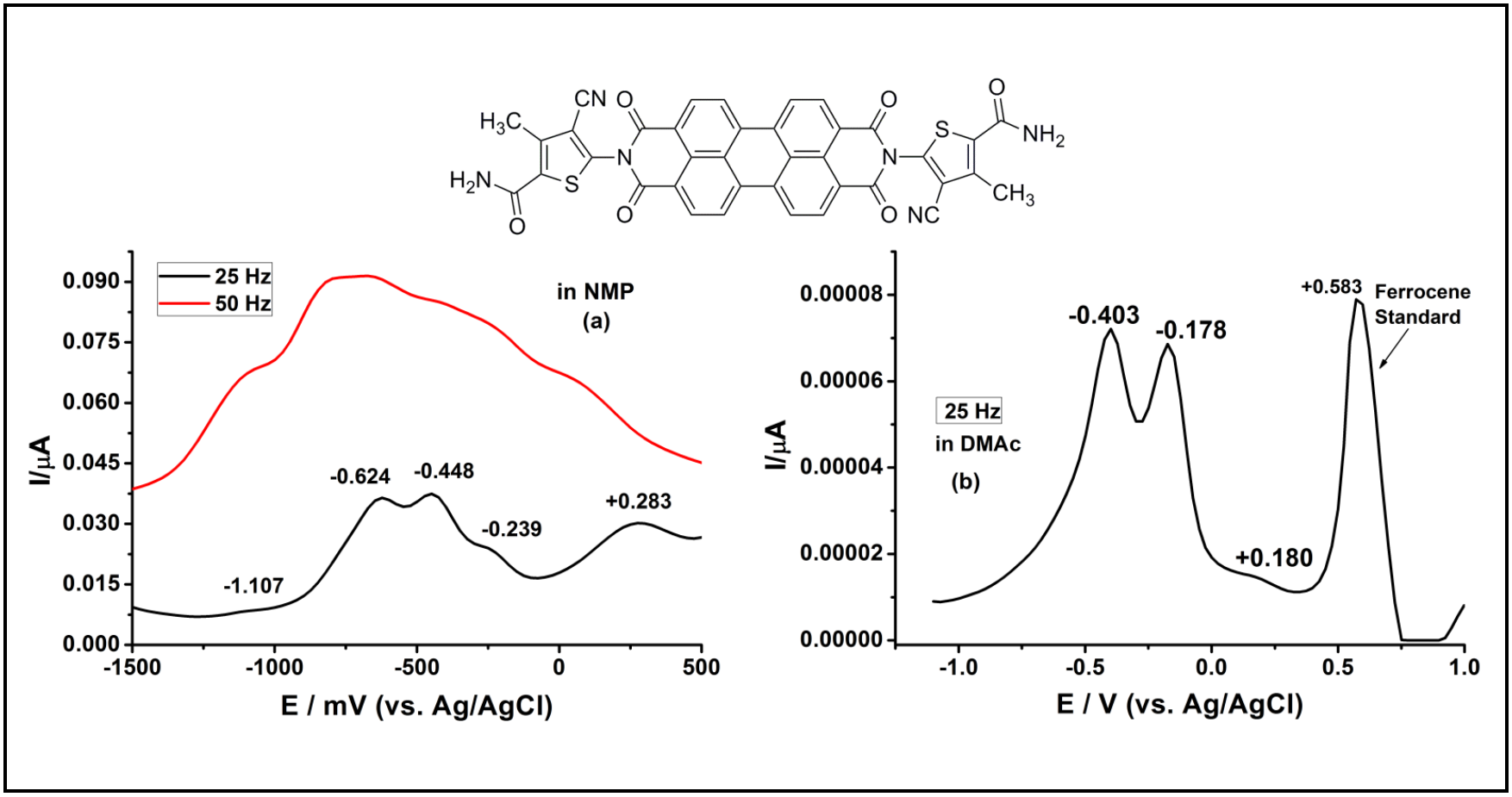

Figure 4.13: The left figure shows Squarewave voltammograms of **TPDI** in NMP and the right figure demonstrates DMAC solutions (Supporting electrolyte: 0.05 M $NaBF_4$)

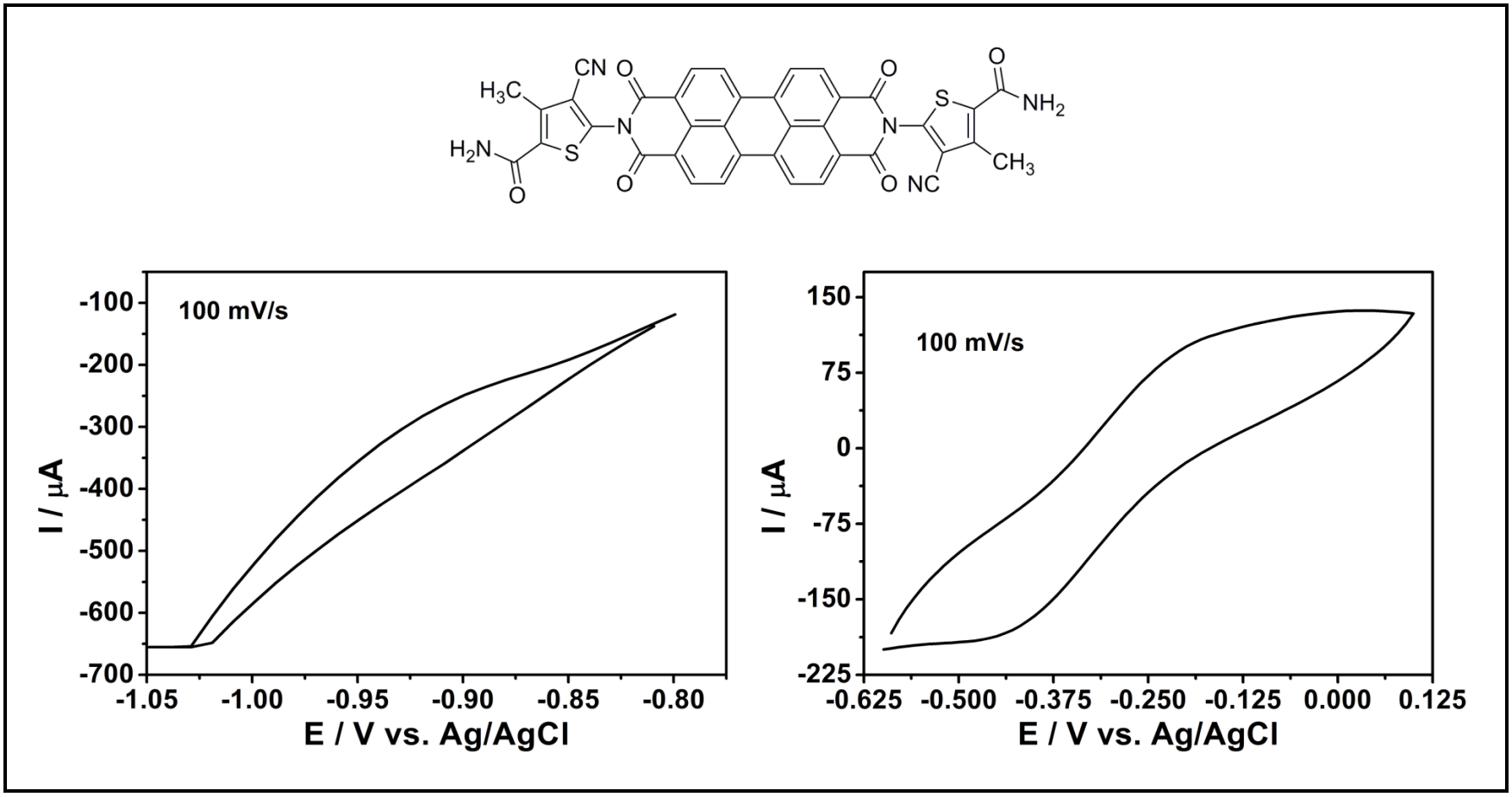

Figure 4.14: **TPDI** in solid-state (supporting electrolyte: 1 M HCl); the left figure demonstrates cyclic voltammogram in the cathodic-region (from –1.05 V to –0.825 V); the right figure shows cyclic voltammogram in the cathodic region (from –0.625 V to +0.125 V)

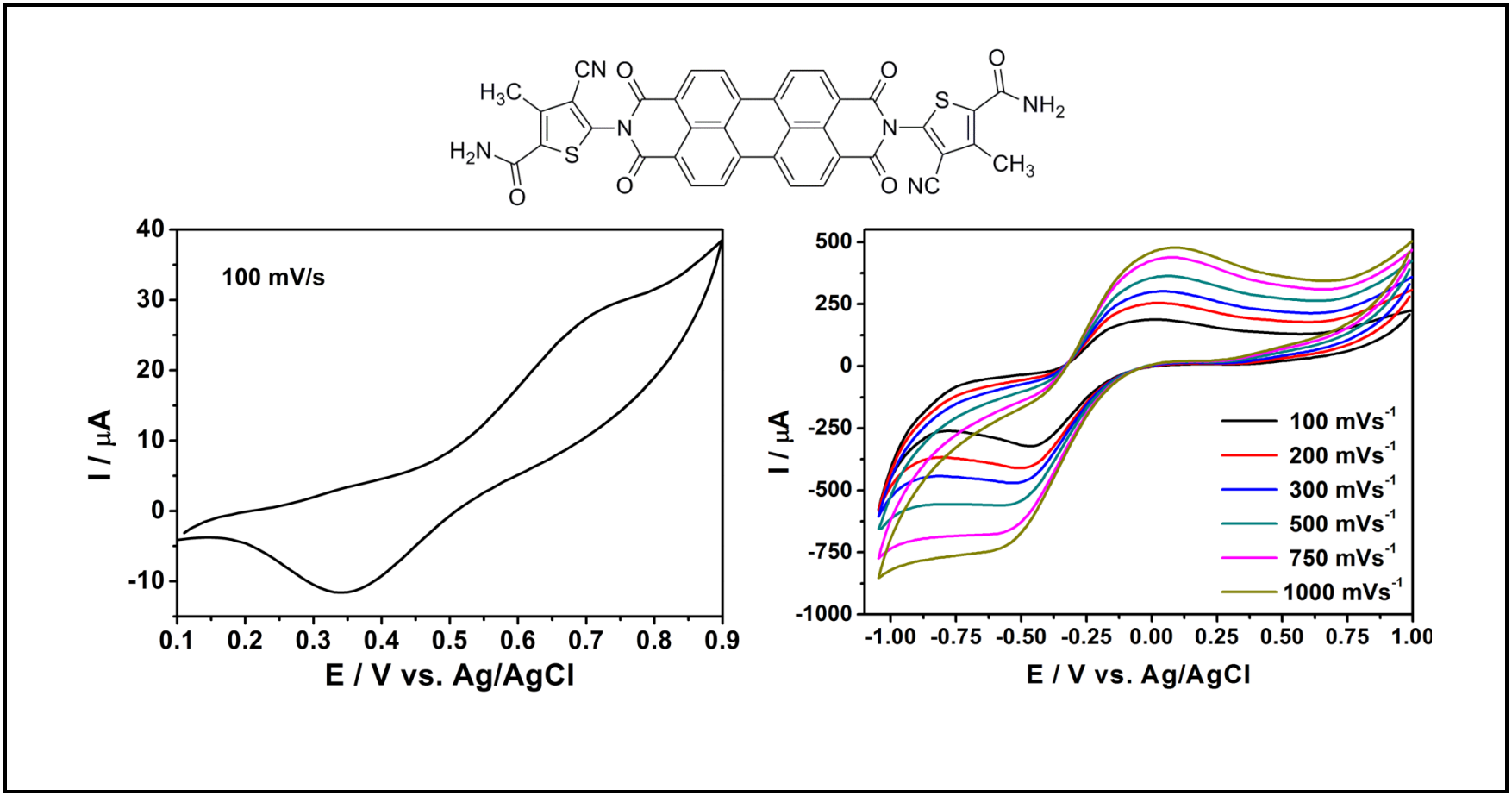

Figure 4.15: **TPDI** in solid-state (supporting electrolyte: 1 M HCl); cyclic voltammogram in the anodic region (from +0.1 V to +0.9 V); scan rate dependent complete cyclic voltammograms from cathodic to anodic region (from –1.00 V to +1.00 V; and the inset shows the CV at 100 mVs^{-1} for clarity)

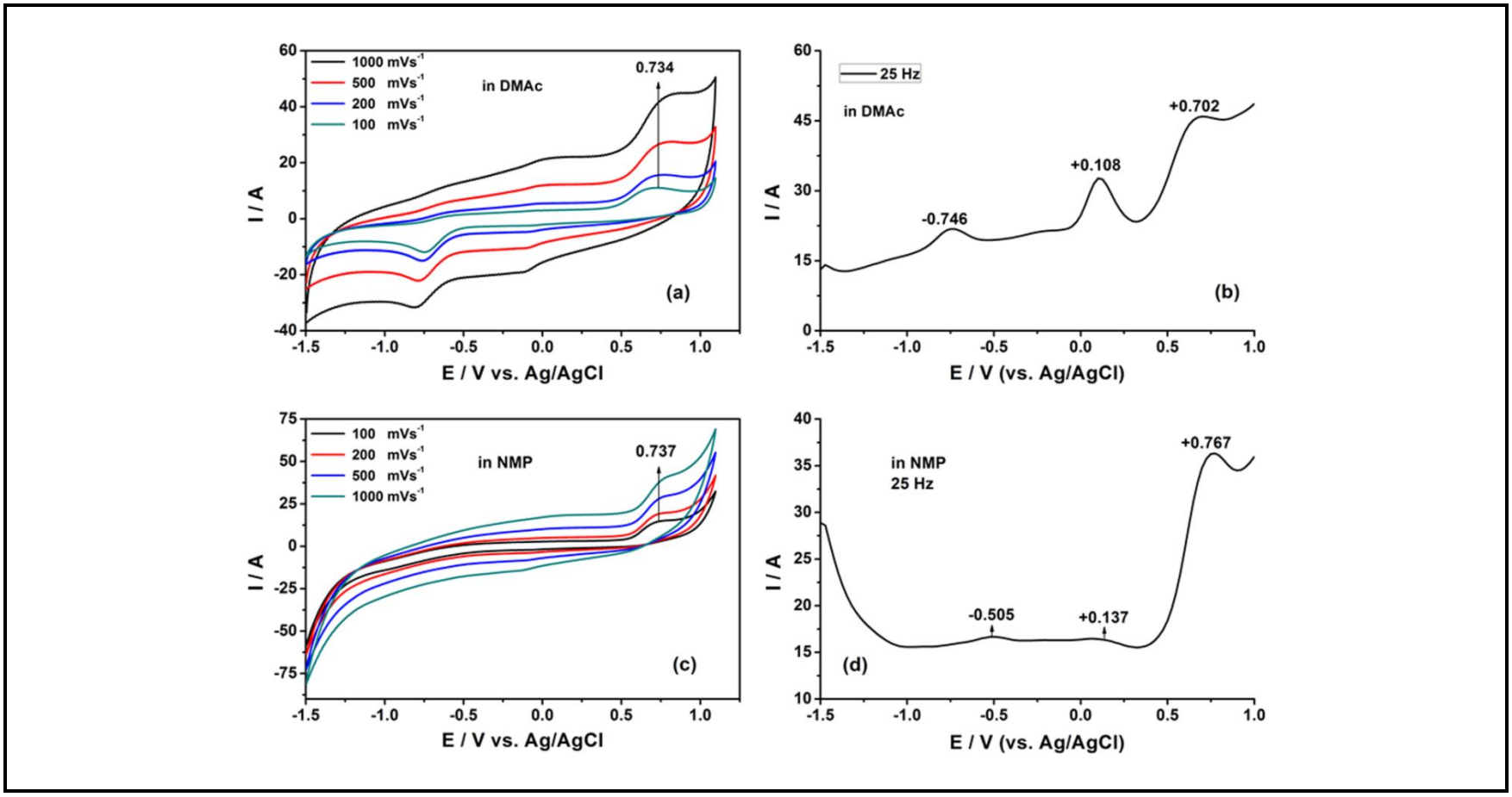

Figure 4.16: (a) Scan rate dependent cyclic voltammograms of **TH** in DMAC; (b) Squarewave voltammograms of **TH** in DMAC; (c) Cyclic voltammograms of **TH** in NMP; (d) Squarewave voltammograms of **TH** in NMP solutions (supporting electrolyte: 0.05 M $NaBF_4$)

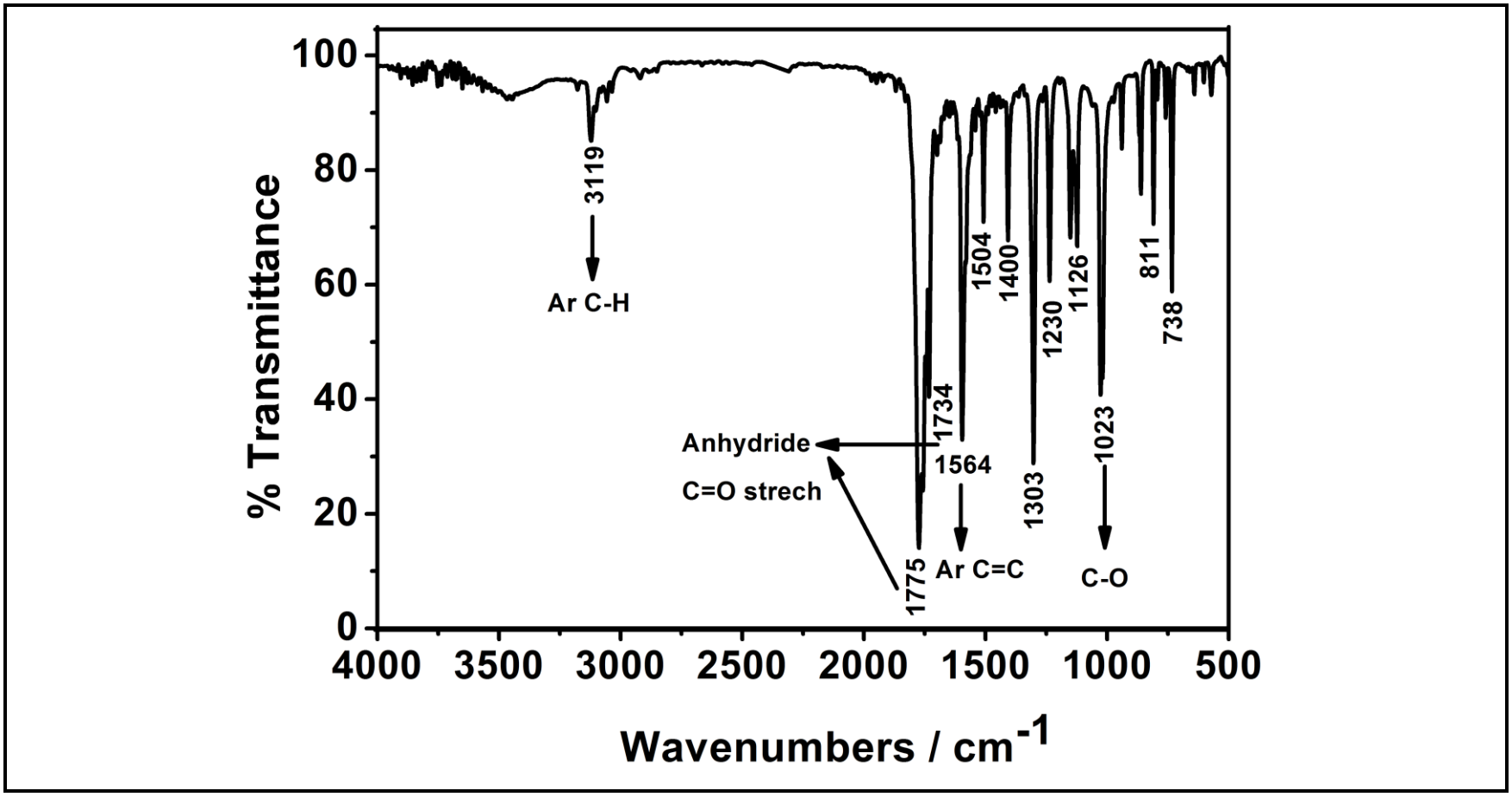

Figure 4.17: Infrared spectrum of perylene tetracarboxylic dianhydride (**PDA**), KBr pellet

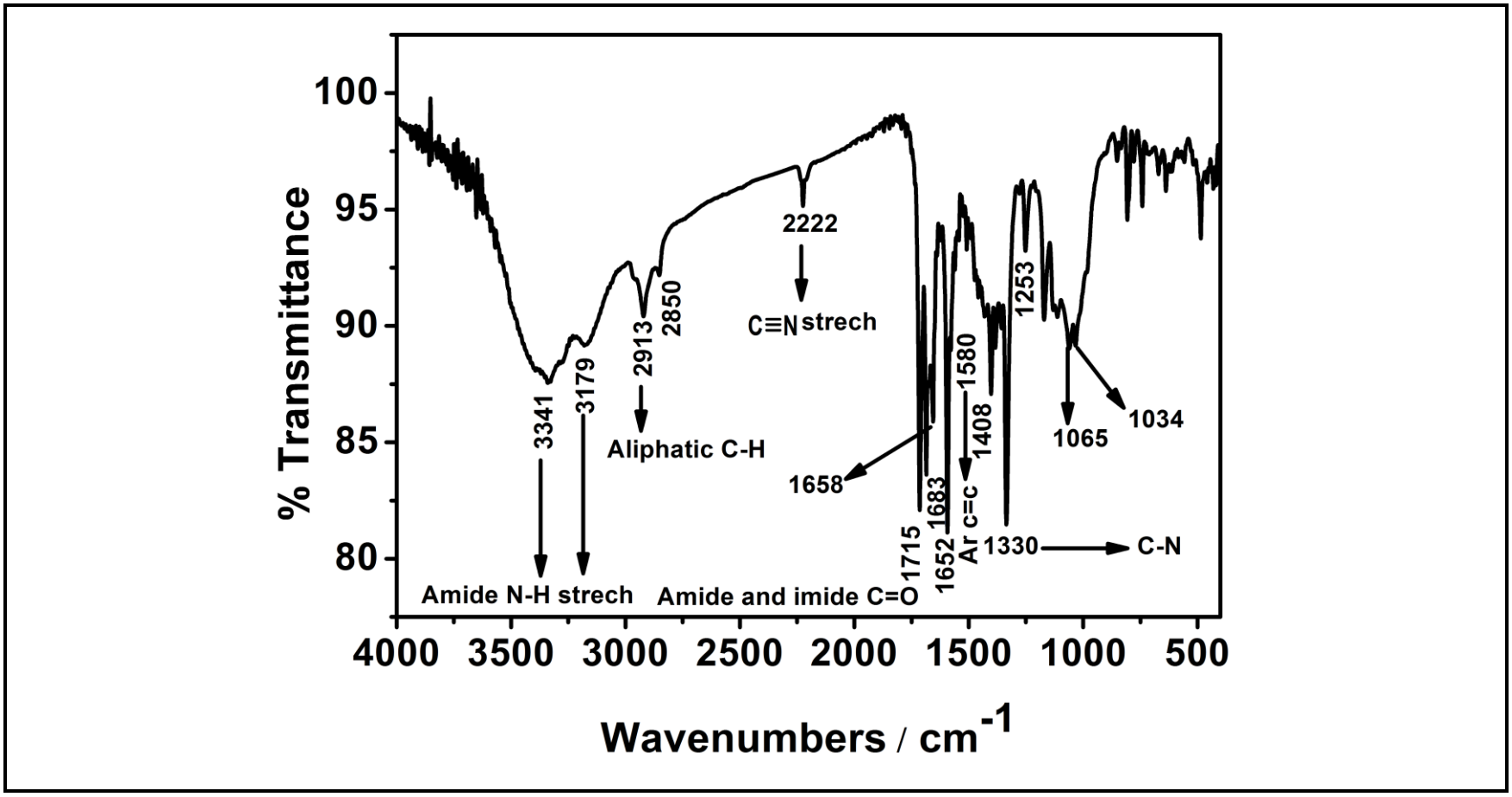

Figure 4.18: Infrared spectrum of **TPDI**, KBr pellet

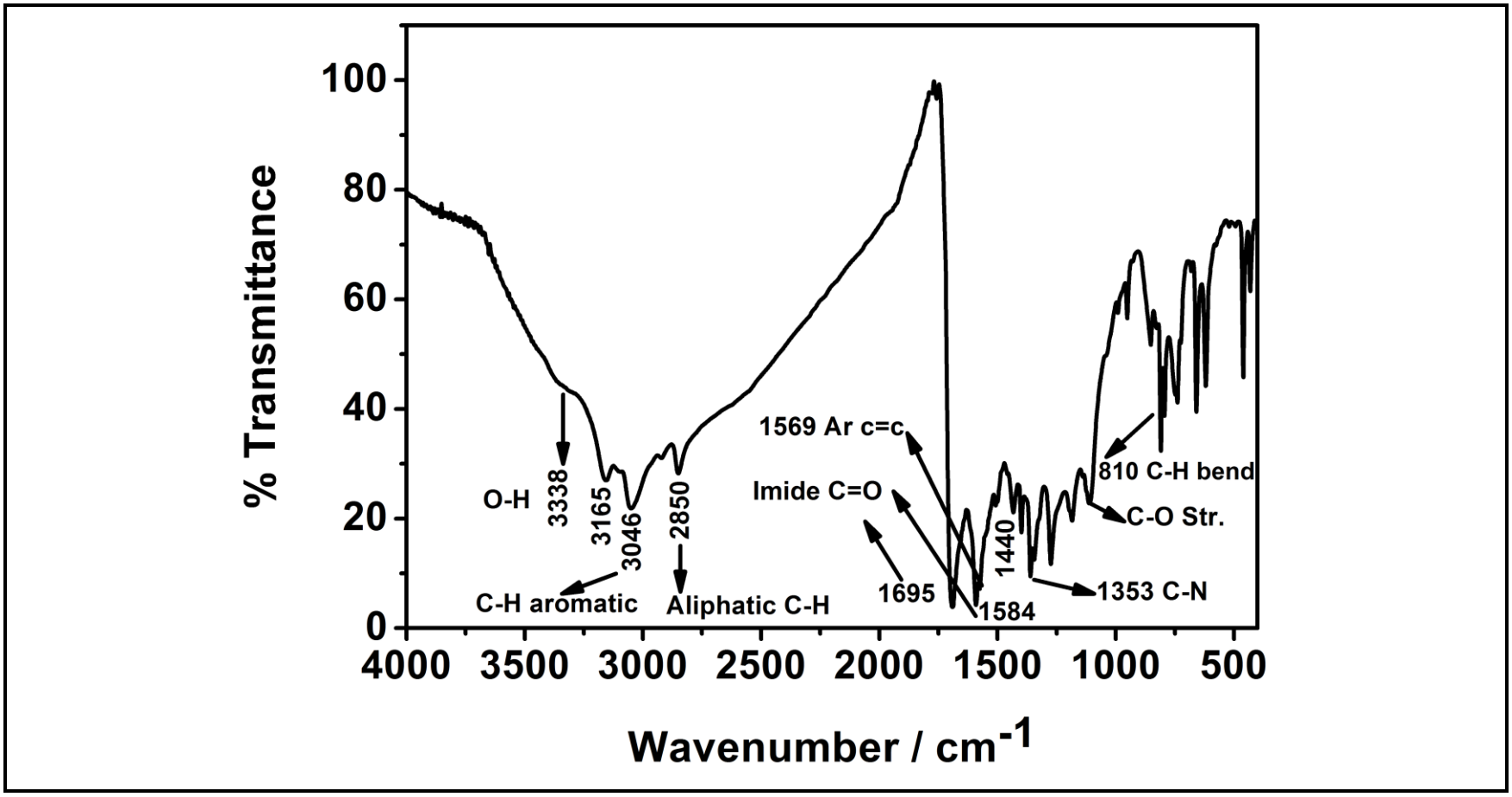

Figure 4.19: Infrared spectrum of **TCPDI**, KBr pellet

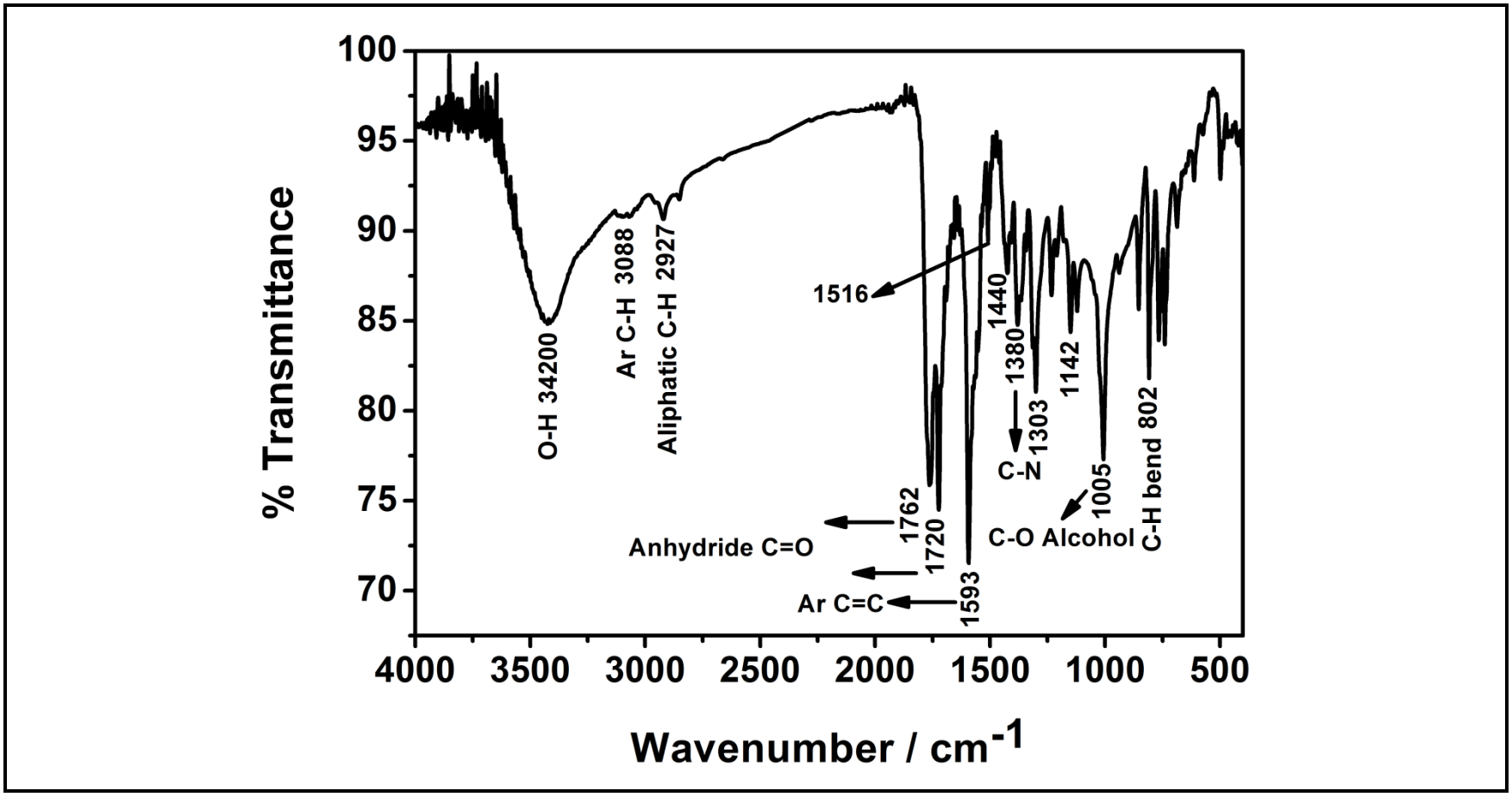

Figure 4.20: Infrared spectrum of **TCPMI**, KBr pellet

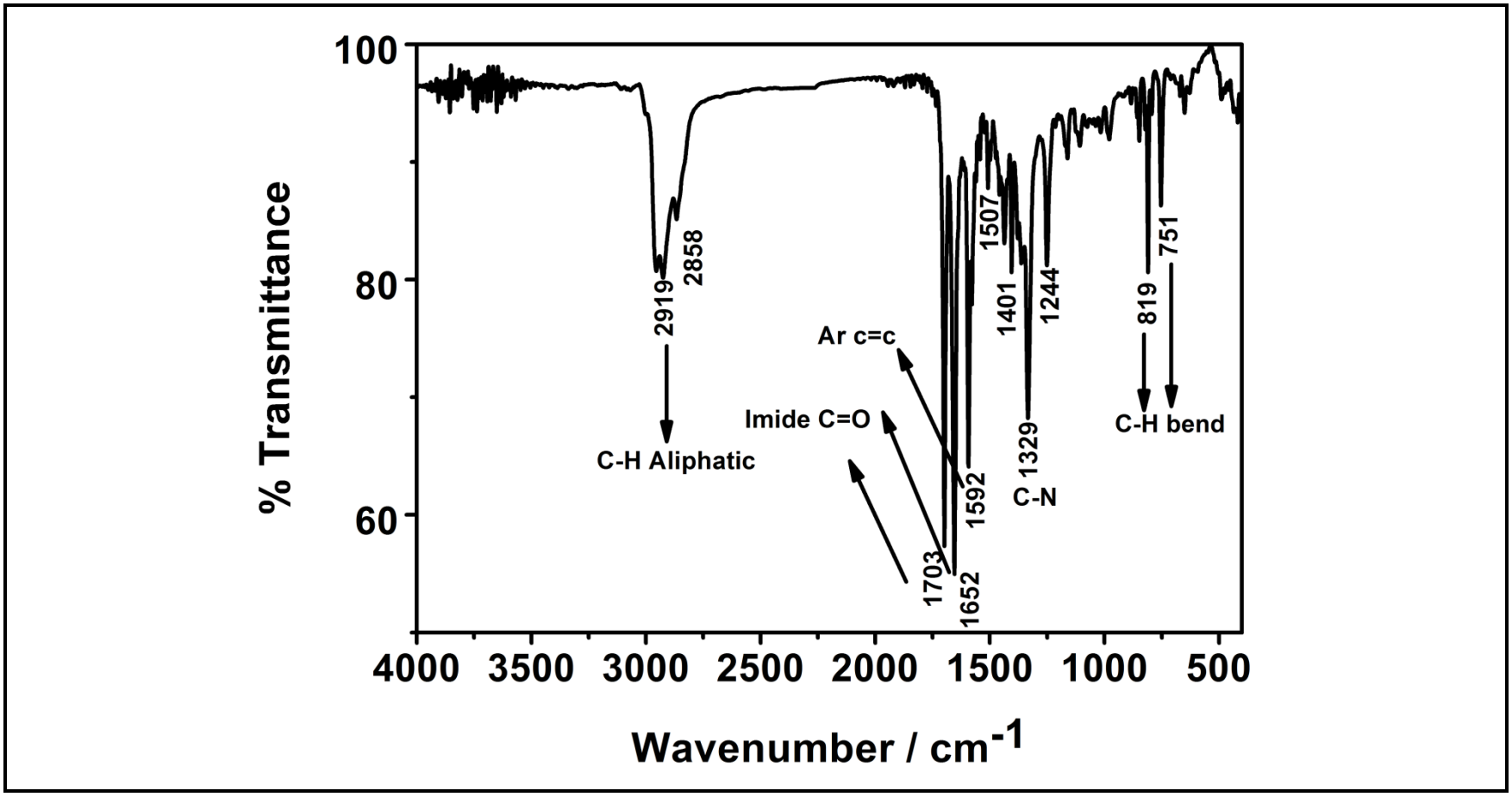

Figure 4.21: Infrared spectrum of **TAPDI**, KBr pellet

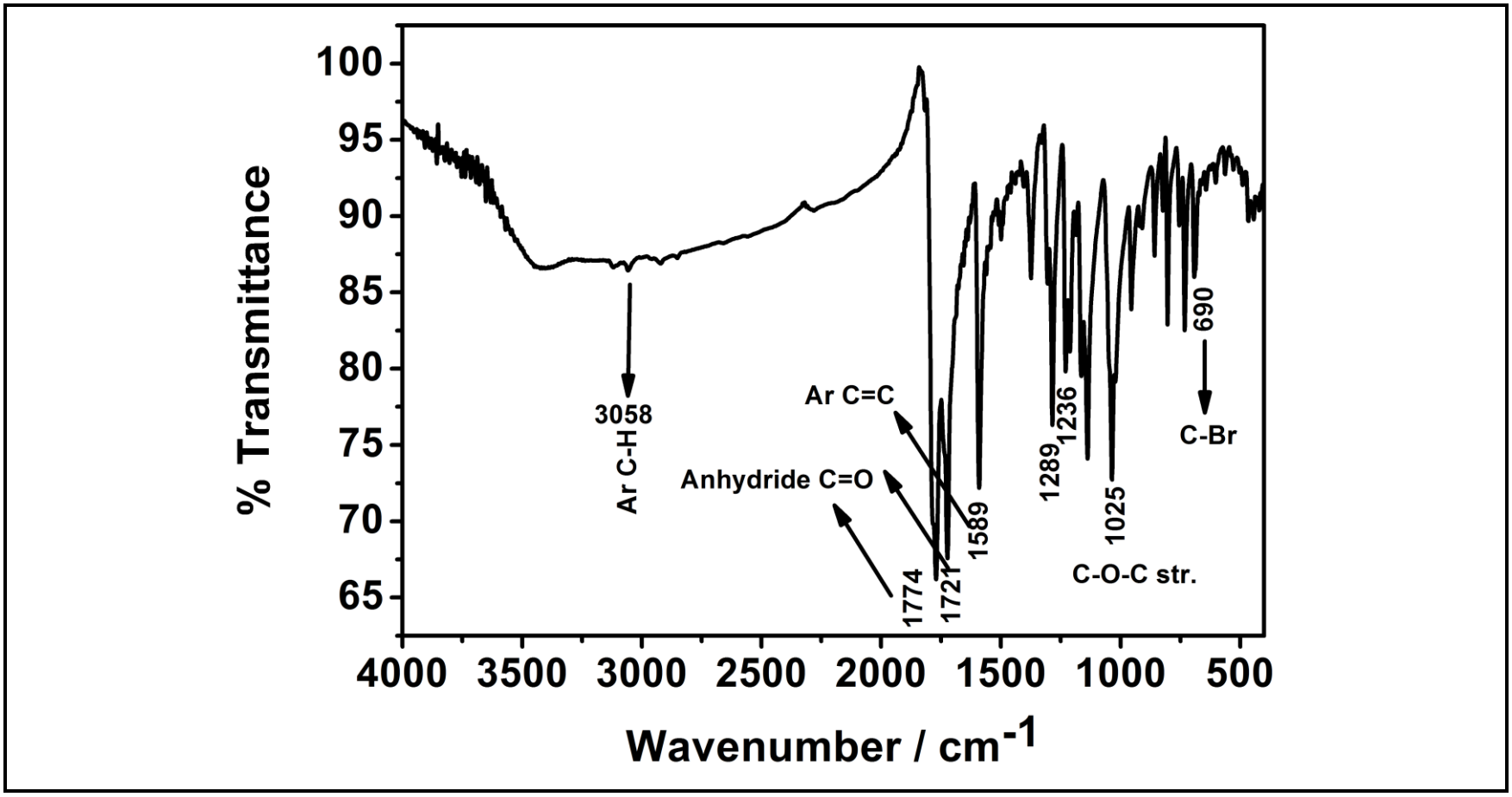

Figure 4.22: Infrared spectrum of **Br-PDA**, KBr pellet

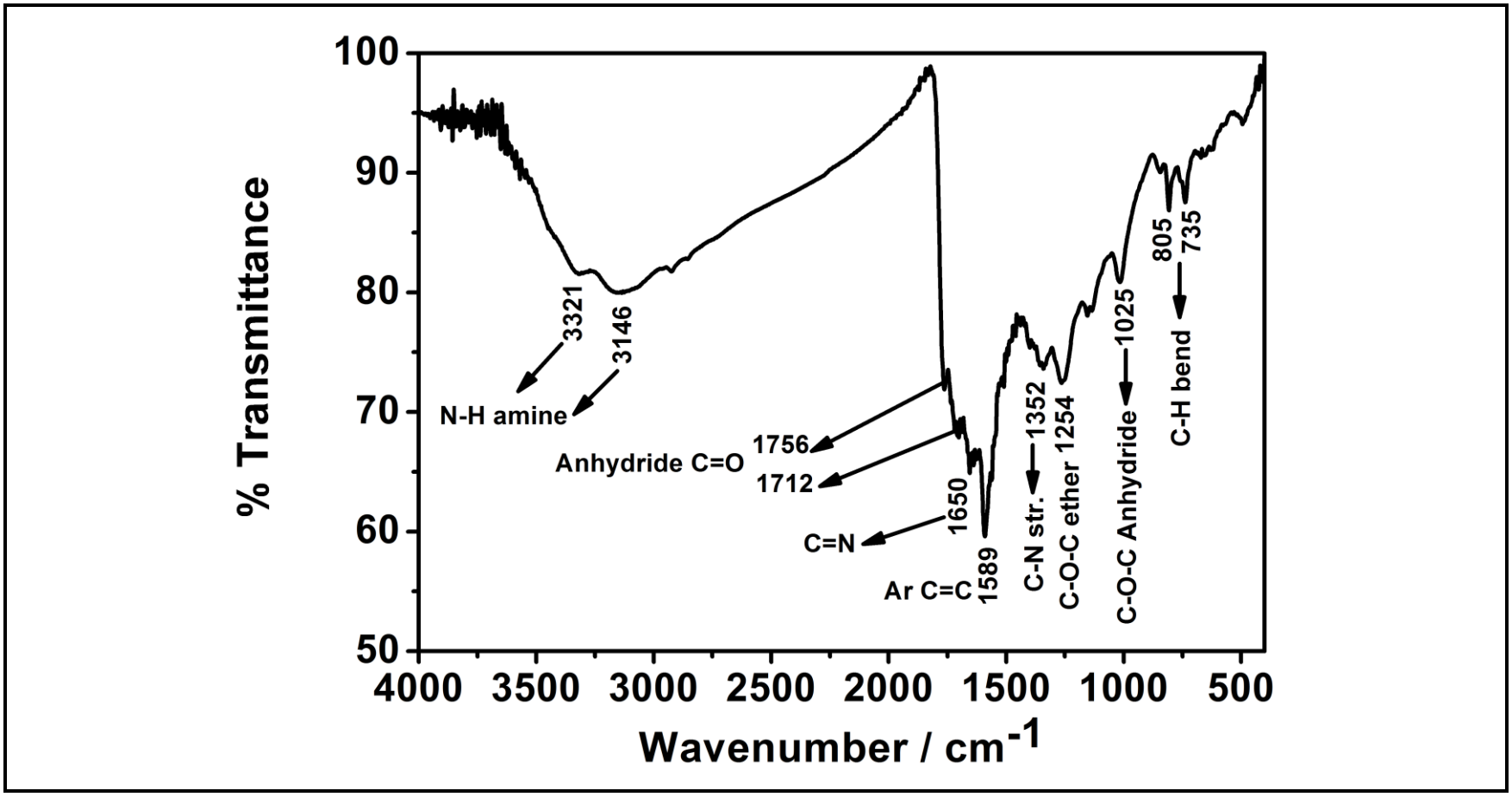

Figure 4.23: Infrared spectrum of **BPY-PDA**, KBr pellet

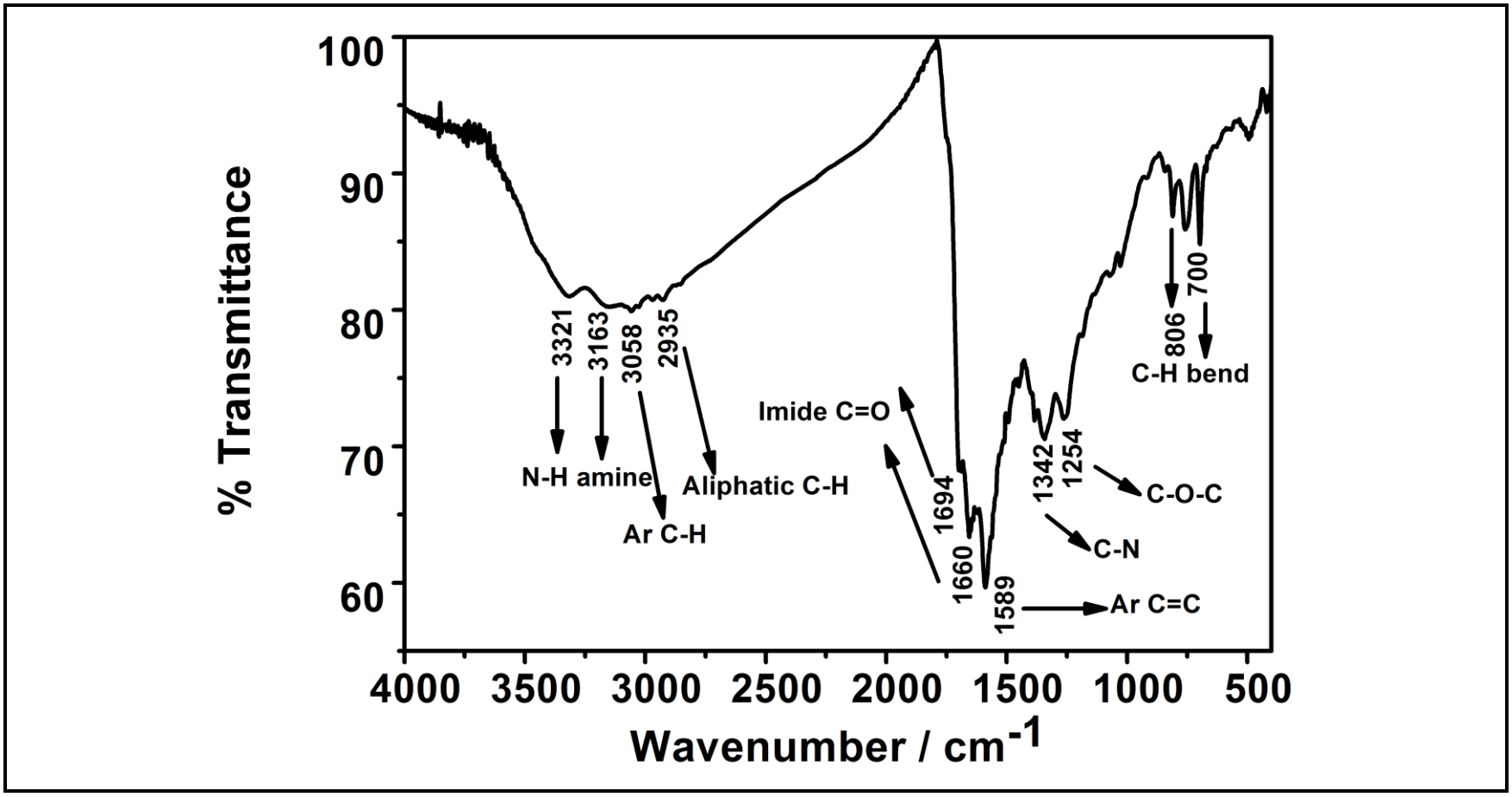

Figure 4.24: Infrared spectrum of **BPY-PPDI**, KBr pellet

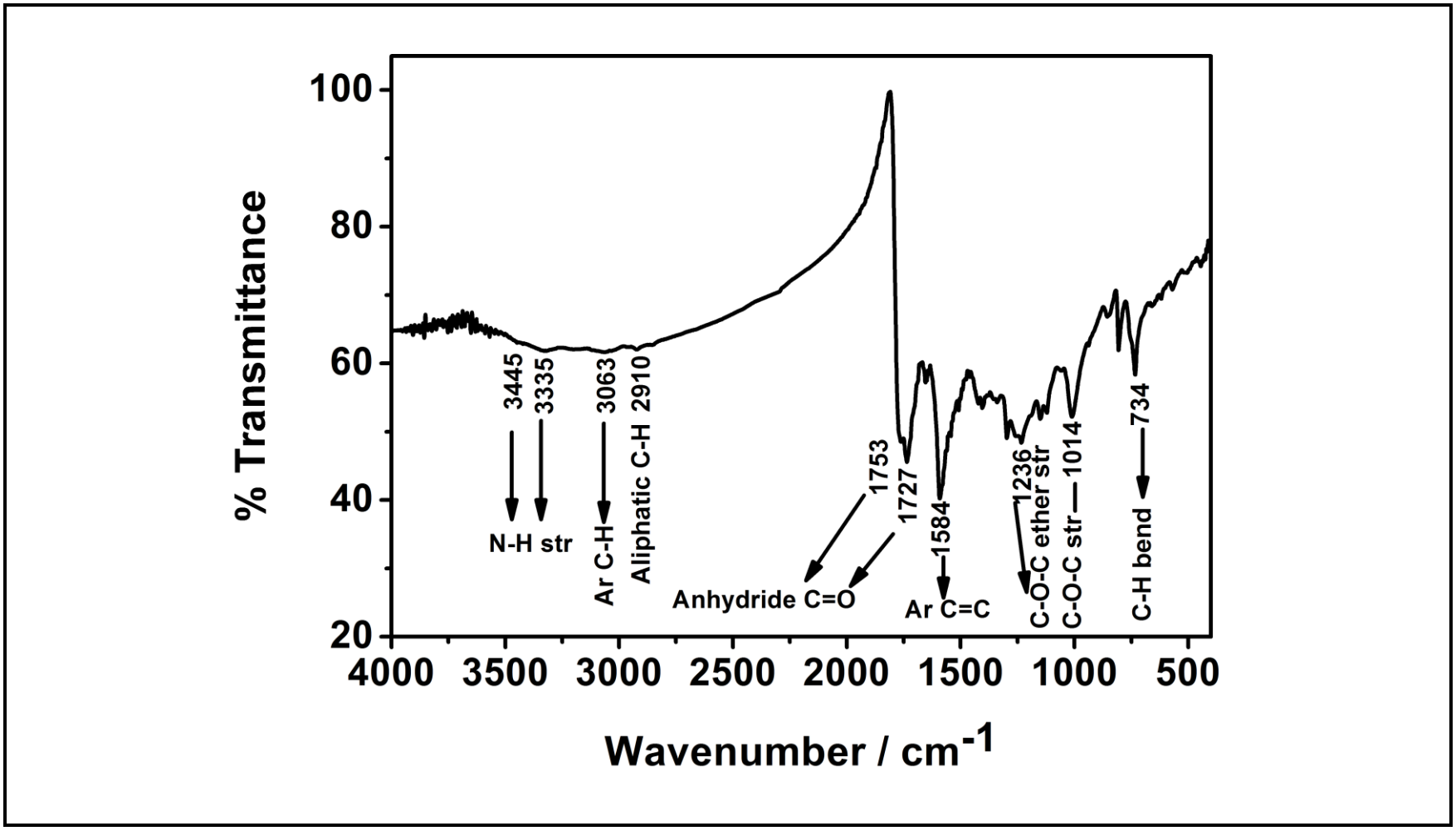

Figure 4.25: Infrared spectrum of **BTC-PDA**, KBr pellet

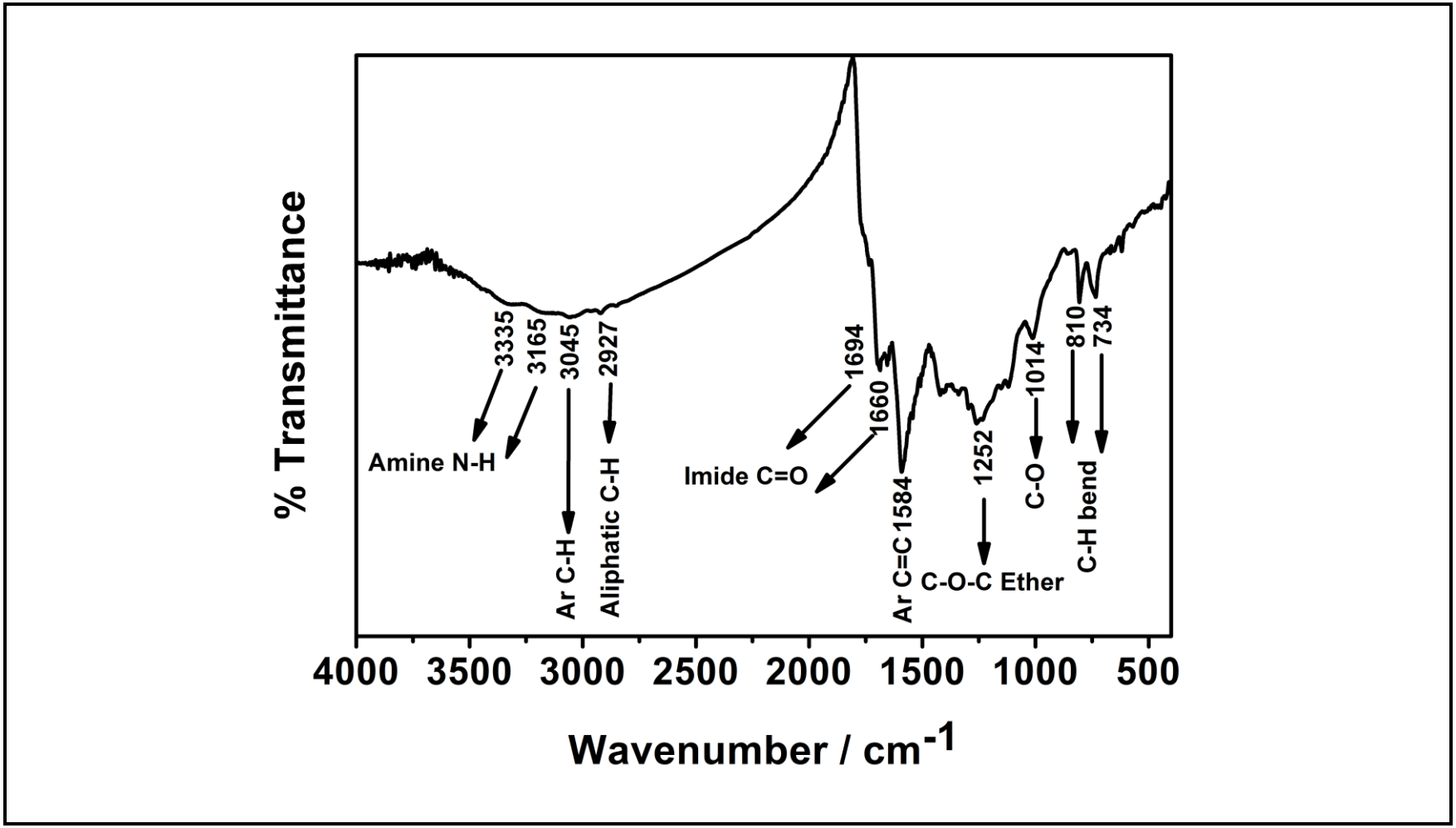

Figure 4.26: Infrared spectrum of **BTC-TCPDI**, KBr pellet

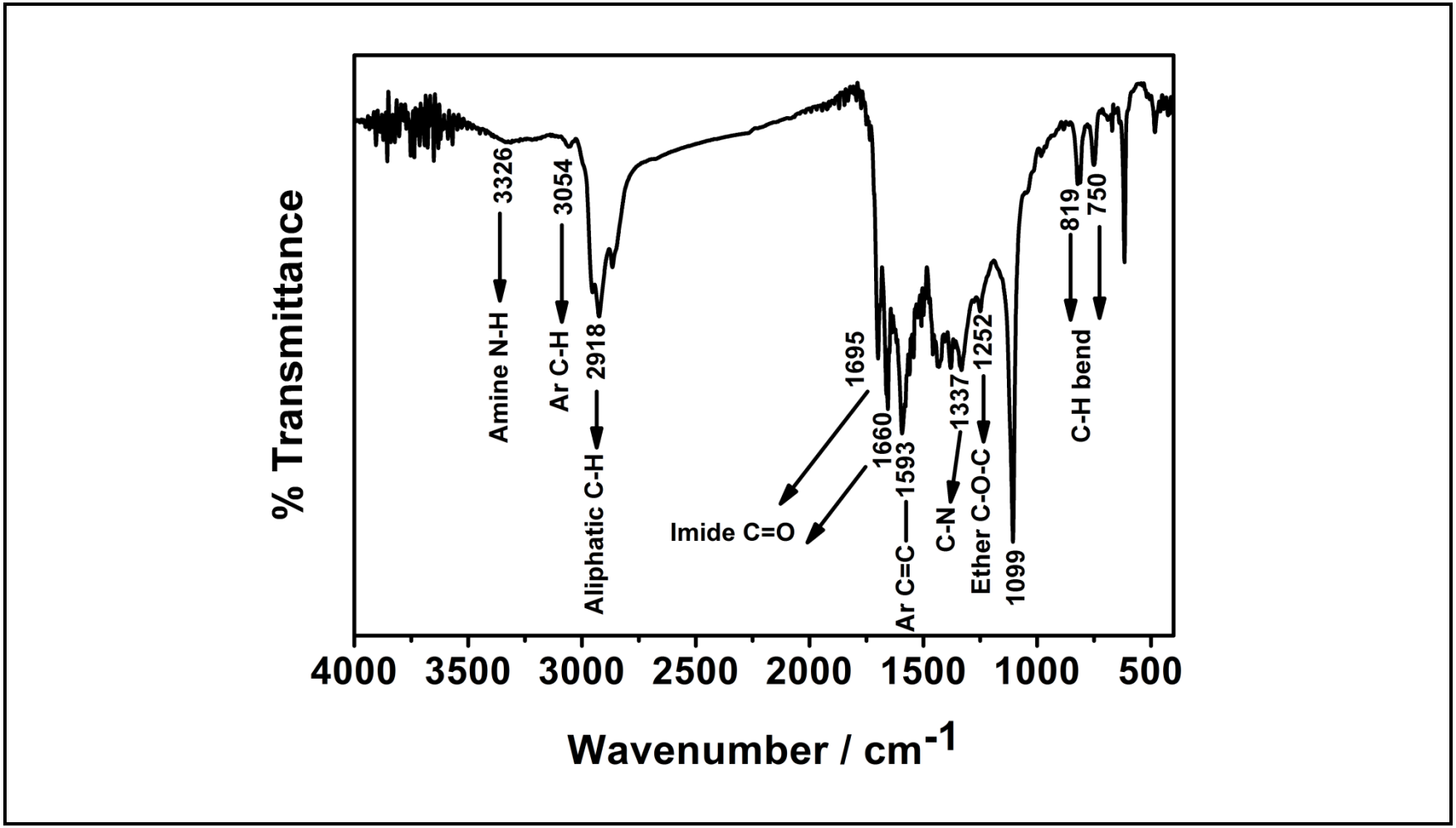

Figure 4.27: Infrared spectrum of **BTC-APDI**, KBr pellet

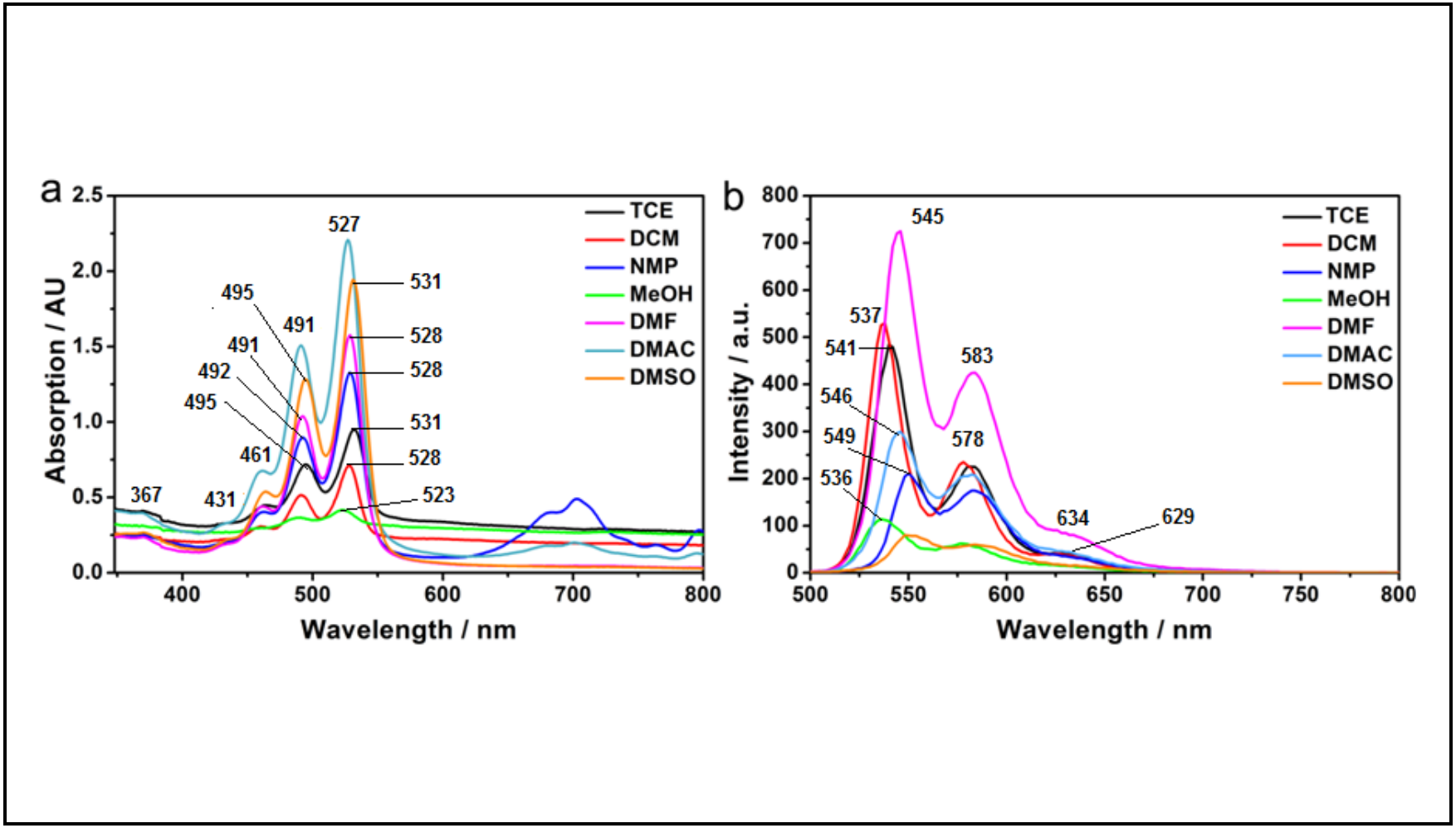

Figure 4.28: (a) Absorptionspectra of **TPDI** in different solvents; (b) Emission spectra of **TPDI** in different solvents at excitation wavelength of 485 nm

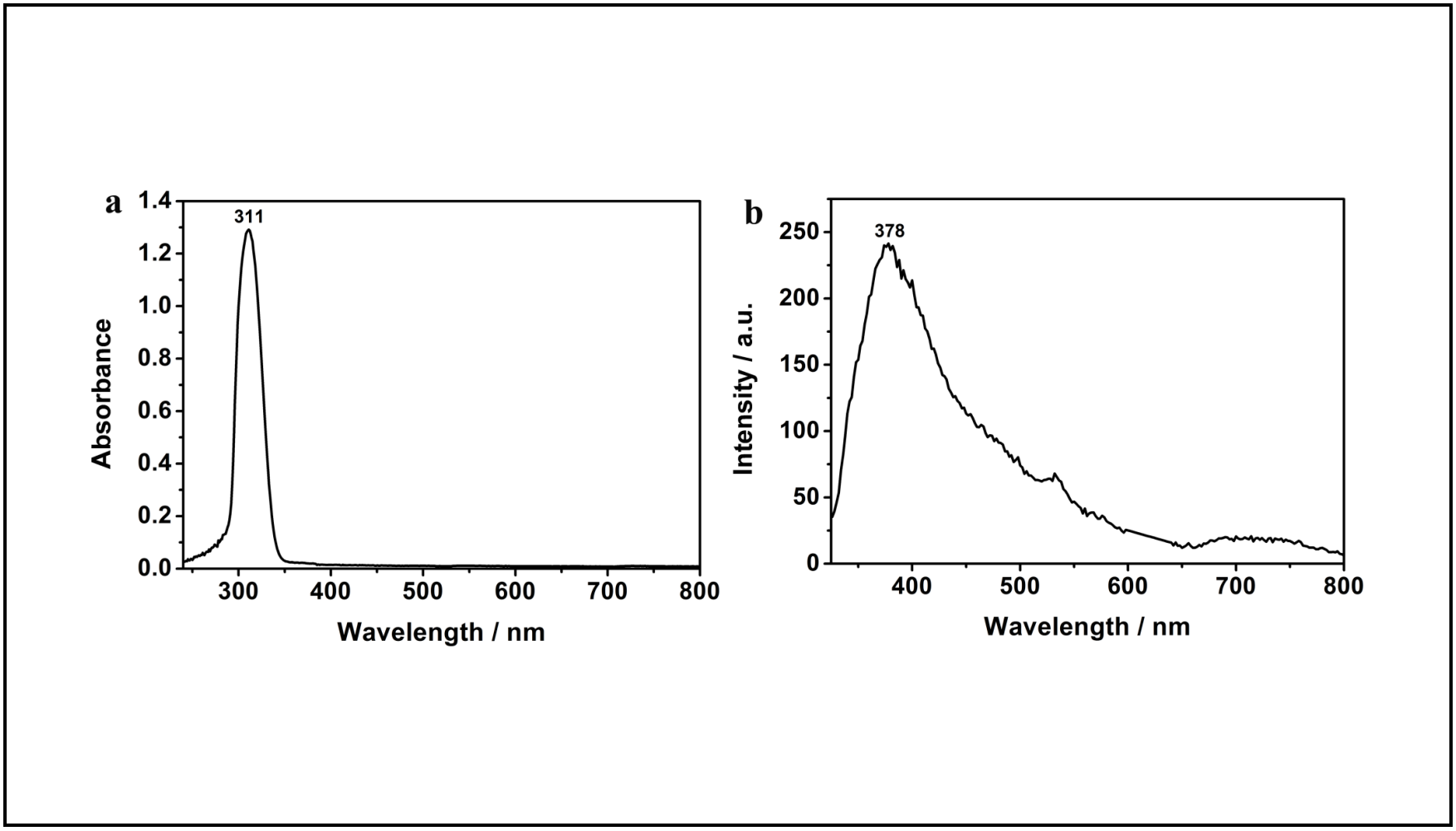

Figure 2.29: (a) Absorptionspectra of **TH** in NMP; (b) Emission spectra of **TH** in NMP at excitation wavelength of 310 nm

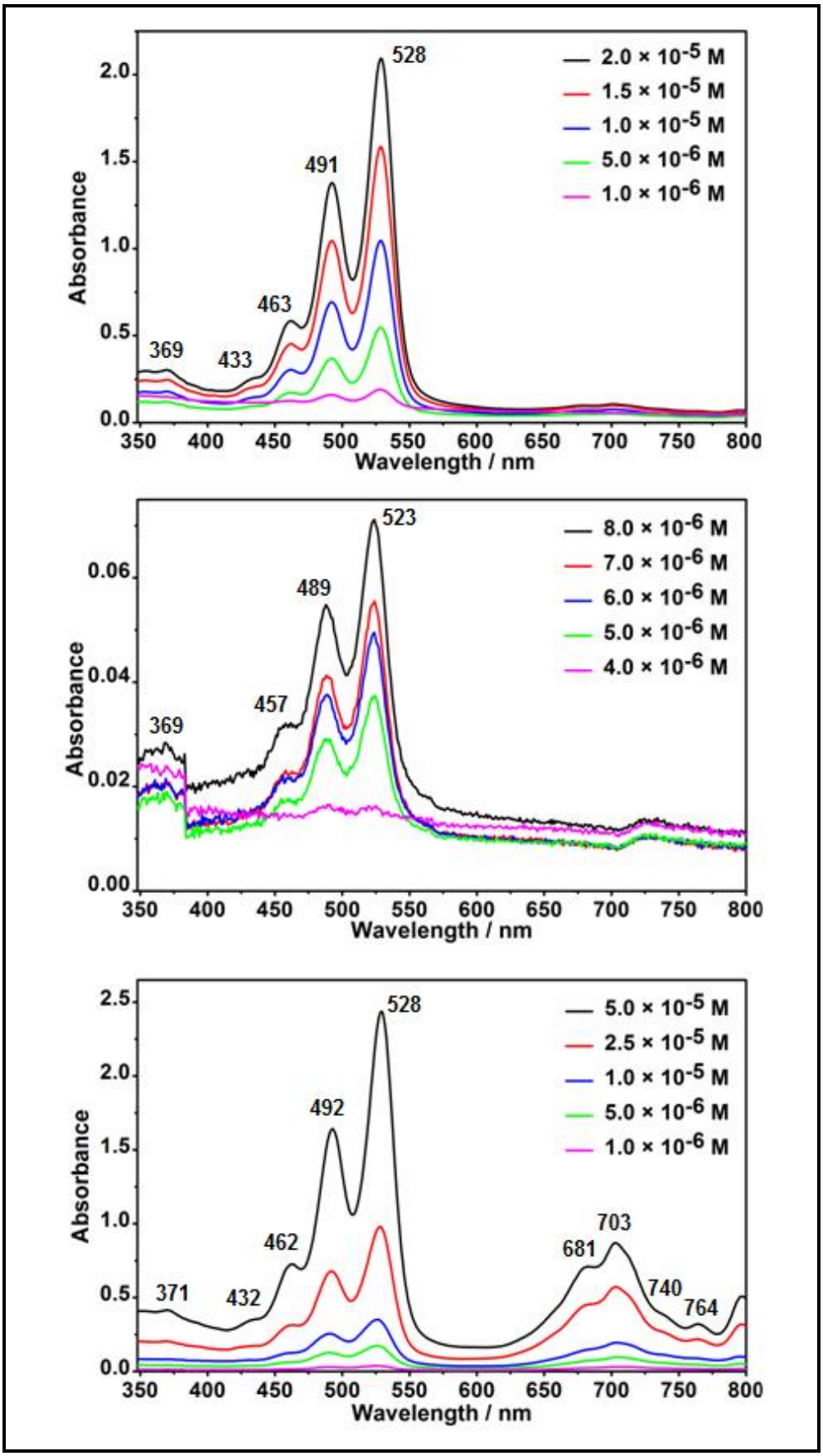

Figure 4.30: Concentration dependent UV measurements of **TPDI** in (a)DMF, (b) MeOH and (c) NMP

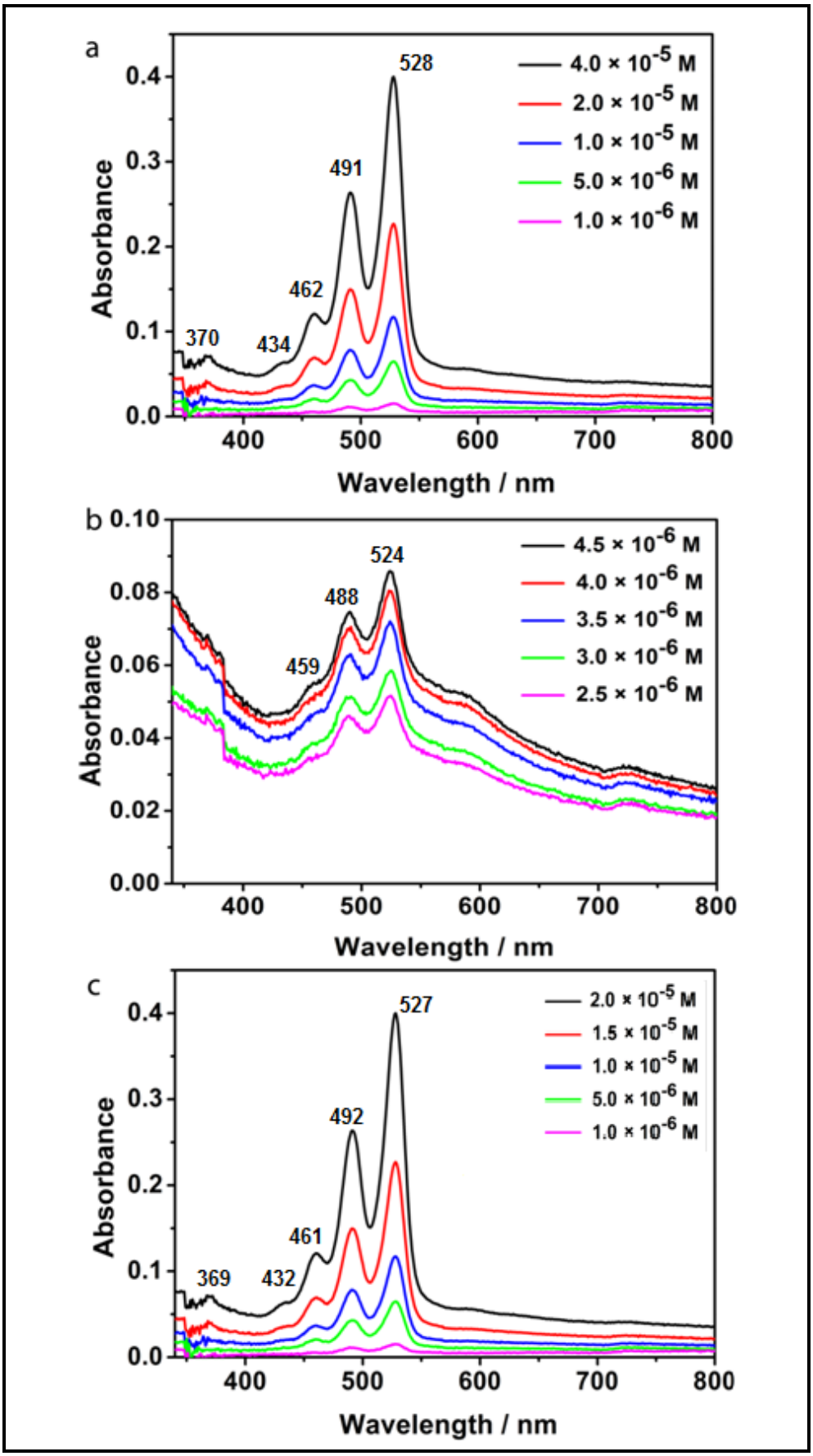

Figure 4.31: Concentration dependent UV spectra of **TPDI** in (a) DCM, (b) EtOH and (c) DMAC

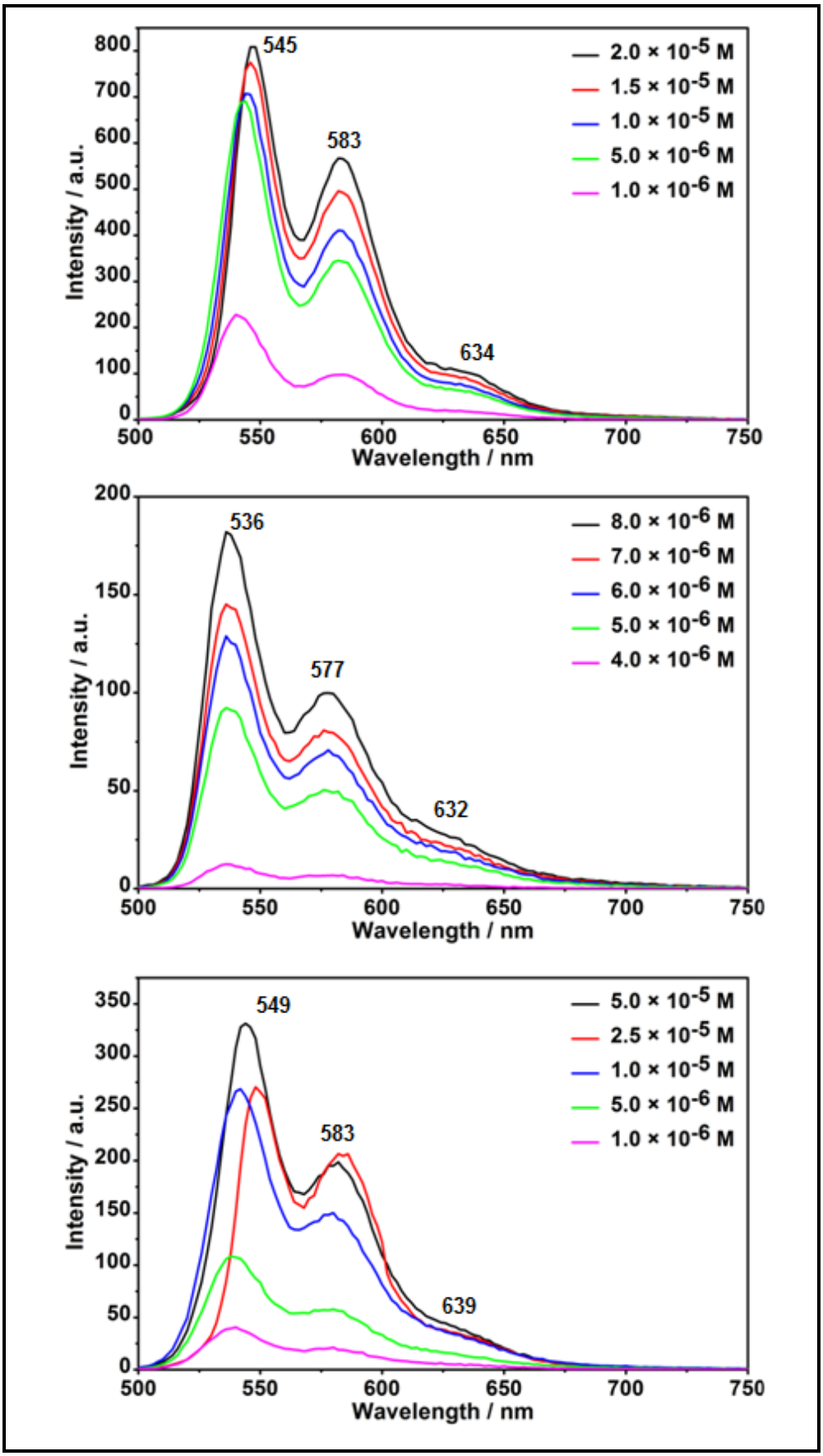

Figure 4.32: Concentration dependent emission spectra of **TPDI** in (a) DMF, (b) MeOH and (d) NMP at excitation wavelength of 485 nm

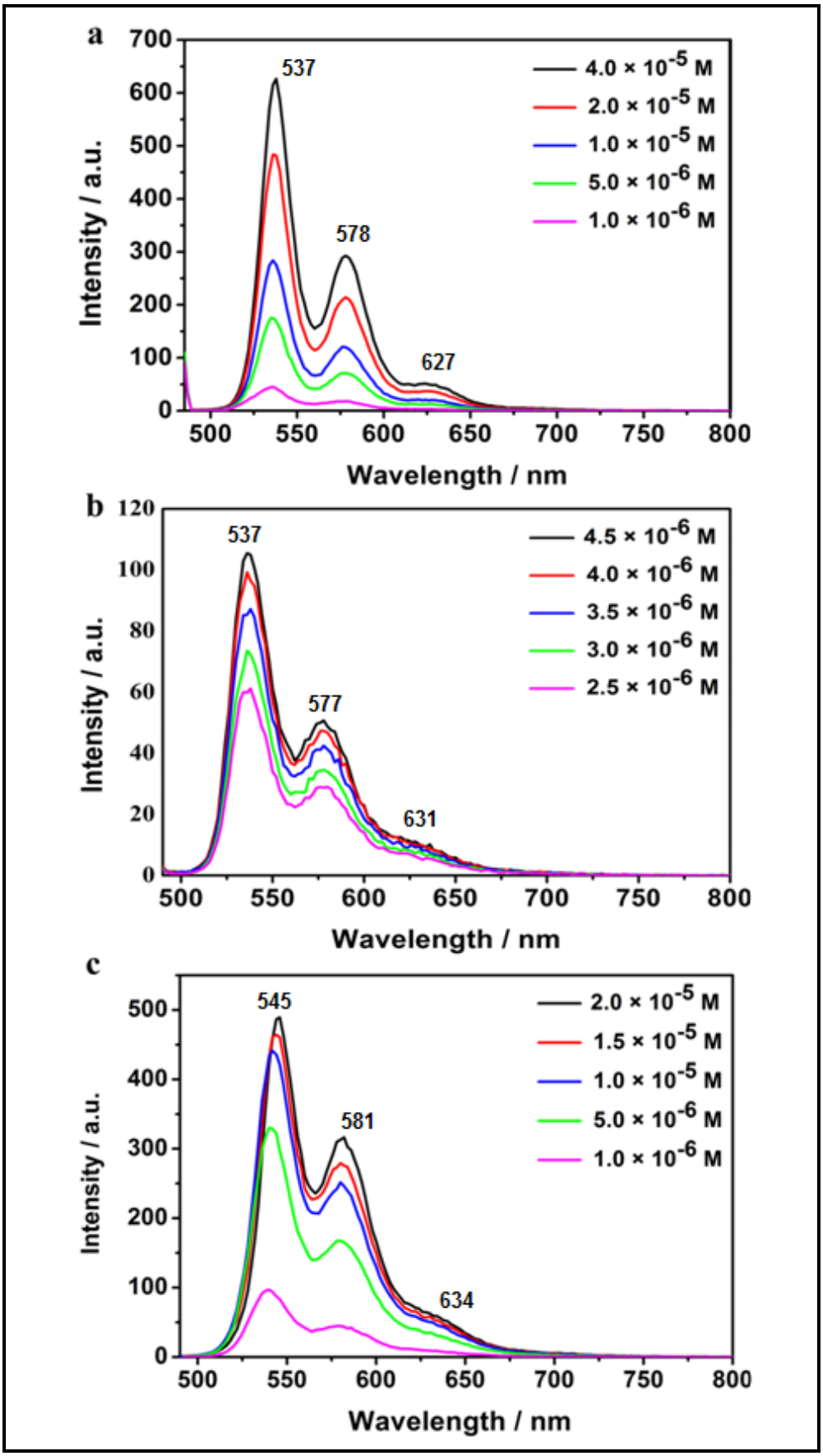

Figure 4.33: Concentration dependent emission spectra of **TPDI** in (a) DCM, (b) EtOH and (d) DMAC at excitation wavelength of 485 nm

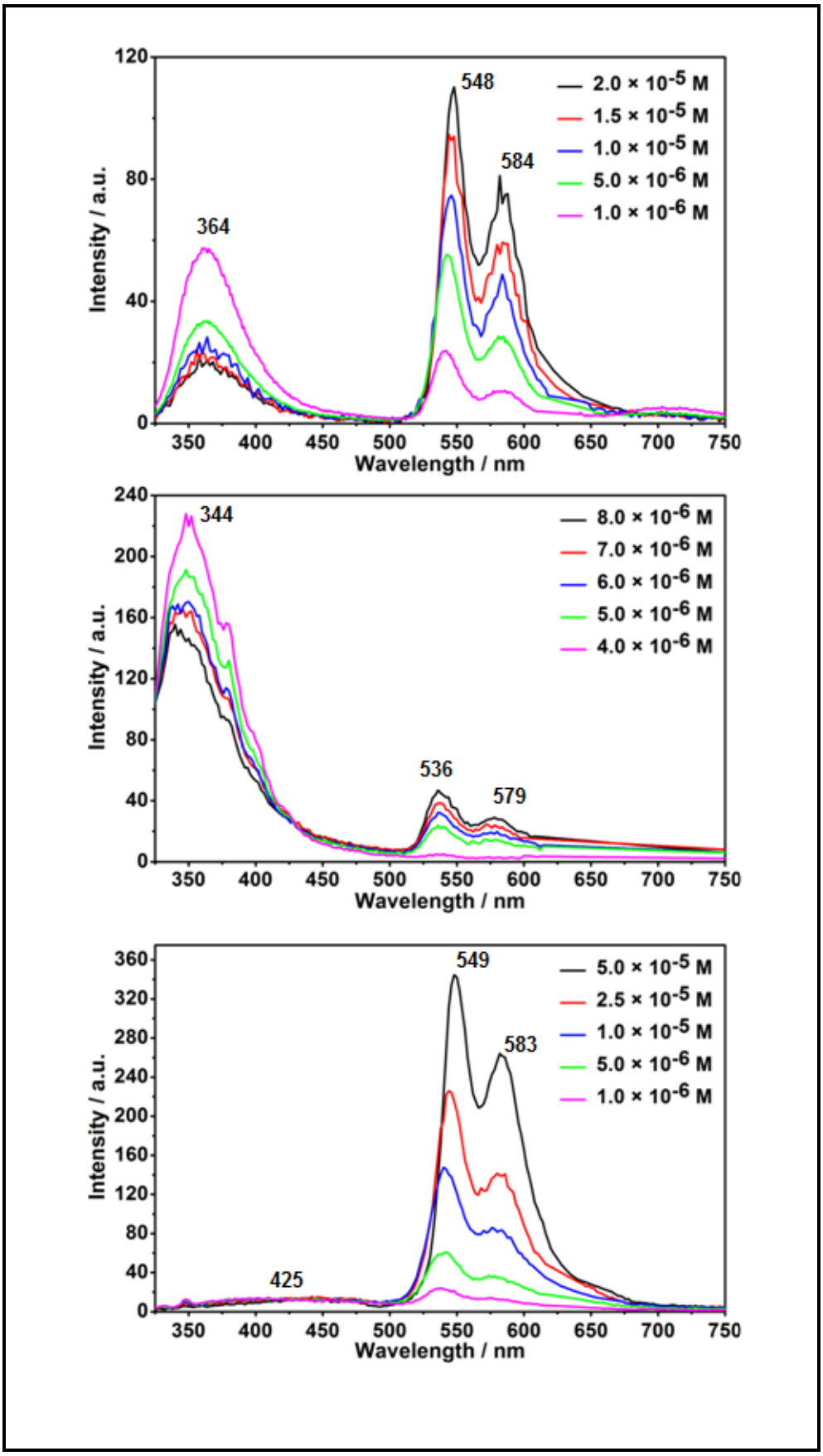

Figure 4.34: Concentration dependent emission spectra of **TPDI** in (a) DMF, (b) MeOH and (d) NMP at excitation wavelength of 315 nm

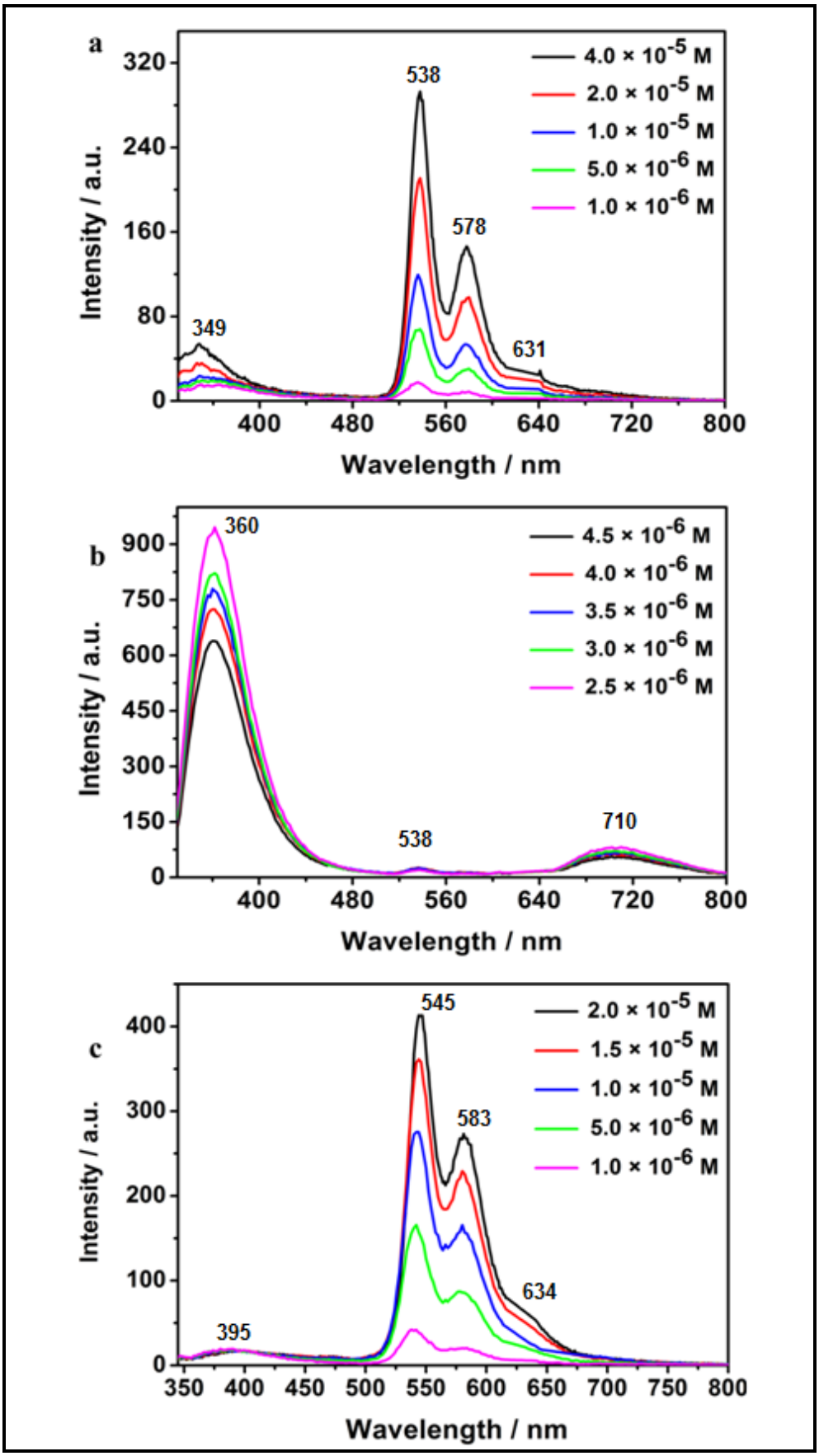

Figure 4.35: Concentration dependent emission spectra of **TPDI** in (a) DCM, (b) EtOH and (d) DMAC at excitation wavelength of 315 nm

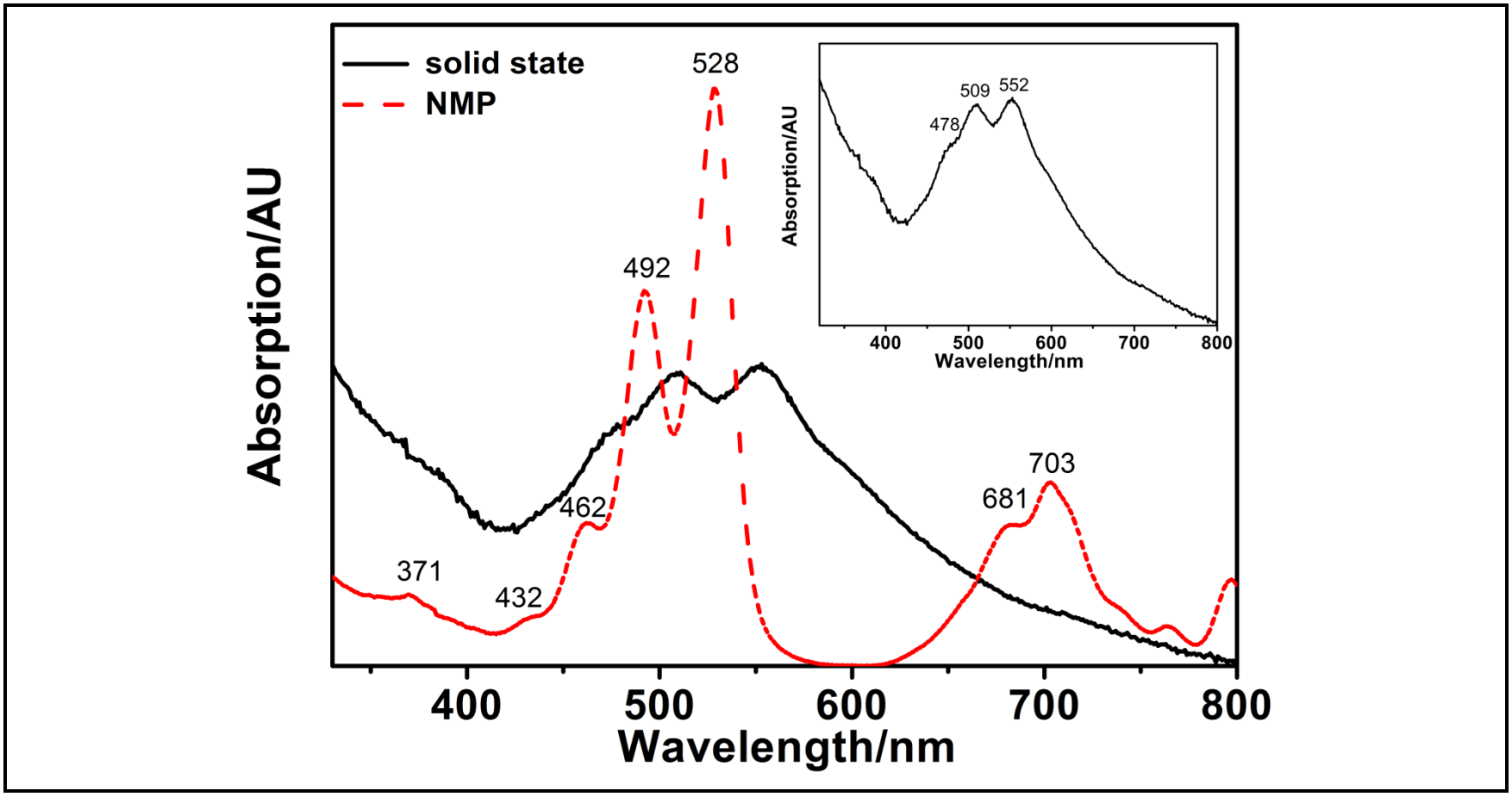

Figure 4.36: Solid-state absorption spectrum of **TPDI** is shown by black color, absorption spectrum of **TPDI** in NMP is shown by red color, in set shows absorption spectrum with wavelengths

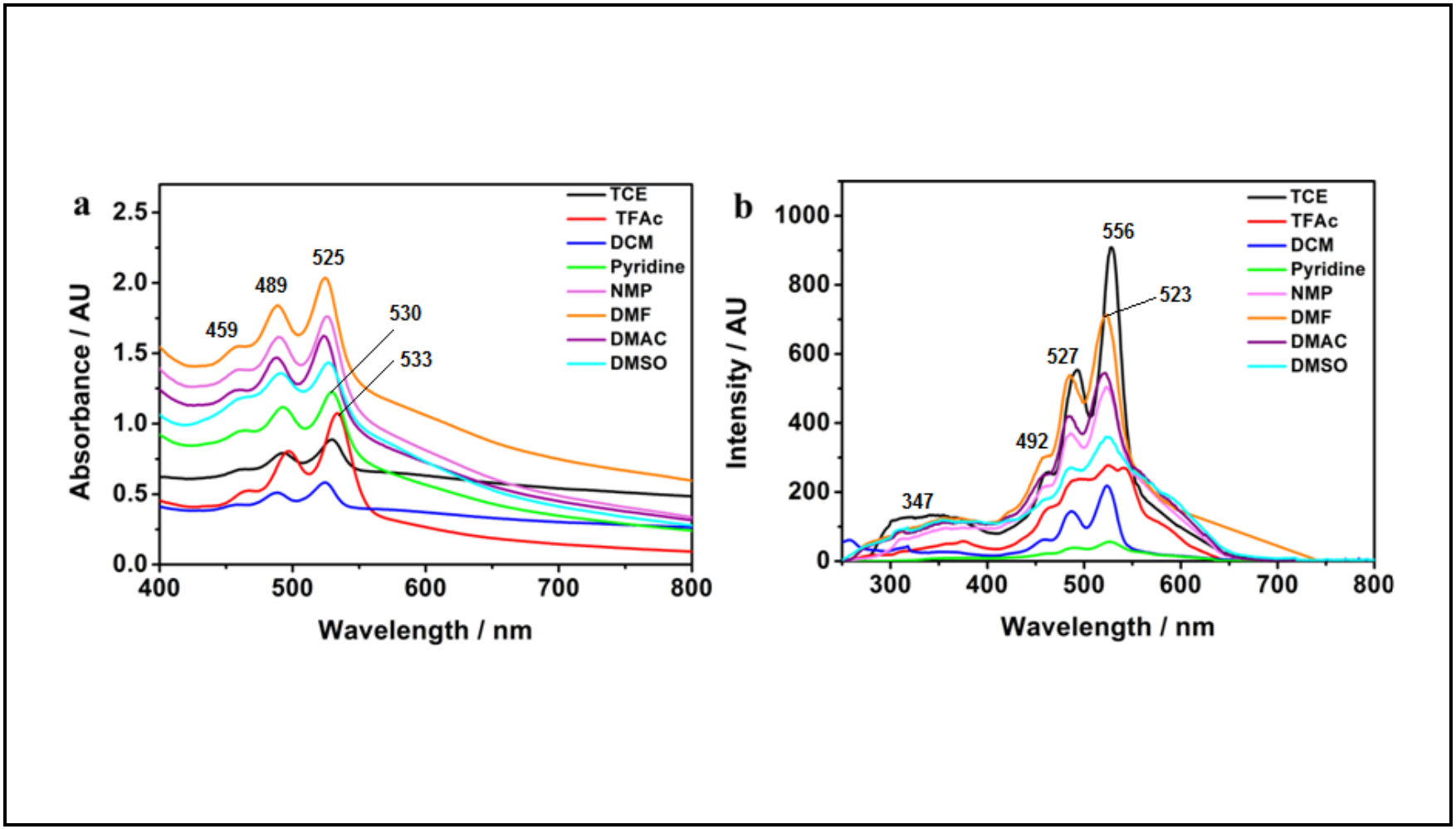

Figure 4.37: (a) **TCPDI** absorption spectra in different solvents. (b) Excitation spectra at emission wavelength of 620 nm in different solvents

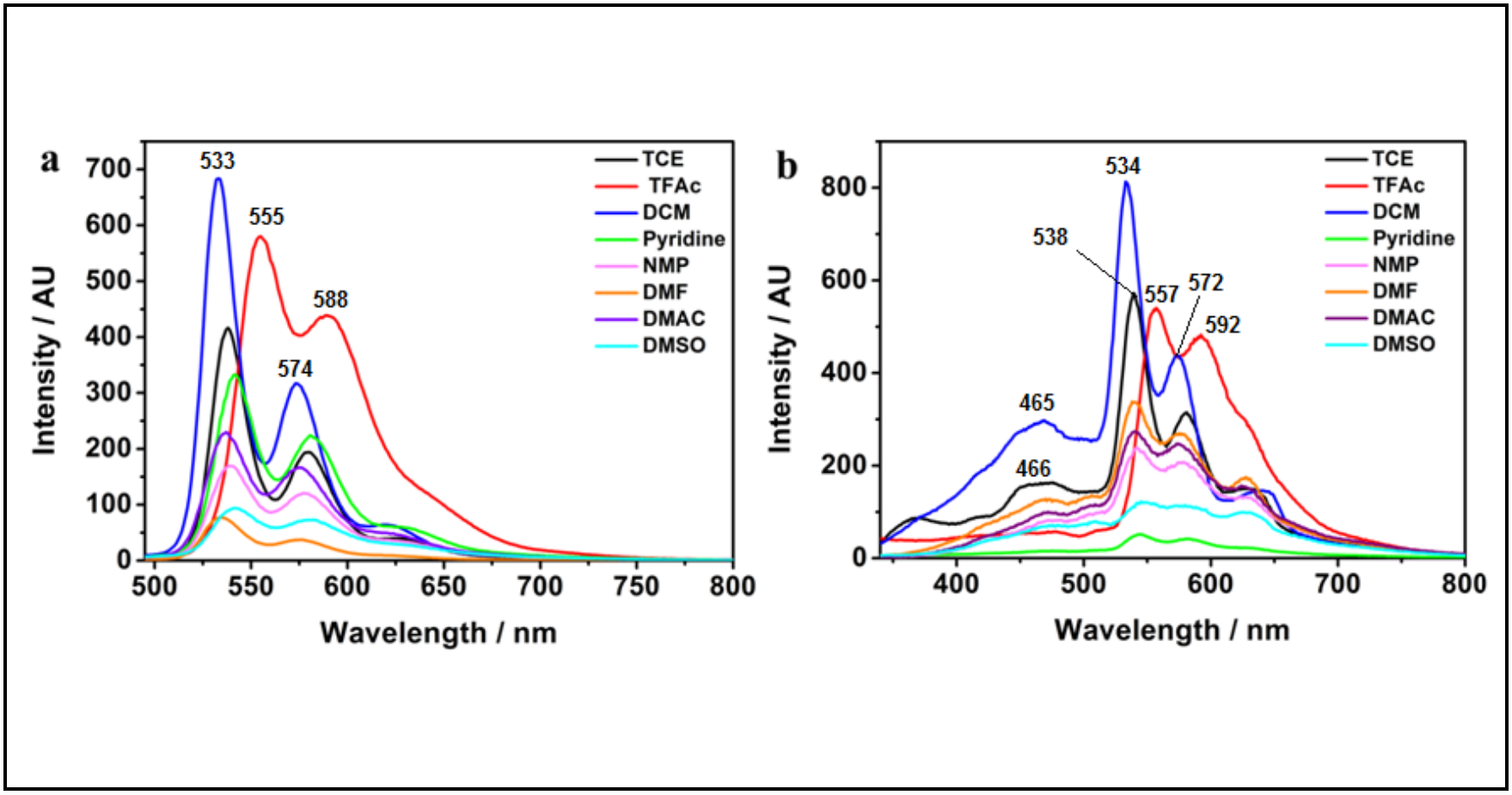

Figure 4.38: Emission spectra of **TCPDI** at (a) Excitation wavelength of 485 nm (b) Excitation wavelength of 315 nm

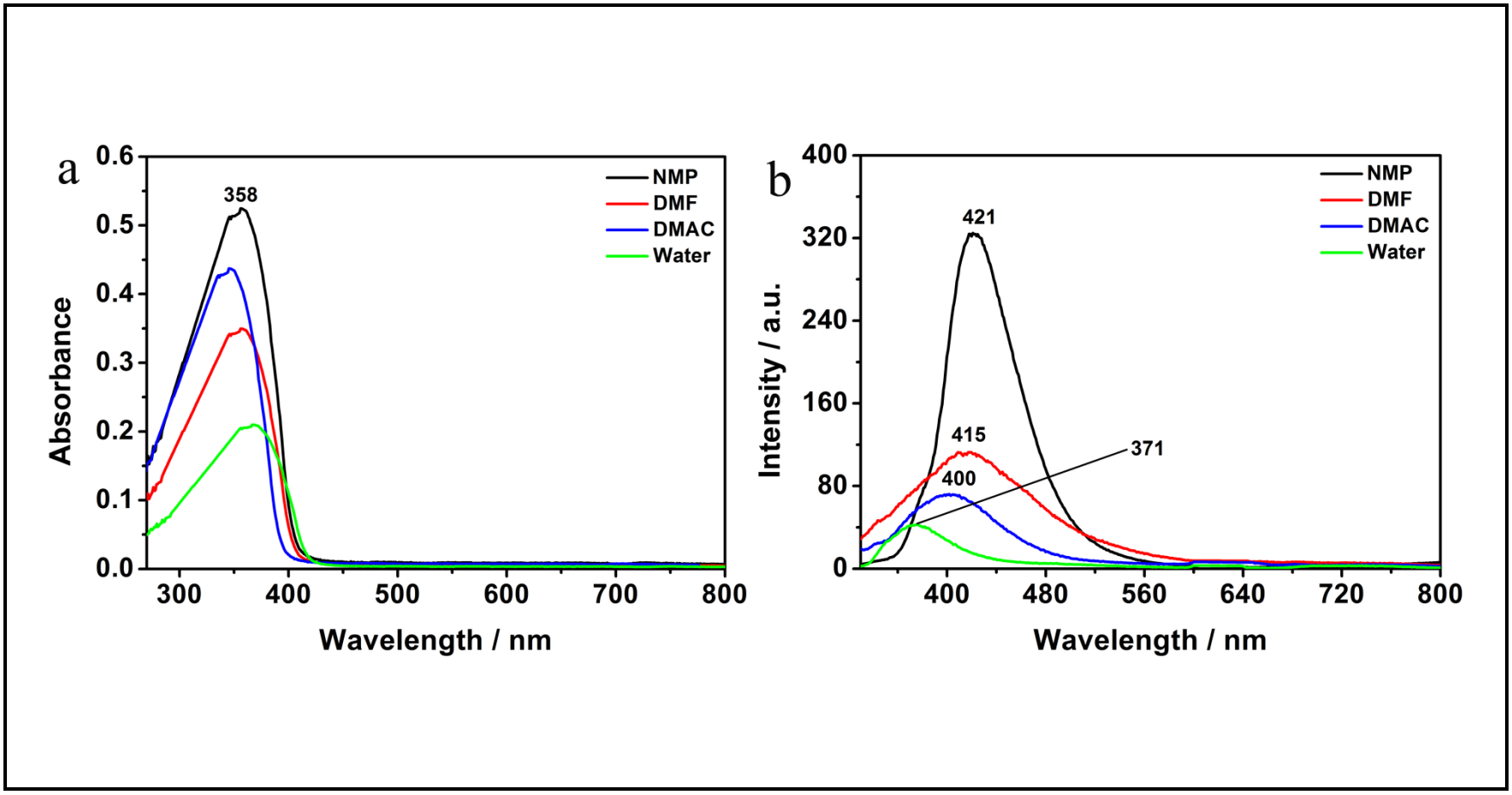

Figure 4.39: (a) Absorption spectra of Vitamin and (b) Emission spectra of Vitamin at excitation wavelength of 310 nm

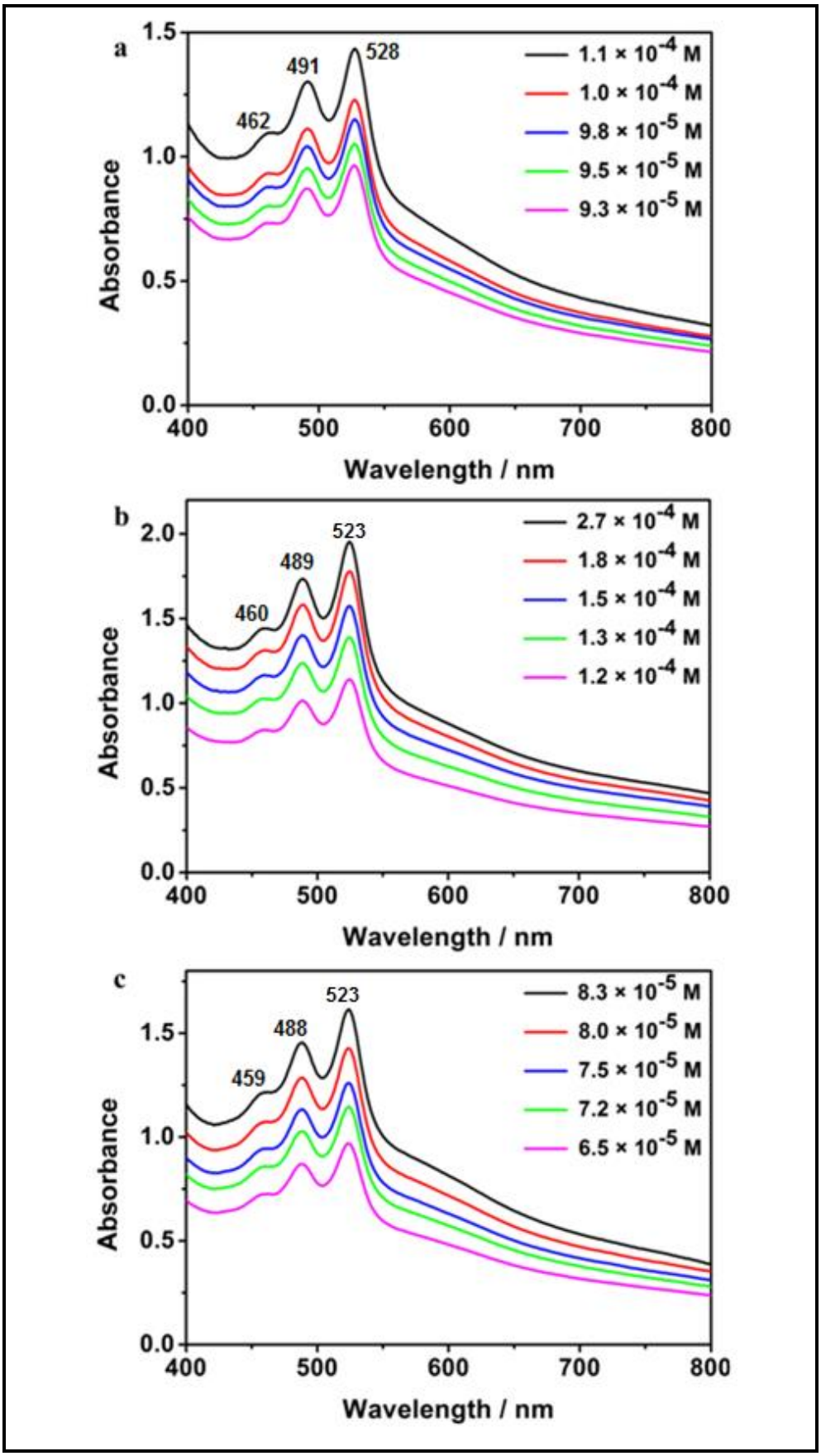

Figure: 4.40: Concentration dependent UV spectra of **TCPDI** in (a) NMP, (b) DMF and (c) DMAC

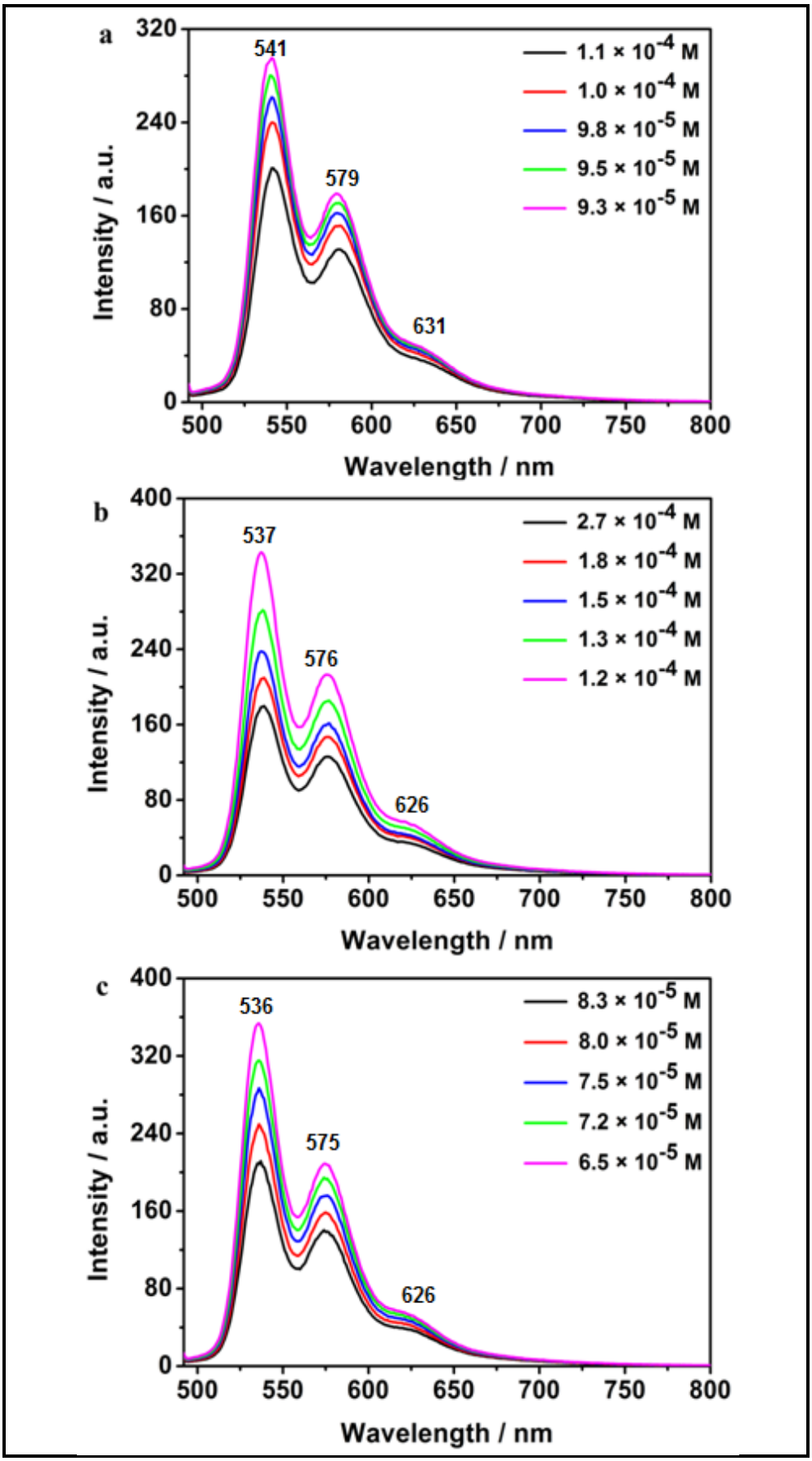

Figure 4.41: Concentration dependent emission spectra of **TCPDI** in (a) NMP, (b) DMF and (d) DMAC at excitation wavelength of 485 nm

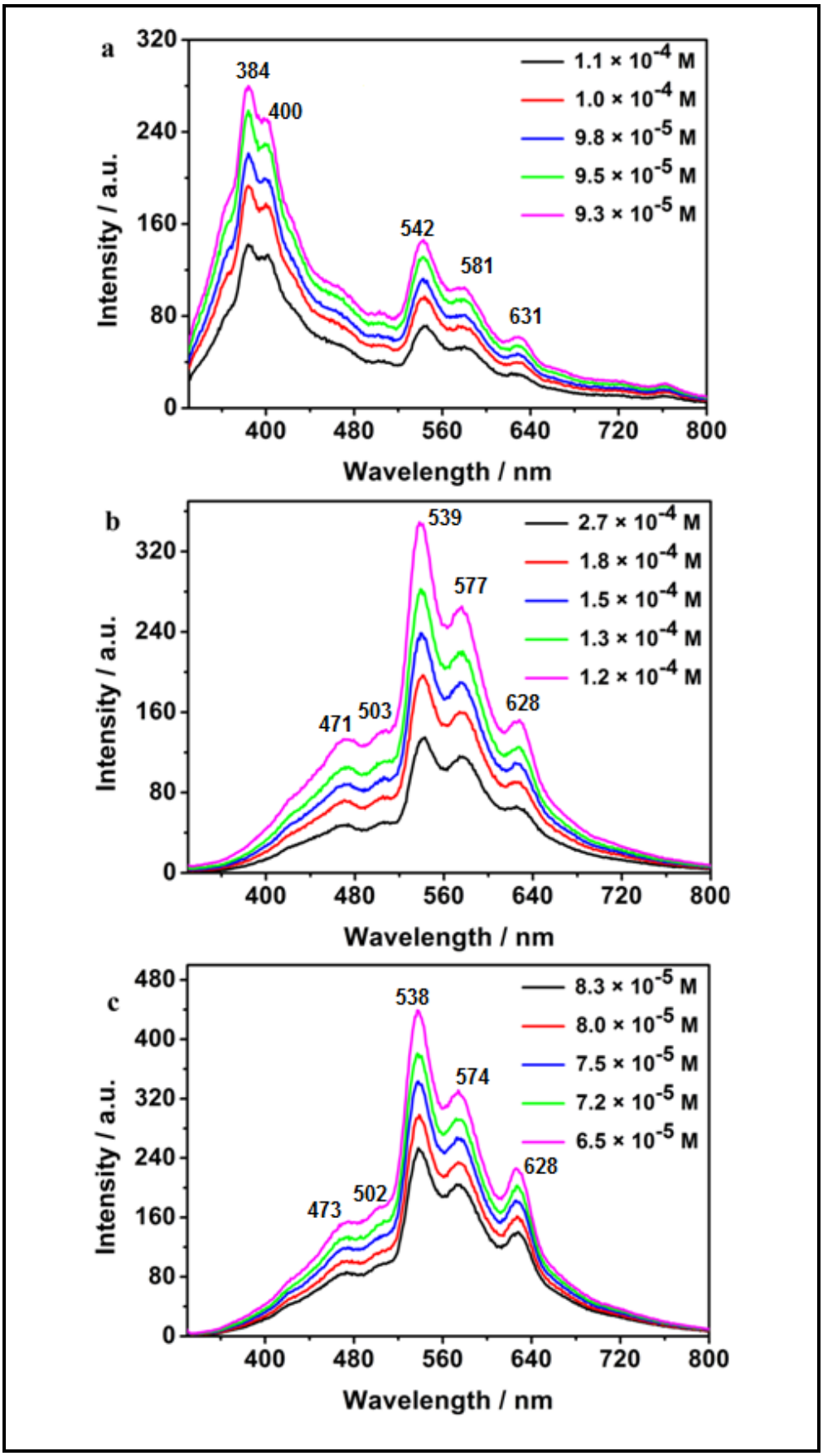

Figure 4.42: Concentration dependent emission spectra of **TCPDI** in (a) NMP, (b) DMF and (d) DMAC at excitation wavelength of 315 nm

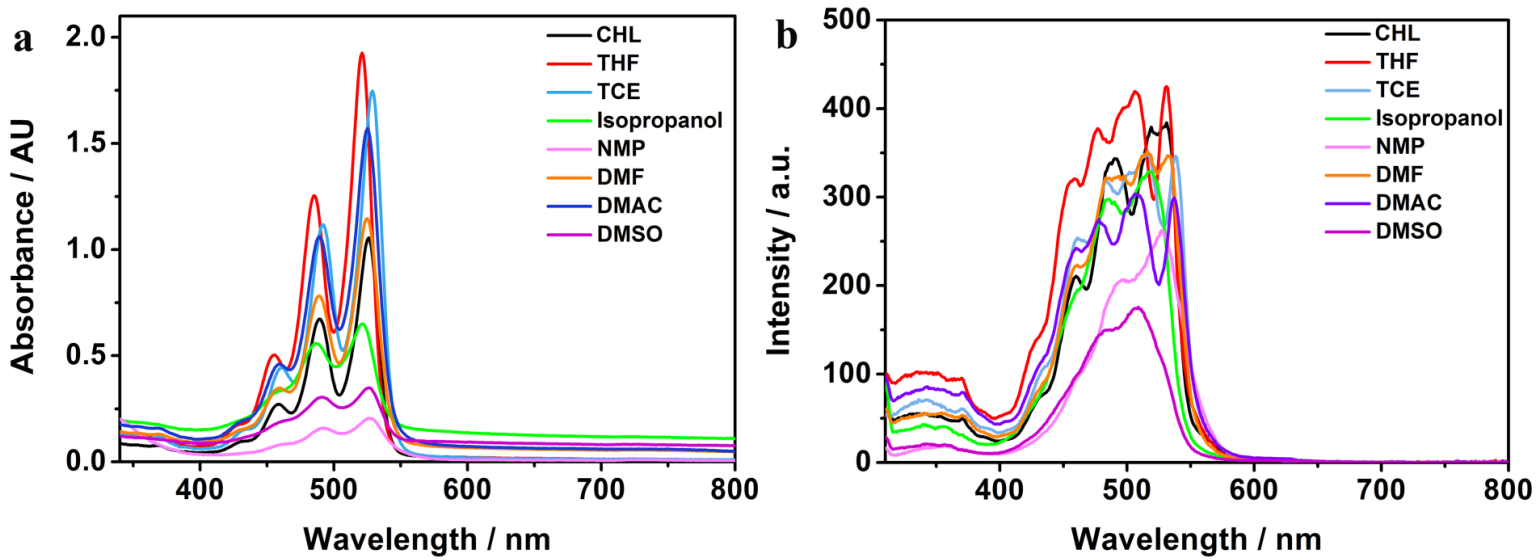

Figure 4.43: (a) **TAPDI**, UV spectra in different solvents. (b) Excitation spectra at emission wavelength of 620 nm in different solvents

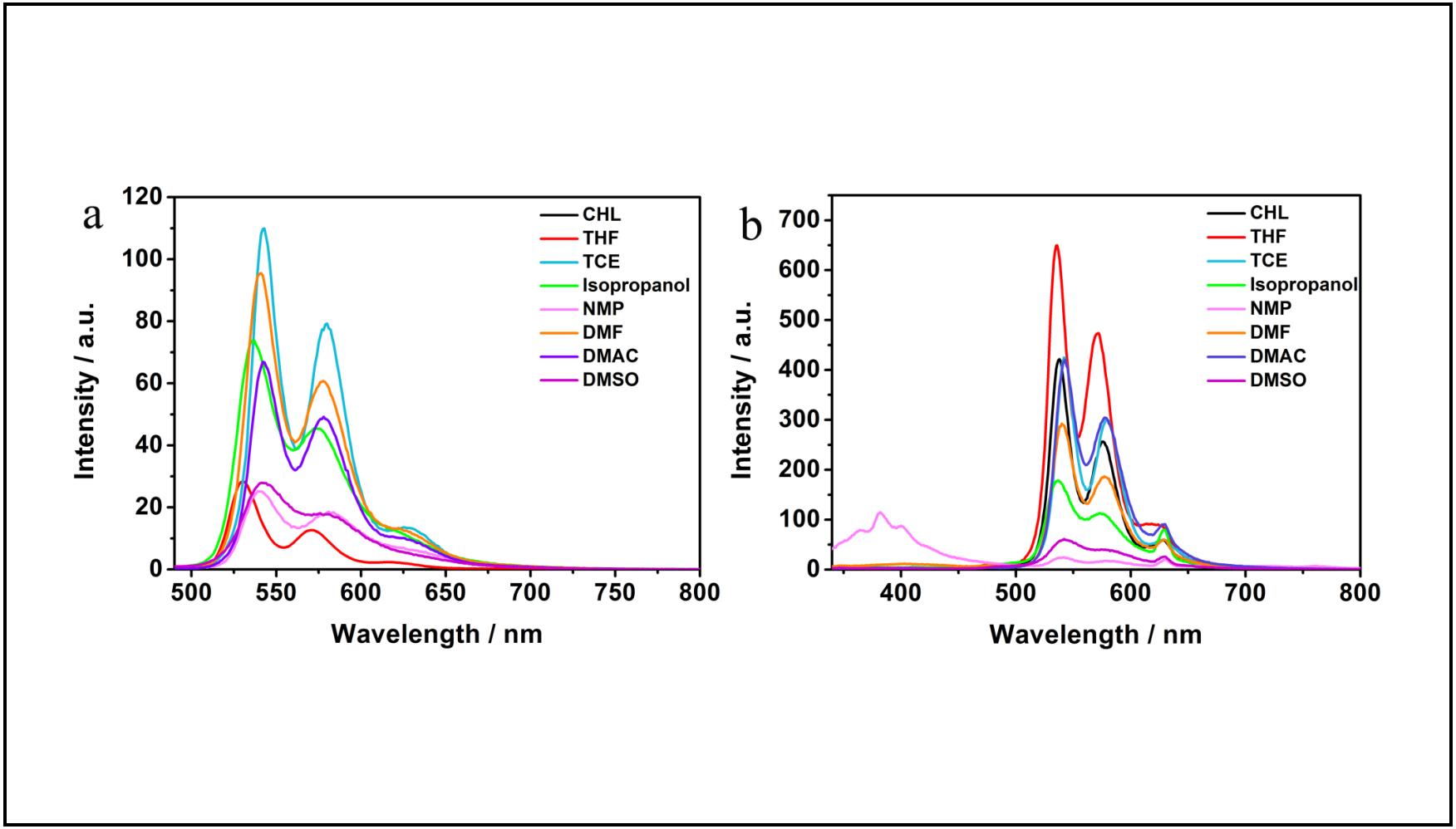

Figure 4.44: Emission spectra of **TAPDI** at (a) Excitation wavelength of 485 nm (b) Excitation wavelength of 315 nm

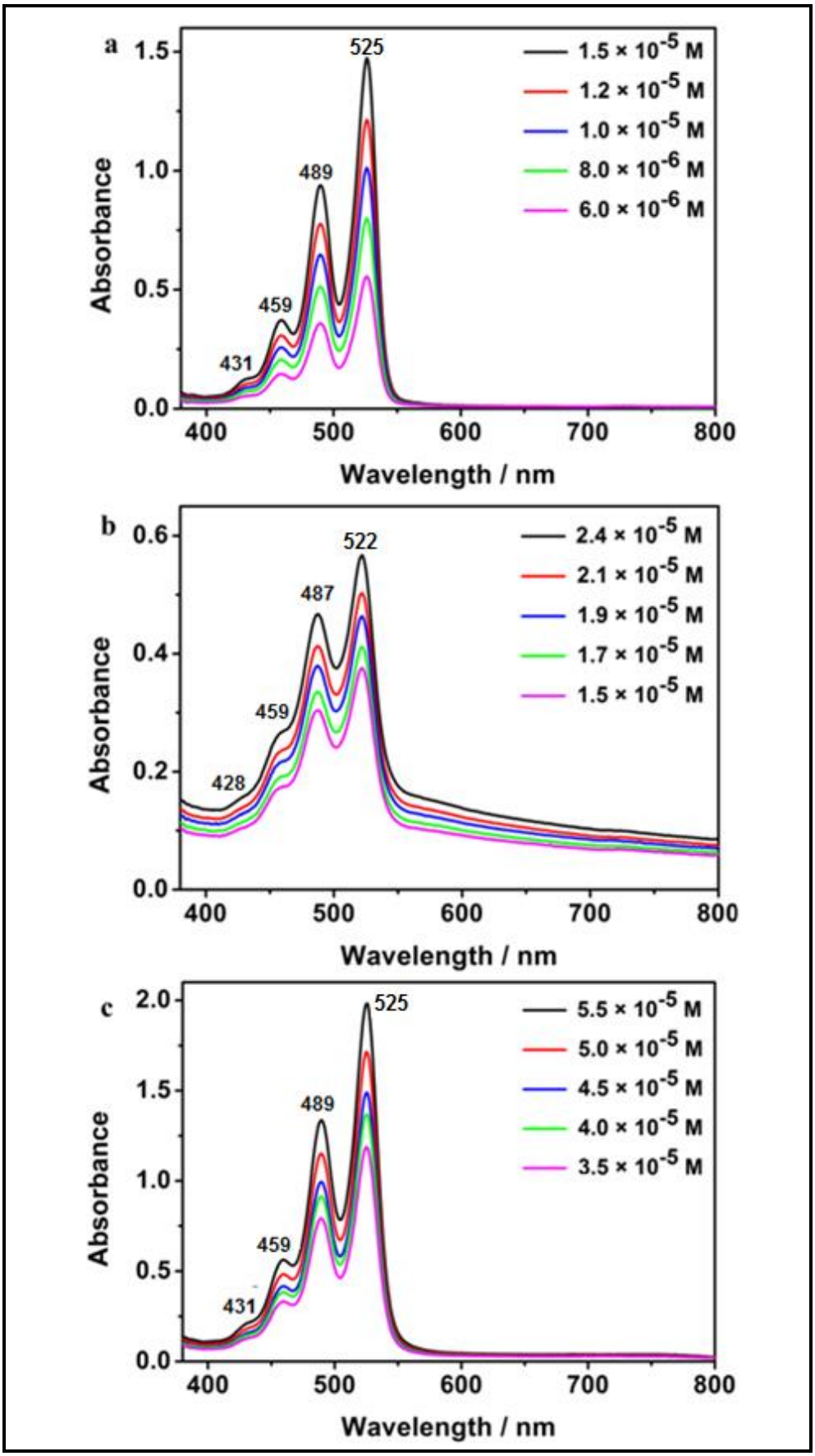

Figure 4.45: Concentration dependent UV spectra of **TAPDI** in (a) CHL, (b) Isopropanol and (c) DMAC

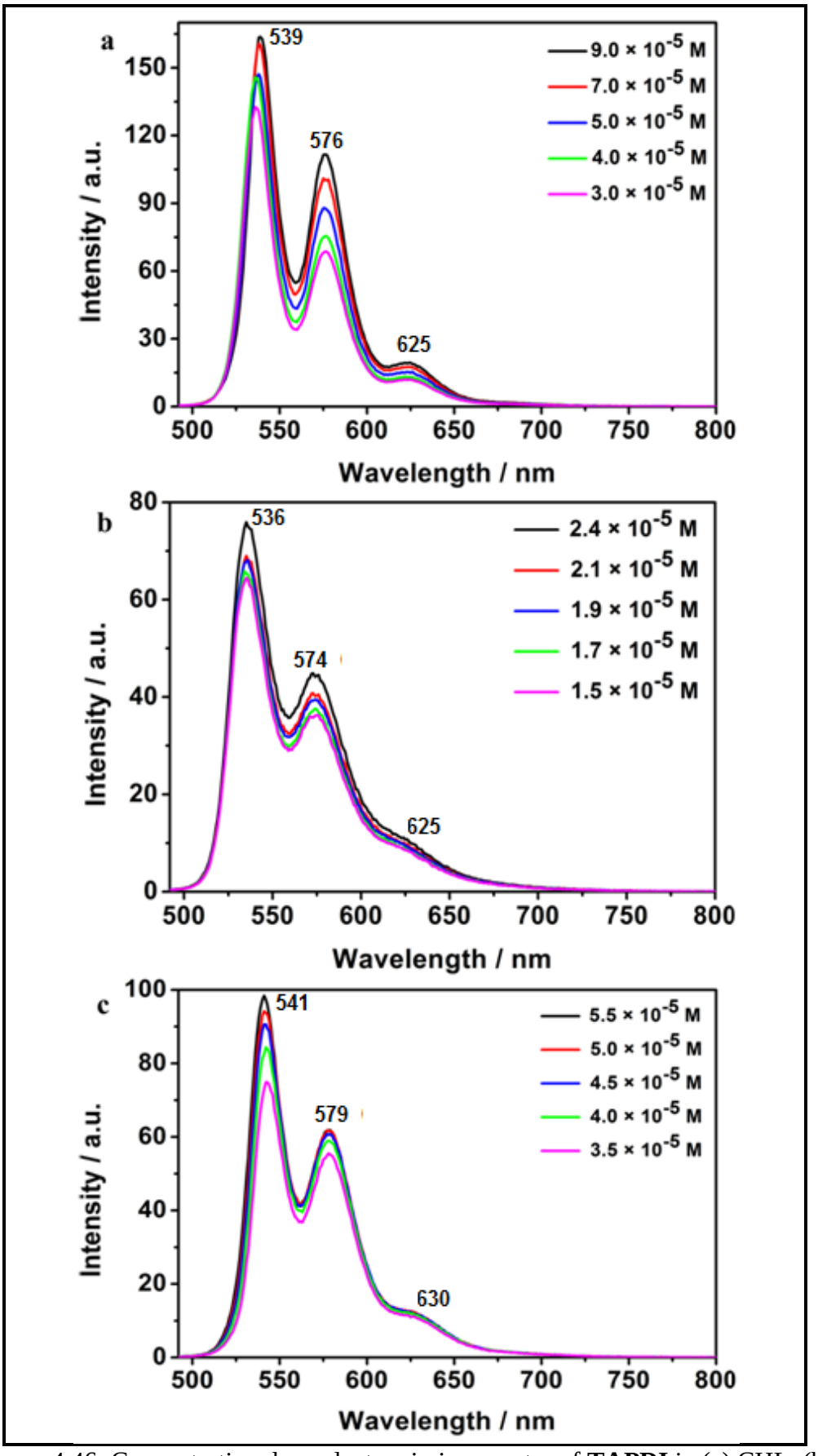

Figure 4.46: Concentration dependent emission spectra of **TAPDI** in (a) CHL, (b) Isopropanol and (c) DMAC at excitation wavelength of 485 nm

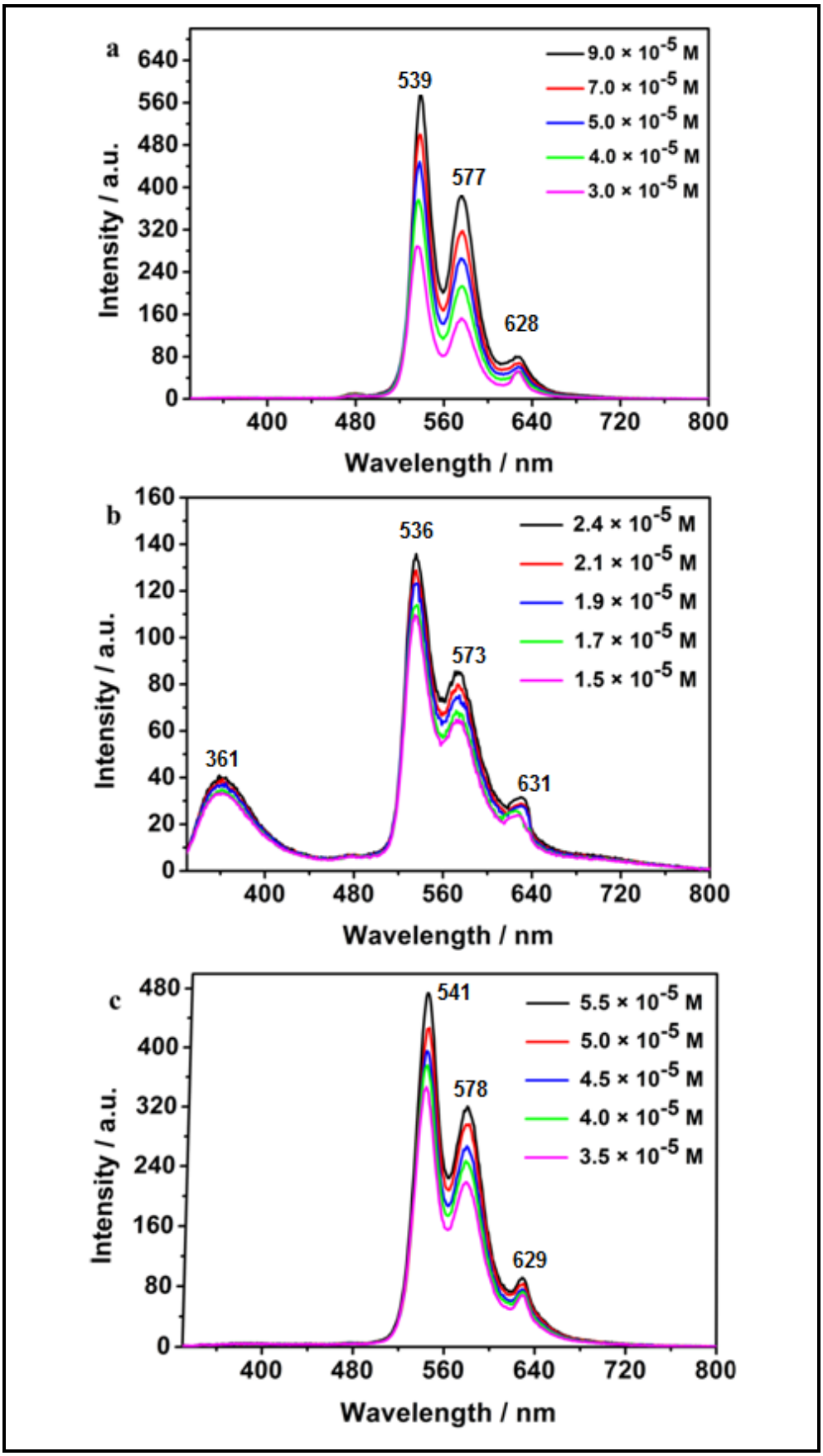

Figure 4.47: Concentration dependent emission spectra of **TAPDI** in (a) CHL, (b) Isopropanol and (c) DMAC at excitation wavelength of 315 nm

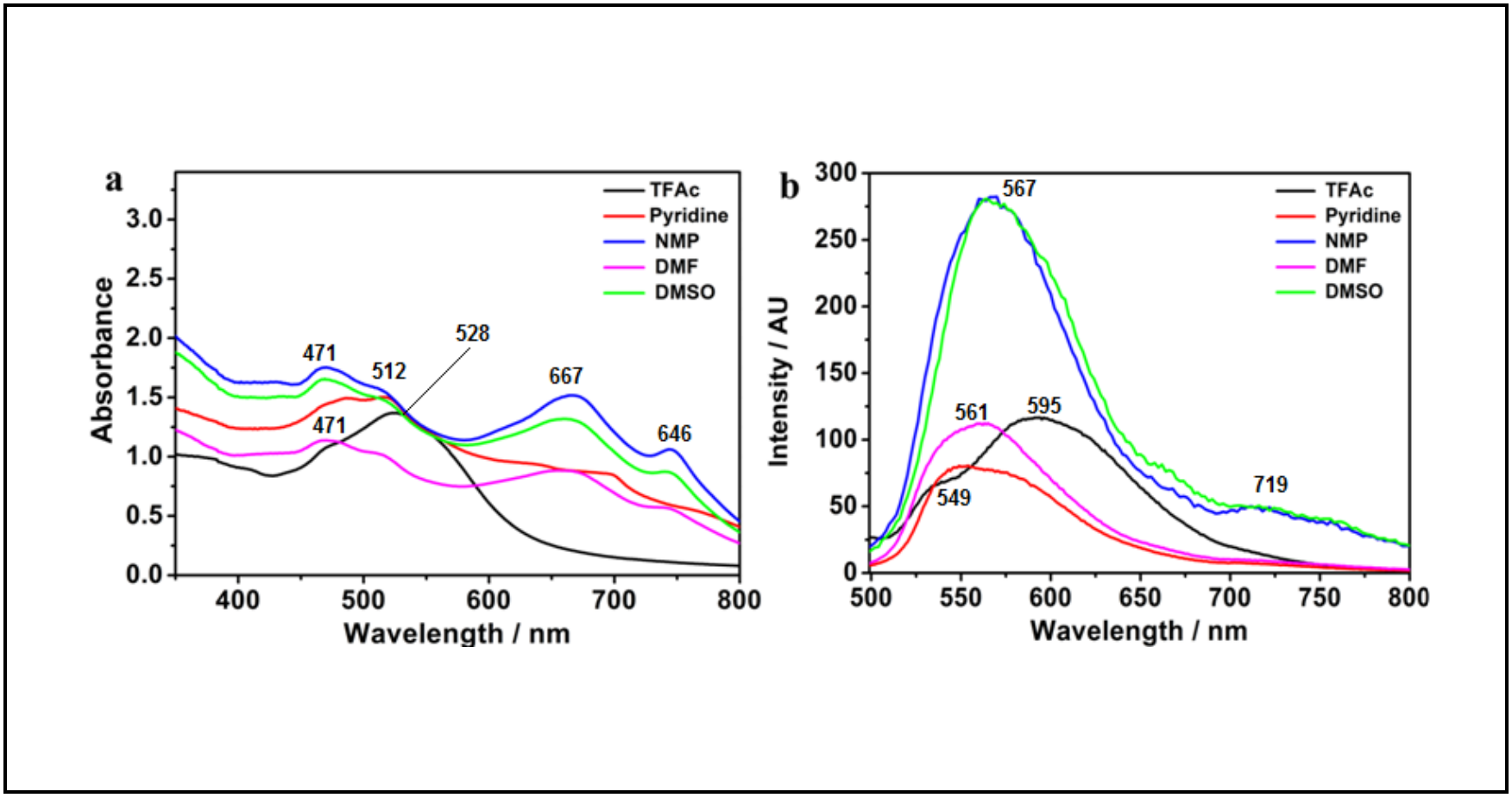

Figure 4.48: (a) UV spectra of **BPY-PDA** and (b) Emission spectra at excitation wavelength of 485 nm in different solvents

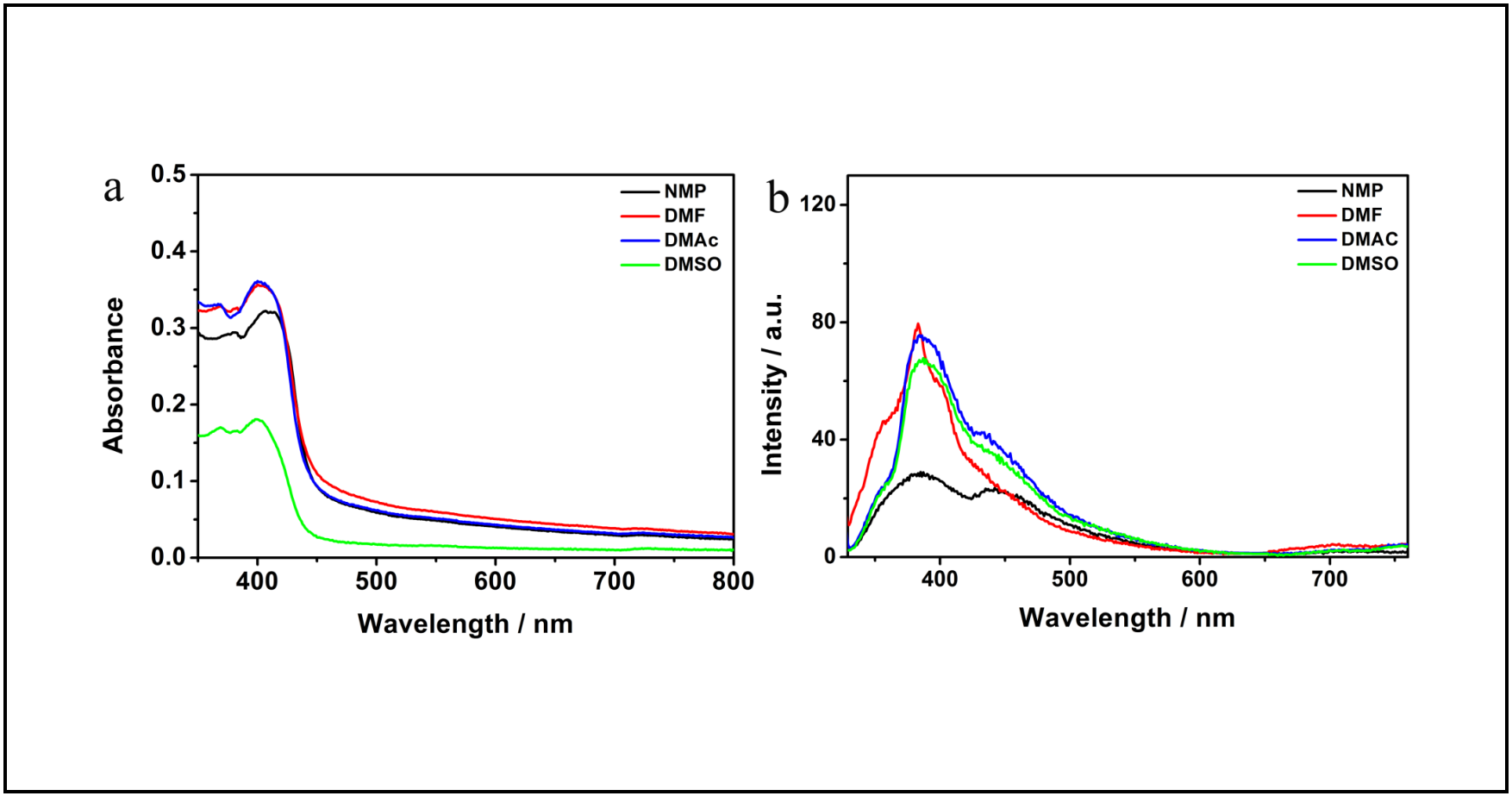

Figure 4.49: (a) UV spectra of **Pyrimidine** and (b) Emission spectra at excitation wavelength of 310 nm in different solvents

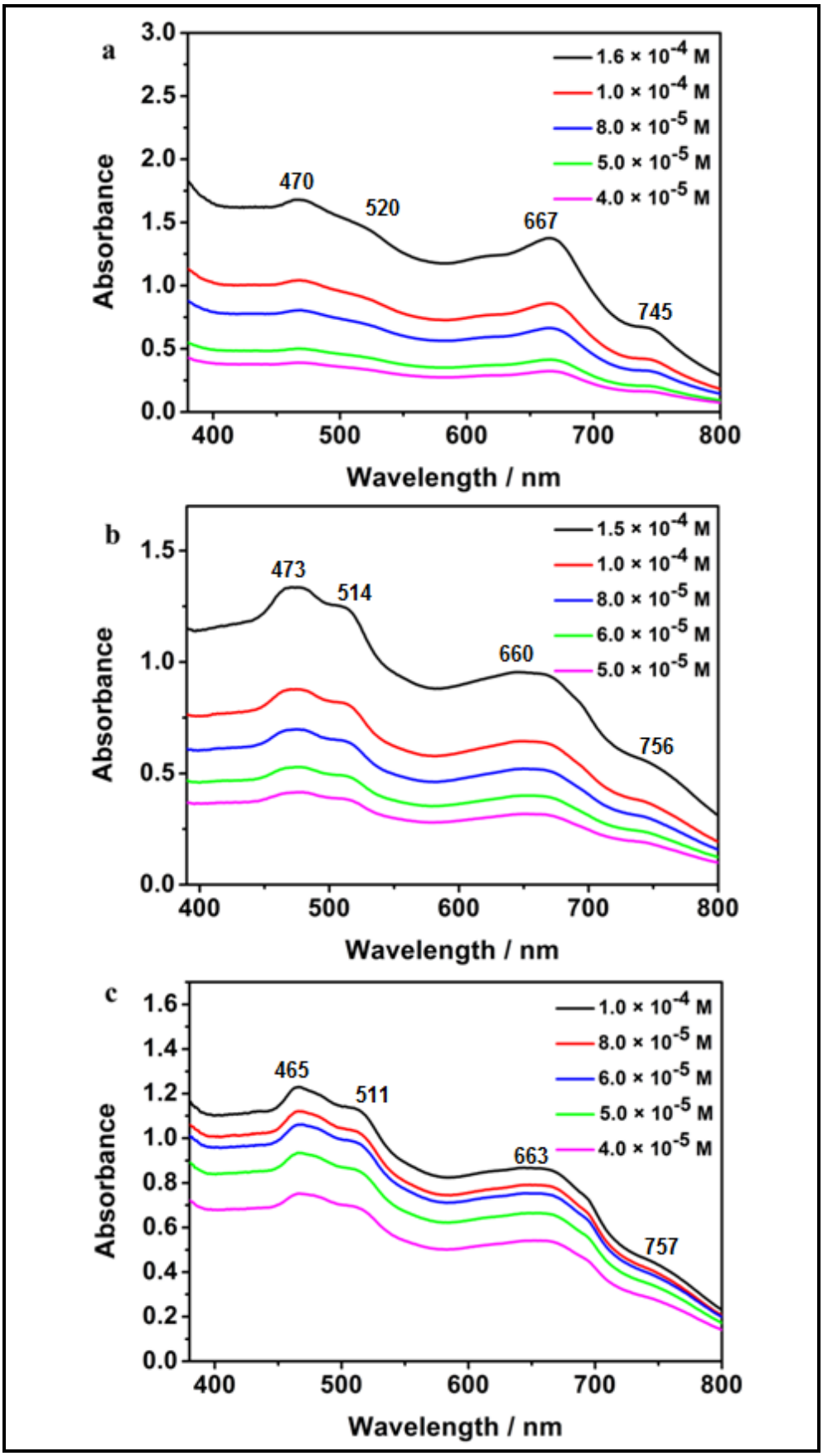

Figure 4.50: Concentration dependent UV spectra of **BPY-PDA** in (a) NMP, (b) DMF and (c) DMAC

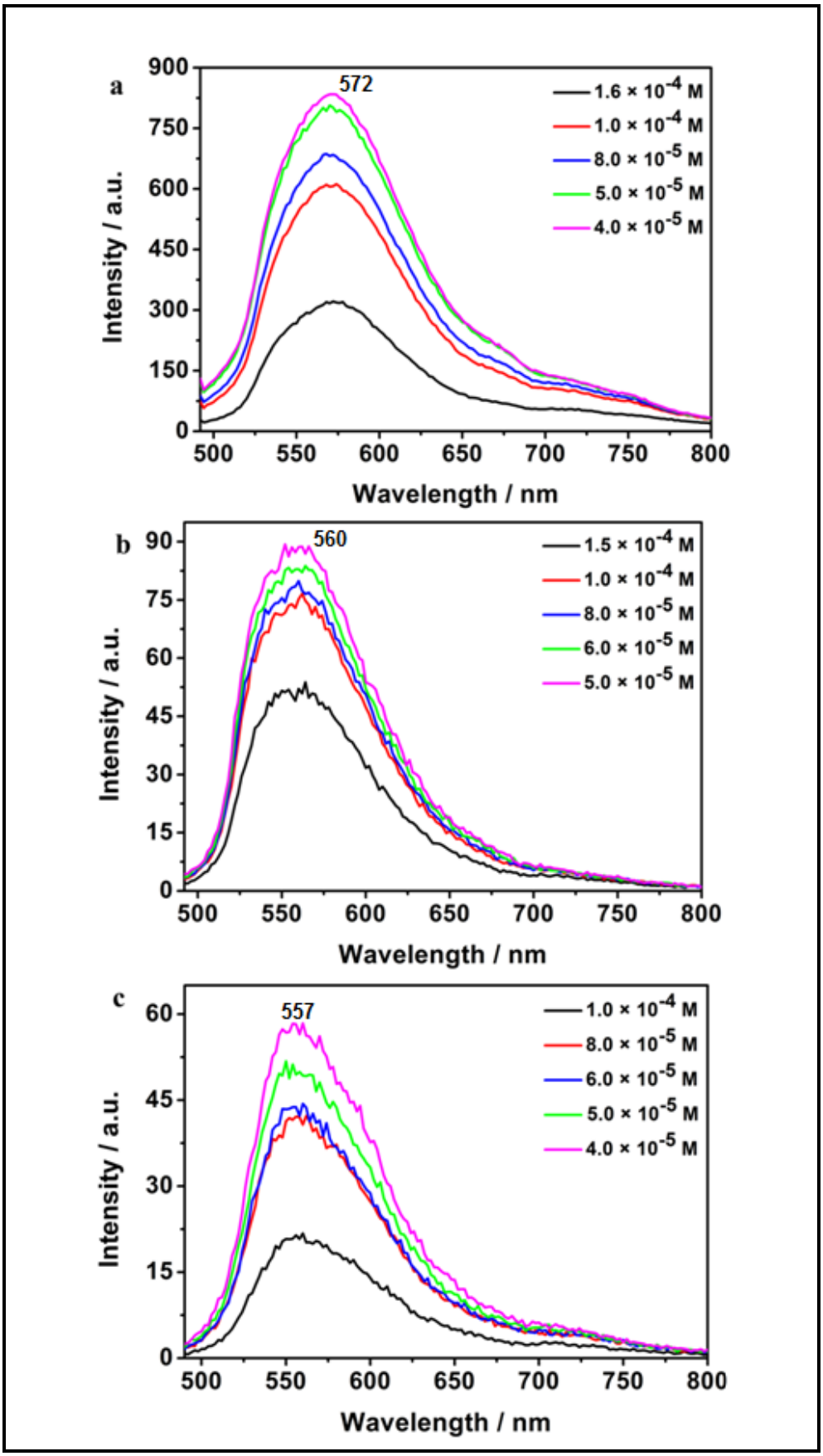

Figure 4.51: Concentration dependent emission spectra of **BPY-PDA** in (a) NMP, (b) DMF and (c) DMAC at excitation wavelength of 485 nm

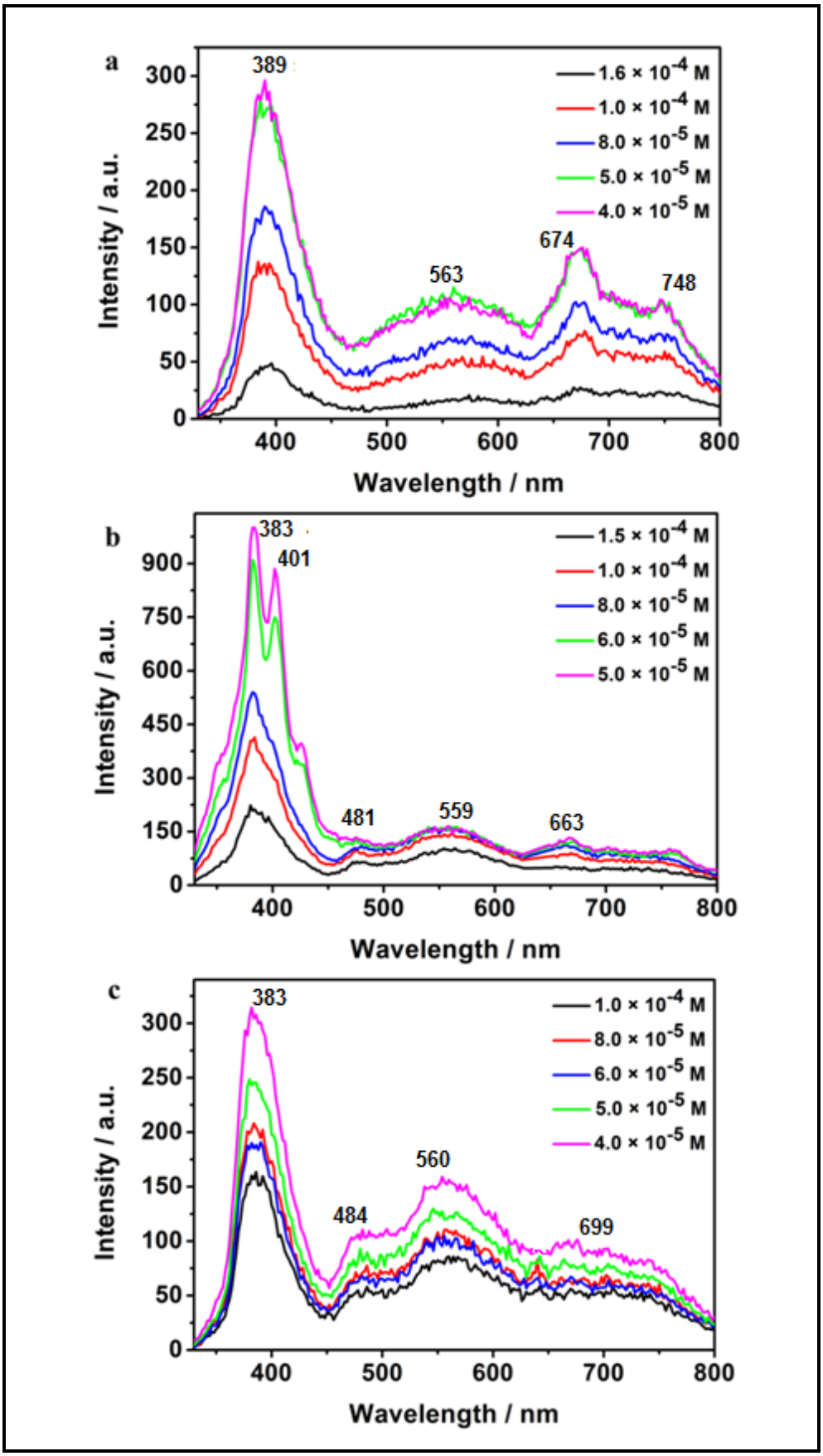

Figure 4.52: Concentration dependent emission spectra of **BPY-PDA** in (a) NMP, (b) DMF and (c) DMAC at excitation wavelength of 315 nm

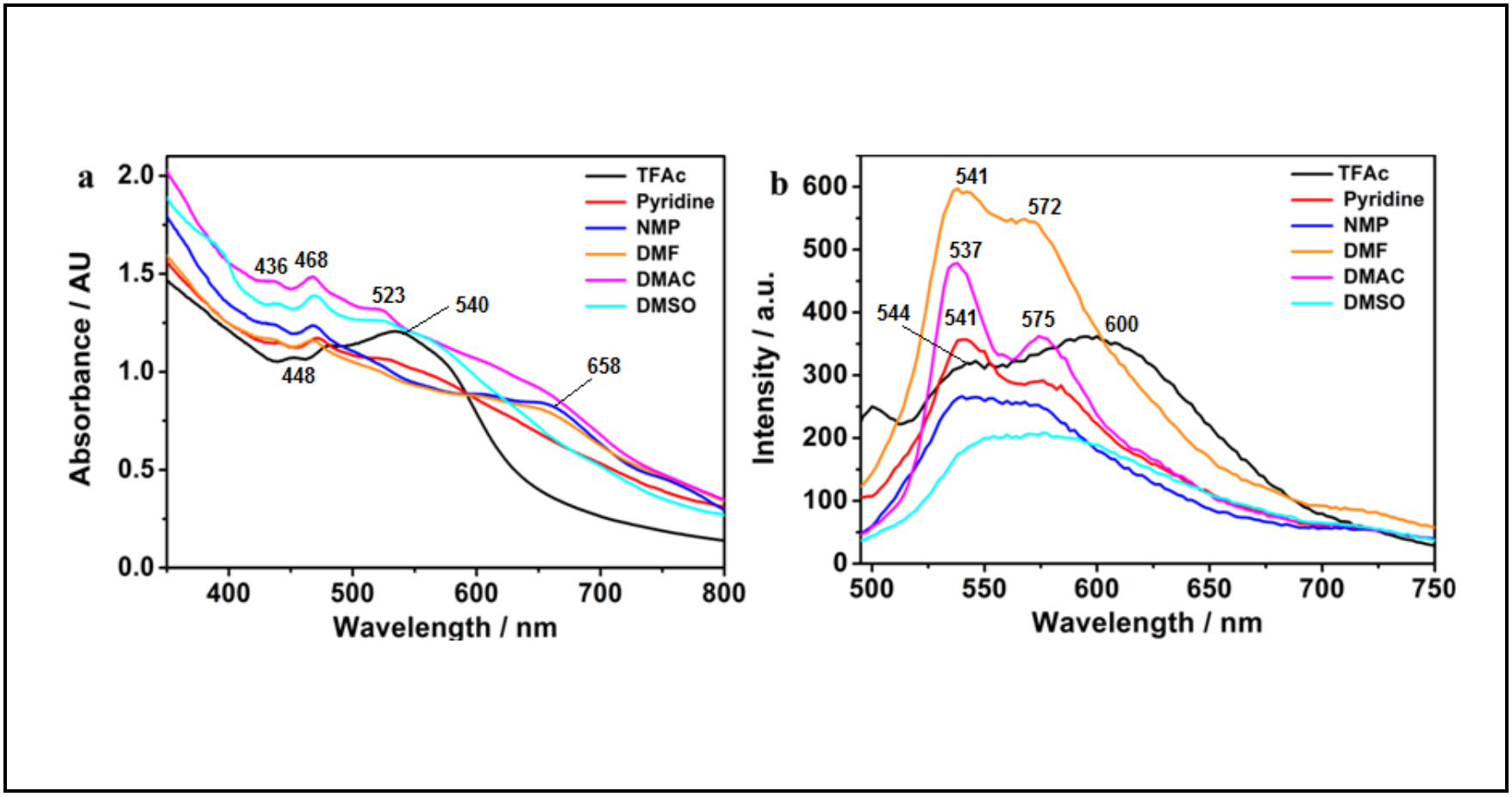

Figure 4.53: (a) UV spectra of **BPY-PPDI** and (b) Emission spectra at excitation wavelength of 485 nm in different solvents

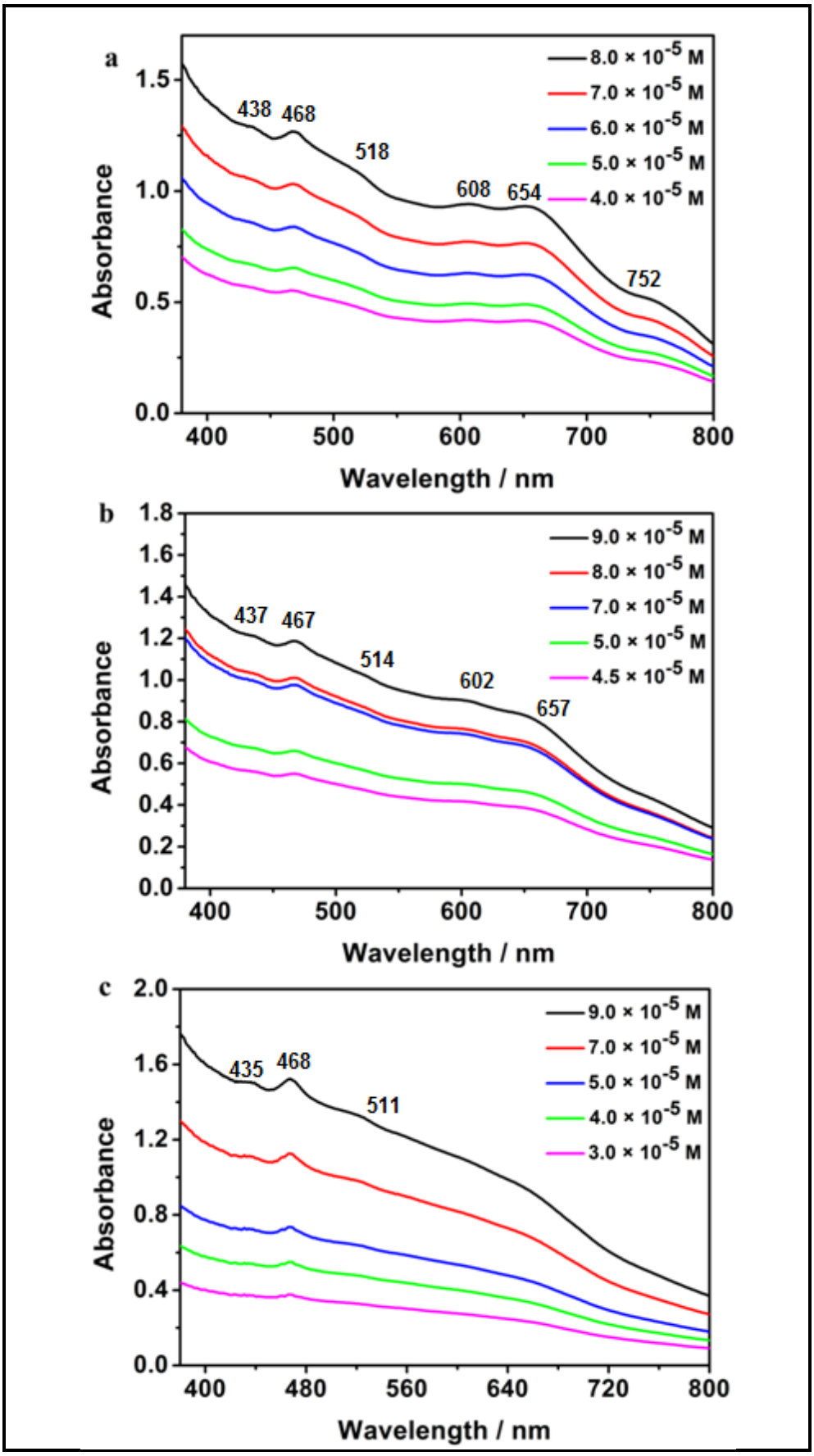

Figure 4.54: Concentration dependent UV spectra of **BPY-PPDI** in (a) NMP, (b) DMF and (c) DMAC

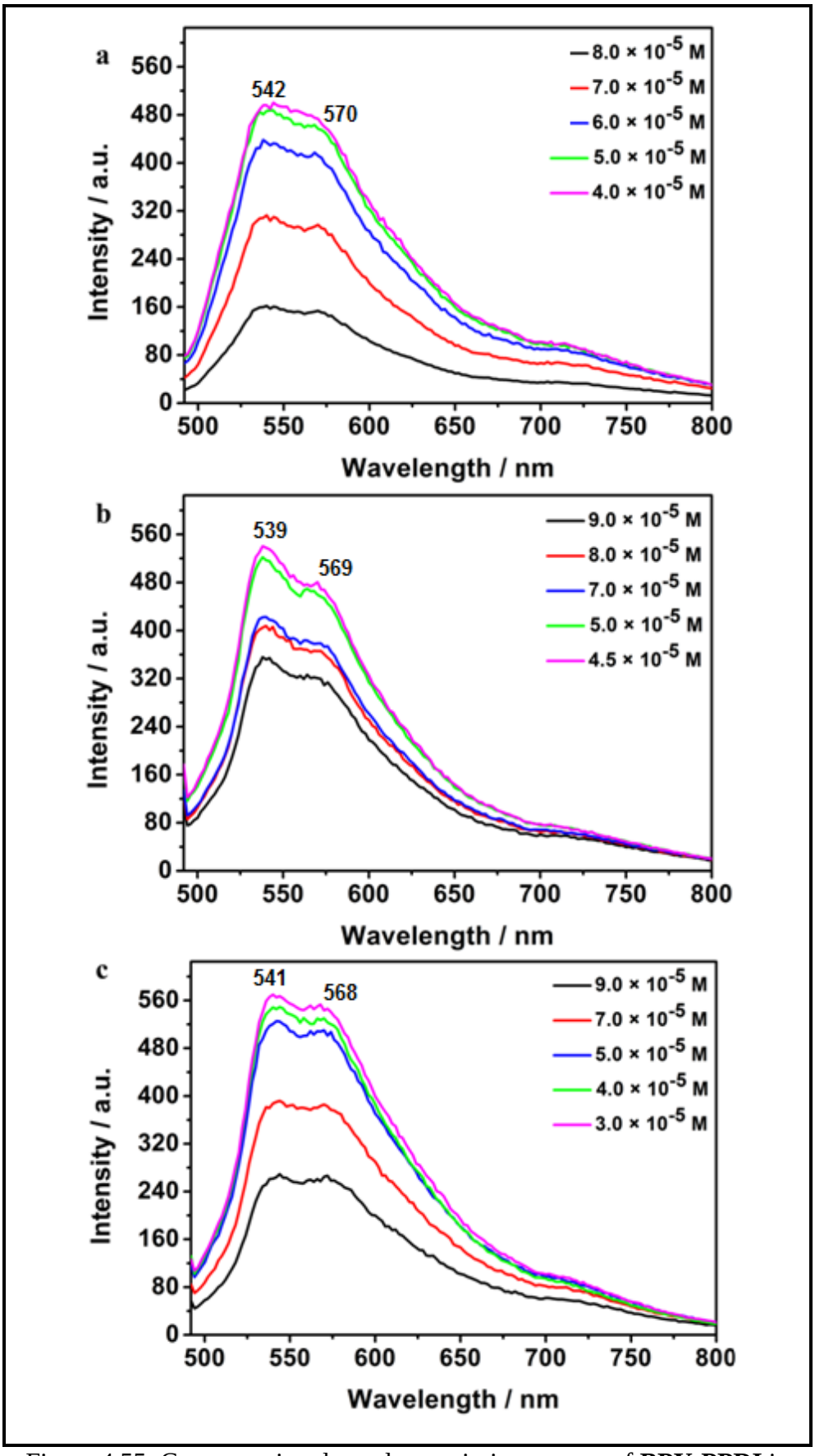

Figure 4.55: Concentration dependent emission spectra of **BPY-PPDI** in (a) NMP, (b) DMF and (c) DMAC at excitation wavelength of 485 nm

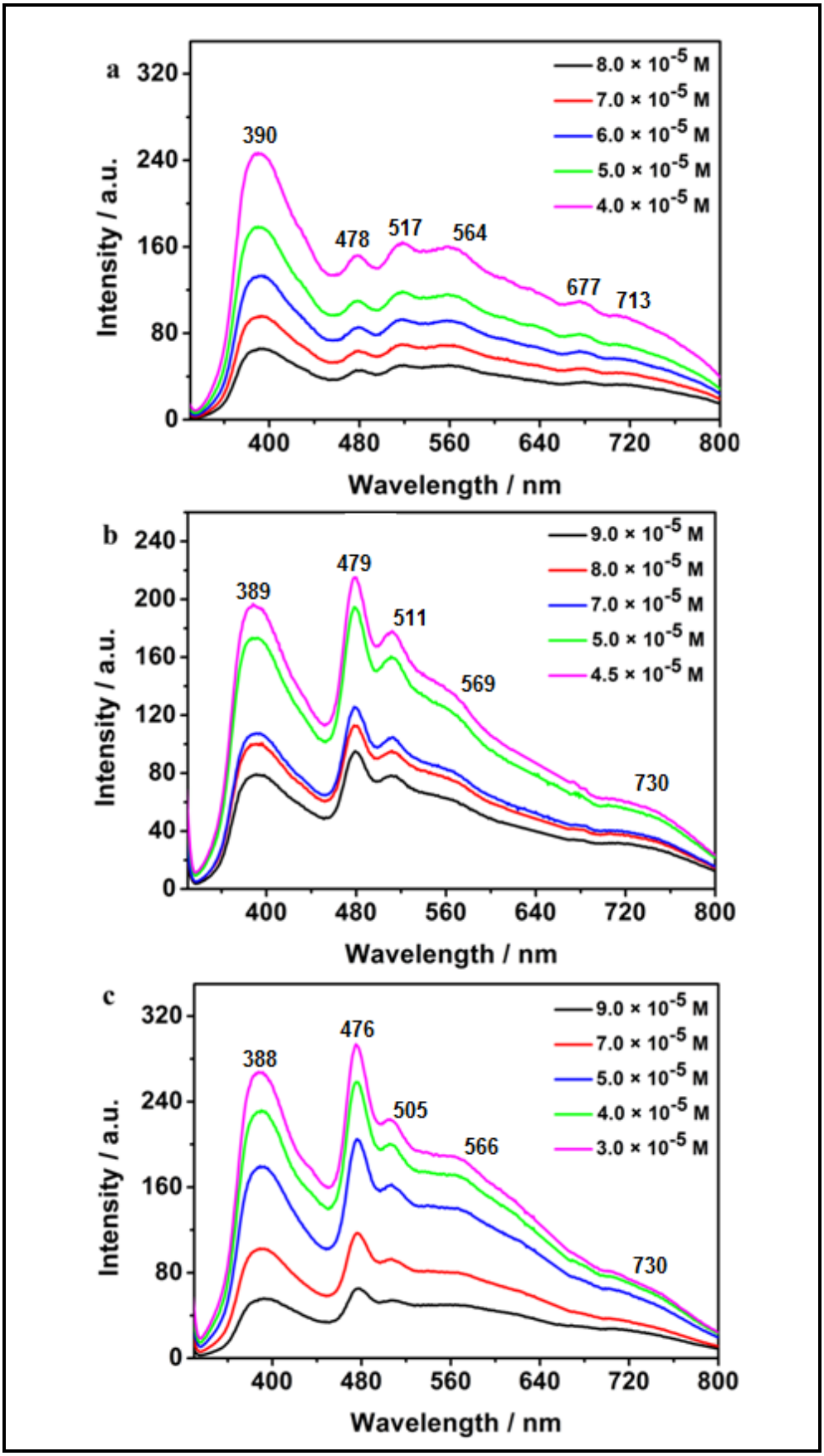

Figure 4.56: Concentration dependent emission spectra of **BPY-PPDI** in (a) NMP, (b) DMF and (c) DMAC at excitation wavelength of 315 nm

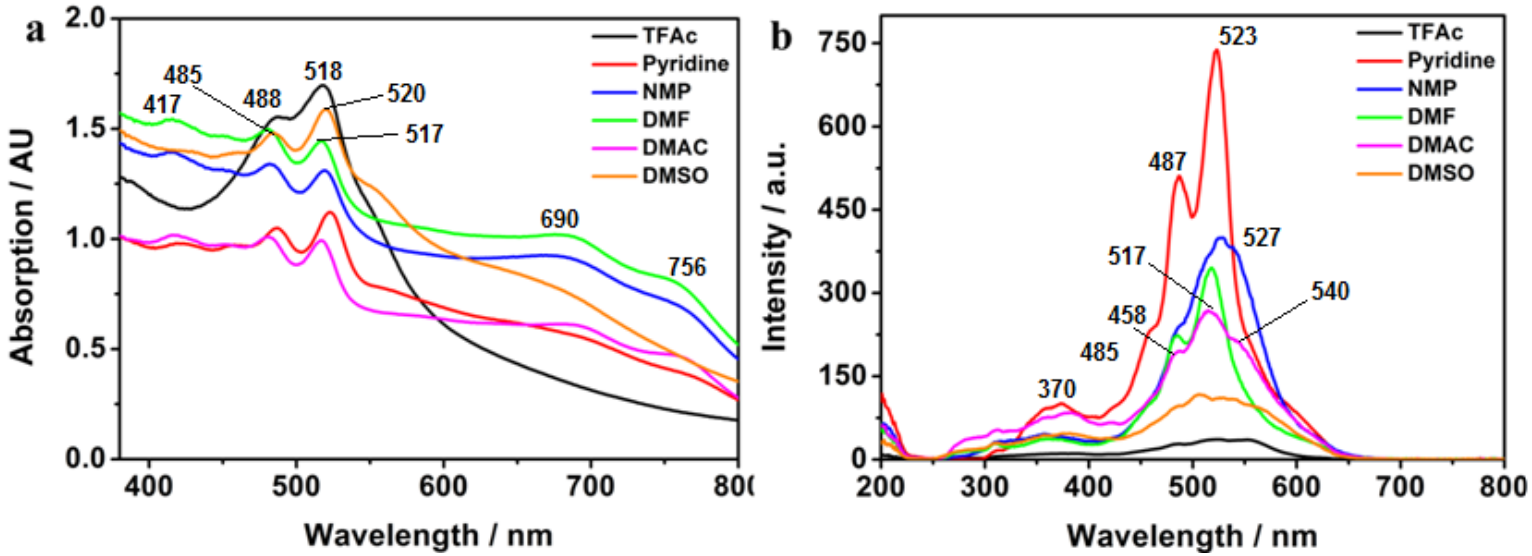

Figure 4.57: (a) UV spectra of **BTC-PDA** and (b) excitation spectra at emission wavelength of 620 nm

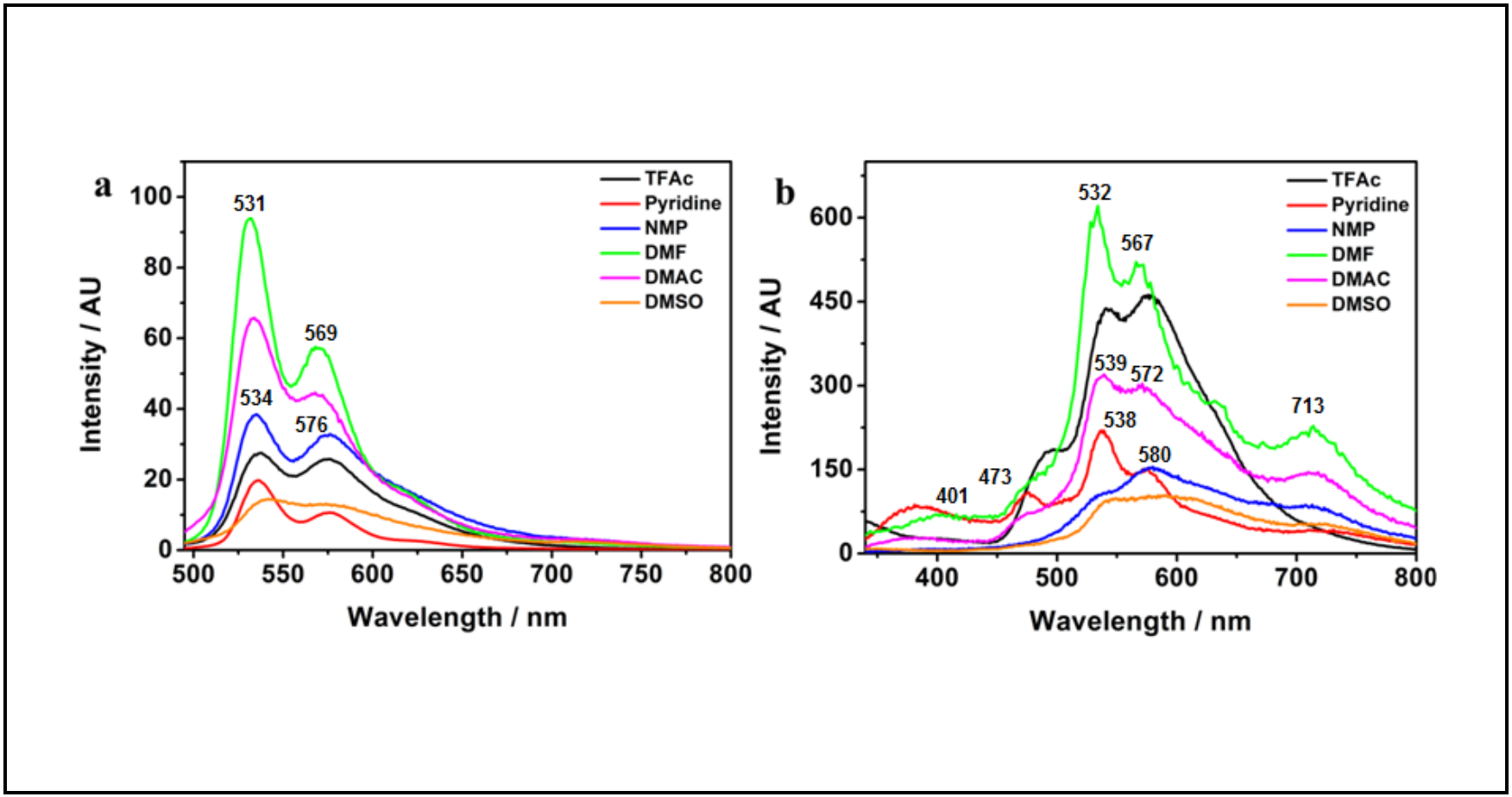

Figure 4.58: Emission spectra of **BTC-PDA** (a) at excitation wavelength of 485nm and (b) 315 nm

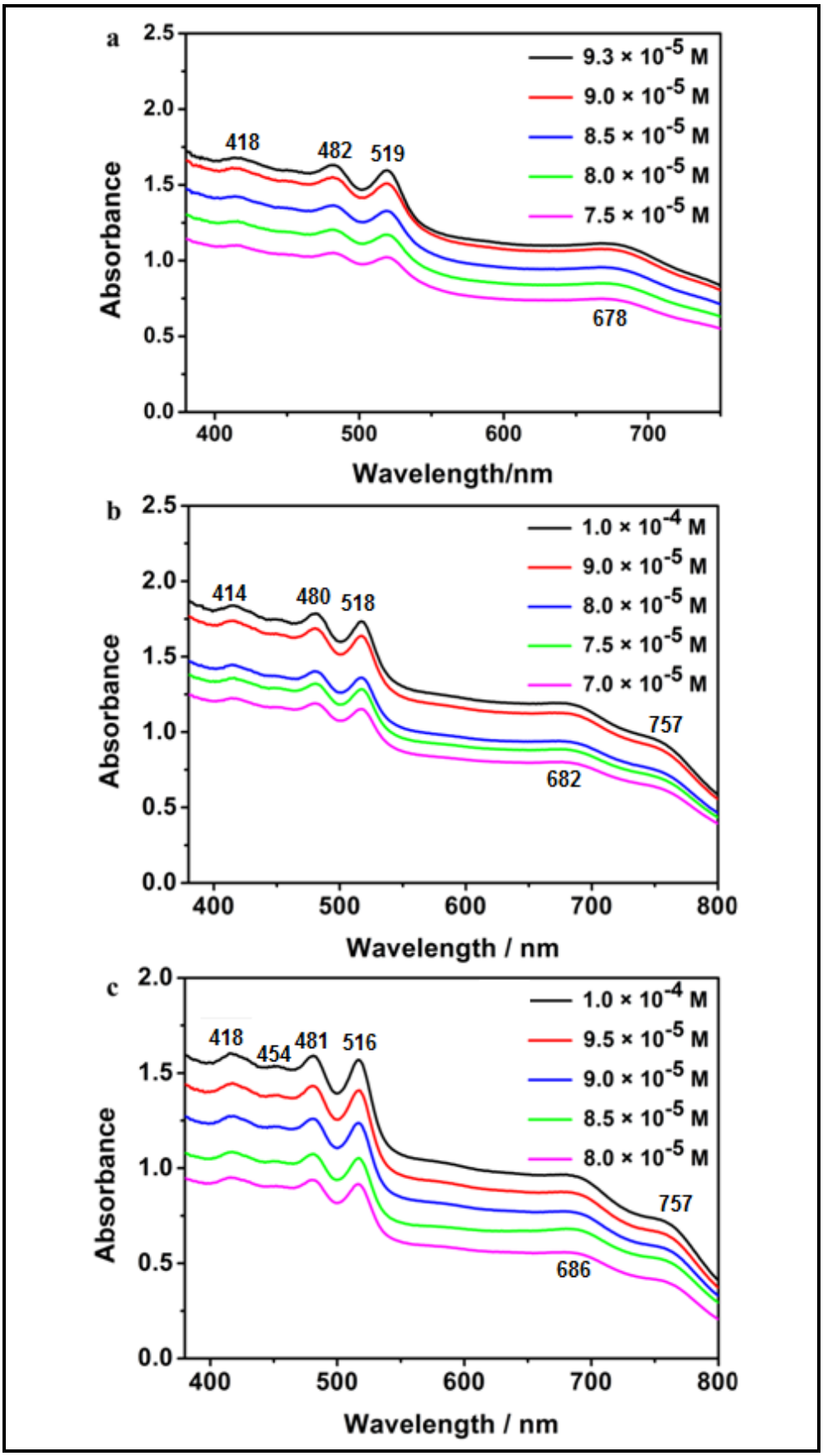

Figure 4.59: Concentration dependent UV spectra of **BTC-PDA** in (a) NMP, (b) DMF and (c) DMAC

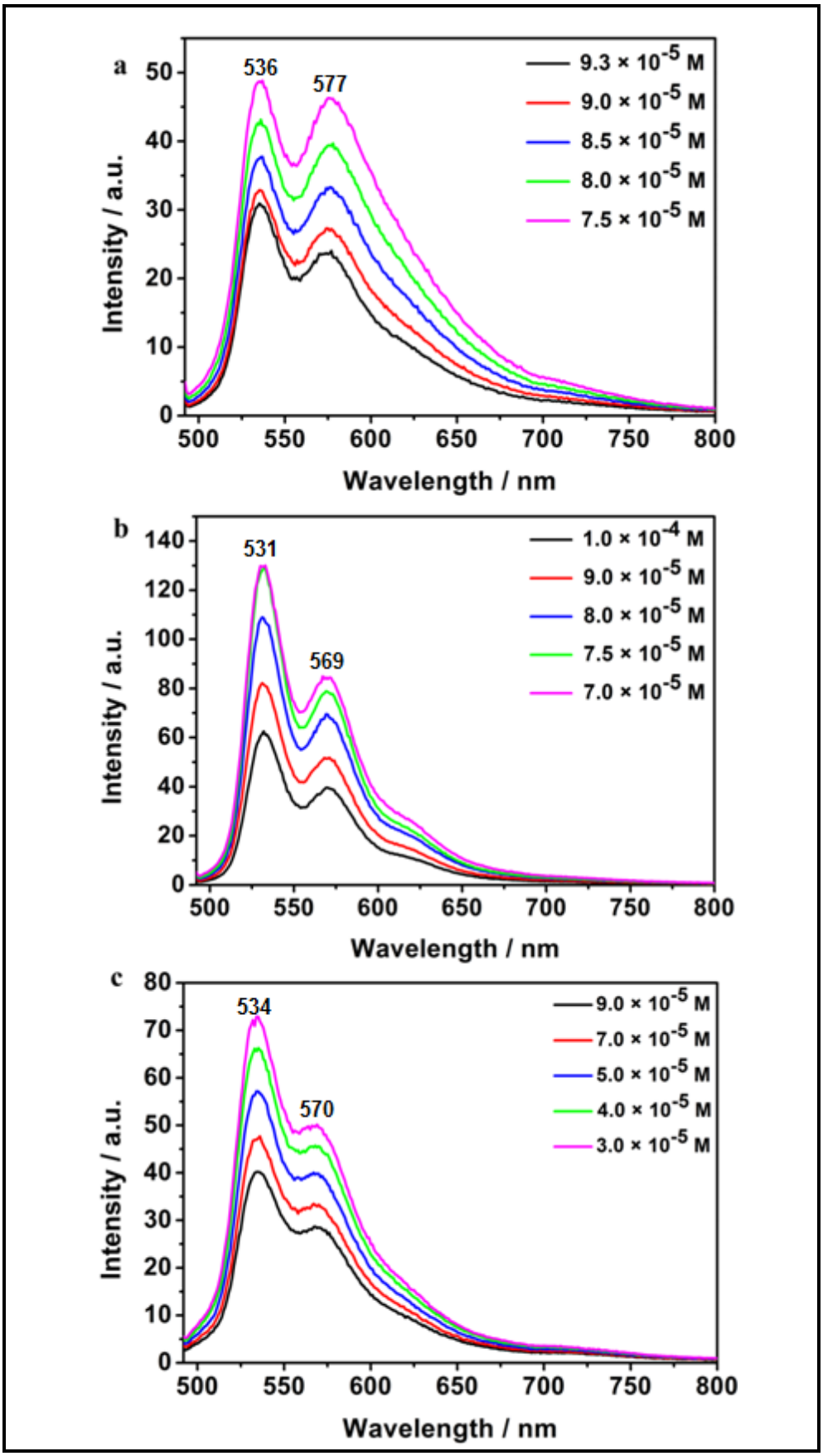

Figure 4.60: Concentration dependent emission spectra of **BTC-PDA** in (a) NMP, (b) DMF and (c) DMAC at excitation wavelength of 485 nm

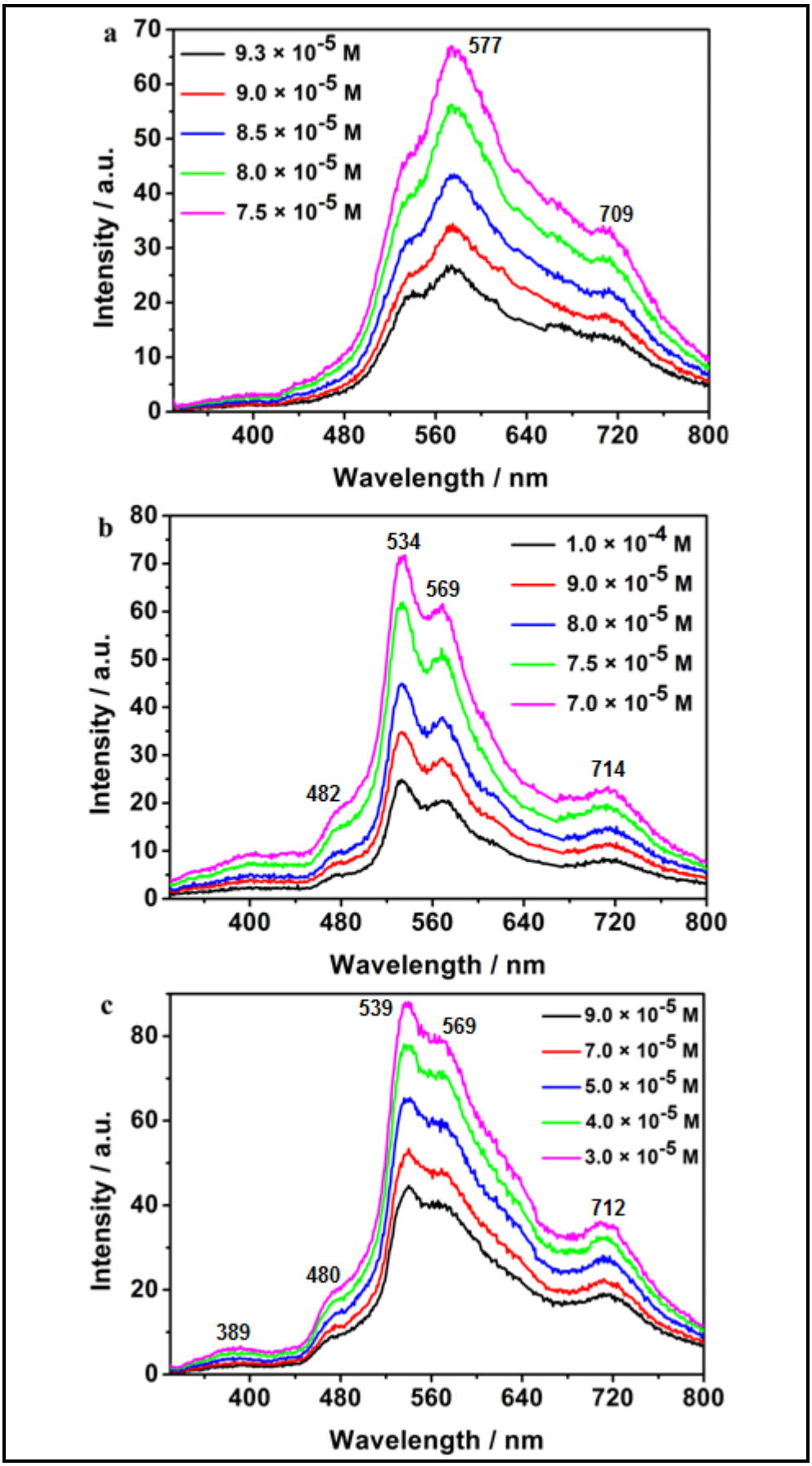

Figure 4.61: Concentration dependent emission spectra of **BTC-PDA** in (a) NMP, (b) DMF and (c) DMAC at excitation wavelength of 315 nm

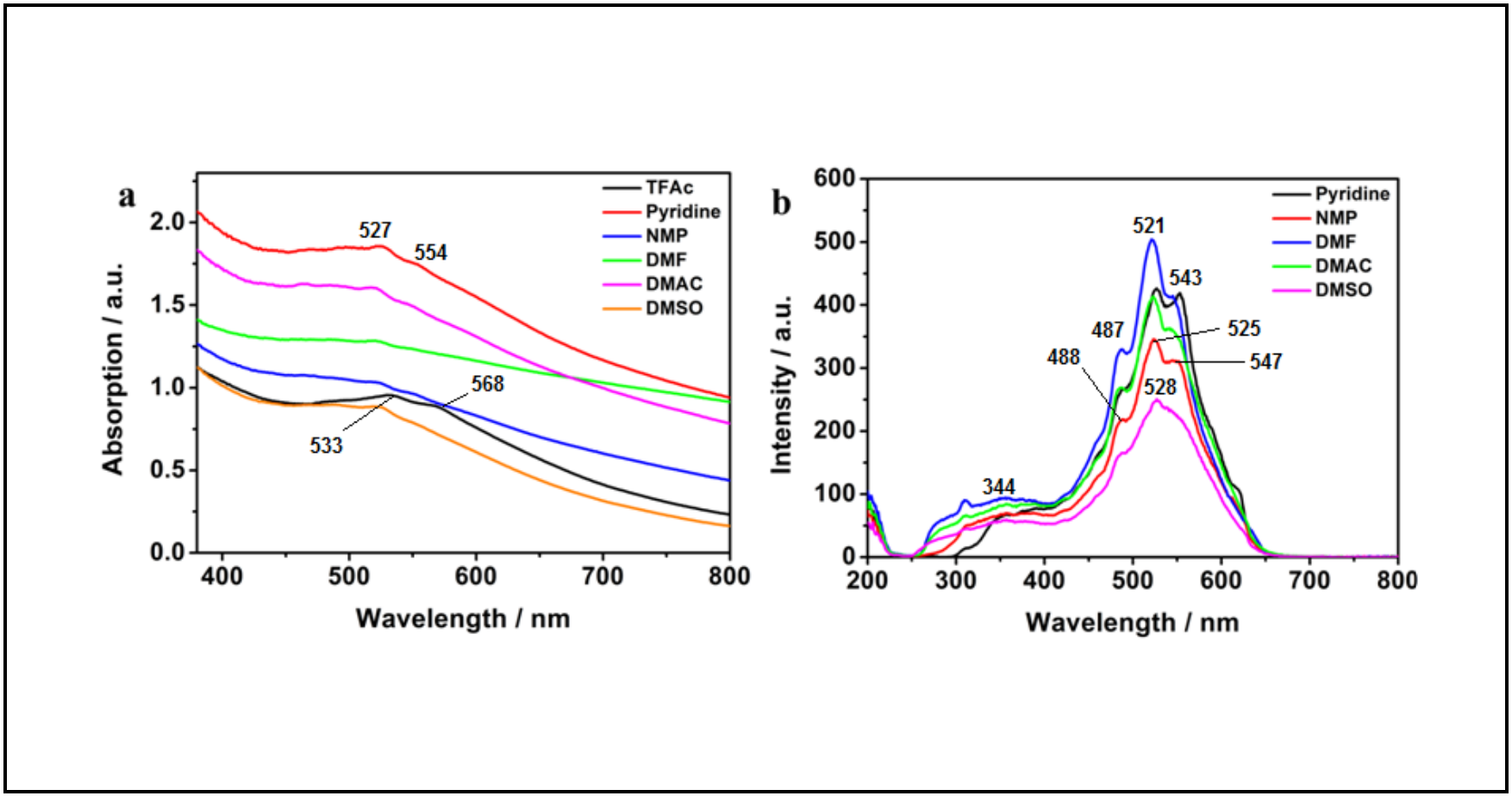

Figure 4.62: (a) UV spectra of **BTC-TCPDI** and (b) Excitation spectra at emission wavelength of 620 nm

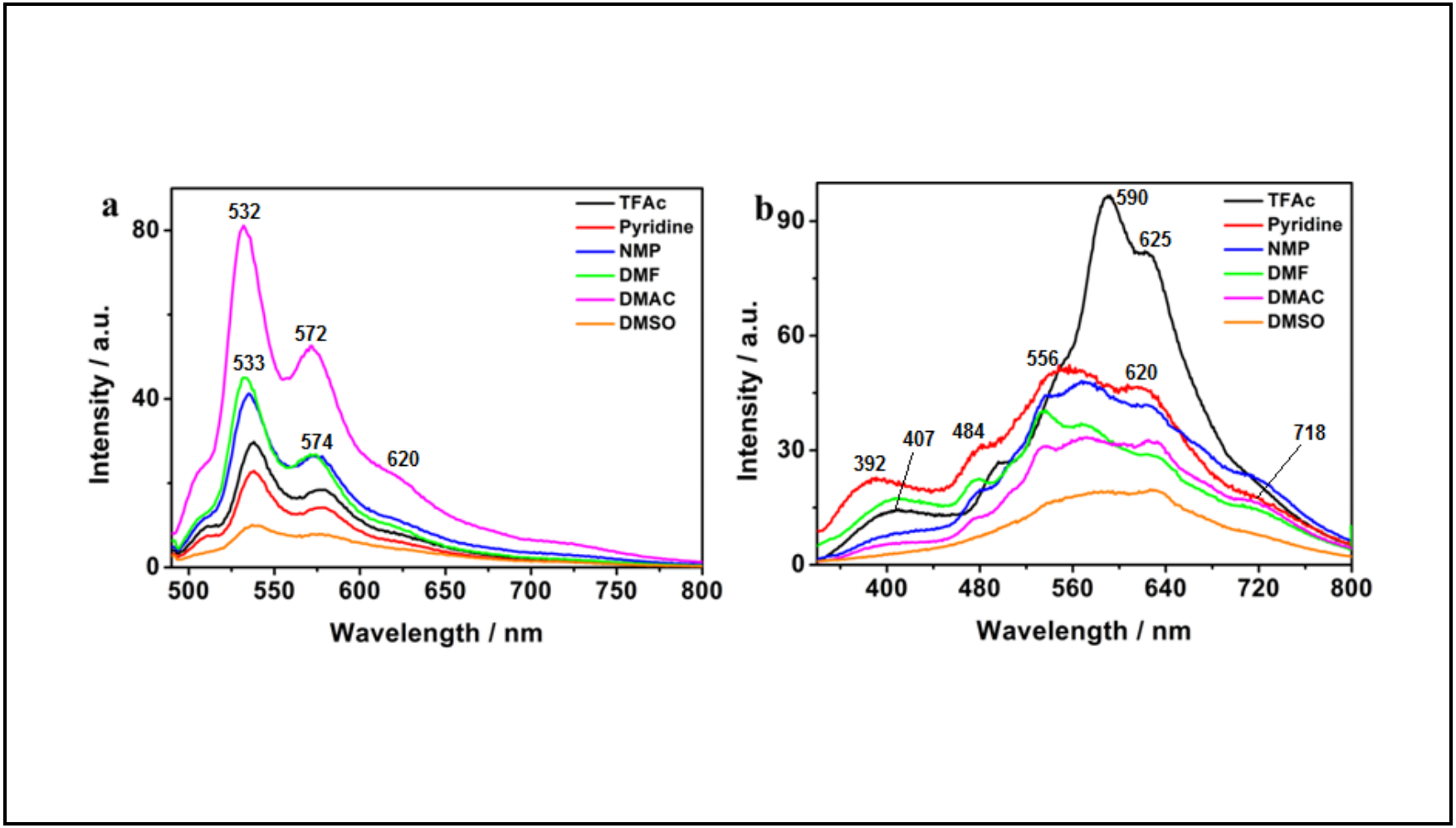

Figure 4.63: Emission spectra of **BTC-TCPDI** (a) at excitation wavelength of 485 nm and (b) 315 nm

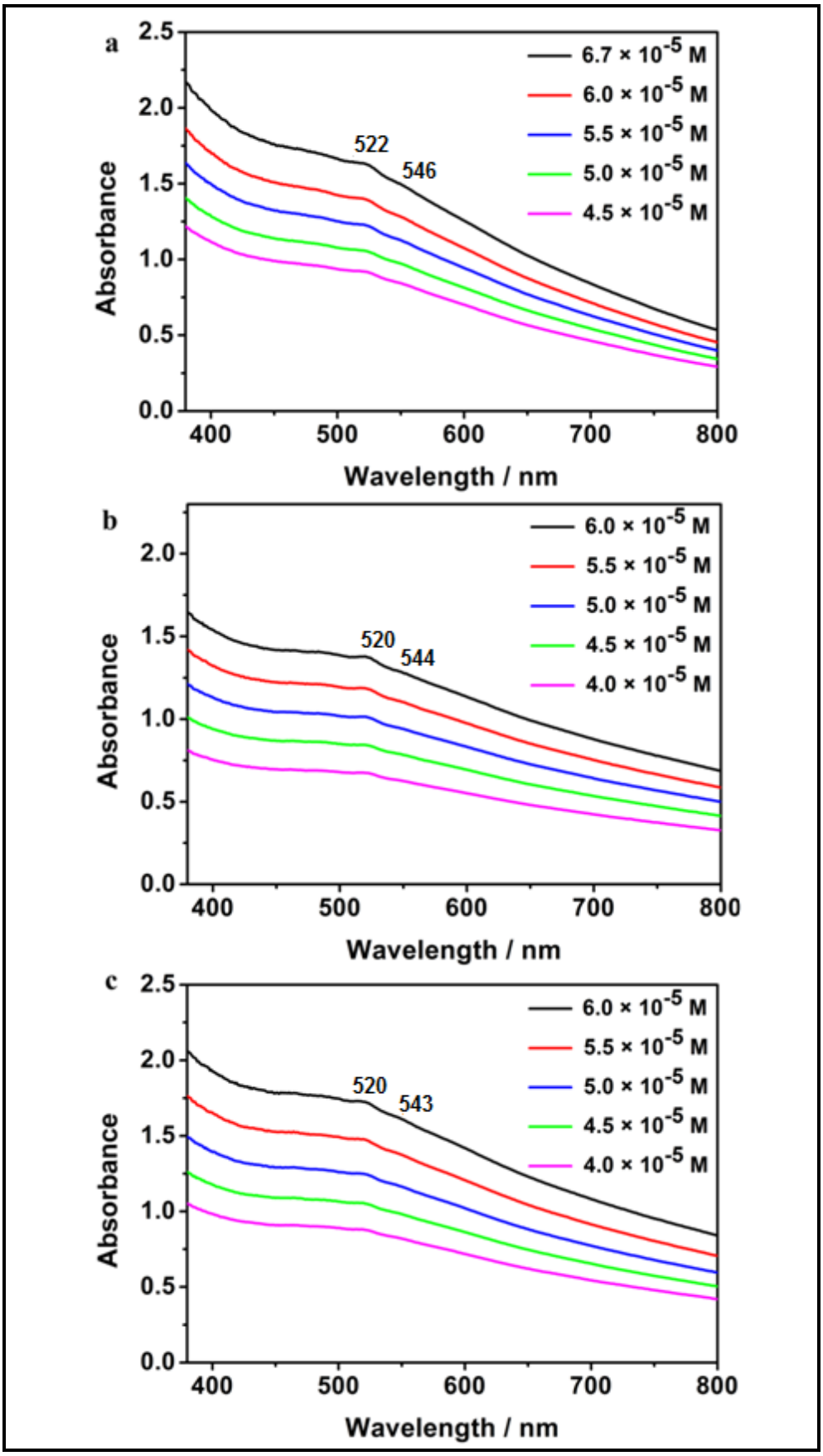

Figure 4.64: Concentration dependent UV spectra of **BTC-TCPDI** in (a) NMP, (b) DMF and (c) DMAC

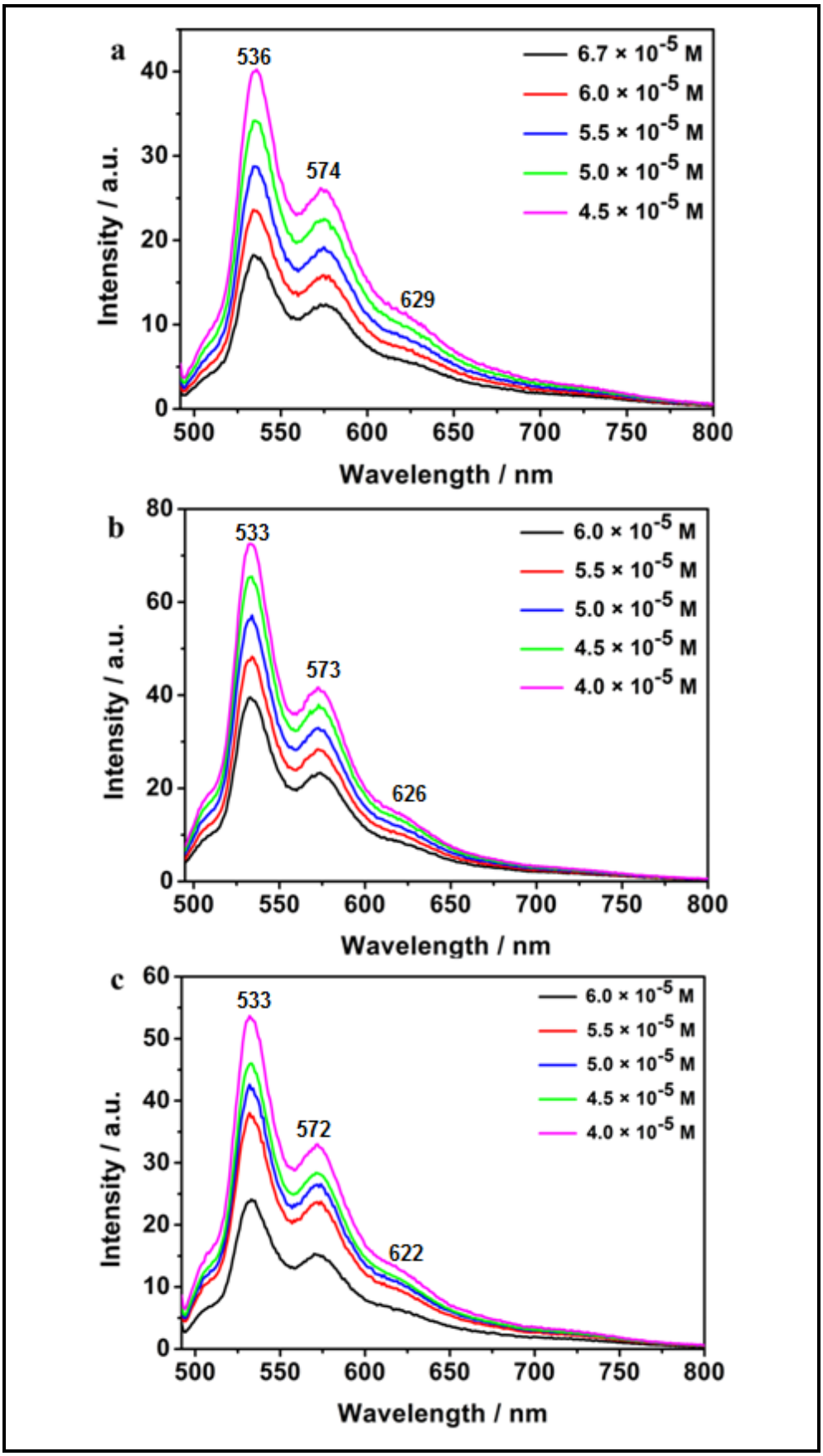

Figure 4.65: Concentration dependent emission spectra of **BTC-TCPDI** in (a) NMP, (b) DMF and (c) DMAC at excitation wavelength of 485 nm

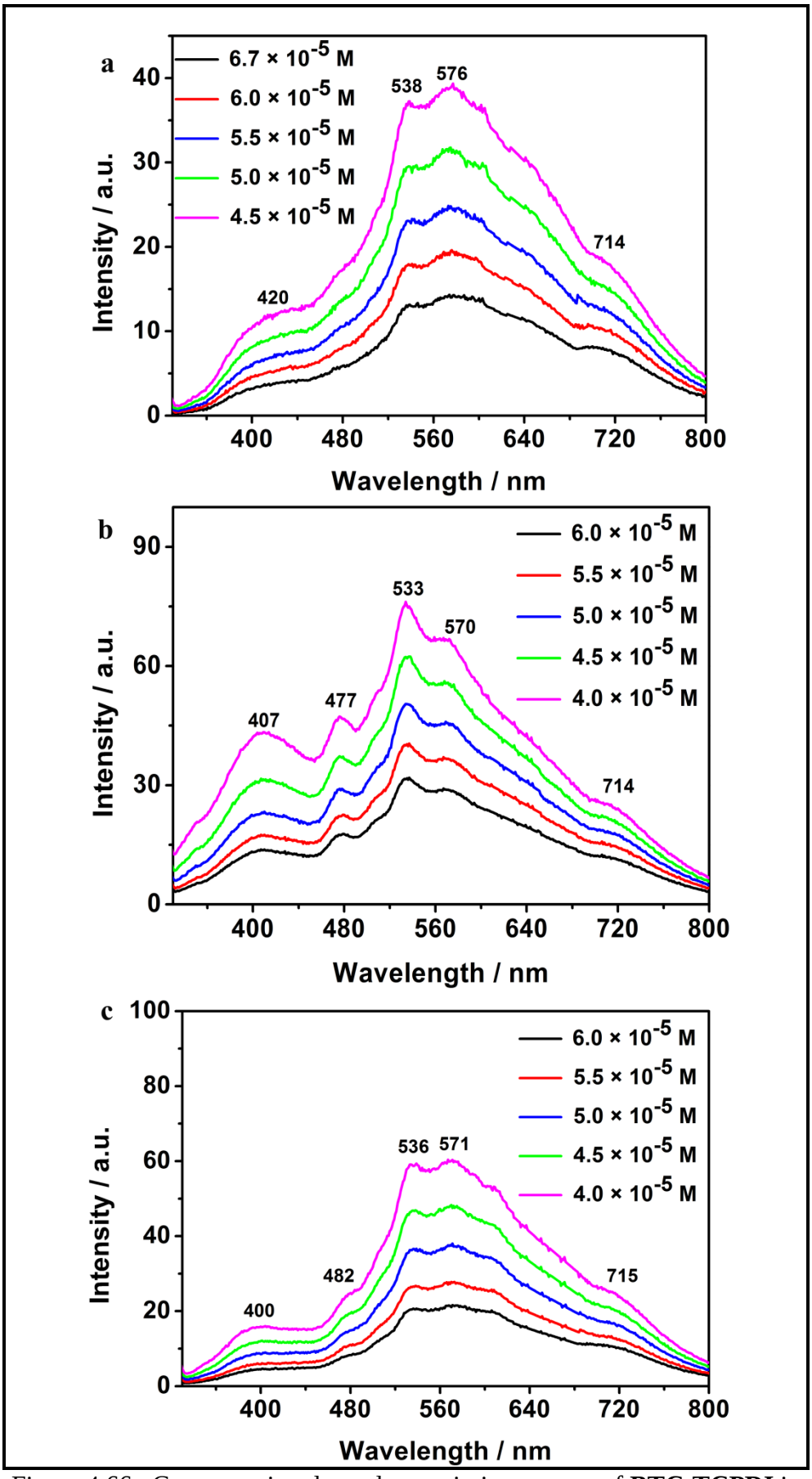

Figure 4.66: Concentration dependent emission spectra of **BTC-TCPDI** in (a) NMP, (b) DMF and (c) DMAC at excitation wavelength of 315 nm

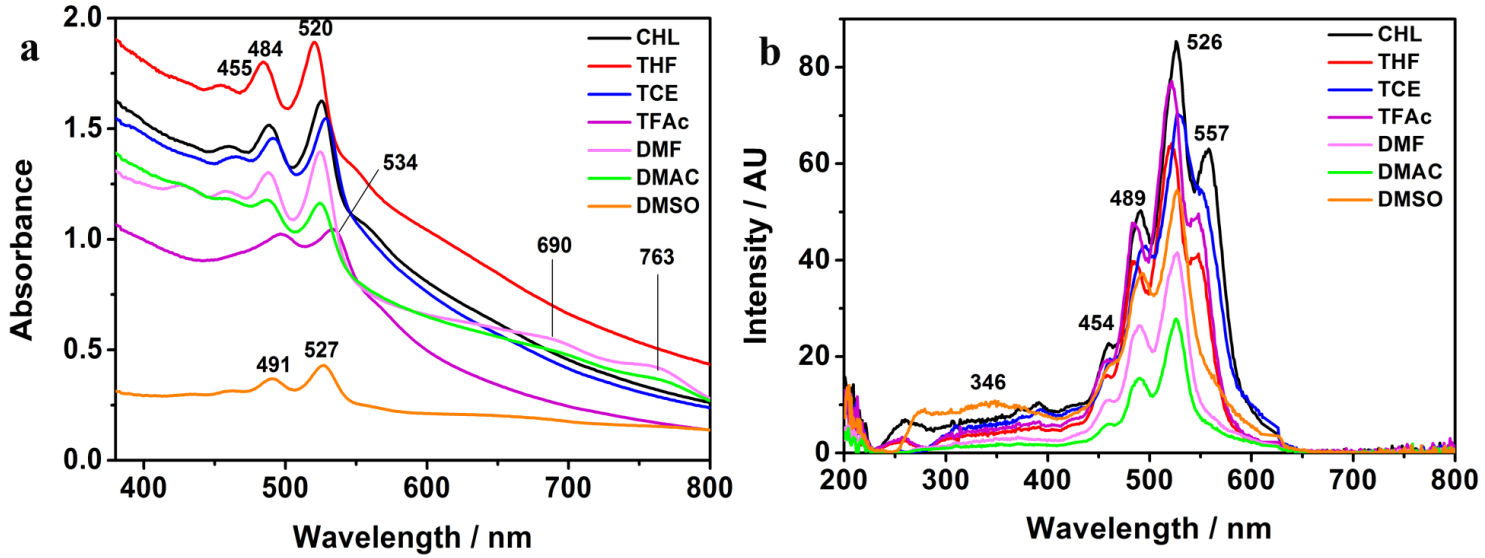

Figure 4.67: (a) UV spectra of **BTC-APDI** and (b) excitation spectra at emission wavelength of 620 nm

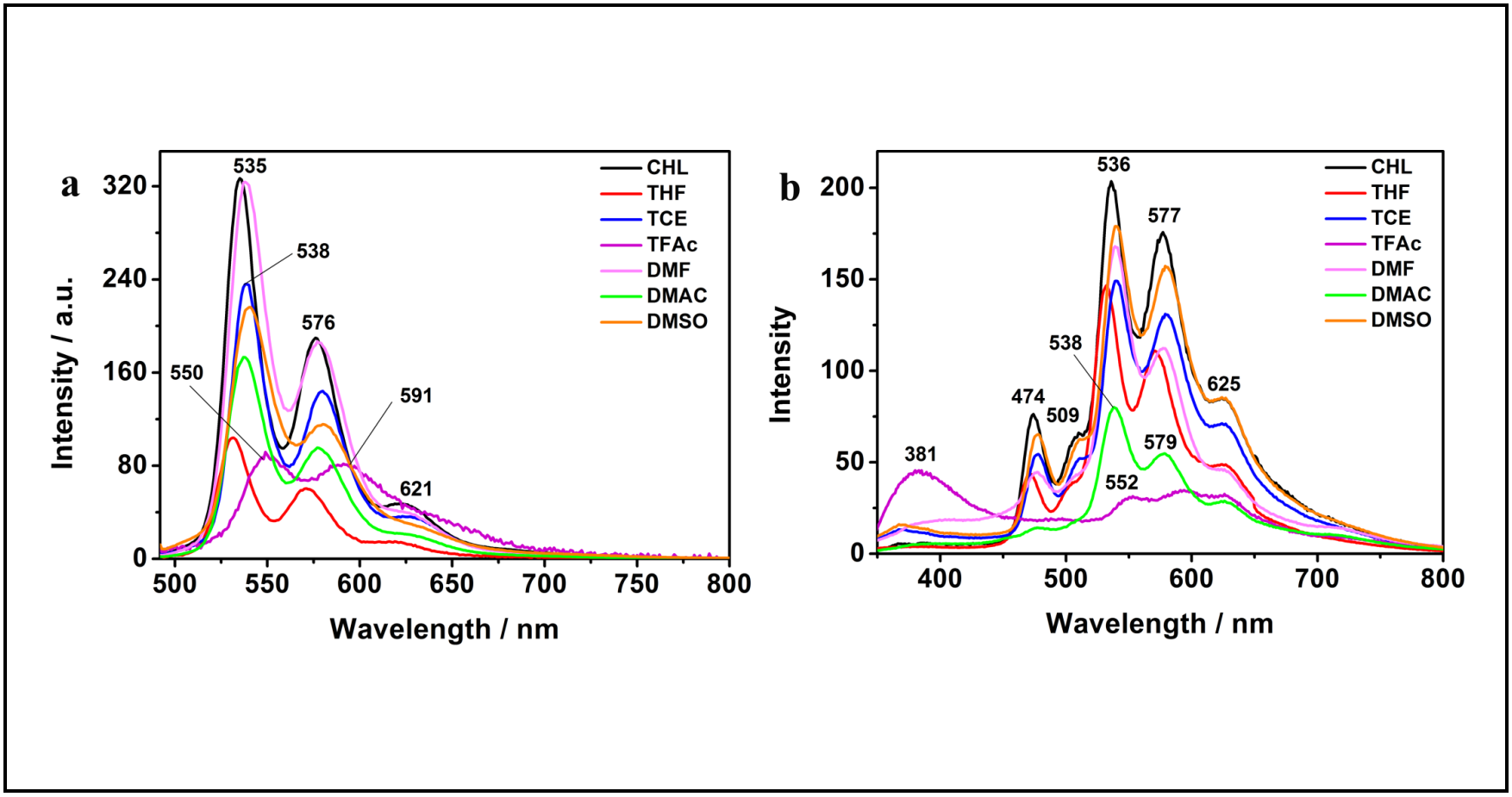

Figure 4.68: Emission spectra of **BTC-APDI** at excitation wavelength of (a) 485 nm (b) 315 nm

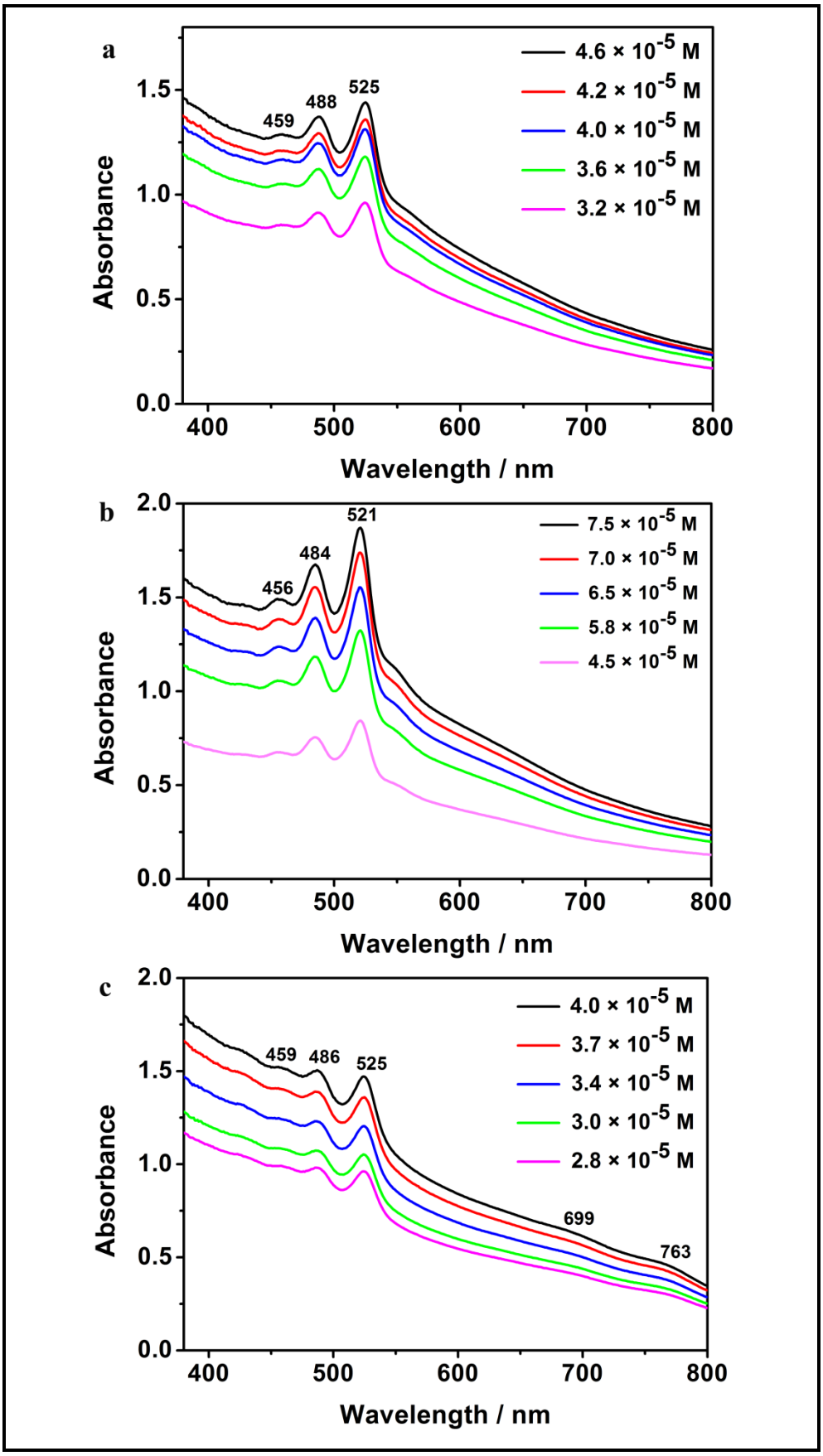

Figure 4.69: Concentration dependent UV spectra of **BTC-APDI** in (a) CHL, (b) THF and (c) DMAC

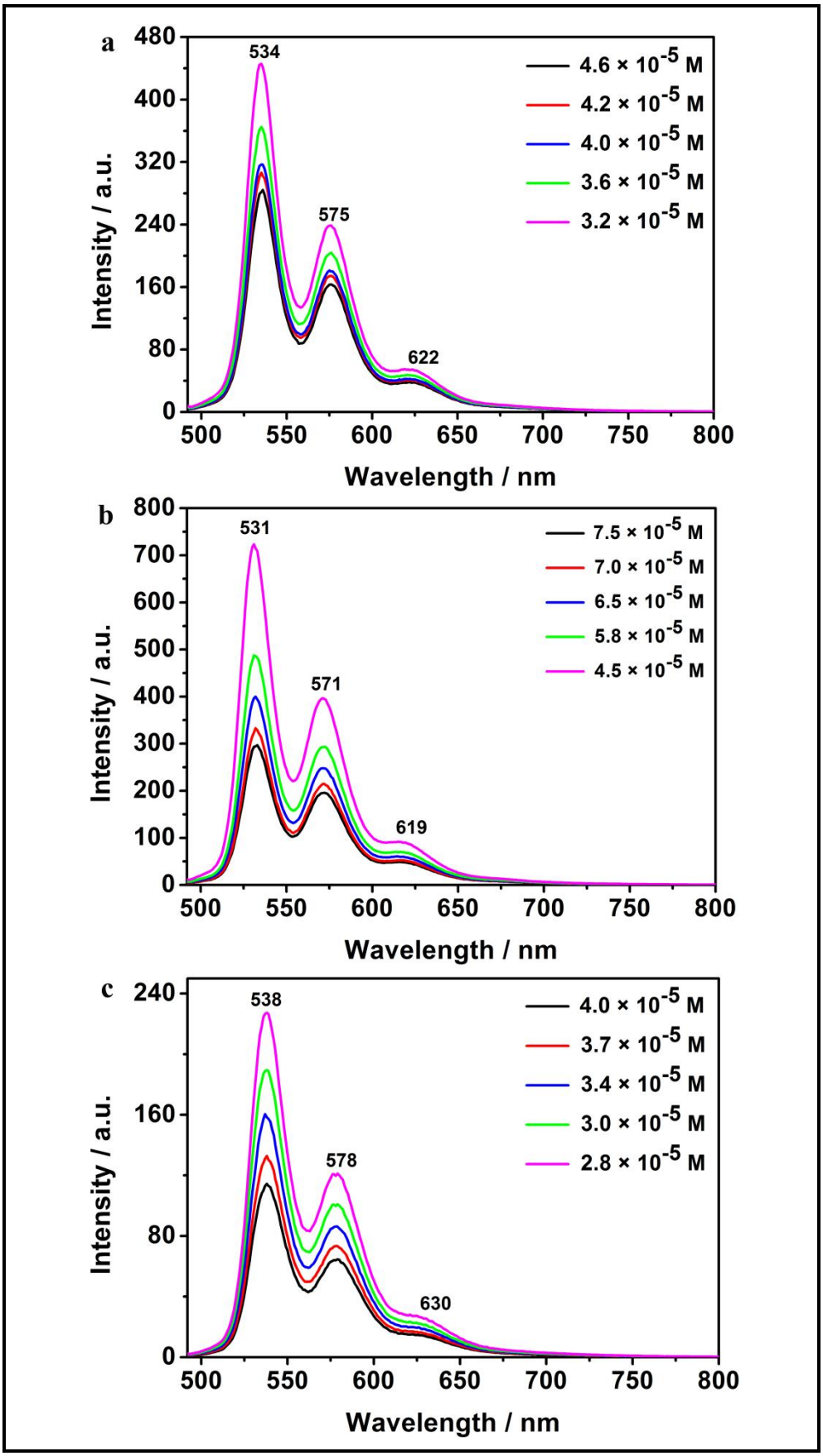

Figure 4.70: Concentration dependent emission spectra of **BTC-APDI** in (a) CHL, (b) THF and (c) DMAC at excitation wavelength of 485 nm

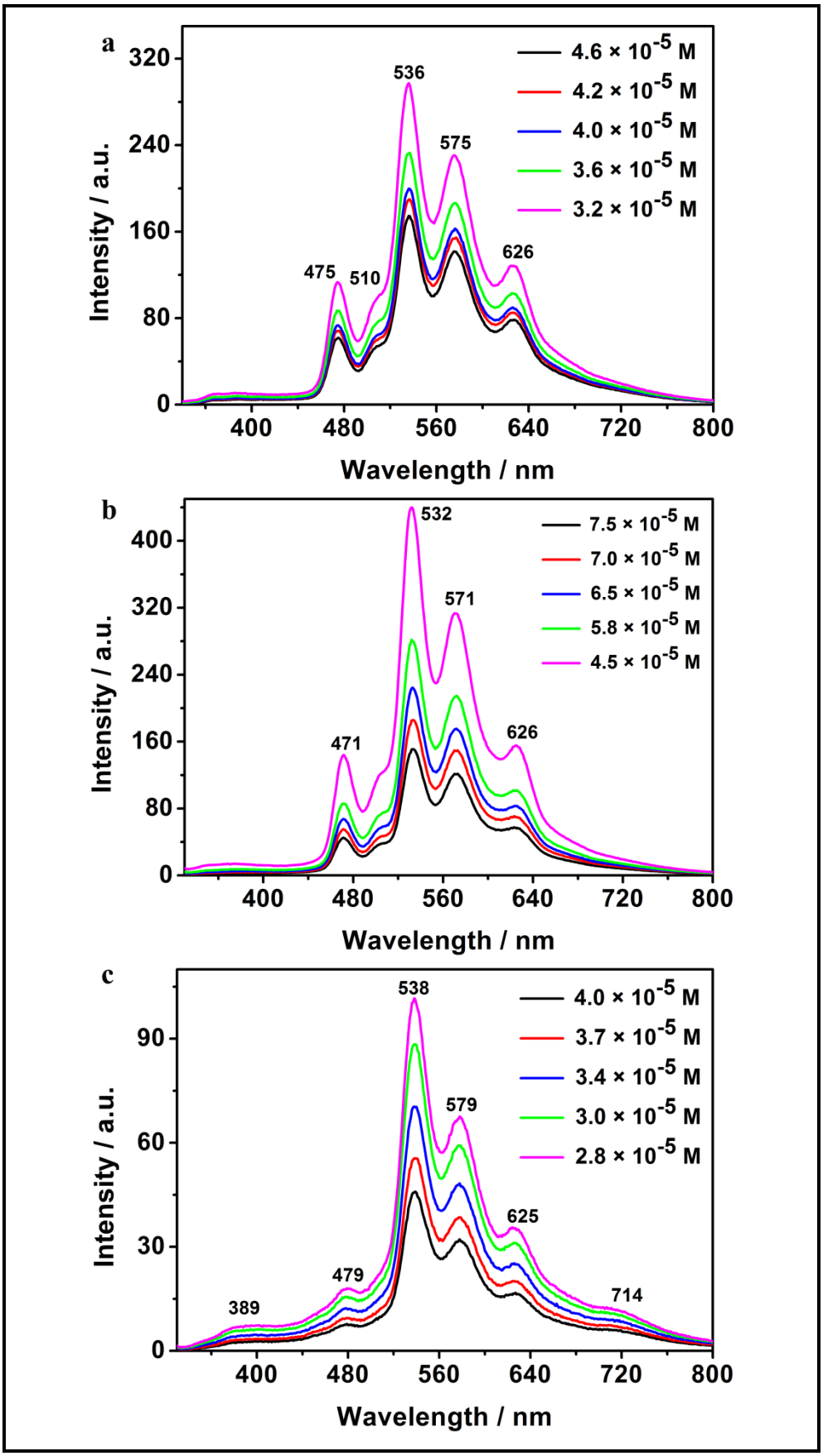

Figure 4.71: Concentration dependent emission spectra of **BTC-APDI** in (a) CHL, (b) THF and (c) DMAC at excitation wavelength of 315 nm

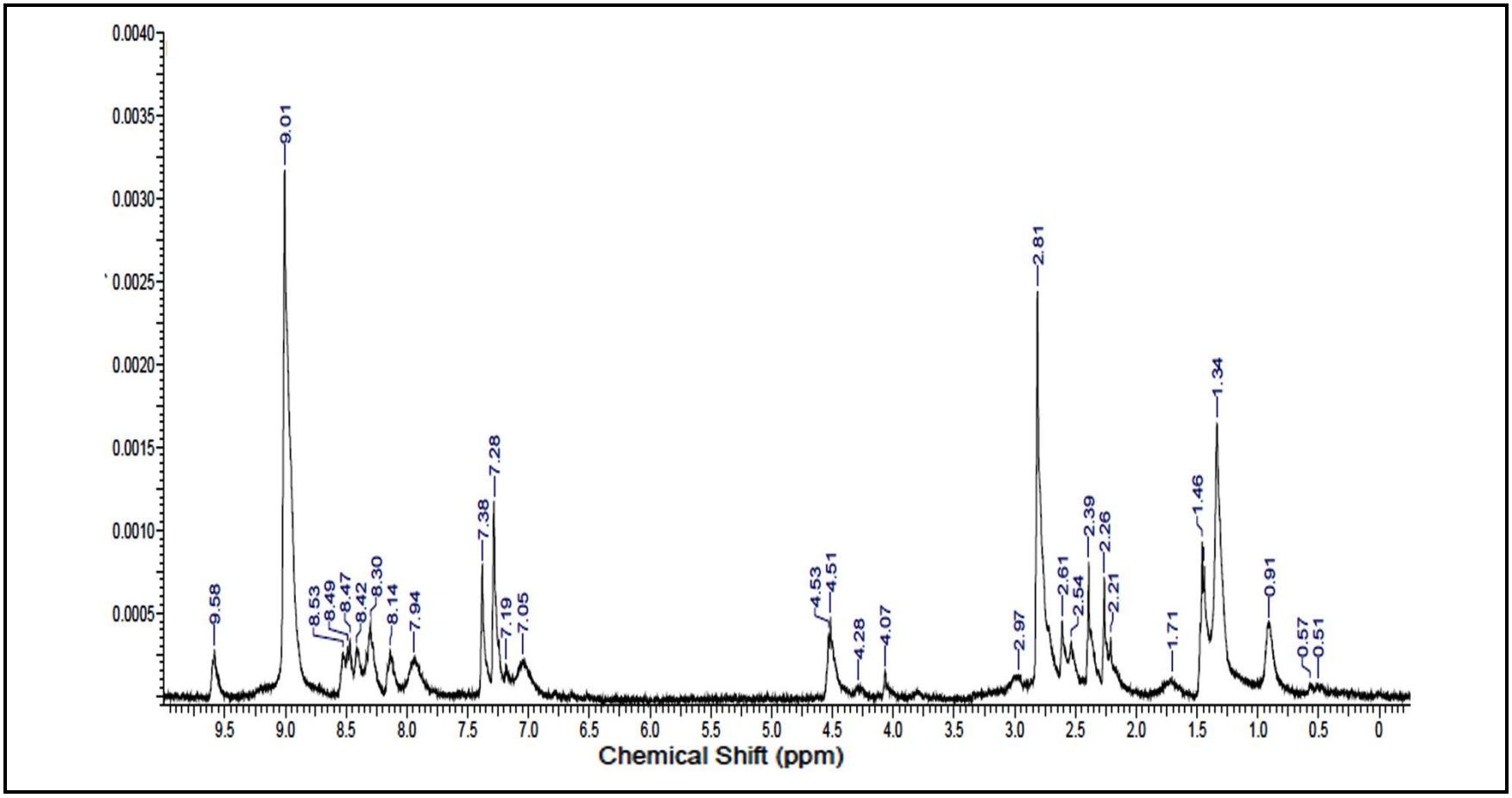

Figure 4.72: H-NMR spectrum of **TPDI** in TFAc:CHL

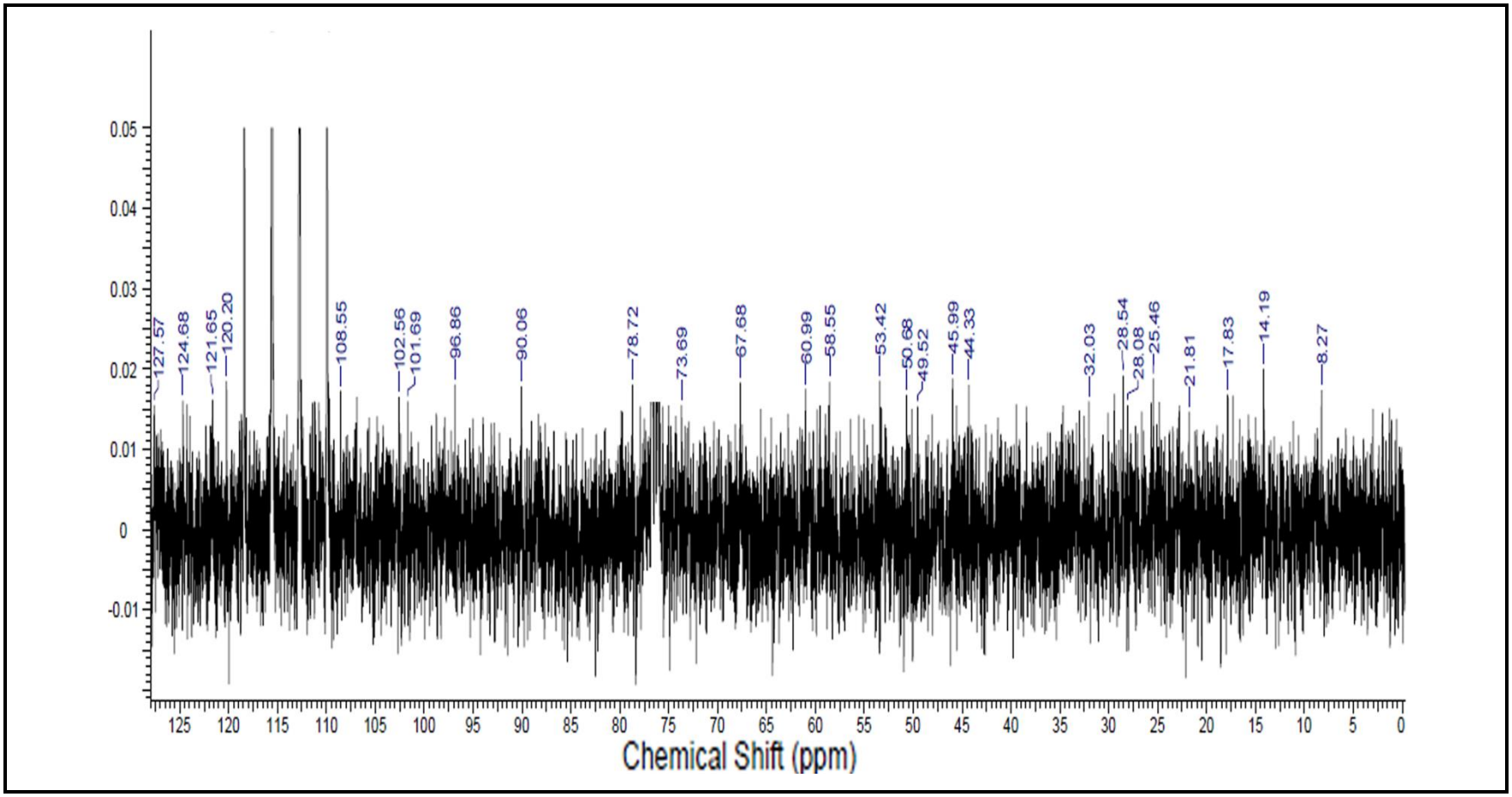

Figure 4.73: C-NMR spectrum of **TPDI** in TFAc:CHL at low ppm

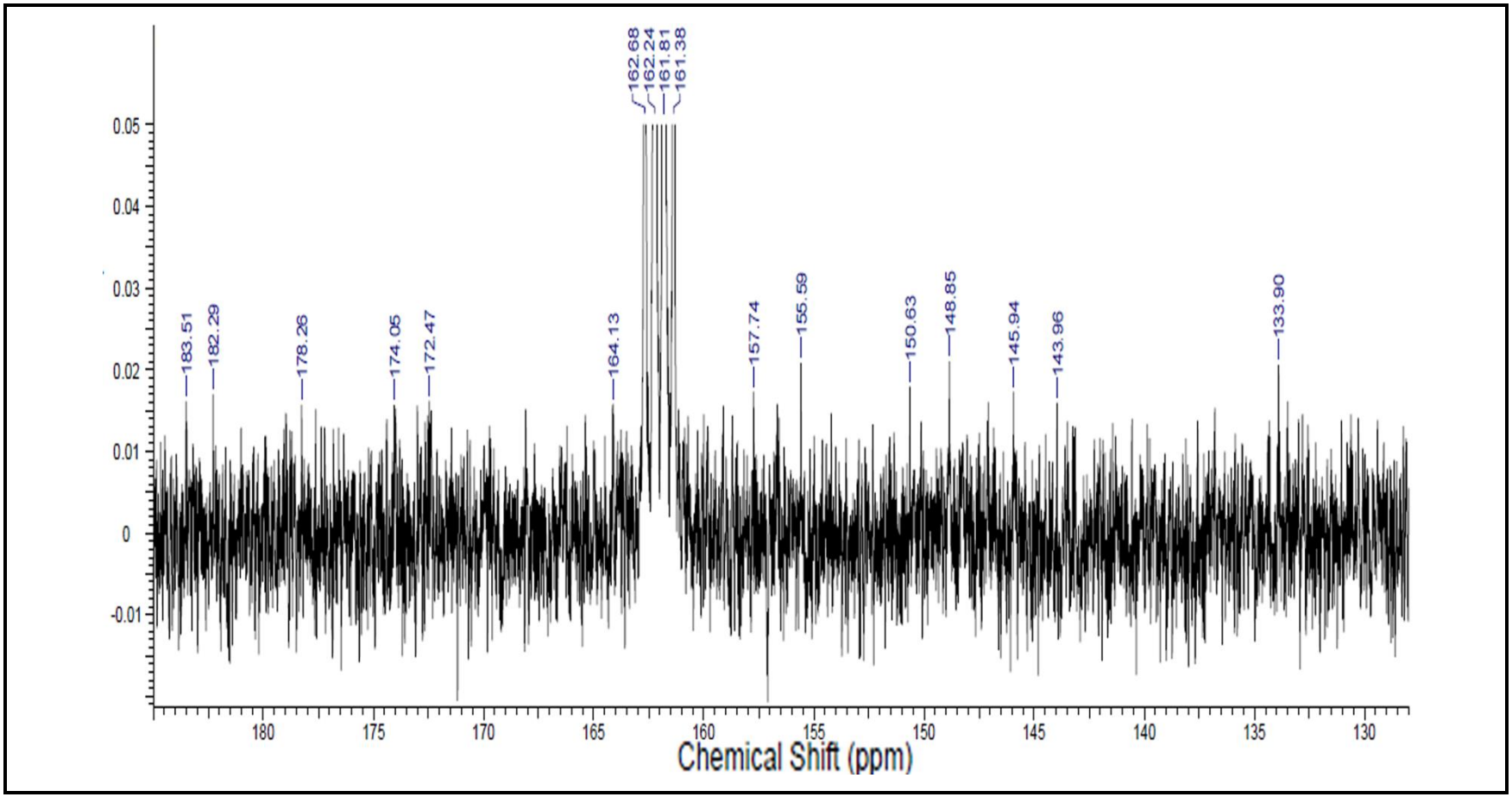

Figure 4.74: C-NMR spectrum of **TPDI** in TFAc:CHL at high ppm

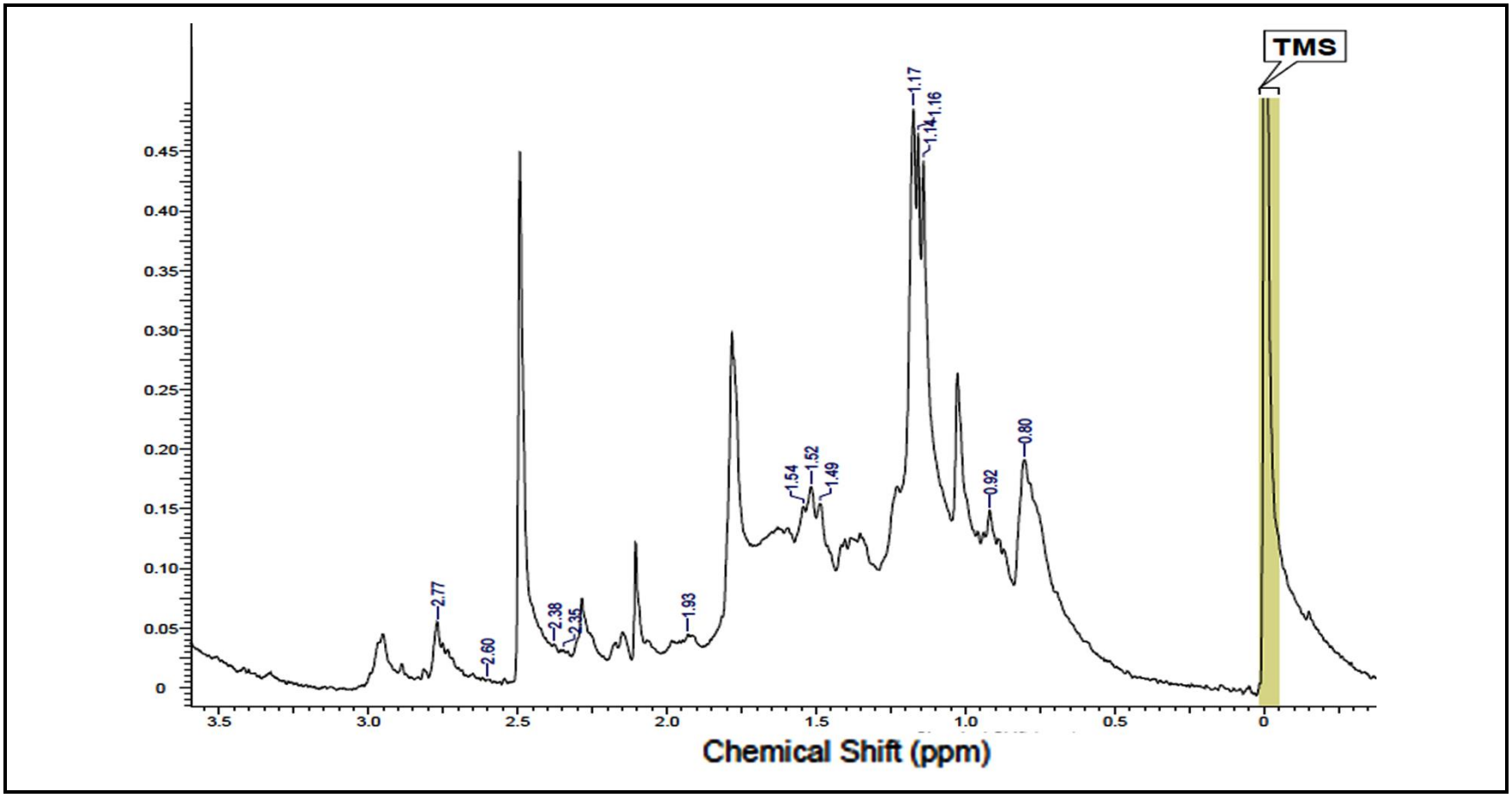

Figure 4.75: H-NMR spectrum of TAPDI in CHL at low ppm

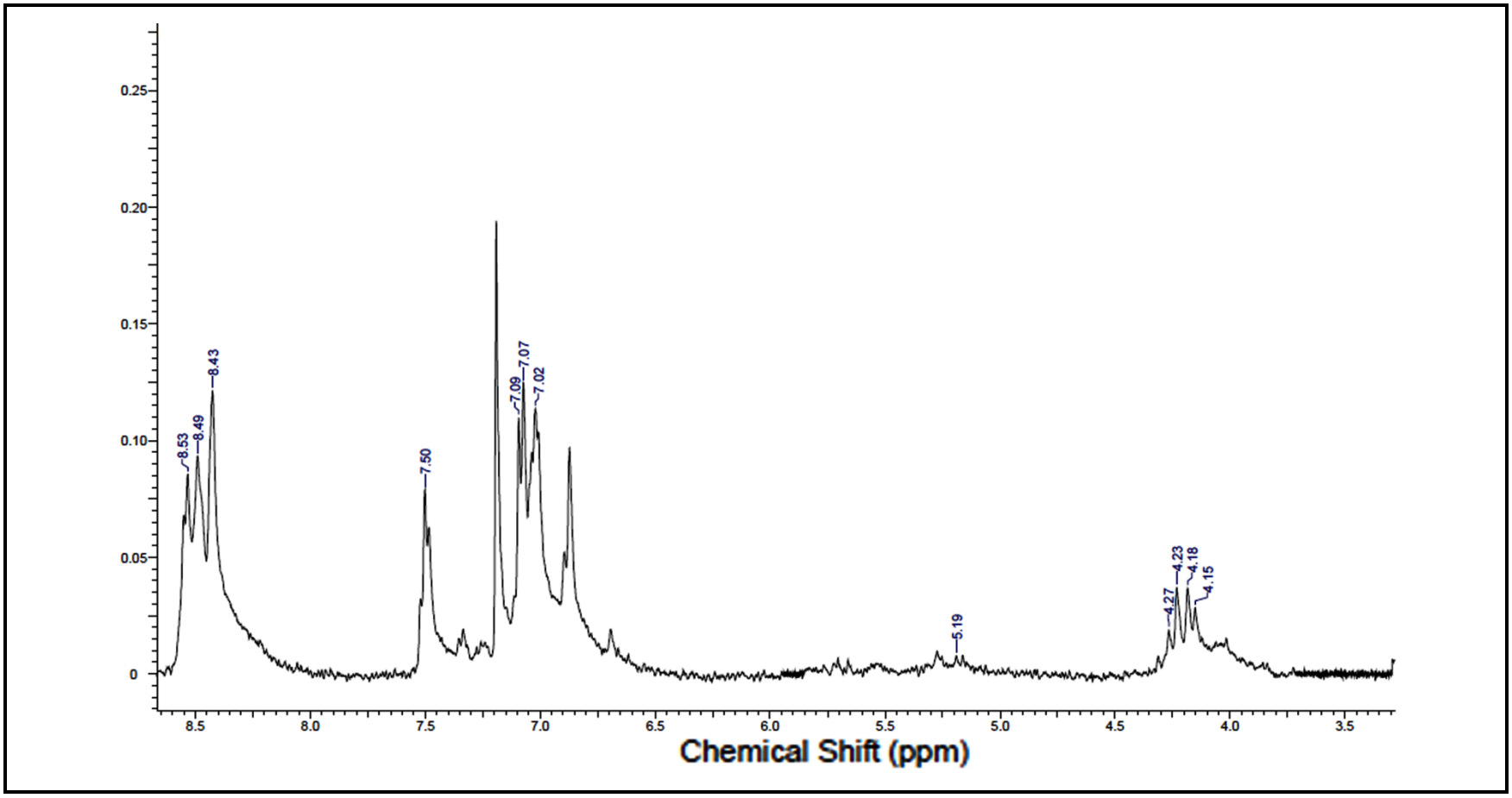

Figure 4.76: H-NMR spectrum of **TAPDI** in CHL at high ppm

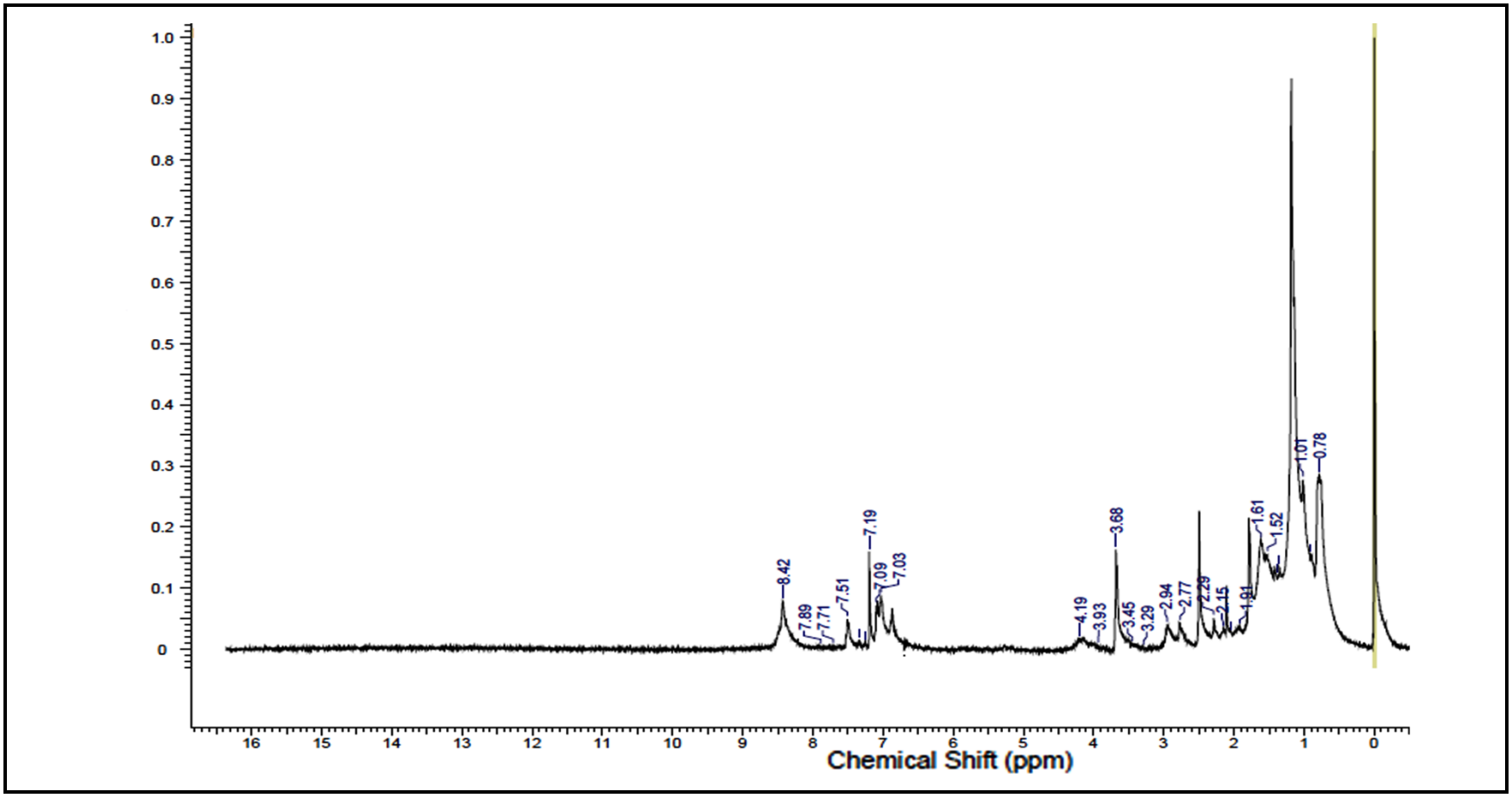

Figure 4.77: H-NMR spectrum of **BTC-APDI** in CHL

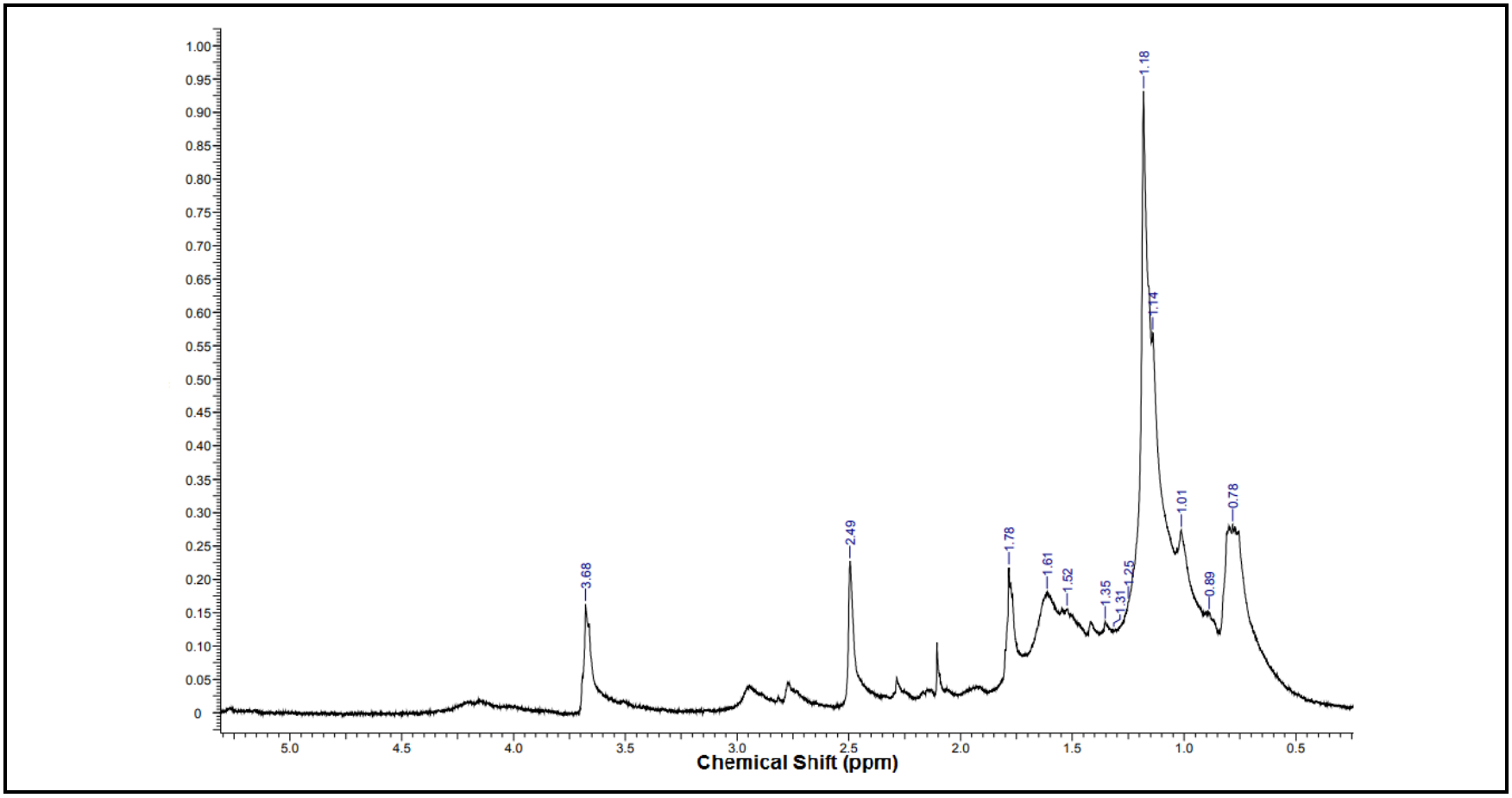

Figure 4.78: H-NMR spectrum of **BTC-APDI** in CHL at low ppm

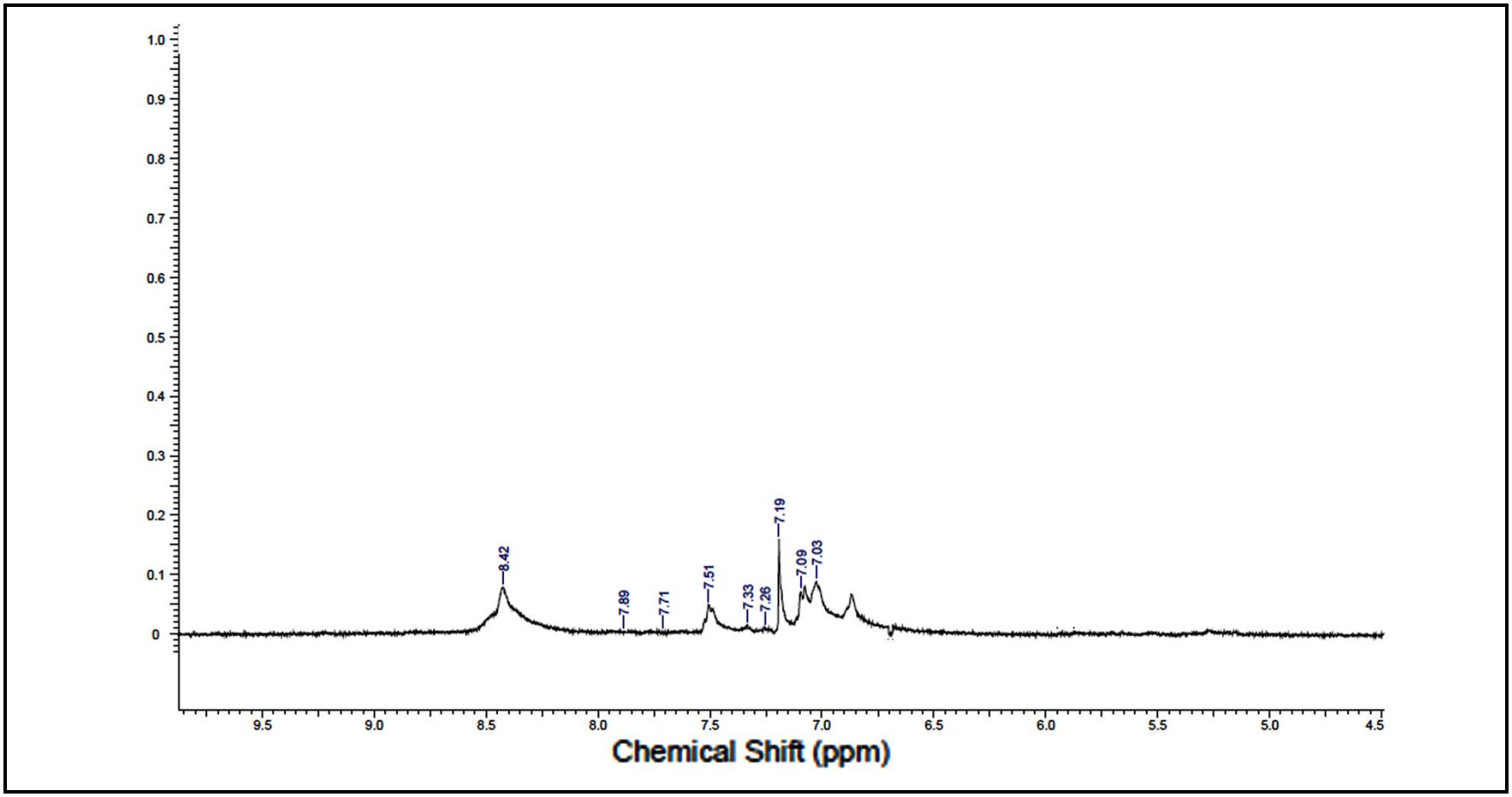

Figure 4.79: H-NMR spectrum of **BTC-APDI** in CHL at high ppm

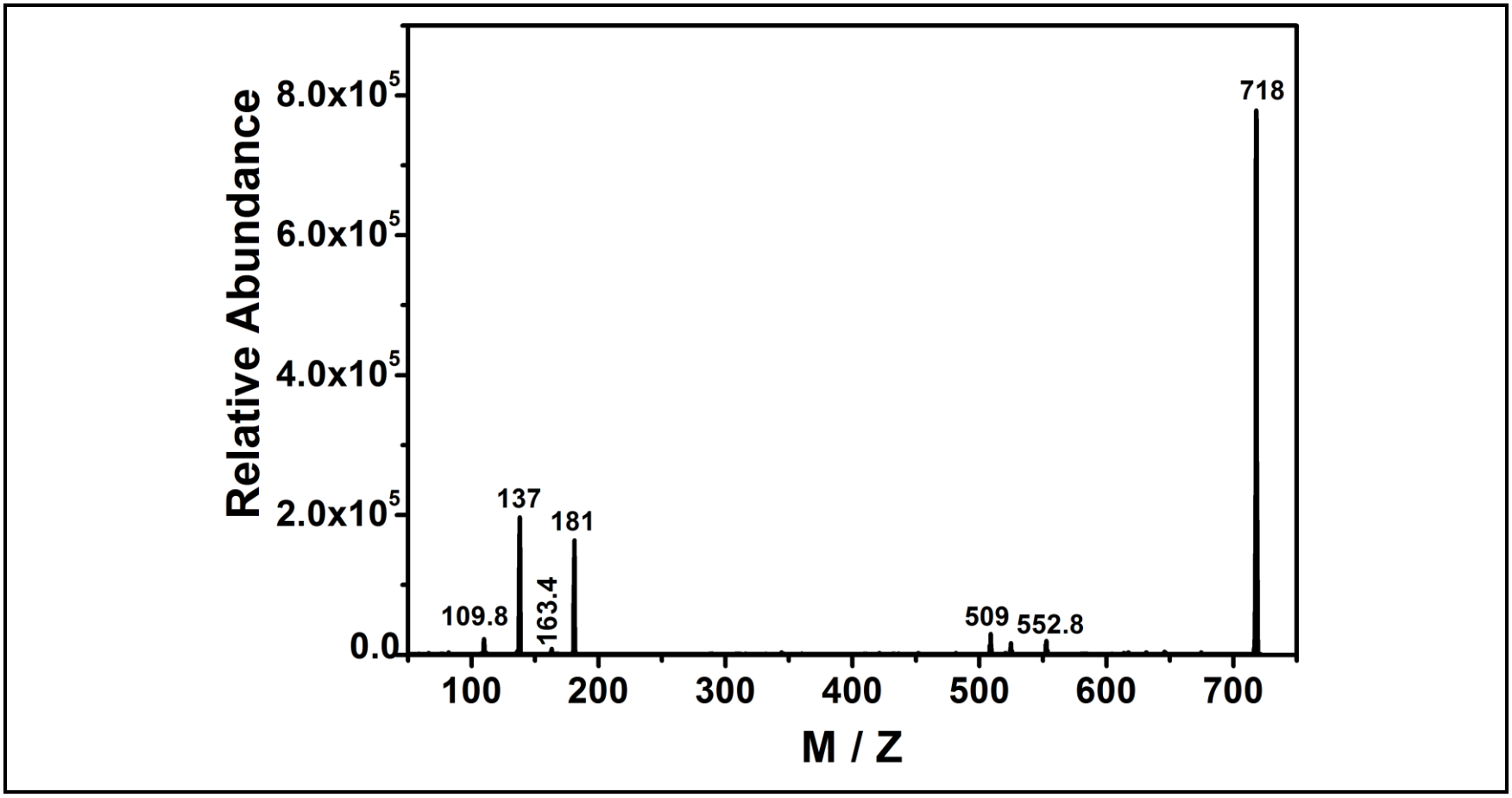

Figure 4.80: Mass-spectrum of **TPDI** in DMF

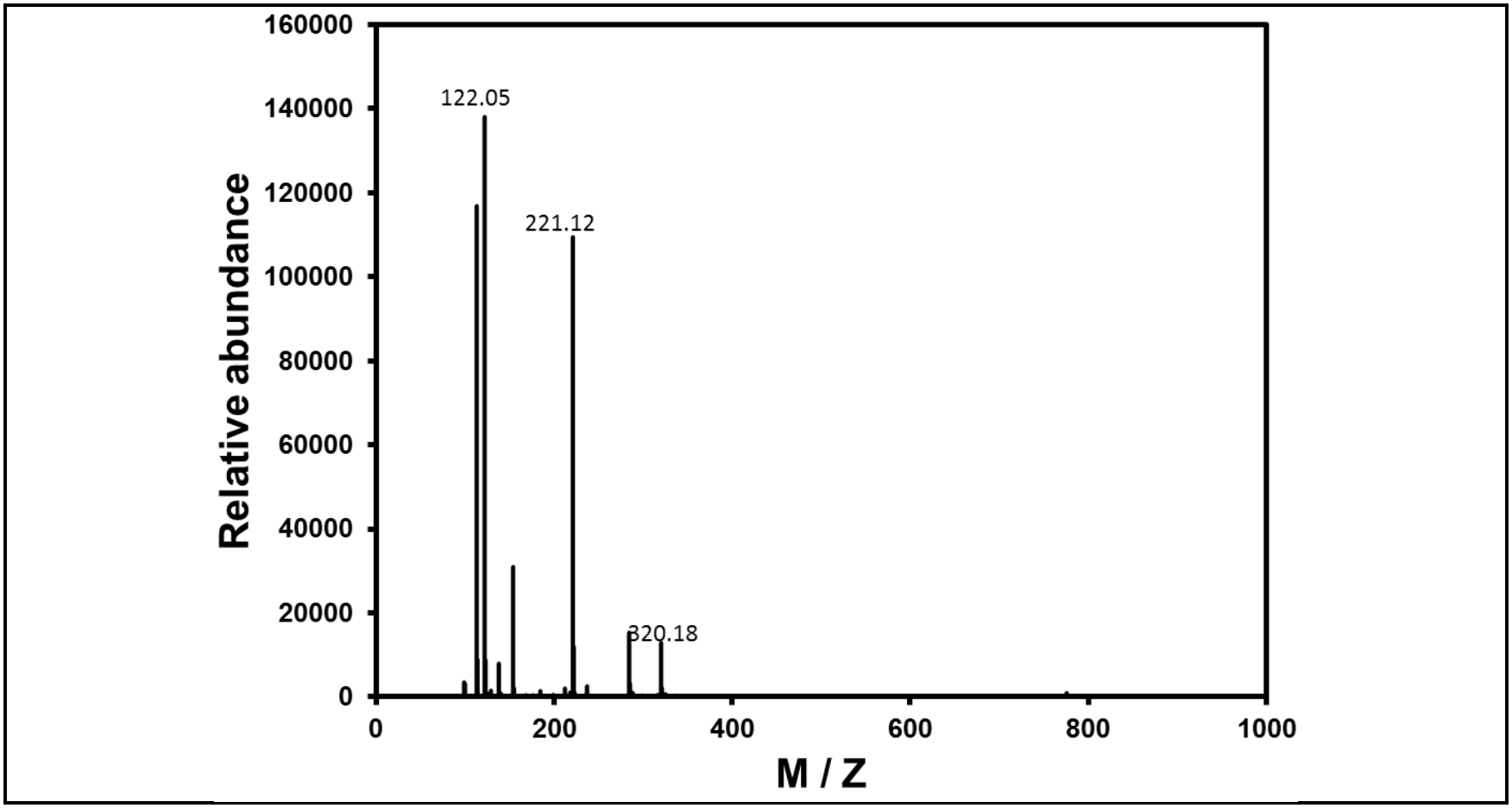

Figure 4.81: Mass-spectrum of **TCPDI** in DMF

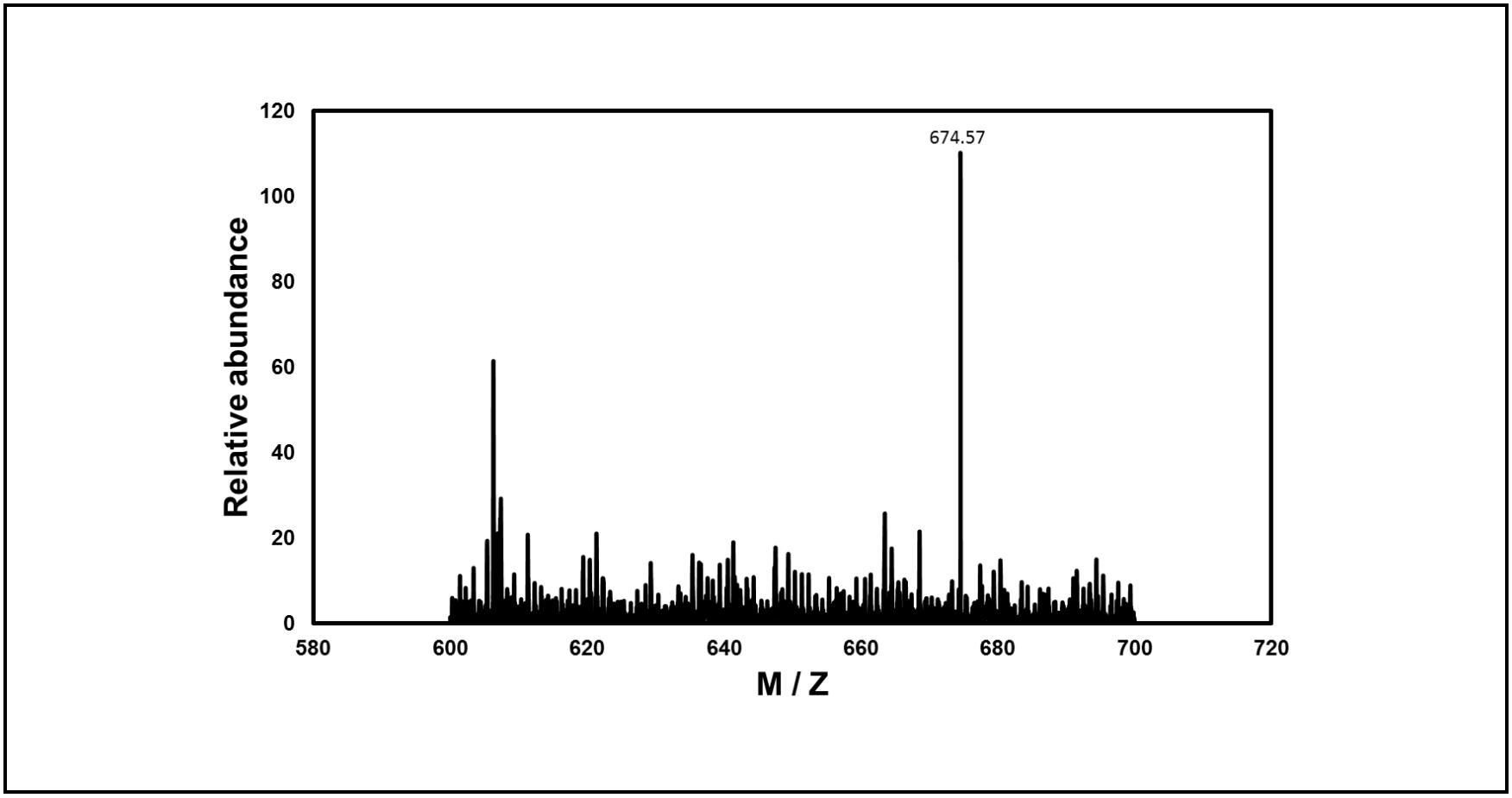

Figure 4.82: Mass-spectrum of **TCPDI** in DMF zoomed in

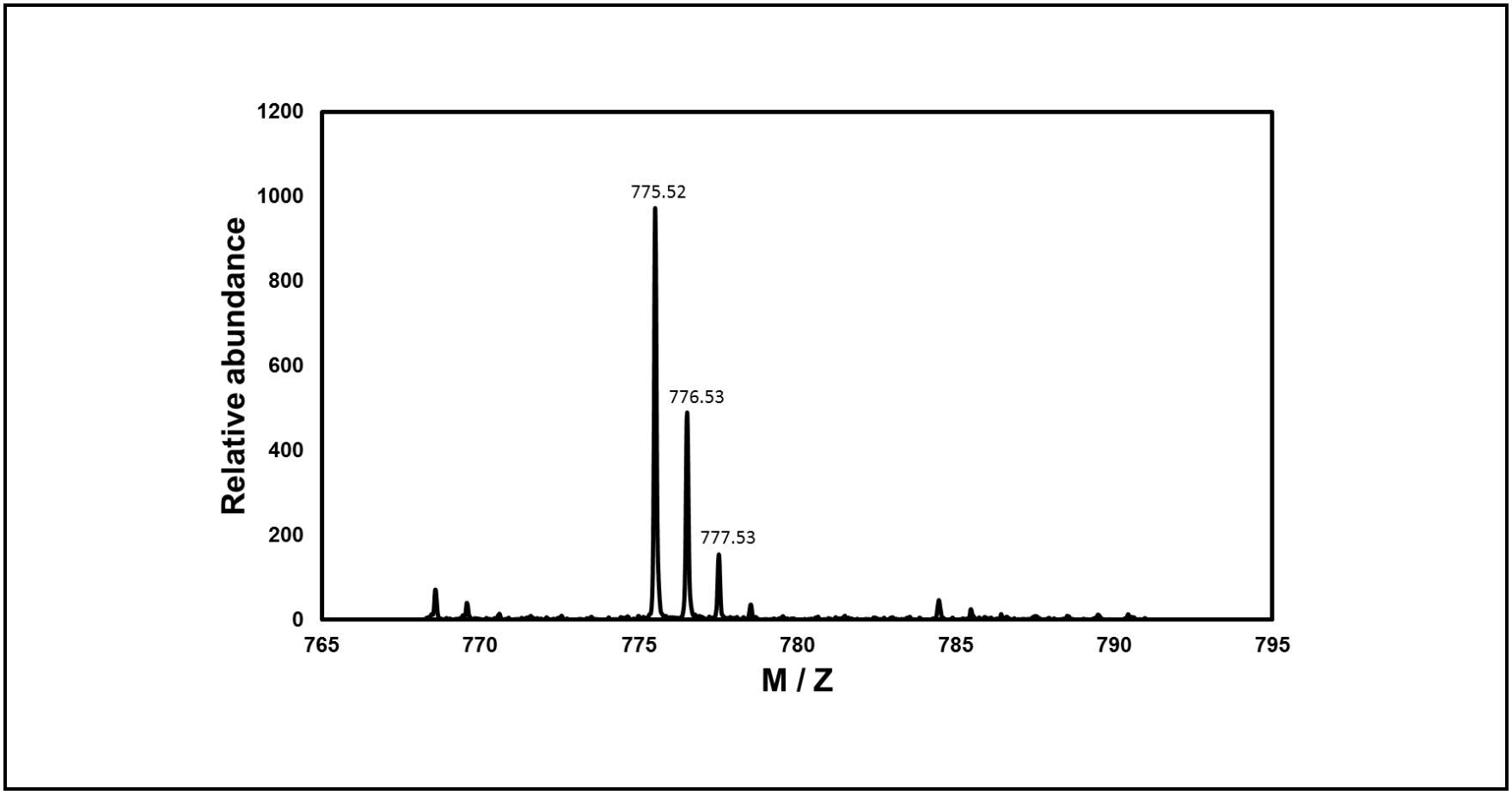

Figure 4.83: Mass-spectrum of **TCPDI** in DMF zoomed in

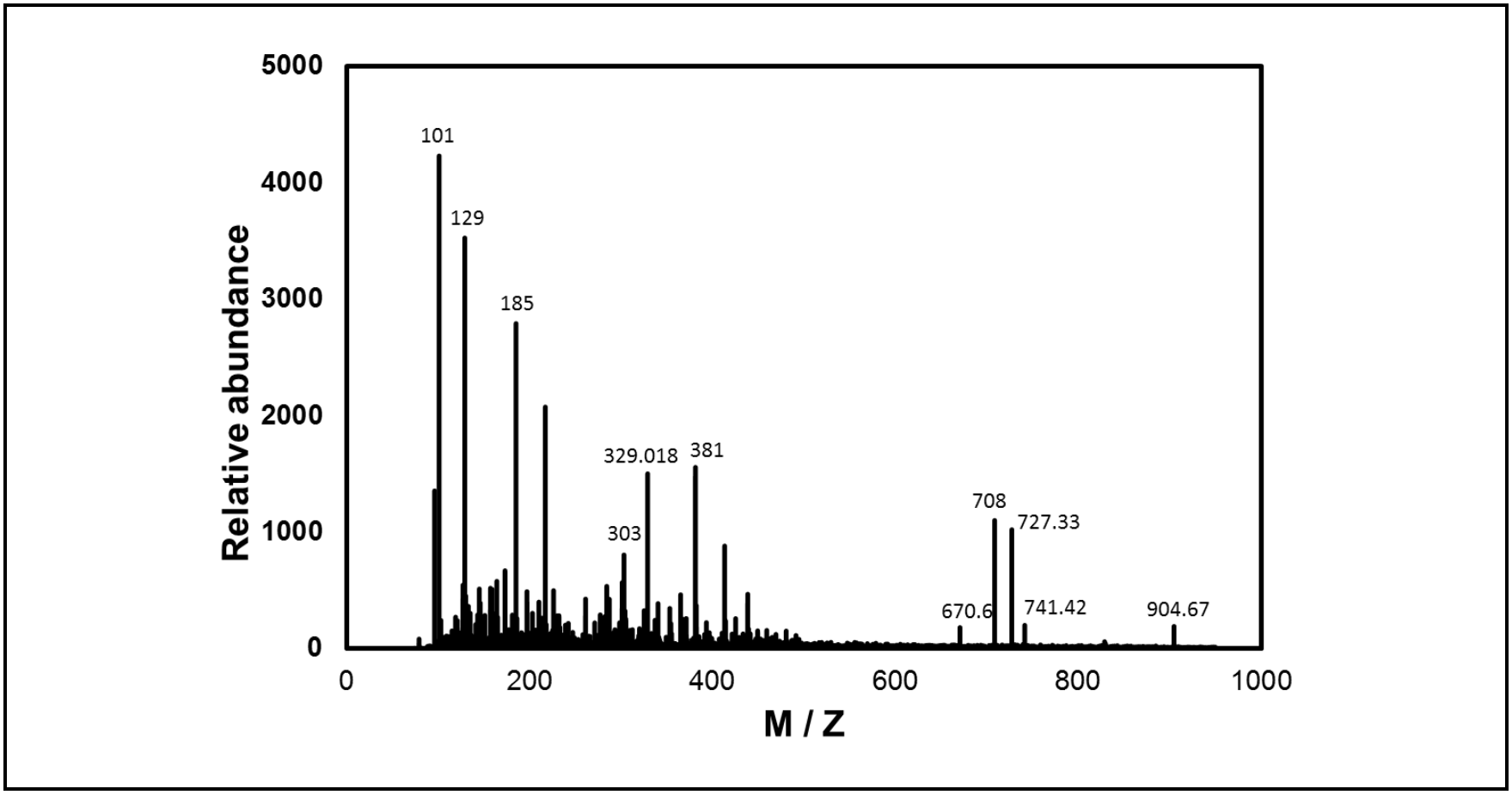

Figure 4.84: Mass-spectrum of **TAPDI** in CHL

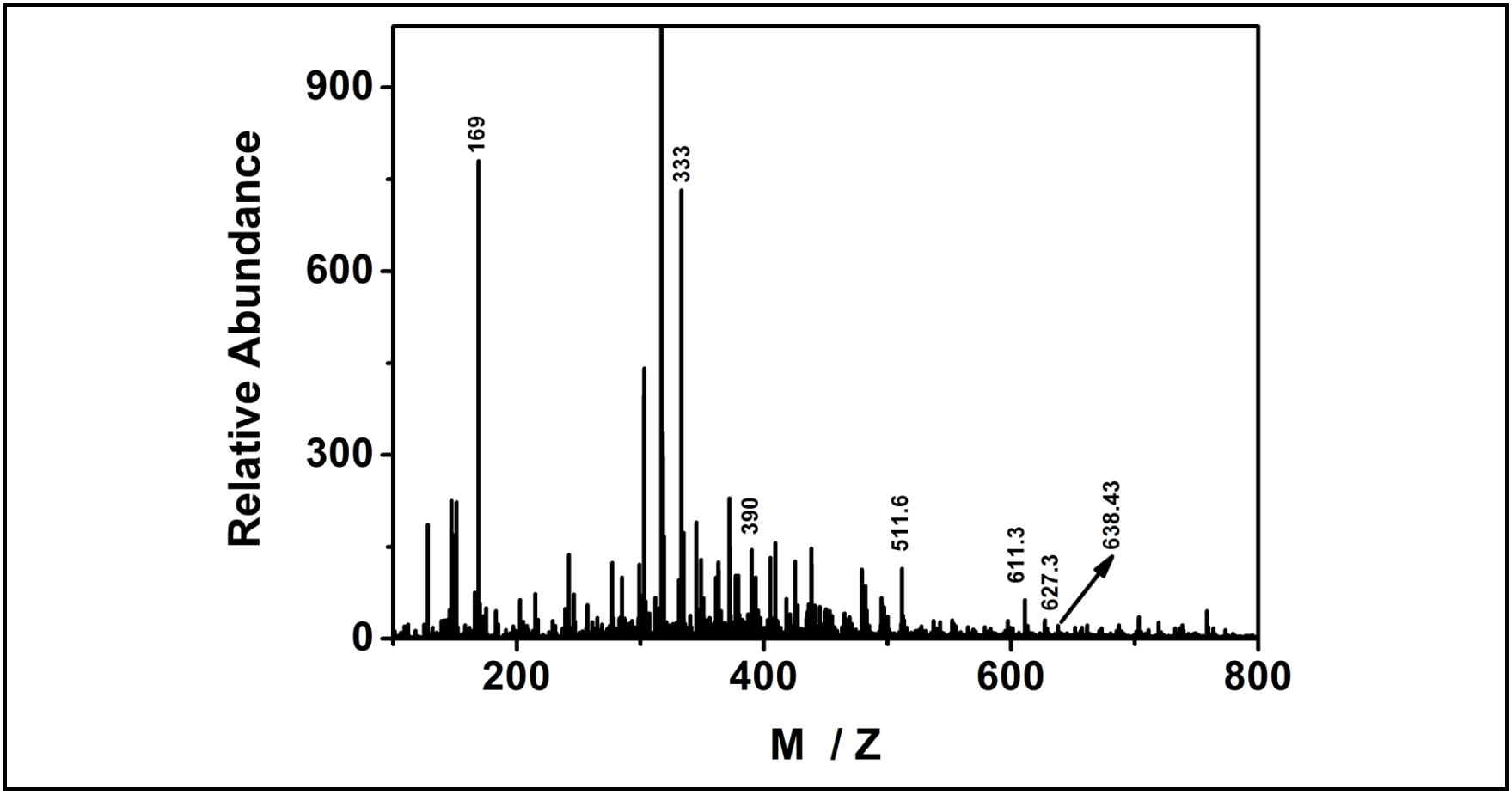

Figure 4.85: Mass-spectrum of **BPY-PDA** in DMF

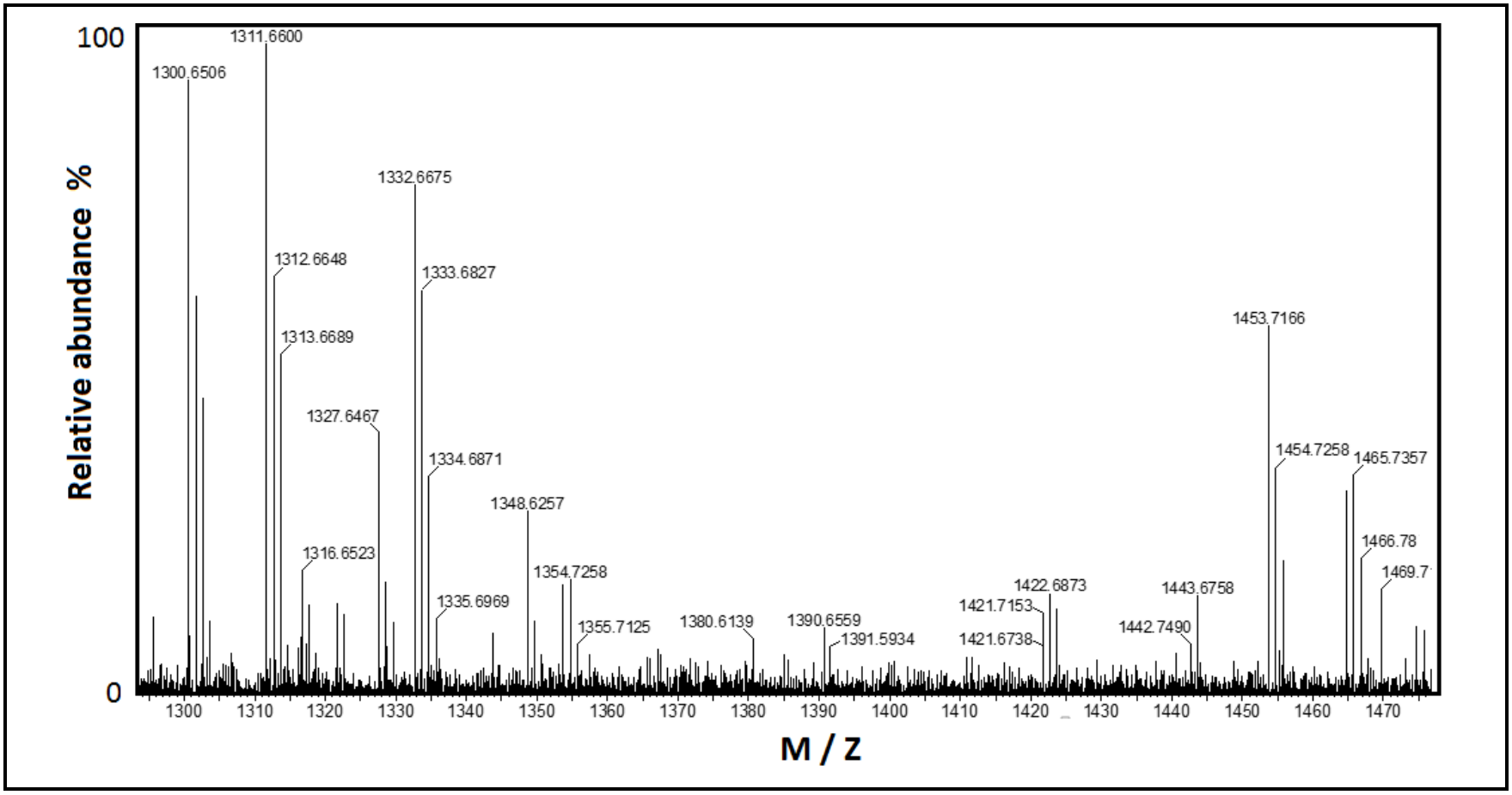

Figure 4.86: Mass-spectrum of **BTC-APDI** in CHL

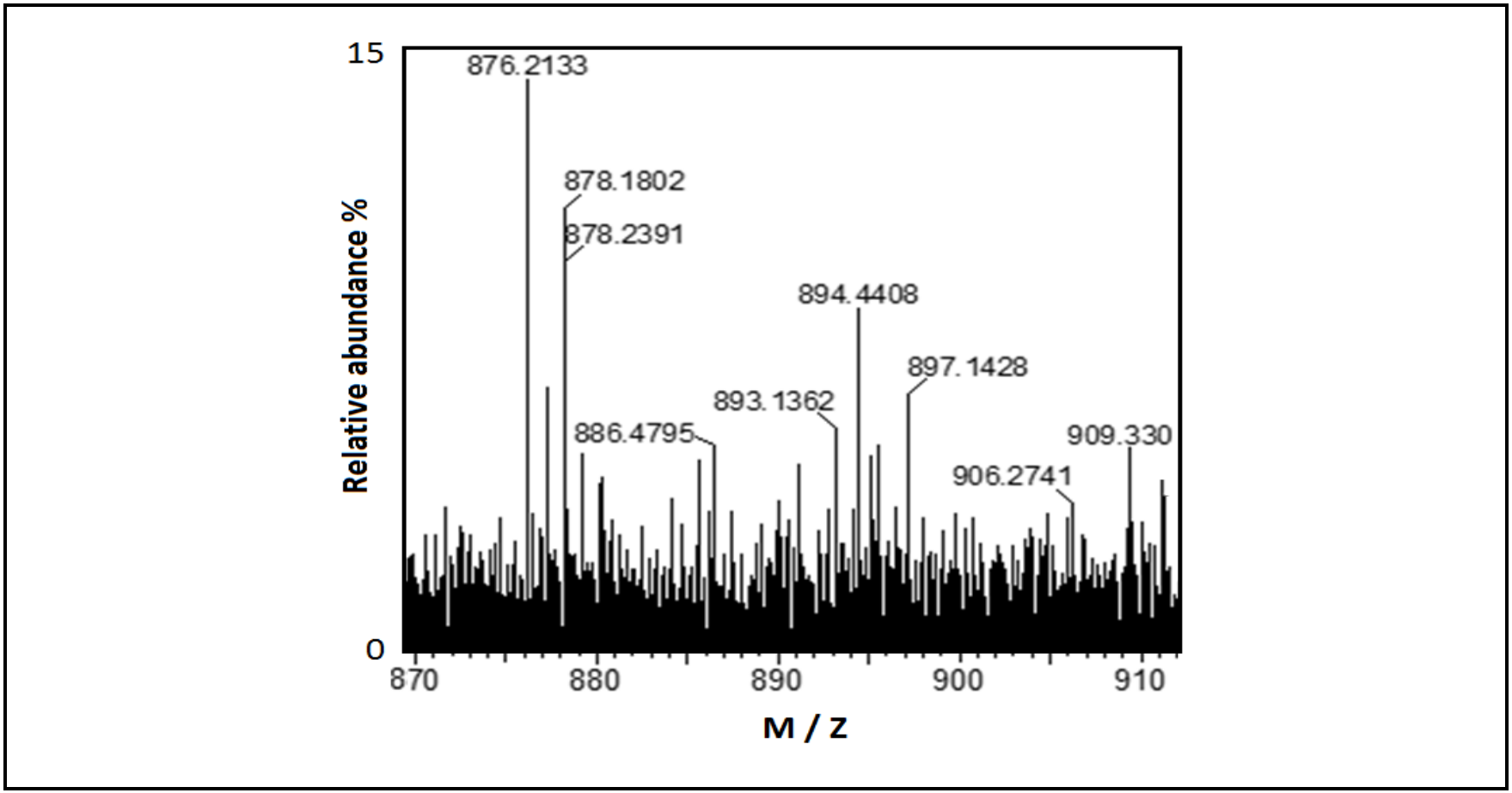

Figure 4.87: Mass-spectrum of **BTC-APDI** in CHL

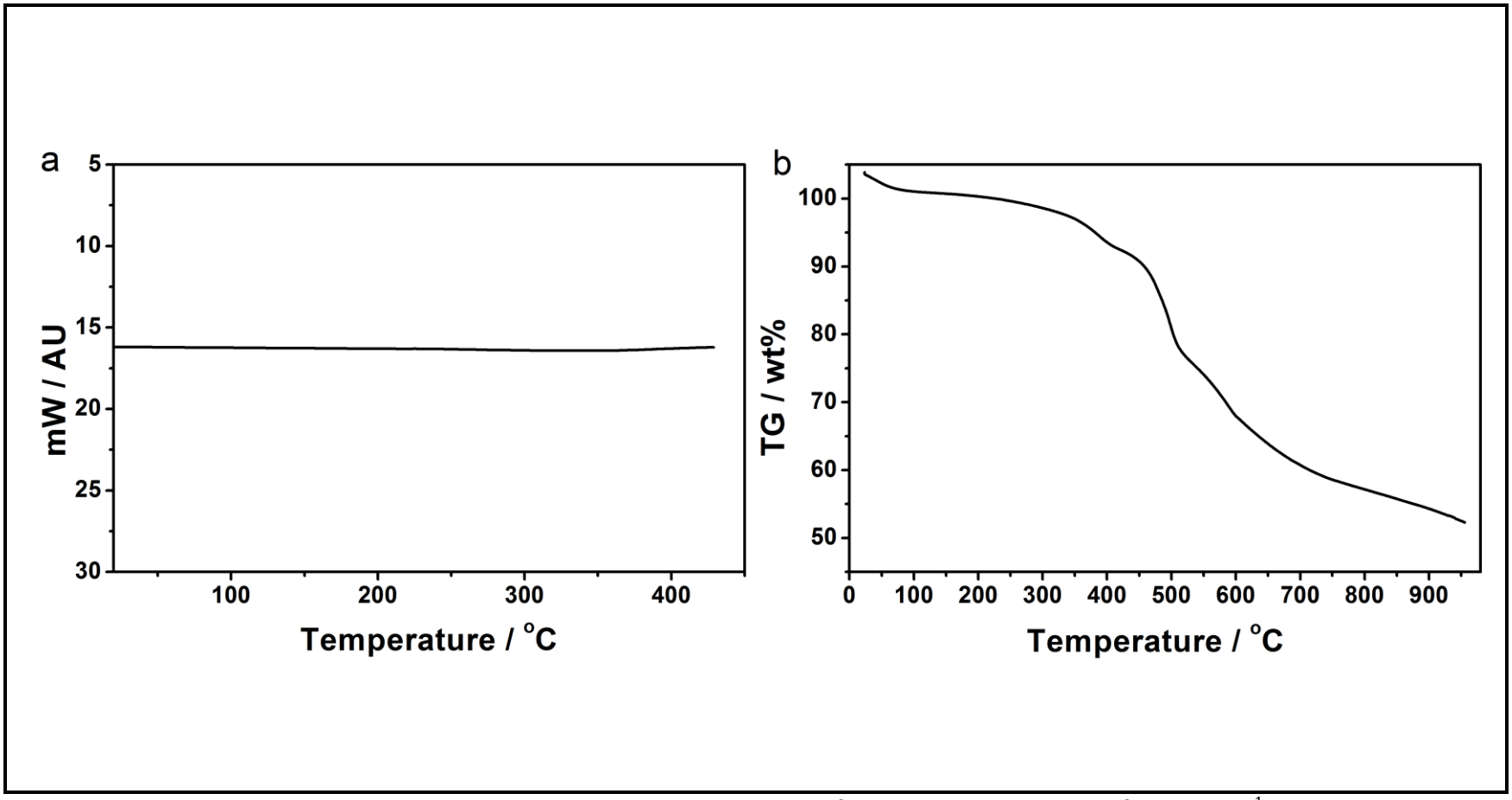

Figure 4.88: (a) DSC thermogram; (b) TGA curves of **TPDI** at a heating rate of 10 ^{o}C min^{-1}

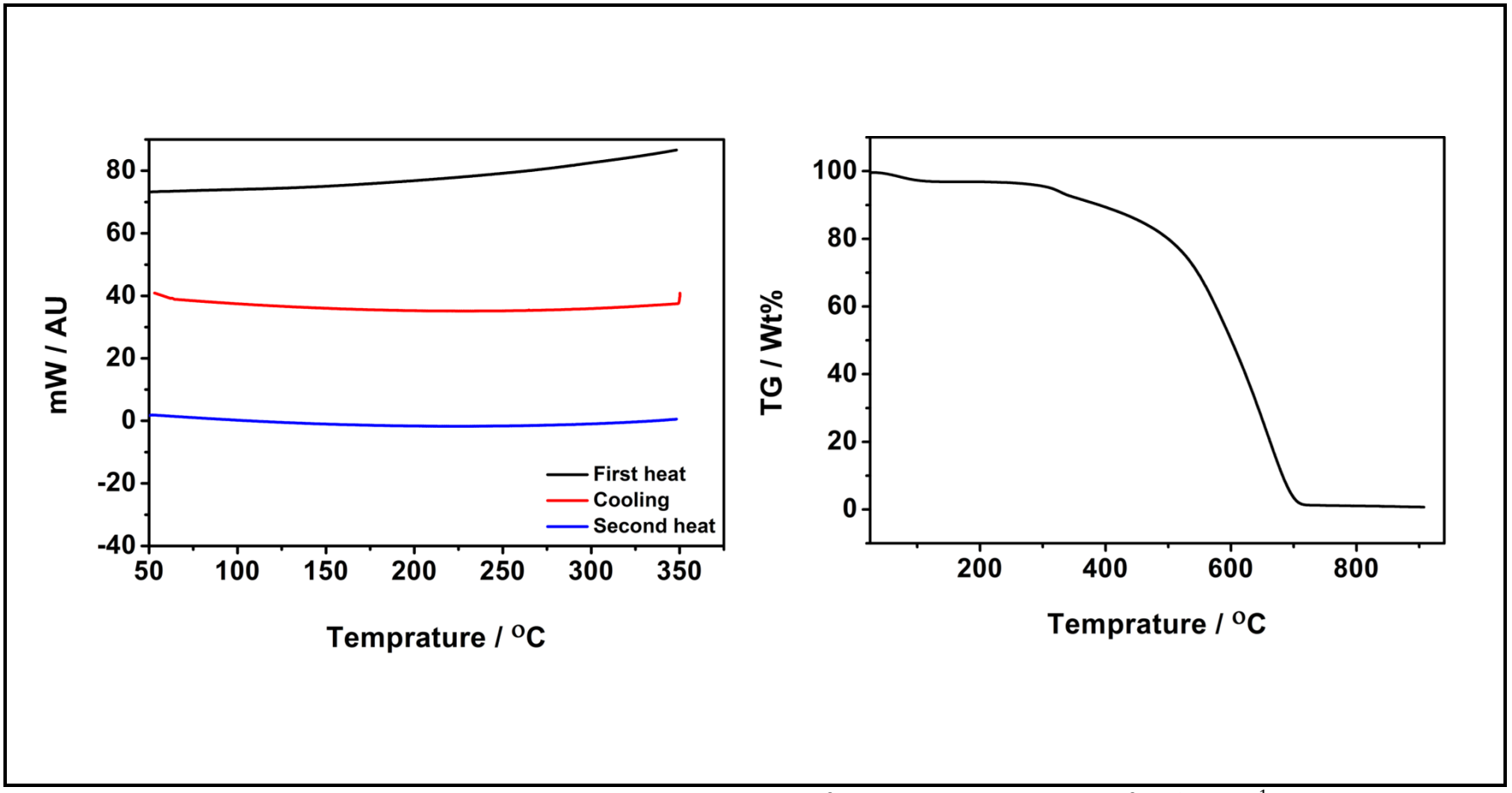

Figure 4.89: (a) DSC thermogram; (b) TGA curves of **TCPDI** at a heating rate of 10 ^{o}C min^{-1}

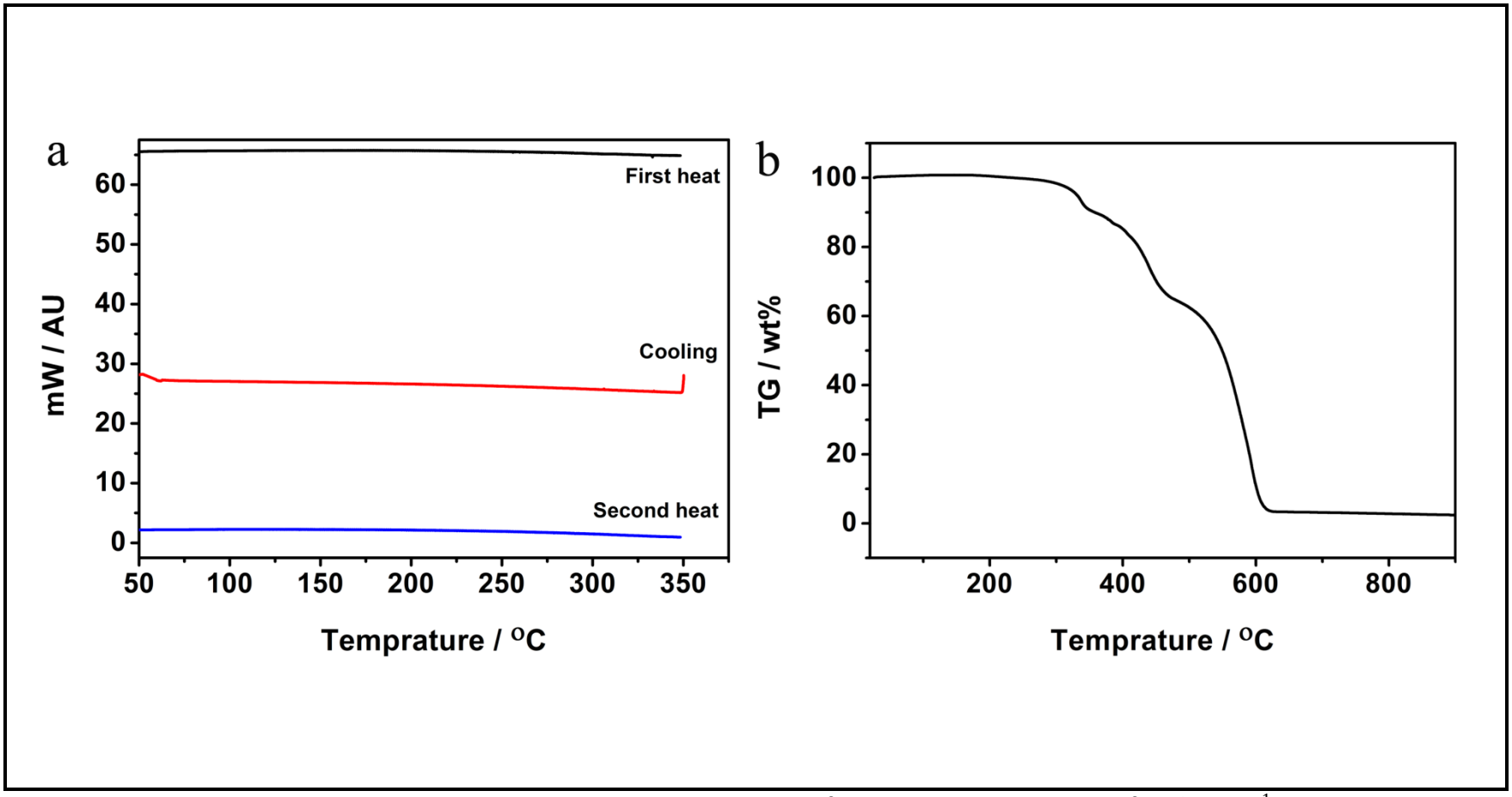

Figure 4.90: (a) DSC thermogram; (b) TGA curves of **TAPDI** at a heating rate of 10 ^{o}C min^{-1}

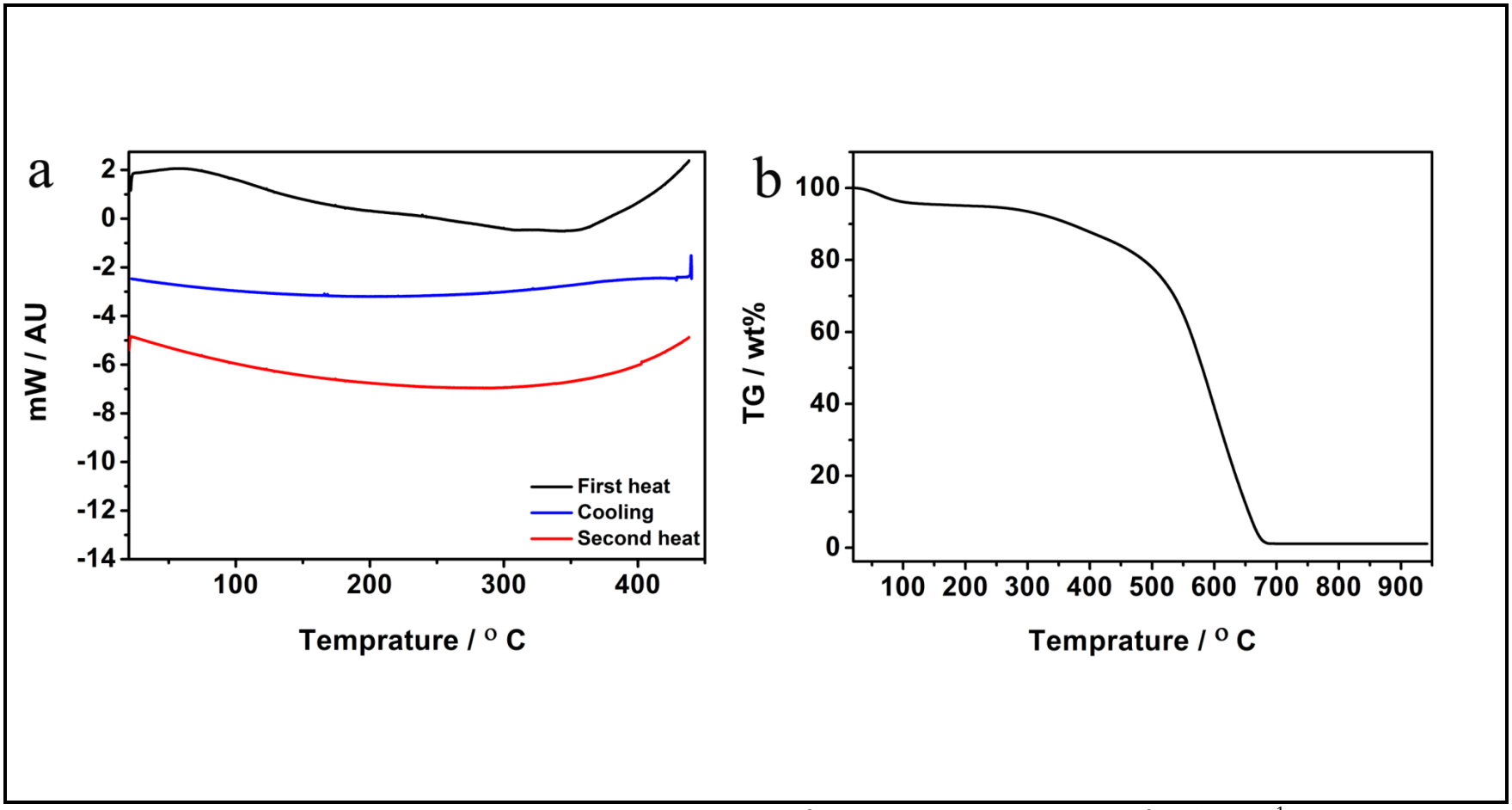

Figure 4.91: (a) DSC thermogram; (b) TGA curves of **BPY-PDA** at a heating rate of 10 ^{o}C min^{-1}.

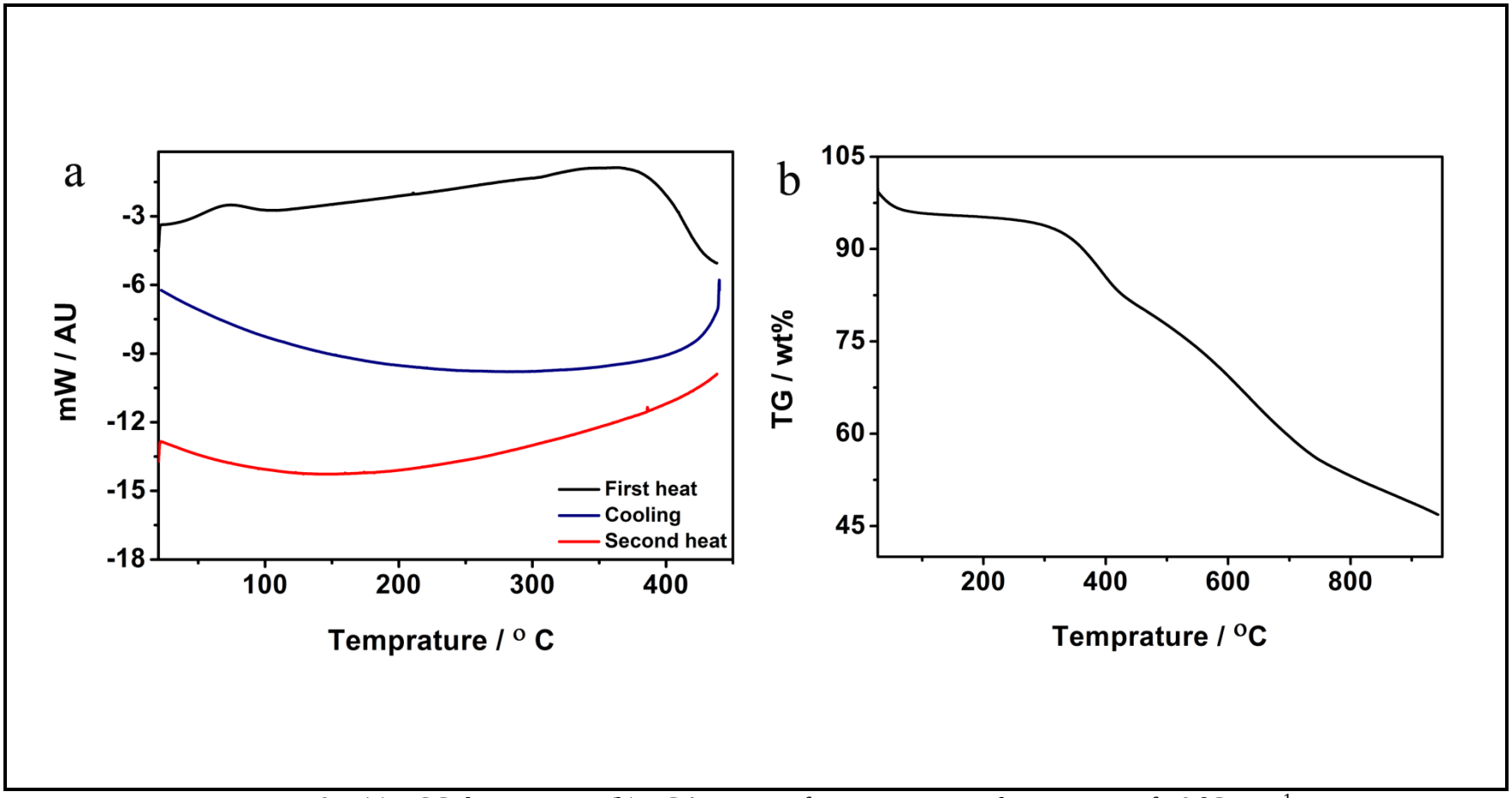

Figure 4.92: (a) DSC thermogram; (b) TGA curves of **BPY-PPDI** at a heating rate of 10 ^{o}C min^{-1}

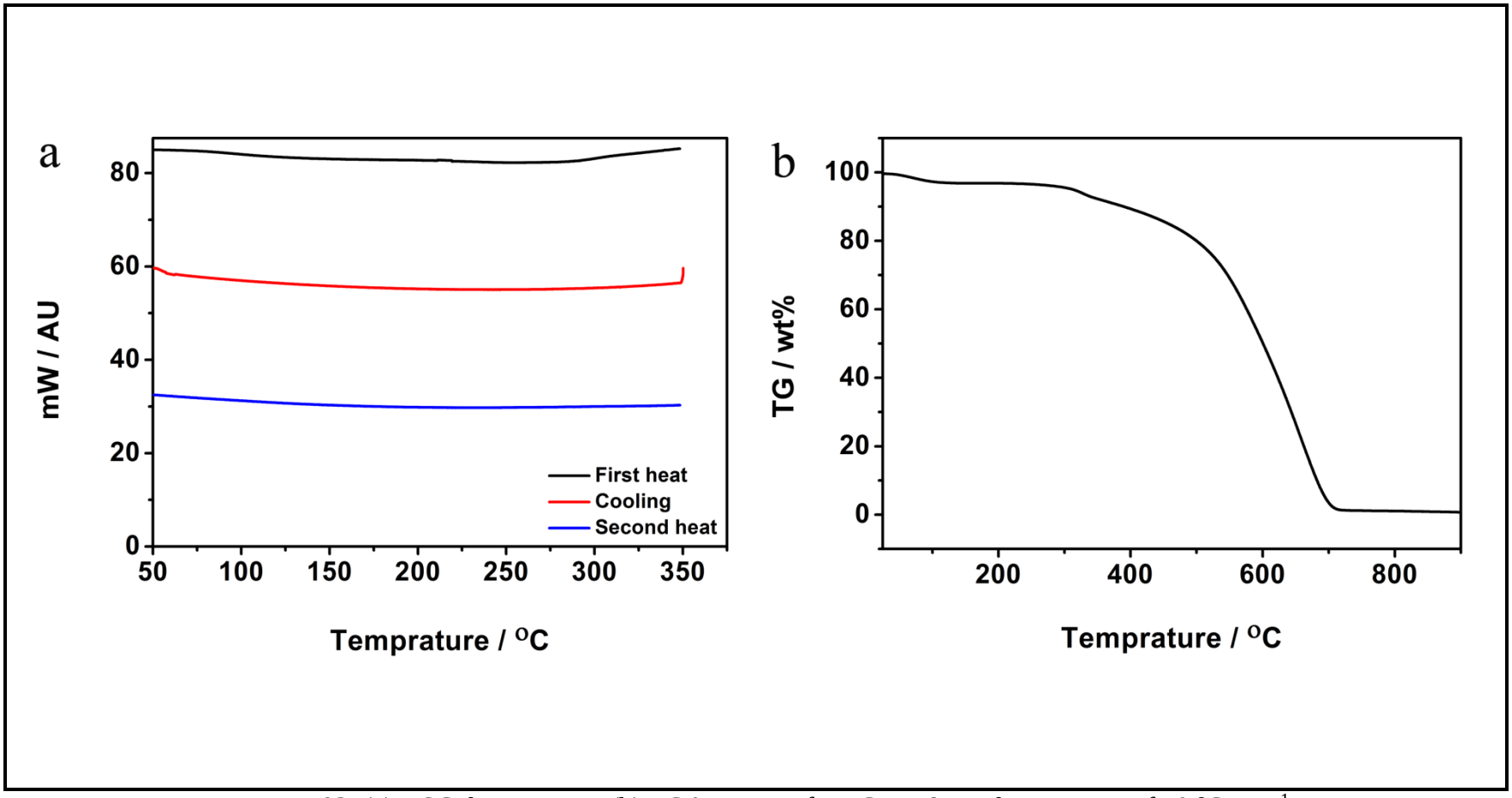

Figure 4.93: (a) DSC thermogram; (b) TGA curves of **BTC-PDA** at a heating rate of 10 ^{o}C min^{-1}

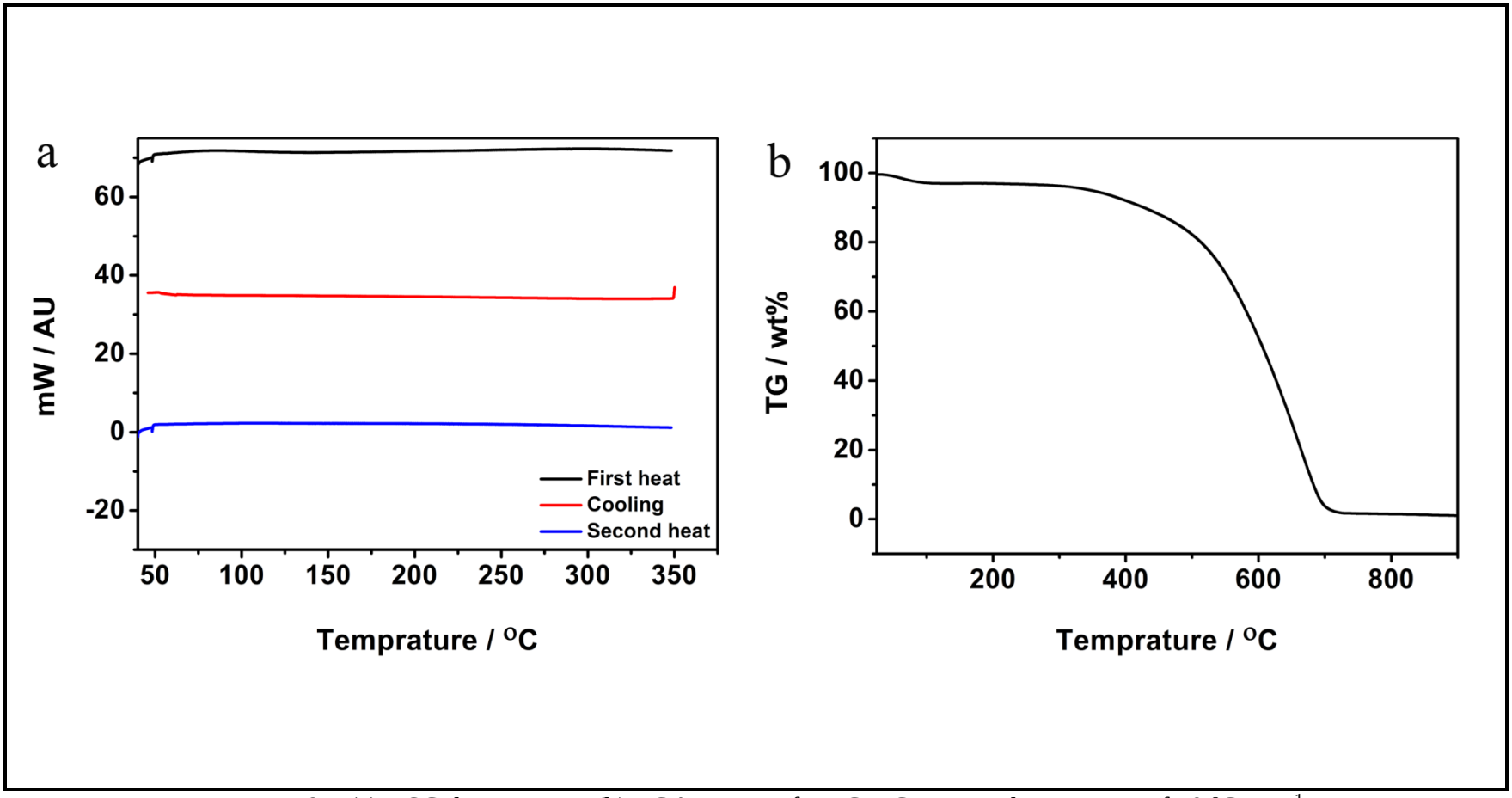

Figure 4.94: (a) DSC thermogram; (b) TGA curves of **BTC-TCPDI** at a heating rate of 10 ^{o}C min^{-1}

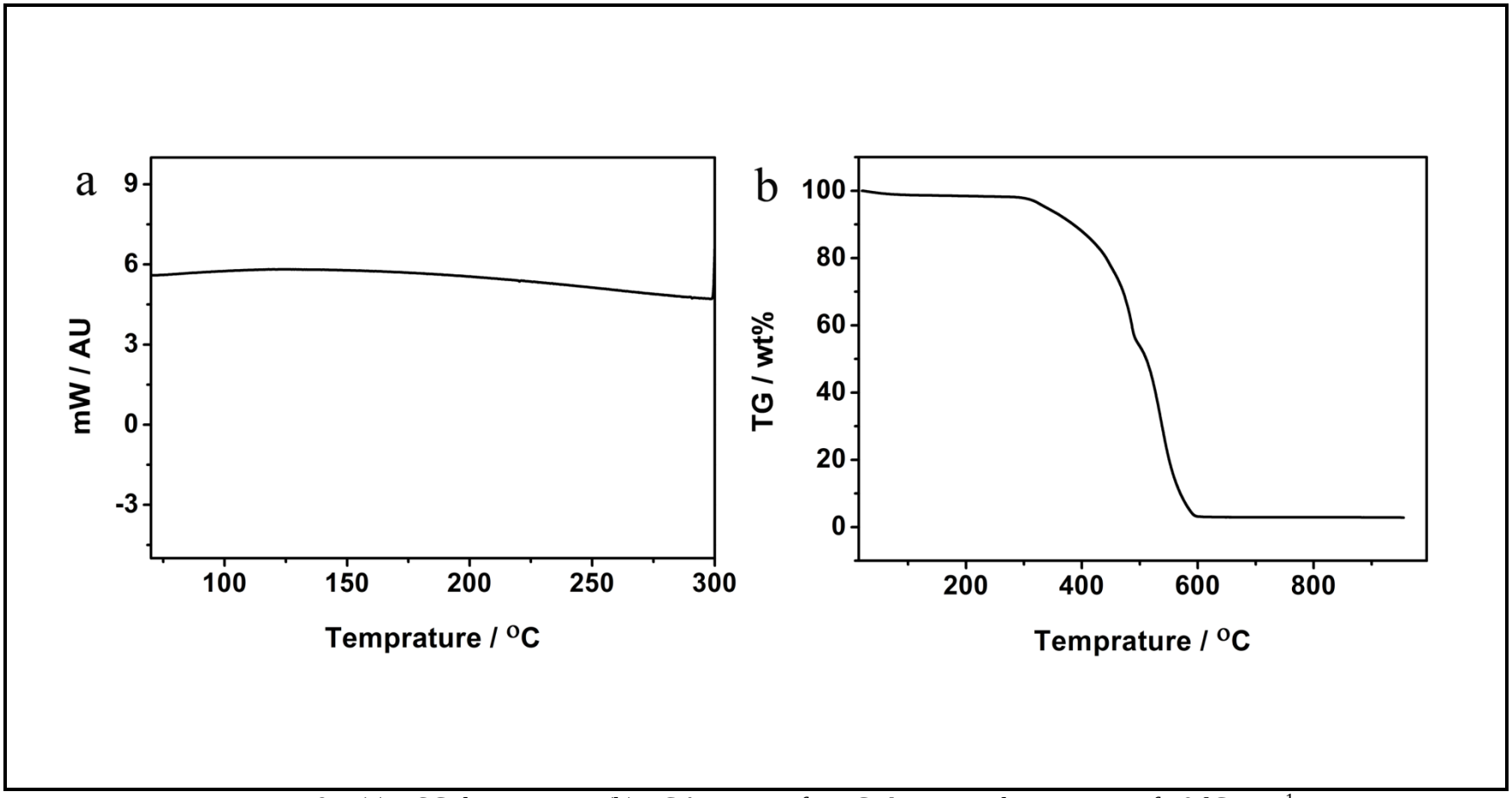

Figure 4.95: (a) DSC thermogram; (b) TGA curves of **BTC-APDI** at a heating rate of 10 ^{o}C min^{-1}

Chapter 5

RESULTS AND DISCUSSION

5.1 Synthesis of Symmetrical and Asymmetrical Perylene Diimide (PDI)

In the present study, three different perylene diimide which two of them were symmetrical (TPDI and TC-PDI) and one was highly soluble asymmetrical (APDI) have been synthesized in high yields, after complete purification of the products characterization have been done by IR spectrophotometer making KBr pellet (Figure 4.18, 4.19, 4.20 and 4.21).

In IR spectrum of TPDI (Figure 4.18) the characteristic peaks are as follow:
3341 and 3179 (amide N-H), 2013 (aliphatic C-H), 2222 (CN stretch), 1658 and 1715 (imide and amide C=O), 1580 (aromatic C=C), 1330 (C-N), 814 and 737 (aromatic C-H bend).

Also the IR spectrum of TCPDI (Figure 4.19) shows the characteristic peaks as follow: 3338 (O-H str.), 3046 (aromatic C-H), 2850 (aliphatic C-H), 1695 and 1584 (imide C=O), 1569 (aromatic C=C), 1353 (C-N), 1109 (C-O str.), 810 (C-H bend).

Comparing the IR-spectrum of perylene dianhydride (Figure 4.17) with the IR peaks of these two compounds clearly shows that in carbonyl region of anhydride 1775 and 1734 cm^{-1} the peaks are replaces with imides carbonyl peaks (1715,1658 for TPDI

and 1695, 1584 for TCPDI) which are at different wave numbers and the anhydride peaks have been totally disappeared.

In the case of TAPDI the reaction has been done in three steps of making K-salt, monoimide monoanhydride (TCPMI) preparation and finally asymmetrical TAPDI. The IR spectrums analyses are as follows:

TCPMI IR spectrum (Figure 4.20): 34200 (O-H), 3088 (aromatic C-H), 2927 (aliphatic C-H), 1680 (imide C=O), 1593 (aromatic C=C), 1380 (C-N), 1005 (alcohol C-O), 802 (C-H bend). TAPDI IR spectrum (Figure 4.21) has shown the characteristic peaks at: 2919 (C-H aliphatic), 1703, 1652 (imide C=O), 1592 (aromatic C=C), 1329 (C-N), 819 and 751 (C-H bend).

5.2 Synthesis of Bay-Substituted Perylene Diimide

In order to change the photophysical and photochemical properties of the diimides, 1,7-symmetrically substituted perylenebis (dicarboximide) dyes (BTC-TCPDI, BPY-PPDI and BTC-APDI) with electron donating groups have been synthesized in good amount of product under mild conditions to achieve this purpose, at first brominated PDA or shortly (Br-PDA) was prepared in accordance with the literature procedure and then modification of perylene core at bay position was done by using different alcoholic substituents. And in the end the synthesis was completed by functionalisation of imide positionsthe IR spectrums of the products are taken by KBr pellet and the results are as below:

Br-PDA IR spectrum (Figure 4.22) shows the following peaks: 3058 (aromatic C-H), 1774 and 1721 (anhydride carbonyl C=O), 1589 (aromatic C=C), 1025 (anhydride C-O-C str.), 690 (C-Br). It has been found that the peak at 690 cm^{-1} compared with pure perylene anhydride (Figure 4.17) has been appeared after bromination.

The IR spectrum of BPY-PDA (Figure 4.23) has shown the characteristics at 3321 and 3146 (amine N-H), 1756 and 1712 (anhydride C=O), 1650(C=N), 1589 (aromatic C=C), 1352 (C-N str.), 1254 (C-O-C ether), 1025 (C-O-C anhydride), 805 and 735 (C-H bend).

The IR spectrum of BPY-PPDI (Figure 4.24) likewise was taken and has the peaks at 3321 and 3163 (amine N-H), 3058 (aromatic C-H), 2935 (aliphatic C-H), 1660 and 1694 (imide C=O), 1589 (aromatic C=C), 1342 (C-N), 1254 (C-O-C ether), 806 and 700 (C-H bend).

As can be seen in IR spectrum of BPY-PDA (figure 4.23) the bromine peak at 690 cm^{-1} has been disappeared and instead the peak at 1254 cm^{-1} which confirmed the formation of product has been produced.

The BTC-PDA IR spectrum (Figure 4.25) has been taken with the peaks at 3445 and 3335 (amine N-H), 3063 (aromatic C-H), 2910 (aliphatic C-H), 1721 and 1753 (anhydride C=O), 1584 (aromatic C=C), 1236 (C-O-C ether), 1014(C-O-C anhydride), 734 (C-H bend).

IR spectrum of BTC-TCPDI (Figure 4.26) has shown the characteristic peaks at 3335 and 3165 (amine N-H), 3045 (aromatic C-H), 2927 (aliphatic C-H), 1660 and 1694 (imide C=O), 1584 (aromatic C=C), 1252 (C-O-C ether), 1014 (alcohol C-O), 810 and 734 (C-H bend).

As can been seen in (Figure 4.27) the IR peaks of BTC-APDI are shown at 3326 (amine N-H), 3054 (aromatic C-H), 2918 (aliphatic C-H), 1695 and 1660 (imide

C=O), 1593 (aromatic C=C), 1337 (C-N), 1252 (C-O-C ether), 819 and 750 (C-H bend).

It is worthy to mentioned that all of the above IR pellets were dried in vacuum oven for 4 hrs at 125 °C and the broadness that can be seen in some of those IR graphs (Figure 4.19, 4.23, 4.24, 4.25, 4.26) probably comes from intermolecular interactions in solid state.

5.3 Solubility of the Perylene Diimides

Table 5.1 shows the solubility of TPDI in various solvents, as can be seen below the compound shows complete solubility in dipolar aprotic (NMP, DMF, DMAC and DMSO) at room temperature and partial solubility in polar protic (EtOH and MeOH) and non-polar solvents (TCE and CH_2Cl_2) at 35 °C. Having cyano group at thiophene ring decreased the planarity of the structure and consequently the π-π stacking of the aromatic rings was prevented as a result the compound shows good solubility in most of organic solvents.

Table 5.1: Qualitative solubility of TPDI

Solvent	**TPDI**	
	Solubility[a]/Color	
TCE	(+ −)[c]	/Pink
TFAc	(+)[b]	/Orange
CH_2Cl_2	(+ −)	/Pale pink
EtOH	(+ −)	/Pale pink
NMP	(+)	/bordeaux
CH_3OH	(+ −)	/Pale pink
DMF	(+)	/Orange
DMAC	(+)	/Orange
DMSO	(+)	/Red

[a] Measured at a concentration of 1 mg mL^{-1} in solvents at 25 °C.
[b] (+): soluble at room temperature.
[c] (+ −): partially soluble on heating at 35 °C in sonicator.

TCPDI has less solubility compared with TPDI, it has complete solubility in dipolar aprotic solvents (NMP, DMF, DMAC and DMSO) at room temperature, mostly soluble in non-polar solvents (DCM, TCE and CHL) and slightly soluble in acetone, surprisingly TCPDI has complete solubility in pyridine and m-cresol as non-polar solvents because of their aromatic nature.

Table 5.2: Qualitative solubility of TCPDI

Solvent	**TCPDI**	
	Solubility[a]/Color	
CHL	(++ −)[c]	/Brown
TCE	(++ -)	/Brown
TFAc	(+)[b]	/Wine red
DCM	(++ −)	/Brown
m-cresol	(+)	/Purple
Pyridine	(+)	/Dark brown
Acetone	(-- +)[d]	/Light brown
NMP	(+)	/Dark brown
DMF	(+)	/Dark brown
DMAC	(+)	/Dark brown
DMSO	(+)	/Dark brown

[a]Measured at a concentration of 1 mg mL^{-1} in solvents at 25 °C.
[b] (+): soluble at room temperature.
[c] (++ −): mostly soluble on heating at 35 °C in sonicator.
[d] (-- +): slightly soluble on heating at 35°C in sonicator.

It has been found that modification of perylene dianhydride with vitamine-B_1 (TCPDI) as a symmetrical diimide hasn't leaded to the formation of highly soluble compound, in order to increase the solubility of the compound an asymmetrical TAPDI has been designed by attaching abiethyl amine at one imide position of TAPDI which could prohibit planarity and stacking of the perylene core and the result amazingly showed high solubility of the compound table 5.3 shows the solubility of TAPDI in various organic solvents. As the results show in the following table the compound has solubility in almost all the studied organic solvents at room temperature.

Table 5.3: Qualitative solubility of TAPDI

Solvent	**TAPDI**	
	Solubility[a]/Color	
CHL	(+)[b]	/Orange
Ethyl acetate	(+ -)[c]	/Orange
THF	(+)	/Orange
TCE	(+)	/Orange
DCM	(+)	/Orange
m-cresol	(+)	/Dark pink
2-propanol	(+-)	/Orange
Acetone	(+ -)	/Orange
NMP	(+)	/Orange
MeOH	(+ -)	/Light red
DMF	(+)	/Orange
DMAC	(+)	/Orange
DMSO	(+)	/Orange

[a] Measured at a concentration of 1 mg mL^{-1} in solvents at 25 °C.
[b] (+): soluble at room temperature.
[c] (+ −): partially soluble on heating at 35 °C in sonicator.

5.4 Solubility of the Bay Substituted PDI

It was expected to have better solubility after modification of the perylene core at

bay position, consequently three different bay-substituted PDIs have been synthesized and the solubility of them were tabulated below (Table 5.4 and 5.5)

Table 5.4: Qualitative solubility of BPY-PDA and BPY-PPDI.

Solvents	**BPY-PDA**	**BPY-PPDI**
	Solubility[a]/Color	Solubility/Color
TFAc	(+)[b]/Purple	(+)/Purple
m-Cresol	(+)/Dark red	(+)/Dark red
Pyridine	(+)/Dark brown	(+)/Dark brown
NMP	(+)/Dark brown	(++ -)/Brown
MeOH	(-+)[c]/Pale brown	-
DMF	(+)/Dark brown	(++ -)/Dark gray
DMAC	(+)/Dark brown	(++ -)/Dark gray
DMSO	(+)/Dark brown	(+)/ Dark gray

[a] Measured at a concentration of 1 mg mL^{-1} in solvents at 25 °C.
[b] (+): soluble at room temperature.
[c] (+ −): partially soluble on heating at 35 °C in sonicator.
[d] (++ -): mostly soluble on heating at 35 °C in sonicator.

The results have shown that before imidization the solubility of BPY-PDA was higher than that of BPY-PPDI. In contrast to BPY-PPDI which has less solubility in dipolar solvents (NMP, DMAC, DMF and DMSO), BPY-PDA was highly soluble in dipolar aprotic (NMP, DMAC, DMF and DMSO) and nonpolar solvents (TFAc and m-cresol) with partial solubility in polar protic solvent (MeOH). The reason can be the increased probable intermolecular interactions after imidization which affected the planarity with reduction of solubility of BPY-PPDI.

Table 5.5: Qualitative solubility of BTC-PDA, BTC-TCPDI and BTC-APDI

Solvent	BTC-PDA	BTC-TCPDI	BTC-APDI
	Solubility[a]/Color	Solubility/Color	Solubility/Color
CHL	-	-	(+)/Orange brown
THF	-	-	(+)/Orange brown
TCE	-	-	(+)/Orange brown
TFAc	(+)[b]/Wine red	(+)/Wine red	(+)/Wine red
DCM	-	-	(-- +)[d]/Pale orange
m-cresol	(++ -)[c]/Purple brown	(++ -)/Purple brown	-
Pyridine	(+)/Dark brown	(+)/Dark brown	-
Acetone	-	-	(-- +)/Pale orange
NMP	(+)/Dark brown	(+)/Dark brown	(+ -)[e]/Brown orange
DMF	(+)/Dark brown	(+)/Dark brown	(+)/Brown orange
DMAC	(+)/Dark brown	(+)/Dark brown	(+)/Brown orange
DMSO	(+)/Dark brown	(+)/Dark brown	(+)/Brown orange

[a] Measured at a concentration of 1 mg mL^{-1} in solvents at 25 °C.
[b] (+): soluble at room temperature.
[c] (++ −): mostly soluble on heating at 35 °C in sonicator.
[d] (-- +): slightly soluble on heating at 35°C in sonicator.
[e] (+ -): partially soluble on heating at 35°C in sonicator.

Likewise the solubility tests for the last three bay-substituted perylene derivatives have been done and the results are tabulated above (Table 5.5), it has been found that modification of the perylene core by vitamin-B_1 at bay position has given complete solubility just in dipolar solvents (DMSO, DMAC and DMF), and protic solvents (TFAc). Among all the non-polar solvents BTC-PDA has shown complete solubility just in pyridine and m-cresol.

In synthesizing BTC-TCPDI the same reagent (vitamin-B_1) has been used for imidization and the product has the unique plus-type structure with vitamin at both bay and imide positions. The solubility of the final product hasn't been improved after imidization and it yielded the same solubility as bay-substituted anhydride (BTC-PDA), which was only soluble in dipolar solvents (DMF, DMAC and DMSO), protic (TFAc) and non-polar solvents such as pyridine and m-cresol.

As the last synthesized bay-substituted derivative, BTC-APDI has been synthesized with the aim of increasing the solubility and changing the photo-physical properties of the compound. Given the circumstances abiethyl-amine was selected as an amine in imidization step. Surprisingly the product has shown great solubility in non-polar solvents such as CHL, THF and TCE with slight solubility in acetone and DCM. Similarly the solubility of the compound has been checked in dipolar solvents (DMF, DMAC and DMSO) and it was found that BTC-APDI has complete solubility in the mentioned organic solvents as well (Table 5.5).

5.5 Analyses of NMR and Mass Spectra

The interpretation of NMR data for all the synthesized compounds is presented below.

Compound TPDI

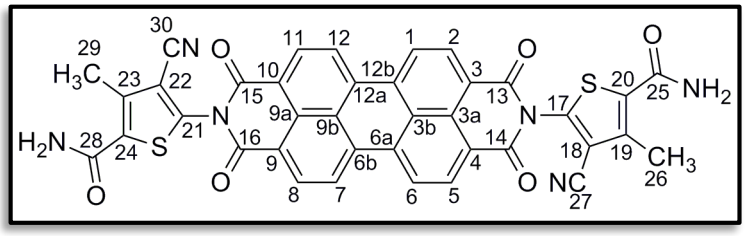

^{1}H NMR, (δ_H pm, 400 MHz, $CDCl_3$): 8.53-8.49 (m, Ar-H, H-C(1), H-C(2), H-C(5), H-C(6), H-C(7), H-C(8), H-C(11), H-C(12)), 8.14 (s, 2H, NH), 7.94 (s, 2H, NH), 2.26 (s, 1CH_3, H_3-C (29)), 2.39(s, 1CH_3, H_3-C (26)).

^{13}C NMR, (δ_c pm, 400 MHz, $CDCl_3$): 164.13 (6 C=O, C(13), C(14), C(15), C(16), C(25), C(28)), 145.94 (4 ArC, C(17), C(20), C(21), C(24)), 133.90 (4 ArC, C(3), C(4), C(9), C(10)), 131.27 (4 ArC, C(6a), C(6b), C(12a), C(12b)), 127.57 (4 ArC,

C(3a), C(9a), C(3b), C(9b)), 124.68 (4 ArC, C(2), C(5), C(8), C(11)), 121.65 (4 ArC, C(1), C(6), C(7), C(12)), 120.20 (2 CN, C(27), C(30)), 108.55 (4(C), C(18), C(19), C(22), C(23)), 53.42 (2 CH_3, C(26), C(29)).

MS (EI, m/z): 718 $[M-1]^+$, 552.8, 524.8, 509, 109.8 the first two m/z correspond to the $C_7H_5N_2OS$ and H_2NCO fragments.

Compound TCPDI

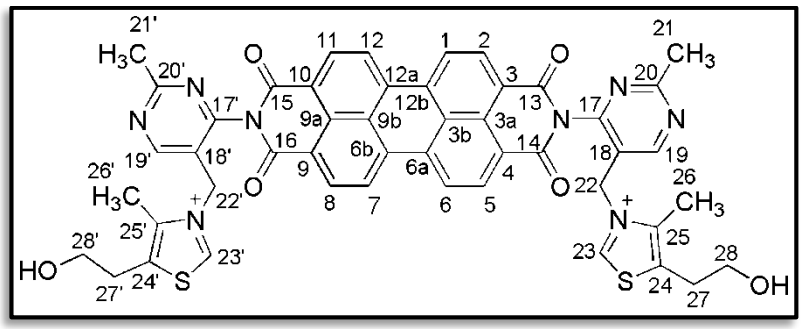

^{1}H NMR and ^{13}C NMR: The NMR spectrum of the compound couldn't be detected because of the low solubility of the compound in deuterated solvents.

MS (EI, m/z) (Mw, 886.994), 775.5, 674.57, 320.18, 122.05. m/z of 775.5 belongs to the loss of C_5H_6NS. m/z of 674.57 corresponds to the loss of C_4H_4NS.

Compound TAPDI

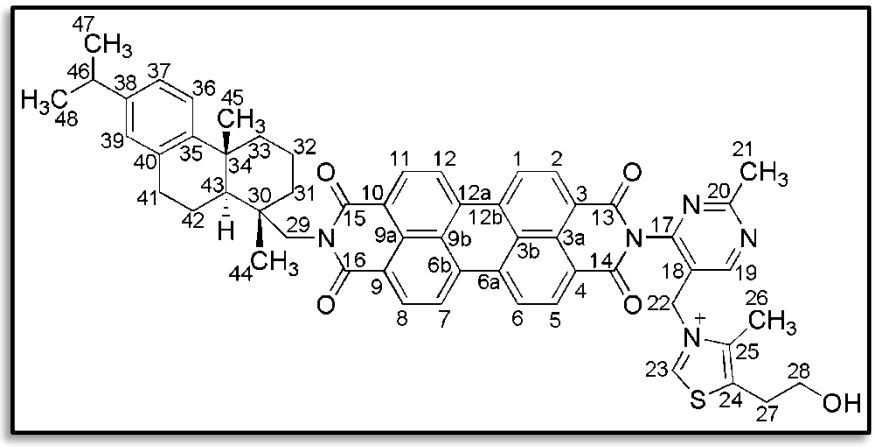

^{1}H NMR, (δ_H ppm, 400 MHz, $CDCl_3$): 8.53-8.43 (m, 8H, H-C(1), H-C(2), H-C(5), H-C(6), H-C(7), H-C(8), H-C(11), H-C(12)), 7.50 (s, 2H, H-C(19), H-C(23)), 7.09-7.02 (m, 3H, H-C(36), H-C(37), H-C(39)), 5.19 (m, 1H, O-H), 4.19 (m, 2H, H-C(29), 2.77 (s, 2H, H-C(22), 2.37 (m, 2H, H-C(28), 2.6 (m, 1H, H-C(46), 1.5 (d, J=12.5, 6H, H_3-C(48), H_3-C(47)), 1.17-1.14 (m, 13H, H_2-C(27), H_2-C(31), H_2-C(32), H_2-C(33), H_2-C(41), H_2-C(42), H-C(43)), 0.92 (br, s, 6H, H_3-C(21), H_3-C(26)), 0.8 (s, 6H, H_3-C(44), H_3-C(45)).

MS (EI, m/z): (Mw, 907.107) 904.67, 741.42, 727.33, 670.6, 329.018. m/z of 904.67 belongs to the loss of hydrogen , m/z of 741.42 corresponds to the loss of $C_6H_{10}NSO$ and CH_3 consequently m/z of 727.33 belongs to the loss of CH_3 fragment and m/z of 670.6 shows the loss of $C_{19}H_{29}$ fragment.

Compound BPY-PDA

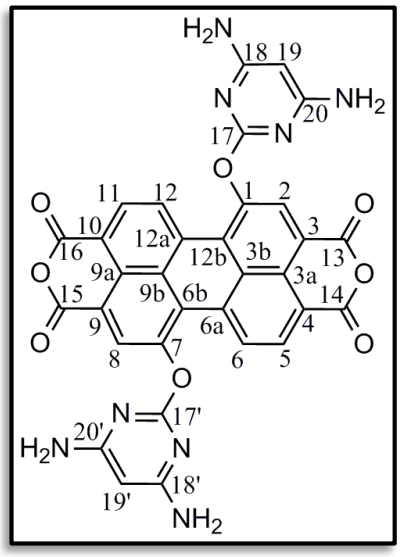

^{1}H NMR and ^{13}C NMR: the NMR spectrum of the compound couldn't be detected because of the low solubility of the compound in deuterated solvents.

MS (EI, m/z): (Mw, 640.52). 627.3, 611.3, 511.6. m/z of 627.3 belongs to the loss of NH_2, m/z of 611.3 corresponds to the loss of $2NH_2$.

Compound BPY-PPDI

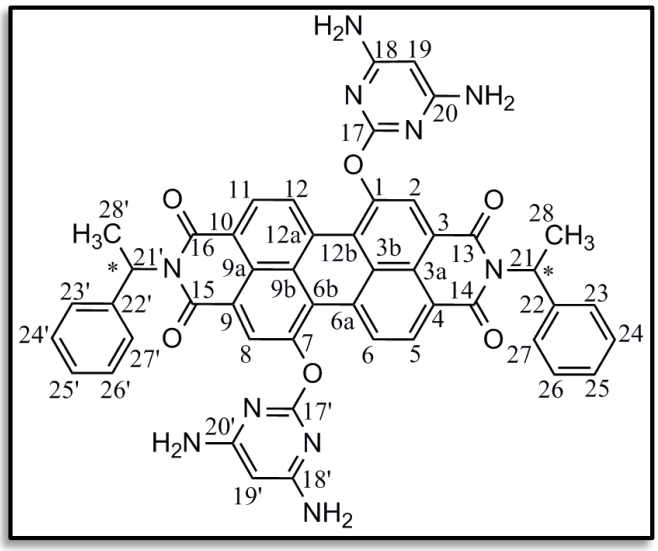

^{1}H NMR and ^{13}C NMR: The NMR spectrum of the compound couldn't be detected because of the low solubility of the compound in deuterated solvents.

MS (EI, m/z): The mass spectrum of this compound due to the low solubility in common organic solvents couldn't be measured.

Compound BTC-PDA

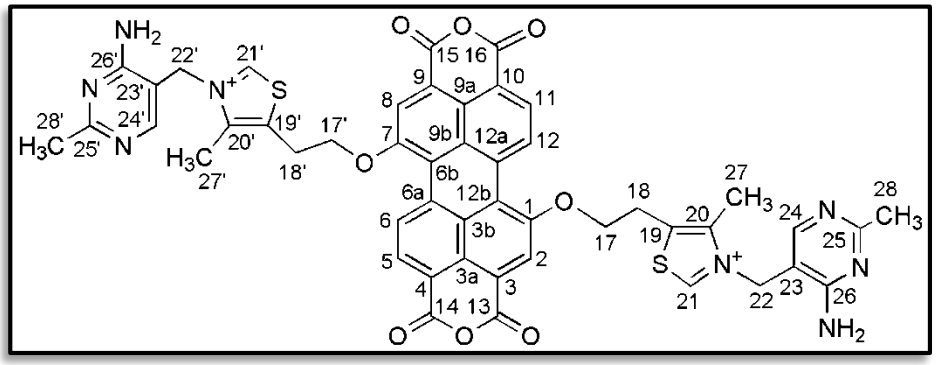

^{1}H NMR and ^{13}C NMR: The NMR spectrum of the compound couldn't be detected because of the low solubility of the compound in deuterated solvents.

MS (EI, m/z): The mass spectrum of this compound due to the low solubility in common organic solvents couldn't be measured.

Compound BTC-TCPDI

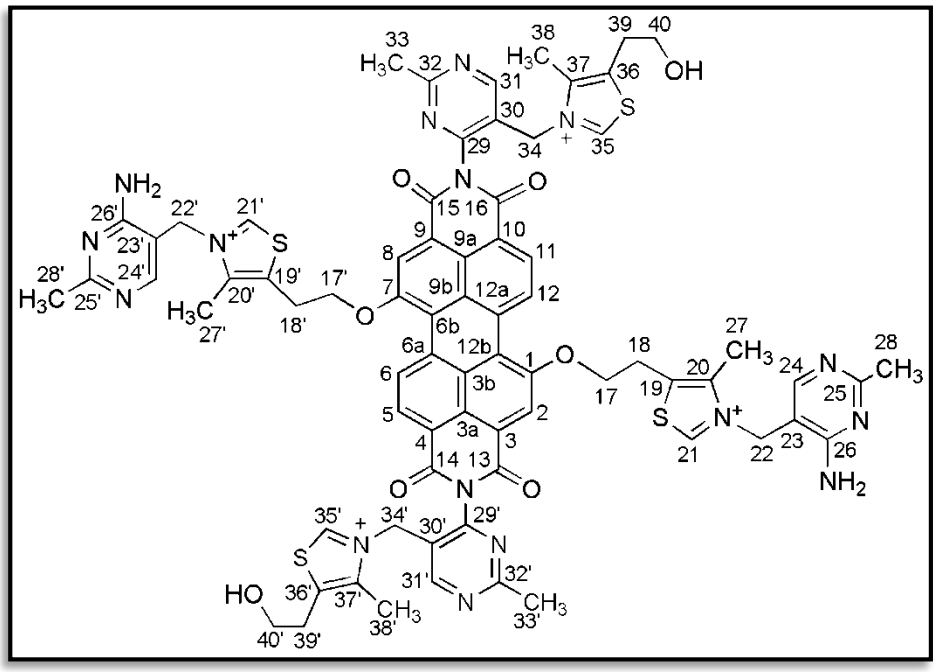

^{1}H NMR and ^{13}C NMR: The NMR spectrum of the compound couldn't be detected because of the low solubility of the compound in deuterated solvents.

MS (EI, m/z): The mass spectrum of this compound due to the low solubility in common organic solvents couldn't be measured.

Compound BTC-APDI

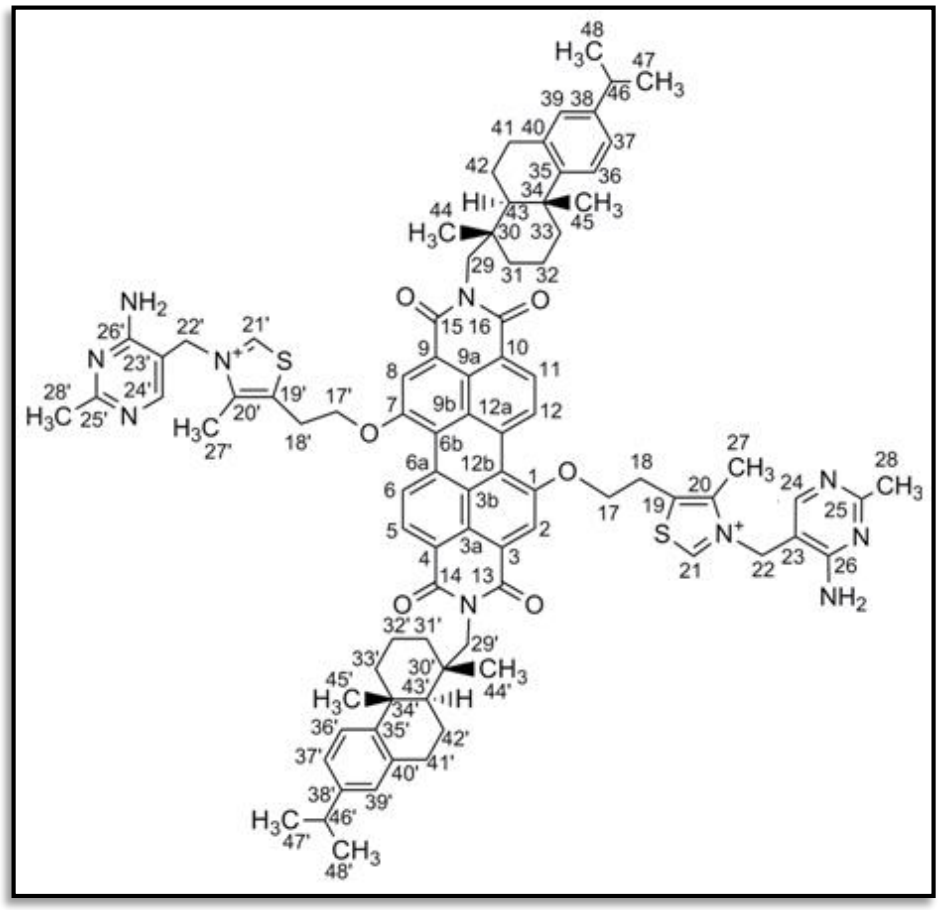

^{1}H NMR, (δ_H ppm, 400 MHz, $CDCl_3$): 8.42 (m, 4H, H-C(11), H-C(12), H-C(6), H-C(5)), 7.89(m, 1H, H-C(24)), 7.71(m, 1H, H-C(24')), 7.51 (br, s, 2H, H-C(2), H-C(8)), 7.33 (m, 1H, H-C(39)), 7.25 (m, 1H, H-C(39')), 7.03-7.9 (m, 4H, H-C(36), H-C(36'), H-C(37), H-C(37')), 3.68(s, 2H, H-C(21), H-C(21')), 2.49(s, 4H, H_2C-(24), H_2C-(24')), 1.78(s,4H, H_2C-(29), H_2C-(29')), 1.61(s,6H, H_3C-(27), H_3C-(27')), 1.52(m,4H, H_2C-(18), H_2C-(18'), 1.35(m,2H, H-C(46), H-C(46')), 1.25(m, 8H, H_2C-(41), H_2C-(41'), H_2C-(42), H_2C-(42')), 1.14-1.31(m, 12H, H_2C-(31), H_2C-(31'), H_2C-(32), H_2C-(32'), H_2C-(33), H_2C-(33')), 1.16(m,12H, H_3C-(47), H_3C-(47'), H_3C-(48), H_3C-(48')), 1.01(s, br, 6H, H_3C-(28), H_3C-(28')), 0.89(m, 4H, H_2C-(43), H_2C-(43')), 0.78(s, 12H, H_3C-(44), H_3C-(44'), H_3C-(45), H_3C-(45')).

MS (EI, m/z): (Mw, 1453.896), 1422.7, 1391.6, 1303, 886.4.

1422.7 corresponds to the loss of $2CH_3$ fragments, 1391.6 shows the loss of two more CH_3, 1303 shows $2C_5H_9N_3$ lost, 886.4 belongs to the loss of two abietyle fragments from both imide sides.

5.6 Analysis of UV-vis and Emission Spectroscopic Measurements

5.6.1 UV-vis and Emission Spectra of TPDI

The absorption-emission spectra of TPDI have been measured in various solvents (polar protic, dipolar aprotic and nonpolar solvents) as well as solid state (Figure 4.28 and 4.36). The absorption spectra of TPDI in solution has shown two sharp vibronic transitions at high wavelengths 400-550 nm which are well matched with characteristic peaks of perylene derivatives [63-65] and can be attributed to the π-π^* transition. At the lower wavelength around 360 nm a weak absorption had been found due to contribution of donor (Figure 4.29). As can be seen in (Figure 4.28-a) a broad band in the range of 600-800 nm has been found specifically in electron donating polar aprotic solvents (NMP, DMAC and DMF) that the intensity of the peak decreases from most electron-donating solvent (NMP) to the least one (DMF) this peak is credited to aggregation of the molecules in solutions. In contrast to absorption spectra which have independency on solvents polarity the emission spectra have been red shifted in dipolar aprotic solvent (DMSO, DMAC, DMF and NMP) which can be indication of sensitivity of emission compared with absorption spectra.

The molar absorption coefficient in seven different solvents has been calculated using the maximum wavelengths in five different solutions of each solvent and the

results are shown in Table 4.3. In all of the solutions the aggregation properties of the compound have been checked using the following table.

Table 5.6: Ratio of absorption intensities of TPDI in various solvents

Solvent	Absorption Intensities of the Peaks		
	$A^{(0\cdot1)}$	$A^{(0\cdot0)}$	$A^{(0\cdot0)}/A^{(0\cdot1)}$
TCE	0.718	0.953	1.327
DCM	0.521	0.729	1.399
NMP	0.895	1.329	1.485
MeOH	0.382	0.419	1.097
DMF	1.038	1.578	1.520
DMAC	1.513	2.200	1.454
DMSO	1.291	1.948	1.508

As indicated in (Table 5.6) the ratio of 0-0 to 0-1 transition in each solvent have been calculated and the results designated the presence of monomeric form of TPDI in the solution because of non-planar structure of the compound. The following scheme can clearly show the non-planarity in the compound's structure.

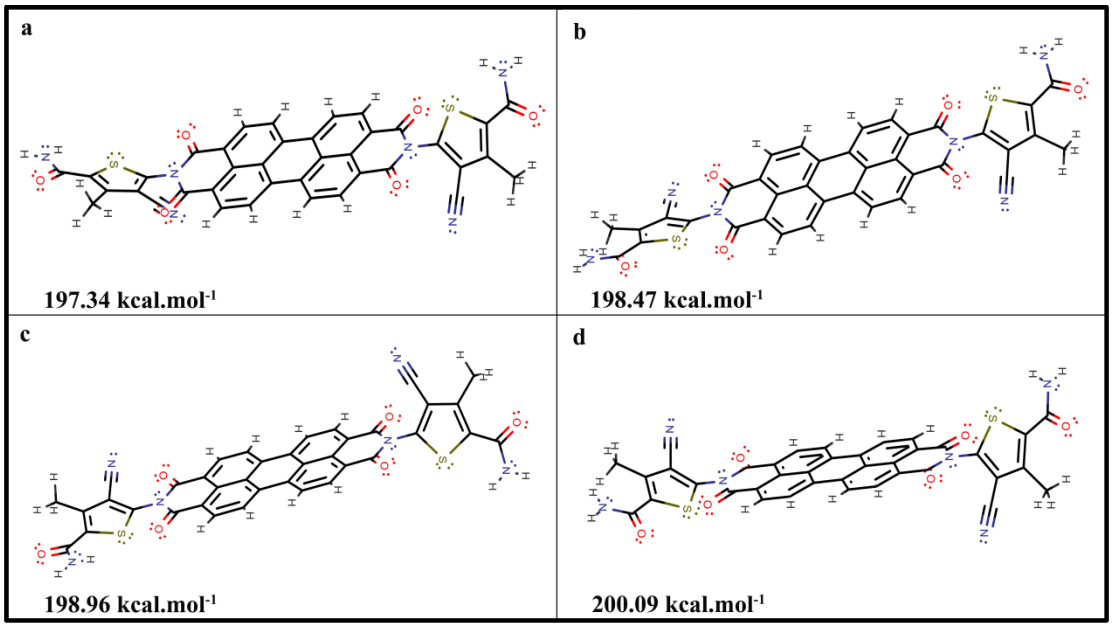

Scheme 5.1: (a)-(d) Representative 3D molecular structure of **TPDI** in different energy levels (all rendered using Marvin by Chem Axon)

As a result of non-planarity, self-assembly and aggregation was minimized for the compound in solutions. The ratio of 0-0 to 0-1 (1.20 in s-state) transition in solid-state also gave weak aggregation possibility the fact can be confirmed by clearly separated vibronic transition spectrum in s-state (Figure 4.36).

For the better understanding of the optical properties concentration dependent absorption and fluorescence (λ_{max} = 485 and 315 nm) measurements of TPDI have been done in various solvents (Figure 4.30, 4.31, 4.32, 4.33, 4.34 and 4.35). As has been discussed before due to the lack of aggregation, well separated peaks with minimum dependency of maximum wavelength on changing of concentration were observed in absorbency of all the measured solvents but fluorescence spectra by changing the excitation wavelengths from 485 to 315 nm showed totally different bands shape. It can be observed in figures (4.30-4.33) that in absorption and emission (λ_{max} = 485 nm) spectra, the intensities of both absorption and emission spectra have been decreased by decreasing the concentrations. Instead at excitation wavelength of

315 nm by reducing the concentration emission in acceptor region will be less intense but by increasing the concentration intensity of the emission in acceptor region will be higher and the energy transfer will be quenched (at 360 and 700 nm). In this excitation wavelength the emission is highly dependent on type of solvent. In polar protic solvents such as MeOH and EtOH (Figures 4.34-b and 4.35-b) because of protonation of donor at amide position the energy transfer had been stopped and the intensity of peaks at donor emission region is much higher than that of acceptor.

The fluorescence quantum yield of TPDI has been calculated using (*N,N'*-bis(dodecyl)-3,4,9,10-perylenebis(dicarboximide) as a reference $\Phi_f = 1$) the results are shown in Table 4.11), due to the low solubility and higher aggregation possibility in DCM and TCE the lowest fluorescence-yield have been achieved.

5.6.2 Intramolecular Fluorescence Quenching of *N,N'*-bis-[2-(5-carboxamidyl-3-cyano-4-methyl)-thienyl]-3,4,9,10-perylenebis(dicarboximide) (TPDI)

It has been found that the fluorescence of donor (thiophene) in TPDI has been strongly over lapped with absorption of TPDI. As has been observed in 4.35 and 4.36 performing excitation of 315 nm strongly enhanced the acceptor peaks compared with energy transfer complexes at 360 or 700 nm which can be indication of charge transfer or aggregation. Using (Figure 4.34-d) the emission of thiophene was quenched by TPDI and the fluorescence-quenching rate-constant (K_q , $M^{-1}S^{-1}$) in NMP has been determined by Stern-Volmer equation (equation 4.17) where I_0 was the emission intensity of the TPDI in lowest concentration (1×10^{-6} M) and I_1, I_2, I_3, and I_4 demonstarate the emission intensities of the TPDI at 5×10^{-6}, 1×10^{-5}, $2.5\times10^{-5}$and 5×10^{-5}M. The quenching rate-constant ($K_q = 9.60\times10^{11}$ $M^{-1}S^{-1}$) could be determined using the slope of the graph (Figure 4.10) that has been plotted in I_0/I *vs.* Concentrations and the lifetime of TPDI in NMP ($\tau_0 = 19.8$ ns)

5.6.3 UV-Vis and Emission Spectra of TCPDI

The absorption-emission and excitation spectra of TCPDI have been measured in various solvents (polar protic, dipolar aprotic and non-polar solvents) (Figure 4.37-4.42). The absorption spectra of TCPDI have shown two vibronic transitions at high wavelengths 490-550 nm which are well matched with characteristic peaks of perylene derivatives and can be attributed to the π-π^* transition with a slight peak at around 460 nm. In absorption spectra (Figure 4.37-a) except TFAc solution which was red-shifted due to the hydrogen bonding ability of the solvent, the peaks show minimum dependency on solvent polarity. Checking the excitation spectra (taken at λ_{em} = 620 nm) in the same figure (4.37-b) clearly showed that the absorption and excitation spectra are well matched in all the solvents except TFAc. The excitation spectrum of the TFAc as a protic solvent has shown two extra shoulder peaks at around 550 and 600 nm which can be attributed to the charge transfer from donor to acceptor (TCPDI) moiety or aggregates formation. Emission spectra of TCPDI in two different wavelengths (λ_{max} = 485 and 315 nm) have been measured and the results showed that the shape of the peaks in these two wavelengths were totally different. At excitation wave length of 485 nm the bands were independent of solvent polarity except TFAc which has shown red shifted peaks for the same reason that has been discussed in absorption spectrum of TFAc. At excitation wavelength of 315 nm a weak broad band at around 465 nm had been observed which can be related to donor (vitamin-B_1) contribution in emission spectrum due to that the absorption and emission (at excitation wavelength of 310 nm) measurements have been done for Vitamine-B_1 separately (Figure 4.39). For more objective investigation in photochemical properties of the compound, TCPDI was subjected to different solvents (NMP, DMF and DMAC) with various concentrations (Figure 4.40-4.42).

As can be seen in figure (4.40) the absorption peaks in all concentrations show well-separated vibronic transitions peak. In contrast to absorption spectra the emission at both excitation wavelengths 315 and 485 nm has shown that by decreasing the concentration from 1.1×10^{-4} to 9.3×10^{-4} the emission intensities have been increased. This can be due to the aggregation in the higher concentration compared with the lower one. It is worthy to mention that the higher degree of sensitivity in emission shows the molecular behaviour of the compound in solutions which could not be seen clearly in absorption spectra. The aggregation behaviour of TCPDI has been checked via the 0-0 to 0-1 transition intensities and the results are demonstrated in (Table 5.7) it's clear that most of the values ($I_{0\text{-}0}/I_{0\text{-}1}$) are lower than 1.5 which confirmed the aggregation phenomenon in solutions. The interaction between the aromatic species and the core perylene ring could be the reason of aggregation. In addition to that the formation of hydrogen bonds because of free O-H group in vitamin structure favoured the formation of aggregates. The emission spectra at excitation wavelength of 315 nm have shown totally different shape in comparison with excitation wavelength of 485 nm, the spectra have a broad shapeless peak at 400 and 503 nm which can be attributed to the donor emission. A better inspection of the (Figure 4.42-a) reveals that the intensity of the peak in donor emission region of NMP solutions is higher than that of acceptor at lower wavelengths. The reason can be the reduction of the polarity from DMAC>DMF> NMP (dielectric constant: 37.8, 36.7 and 32 respectively) which destabilized the donor moiety and consequently, the energy transferred has been stopped from donor to acceptor and the peaks are blue-shifted in NMP. The quantum yield of TCPDI also has been calculated (Table 4.11) and the results revealed low quantum yield in majority of the investigated solutions.

Table 5.7: Ratio of absorption intensities of TCPDI in various solvents

Solvent	Absorption Intensities of the Peaks		
	$A^{(0\cdot1)}$	$A^{(0\cdot0)}$	$A^{(0\cdot0)}/A^{(0\cdot1)}$
TCE	0.62	0.69	1.13
TFAc	1.3	1.7	1.31
DCM	0.52	0.59	1.13
Pyridine	1.4	1.5	1.06
NMP	1.6	1.7	1.06
DMF	1.7	1.9	1.12
DMAC	1.6	1.8	1.12
DMSO	1.7	1.8	1.06

5.6.4 UV-Vis and Emission Spectra of TAPDI

Likewise the absorption-emission and excitation spectra of TAPDI have been measured in various solvents (polar protic, dipolar aprotic and non-polar solvents) (Figure 4.43- 4.47). The absorption spectra of TAPDI have shown three sharp vibronic transitions at high wavelengths 400-550 nm which are well matched with characteristic peaks of perylene derivatives and can be attributed to the π-π^* transition with a slight peak at around 430 nm. The maximum values of red and blue shifted spectra have been observed in TCE and isopropanol respectively. The aggregation behaviour of TAPDI indifferent solutions was checked using the following table (Table 5.8)

Table 5.8: Ratio of absorption intensities of TAPDI in various solvents

Solvent	Absorption Intensities of the Peaks		
	$A^{(0\cdot0)}$	$A^{(0\cdot1)}$	$A^{(0\cdot0)}/A^{(0\cdot1)}$
CHL	1.06	0.68	1.60
THF	1.90	1.26	1.51
TCE	1.75	1.12	1.56
Isopropanol	0.65	0.57	1.14
NMP	0.21	0.16	1.31
DMF	1.38	0.94	1.47
DMAC	1.88	1.27	1.48
DMSO	0.35	0.31	1.13

As can be seen the table the ratio of absorption intensities in most of the solvents ($I_{0\text{-}0}/I_{0\text{-}1}$) are higher or close to 1.5 that can be a good indication of monomeric form of the compound in solutions. Having narrow peaks of absorption is also another indication of monomerized molecules. The absorption an emission (in both excitation wavelengths 315 and 485 nm) spectra were independent of the solvent polarity, at excitation wavelength of 315 nm the compound has shown a broad peak at 381 nm which probably shows donor's contribution in emission spectrum. More investigation in photo-chemical properties of TAPDI has been done, due to that the concentration dependent measurements of the compound in CHL, isopropanol and DMAC were performed (Figure 4.45-4.47). In absorption spectra showed independency of changing of the concentrations. Emission spectra have been measured by excitation at various wavelengths (485 and 315) through the absorption spectrum. The results are shown that changing the excitation wavelength have not substantially changed the emission spectra except in isopropanol (Figure 4.47-b) at excitation wavelength of 315 the donor emission at 361 nm can be seen. The

fluorescence yield of the compound has been calculated in different solvents using equation (4.8) and the results are summarized in table (4.11).

5.6.4 UV-Vis and Emission Spectra of BPY-PDA

The photo-chemical properties of BPY-PDA as bay-substituted perylene have been study in various solvents (polar protic, dipolar aprotic and nonpolar solvents) by absorption and emission spectroscopic measurements (Figure 4.48- 4.52). the absorption spectrum of BPY-PDA has shown different shapes in dipolar solvents (4.48-a) like NMP, DMF and DMSO compared with non-polar (pyridine) and protic solvents (TFAc). In dipolar solvents a broad peaks at around 667 and 646 nm have been found which can be attributed to charge transfer from donor (pyrimidine) to acceptor moiety or aggregation of the molecules in the following solutions. In contrast to dipolar solvent in protic solvent (TFAC) due to the protonation of amines at bay position the charge transferred bands have been totally diminished in addition to that the 0-0 transition in TFAc solution has been red-shifted compared with other solutions this shows the fact that the structure of the compound is clearly affected by solvents polarity and consequently the absorption bands were shown interesting different shapes. In comparison with the other synthesized compounds the absoption spectra of BPY-PDA have not demonstrated the well-resolved vibrational transitions that can be an indication of aggregation or intermolecular interactions such as H-bonding due to the presence of free ($-NH_2$)s in pyrimidine structure. The aggregation possibility of the molecules was examined using the following table (Table 5.9). As can be seen the table the ratio of absorption intensities in most of the NMP, DMF and DMSO ($I_{0\text{-}0}/I_{0\text{-}1}$) became lower than one that confirm the aggregates formation.

Table 5.9: Ratio of absorption intensities of BPY-PDA in various solvents

Solvents	Absorption Intensities of the Peaks		
	$A^{(0\cdot0)}$	$A^{(0\cdot1)}$	$A^{(0\cdot0)}/A^{(0\cdot1)}$
TFAc	1.38	1.10	1.25
Pyridine	1.50	1.49	1.00
NMP	1.58	1.77	0.89
DMF	1.02	1.15	0.88
DMSO	1.48	1.65	0.89

The emission spectrum of the compound has been studied in various solvents at excitation wavelength of 485 nm (Figure 4.48-b), and the excimer fluorescence bands have been observed in all of the solutions, the band in TFAc is red-shifted and a hypsochromic shift has been observed in pyridine solution. The absorption and fluorescence behaviour of pyrimidine have been separately studied in NMP, DMF, DMAC and DMSO and the results are shown in (Figure 4.49). Concentration-dependent measurements on absorption-emission properties of the compound revealed interesting results that are shown in (Figure 4.50-4.52) one can see that the absorption and emission were independent of concentration and upon changing the concentration no big difference has been observed but emission spectrum of the compound reveals different shape versus changing of excitation wavelength from 485 to 315nm. In contrast to excitation wavelength of 485, at excitation wavelength of 315 nm the donor emission has been more intense than that of acceptor. In (figure 4.52) it can be said that the emission spectra of BPY-PDA are more or less following the same pattern with this difference that in the region of acceptor emission, the intensities of the peaks in these three solvents are ordered as follows: NMP>DMAC>DMF, the maximum emission loss of acceptor was recorded in DMF. These meaningful differences can be interpreted by the fact that the free (-NH_2) s

which are located at bay-positions of the perylene core can have inter-molecular interaction by these three solvents, i.e. hydrogen-bonding intermolecular interaction in NMP solution is much stronger than DMAC, and DMAC will have stronger interaction than DMF or more clearly the donation of NMP>DMAC>DMF, which can accelerate the energy transfer from donor (pyrimidine) moiety to acceptor.

The quantum-yield of the compound is calculated in various solvents and the results are summarized in Table (4.12) as can be seen due to aggregation in solution the values are quite low.

5.6.5 UV-vis and Emission Spectra of BPY-PPDI

Likewise the photo-physical properties of BPY-PPDI have been investigated in various organic solvents. And the results are shown in (Figures 4.53-4.56). By checking the solubility table of these two compounds (Table 5.4) one can recognize that the solubility of the bay-substituted diimide compared with its bay-substitited anhydride has decreased tremendously, probably imidization by a chiral amine at imide position has twisted the whole structure toward having more inter-moreculra interaction specify at bay-positions which have H-bonding possibilities. This fact was shown itself in absorption spectra of BPY-PPDI as can be seen in (Figure 4.53-a) the bans are more structure less in comparison with BPY-PDA and the vibronic bands have not been separated well. In addition to that the bands are highly affected by polarity of the solvents with the most red-shifted band in TFAc solution. The aggregation probability in each solution has been check by 0-0 to 0-1 transitions intensities and the results are summarized in (Table 5.9)

Table 5.10: Ratio of absorption intensities of BPY-PPDI in various solvents

Solvents	Absorption Intensities of the Peaks		
	$A^{(0\cdot0)}$	$A^{(0\cdot1)}$	$A^{(0\cdot0)}/A^{(0\cdot1)}$
TFAc	1.21	1.13	1.07
Pyridine	1.06	1.17	0.91
NMP	1.08	1.24	0.87
DMF	1.00	1.17	0.85
DMAC	1.33	1.49	0.89
DMSO	1.25	1.40	0.89

Comparison of table 5.9 with 5.10 show that the final compound has been slightly more aggregated after imidization. Similar to the bay-substituted anhydride (BPY-PDA) the charge transfer or aggregation peaks can be observed in NMP, DMF and DMAC solutions at around 658 nm which can be attributed to specific structure of donor that makes it probable to have charge transfer to acceptor. For the same reason that has been discussed above, in TFAc because of protonation of ($–NH_2$) s the charge transfer stopped in this solution. Interestingly the emission spectrum of BPY-PPDI in contrast to absorption spectra show the vibronic transitions more clearly in DMF, DMAC and pyridine, the bands in TFAc, DMSO, and NMP solutions were more likely to excimer type emission.

Like the other synthesized compounds the concentration dependent measurements in NMP, DMF and DMAC were performed and the emission properties of the compound was checked in both 485 and 315 nm excitation wavelengths (Figure 4.54-4.55). As can been seen in (Figure 4.54) the absorption spectra in all three solvents were structure-less wide bands with charge transfer or aggregation peaks at 752, 654 and 608 nm in NMP, these peaks are less intense in DMF and DMAC, the absorption in TFAc demonstrated different shape caused by porotonation of free amine at bay position the charge transfer bands were diminished. In emission at

excitation wavelength of 485 nm from higher to lower concentration the intensities of the peaks increases due to the reduction of aggregation, and excimer type emission can be observed in all of the three solutions (Figure 4.55). Instead in emission with excitation wavelength of 315 nm the shape of the spectra were totally different compared with other excitation wavelength (485 nm). The intensities of the bands in acceptor region (Figure 4.56) follow the behaviours as that of BPY-PDA in NMP, DMF and DMAC (Figure 4. 52) which have been discussed in detail before (part 5.6.4). Fluorescence yields of BPY-PPDI are tabulated in (Table 4.12) and the values are tremendously lower than that of BPY-PDA as a result of increasing aggregation after imidization.

5.6.6 UV-Vis and Emission Spectra of BTC-PDA

The photo-physical studies of BTC-PDA also have been done in different solvents by absorption, emission and excitation measurements (Figure 4.57-4.61). Since the substitution has been done using vitamin at bay-position the results were quite interesting compared with TCPDI which had vitamin at imide position. The peaks sharpness in BTC-PDA was decreased which can be an indication of aggregation, inter or intra-molecular interactions. Comparing the solubility table of these two compounds shows the reduction in solubility of BTC-PDA. The absorption spectra of BTC-PDA have a broad band in NMP, DMF and DMAC at near infrared region which can be attributed to charge transfer from donor to acceptor moiety or aggregation of the molecules but in TCPDI the following peaks in the same solutions had not been observed. It's worthy to mention that the NIR peaks appeared in all the derivatives which had free ($-NH_2$) in the structure (TPDI, BPY-PDA, BPY-PPDI, BTC-PDA and BTC-APDI) that can be an evidence of strong donation of free amine group. In absorption spectra of BTC-PDA (Figure 4.57-a) in addition to 0-0 and 0-1

vibronic transitions one small shoulder peaks at lower wavelength (417 nm) was observed which can be ascribed to the absorption spectrum of donor. The aggregation of the compound have been examined in all the solutions using the following table (Table 5.11)

Table 5.11: Ratio of absorption intensities of BTC-PDA in various solvents

Solvents	Absorption Intensities of the Peaks		
	$A^{(0\cdot0)}$	$A^{(0\cdot1)}$	$A^{(0\cdot0)}/A^{(0\cdot1)}$
TFAc	1.70	1.50	1.13
Pyridine	1.10	1.00	1.10
NMP	1.30	1.30	1.00
DMF	1.45	1.50	0.96
DMAC	0.99	1.01	0.98
DMSO	1.59	1.48	1.07

The values reveal aggregates formation in all the investigated solvents since the ratios are less than 1.5.

Emission spectra of TC-PDA (Figure 4.58-a) at excitation wavelength of 485 nm showed less dependency on solvent polarity and almost all the peaks shape were the same, except DMSO solution that has excimer type emission. In excitation wavelength of 315 nm the peaks were more structure-less and in the acceptor region eximer type emission has been noticed along with charge-transfer complex emission at 713 nm. The concentration dependent measurements have been performed in NMP, DMF and DMAC with the fluorescence spectroscopic measurements at two different wavelengths of 485 and 315 nm (Figure 459-4.61). In all three solvents the absorption bands were broad with NIR charge transfer or aggregation bands around 686 and 757 nm. The shape of the spectrum was independent of the concentration. In

emission spectra at excitation wavelength of 485 nm the energy transfer peaks were totally quenched. At excitation wavelength of 315 nm in contrast to TCPDI the emission in donor region was diminished in NMP, the reason can be highly donative nature of NMP compared with DMAC and DMF which can enhance the energy transfer from donor to acceptor. Quantum-yield of BTC-PDA was calculated in different solvents and the results are shown in (Table 4.13).

5.6.7 UV-Vis and Emission Spectra of BTC-PPDI

Figures 4.62-4.66 show the spectroscopic measurements of BTC-PPDI in various solvents and different concentrations. Absorption spectra (Figure 4.62-a) of BTC-PPDI in compared with BTC-PDA have been totally structure-less that the vibronic transitions were not separated well. The bands are quite broad and show aggregation type absorption probably due to the increasing the stacking behaviour of the compound after imidization and intermolecular interaction at bay-positions. Excitation spectra of the compound (Figure 4.62-b) clearly show the formation of aggregates in solution as can be seen in that figure the 0-1 transition has higher intensity than 0-0 transition. In the following table (Table 5.12) the ratio of absorption intensities have been calculated and the results reveal that ($A^{(0\cdot0)}/A^{(0\cdot1)}<1.5$) that can be indication of aggregates formation.

Table 5.12: Ratio of absorption intensities of BTC-TCPDI in various solvents

Solvents	Absorption Intensities of the Peaks		
	$A^{(0\cdot0)}$	$A^{(0\cdot1)}$	$A^{(0\cdot0)}/A^{(0\cdot1)}$
TFAc	0.89	0.96	0.93
Pyridine	1.75	1.85	0.95
NMP	0.97	1.03	0.94
DMF	1.24	1.28	0.97
DMAC	1.50	1.61	0.93
DMSO	0.79	0.89	0.89

The Fluorescence property of BTC-PPDI has been checked at two different excitation wavelengths of 485 and 315 nm, the results can be seen in (Figure 4.63). The emission spectra at excitation wavelength of 485 nm showed three vibronic transitions at 532, 572 and 620 nm with a small shoulder band at lower wavelength which is perhaps attributed to donor moiety. Changing the excitation wavelength from 485 to 315 nm gave totally different shapes of emission spectra of the compound (Figure 4.63-b). The bands in acceptor region were more likely to excimer type emission with the charge-transfer complex peaks at 718 nm in NMP, DMF and DMAC, similar to bay-substituted derivative (BTC-PDA). The reason was discussed in detail in pervious section (part 5.6.6).

The photo-physical properties of BTC-TCPDI were examined in various concentrations of NMP, DMF and DMAC solutions (Figure 4.64-66). One can see that in most of the concentration-dependent measurements the solutions were prepared in these three solvents (NMP, DMF and DMAC) due to the donative properties of the solvents charge-transfer complexes formation can be more noticeable. Absorbency of the compound in these three solvents at different concentrations has not shown any specific difference, the bands in all of them were broad and shape-less ascribe to aggregates formation, at excitation wavelength of 485 nm the bands are separated well as a result of higher degree of sensitivity of fluorescence compared with absorbency. At 315 nm excitation wavelength the donor emission can be monitored clearly, in NMP as the more donative solvent the emission in donor region is less intense in comparison with the same region in DMF and DMAC, the reason can be the energy transfer from donor to acceptor which was accelerated in more donative solvent (NMP) than the other ones (DMF and MDAC)

and consequently the emission spectra in acceptor section of NMP solution was more intense than DMF and DMC additionally the acceptor bands at this excitation wavelength were more likely to excimer type emission. More or less the compound behaviour at 315 nm excitation wavelength was similar to bay-substituted derivative (BTC-PDA) just the energy-transfer after imidization was less intense than that of BTC-PDA. Fluorescence yield of the compound in different solvents was calculated and summarized in (Table 4.13) the results were quite lower than that of BTC-PDA caused by higher aggregation possibility.

5.6.8 UV-Vis and Emission Spectra of BTC-APDI

As the last synthesizing compound, BTC-PDA was treated by abiethyl amine in imidization step which has surprisingly increased the solubility of the compound, the photo-physical properties of the compound has been examined and the results can been observed in (Figure 4.67-4.71). Checking the absorbency of the compound in various solvents denoted three structural vibronic transitions with a small band at 557 nm. In DMF solution the charge transfer at NIR region distinctly can be observed, which could not be seen in BTC-TCPDI as reason of having aggregation. The excitation spectra (at emission wavelength of 620 nm) of BTC-APDI are totally matched with absorption bands (Figure 4.67-b). Aggregation possibility of the compound has been checked by the following data (Table 5.13).

Table 5.13: Ratio of absorption intensities of BTC-APDI in various solvents

Solvents	Absorption Intensities of the Peaks		
	$A^{(0\cdot0)}$	$A^{(0\cdot1)}$	$A^{(0\cdot0)}/A^{(0\cdot1)}$
CHL	1.25	1.17	1.07
THF	1.47	1.39	1.06
TCE	1.03	0.97	1.06
TFAc	1.05	1.03	1.02
DMF	1.40	1.30	1.08
DMAC	1.17	1.18	0.99
DMSO	0.36	0.31	1.16

Similar to other derivatives the emission in two different excitation wavelengths was studied. The peaks at these two wavelengths were almost similar, just at excitation wavelength of 315 nm the donor emission could be detected. The band in TFAc in both excitation wavelengths were shown excimer type fluorescence and in THF the peaks were more blue-shifted. Various concentrations of the compound in CHL, THF and DMAC have been prepared and the absorption-fluorescence measurements of BTC-APDI were studied (Figure 4.69-4.71). The absorption bands in all three solvents showed three vibronic transitions and in DMAC the charge transfer or aggregation bands at 699 and 763 nm can be observed because of donative nature of DMAC these peaks were noticed just in this solvent. Fluorescence properties of the compound in 485 and 315 nm wavelengths were measured (Figure 4.70 and 4.71), at 485 nm the compound showed three vibronic bands which were separated well. The intensities of the bands were increased from higher (7.5×10^{-5}) to lower (4.5×10^{-5}) concentration as a result of aggregation reduction in lower concentration solution. At 315 nm excitation wavelength the shape of the peaks were different from that of 485 nm, around 510, 475 and 389 nm three small bans were detected that can be attributed to charge-transfer complex emission of donor, with focusing in (Figure

4.71-c) it was noticeable that at 389 and 479 nm the bands intensities have been reduced which can be credited to donative feature of DMAC that can accelerate the energy-transfer of donor to acceptor consequently the peaks at lower wavelength will have lower intensity.

Quantum yield of the compound in various solvents have been calculated the results can be observe in (Table 4.13) comparing the value with other bay-substituted derivatives (BTC-PDA and BTC-TCPDI) show quite higher values because of higher solubility of the compound and less aggregates-formation possibility (Table 5.11).

5.7 Analysis of Intra-Molecular Fluorescence-Quenching in TPDI

It has been seen that at emission spectrum with the excitation wave length of 315 nm the emission at donor region was diminished in contrast to acceptor's emission which was more enhanced, that could be an indication of energy or electron transfer from thiphene as a donor to the acceptor moiety. Using (Figure 4.34) in NMP as the most donative solvent the quenching rate-constant was calculated from Stern-Volmer plot (Figure 4.10) where the slope is $\mathbf{K_q \times \tau_0}$ since the life-time was obtained before (Table 4.40) K_q has been found (9.670×10^{11} $M^{-1}S^{-1}$) the high amount of K_q upholds the energy or electron transfer of donor to acceptor.

5.8 Electro-Chemical Information and Analysis of *N,N'*-bis-[2-(5-Carboxamidyl-3-cyano-4-methyl)-thienyl]-3,4,9,10-perylenebis-(dicarboximide) (TPDI)

The electro-chemical properties of TPDI have been studied by cyclic (CV) and square-wave (SWV) voltammatry method, the measurements have been done in solutions including DMF, DMAC and NMP (supporting electrolyte: 0.1 M $NaBF_4$) and solid state (supporting electrolyte: 1 M HCl). The redox potential of TPDI in both solution and solid state have been gained in contrast with Ag/AgCl and standardized with Ferrocene/ferrocenium (Fc/Fc^+). The results are demonstrated in (Figures 4.9, 4.11, 4.12, 4.13, 4.14 and 4.15) and summarized in (Table 4.1). In order to show that the redox waves are reproducible the measurements were repeated in same region with different scan rates. The redox potentials of TPDI in both solution and solid-state have been standardized with ferrocene/ferronium (Fc/Fc^+) couple as a reference. The CV measurement of TPDI in DMF (Figure 4.9) demonstrated two reduction peaks at $E_{1/2,red1}$= -0.734 V and $E_{1/2,red2}$= -0.951 V (*vs*. Fc/Fc^+) with the peak-potential separations (ΔE_p) of 88 and 108 mV, at scan rate of 100 mVs^{-1} which can be seen in (Figure 4.9 inset), the results reveals two radical-anion formation ($TPDI^{-\cdot}$) due to donor-acceptor-donor structure of the compound.

The CV measurement of TPDI in DMAC (Figure 4.12) also showed reversible reduction. As illustrated in the figure at scan rate of 100 mVs^{-1} two reduction peaks at $E_{1/2,red1}$= -0.779 V and $E_{1/2,red2}$= -1.015 V with respectively ΔE_p of 87 and 94 mV were observed. The same trend at scan rate of 100 mVs^{-1} was observed for TPDI in NMP with two reversible reduction potential at -0.791 V and -1.022 V and peak separation of ΔE_{p1} = 91 and ΔE_{p2} = 91 mV, in all above mentioned measurements

(DMF, DMAC and NMP) the reduction potentials revealed consecutive formation of radical anion and di-anion that at higher scan rates the peaks were dissipated without any substantial oxidation peaks of TPDI. Since squarewave voltammetry has been known as more sensitive measurement the oxidation behaviour of TPDI were checked by this technique and has shown a weak broad peak at around 0.25 V in DMF solution that has been attributed as donor oxidation peak (Figure 4.9 the right part). Later on additional measurements on electro-chemical properties of donor unit (5-amino-4-cyano-3-methylthiophene-2-carboxamide, TH) (Figure 4.16) in DMAC and NMP with oxidation peaks respectively at 0.734 and 0.737 confirmed the oxidative nature of the donor units that the peaks are totally different from that of TPDI.

The solid state redox behaviour of TPDI has been also examined in anoidic and catodic regions (Figure 4.14 and 4.15) and due to the intensive interactions in s-state different results have been collected compared with solution measurements. It has been found that the compound has a weak irreversible reduction between -1.08 to +0.8 V and weak reversible peak at -0.625 to +0.125 V (Figure 4.14). In anodic region a weak oxidation peak has been found due to the oxidation of sulfur of in thio-ring, and the scan rate dependent measurement in the region of -1 to +1 has shown reversible reduction potential (Figure 4.15).

The HOMO and LUMO energy levels and E_g have been calculated by optical data and the results are tabulated in (Table 4.1). Using $E_{LUMO} = - (4.8+E_{1/2})$ the LUMO energy level was calculated and the bond-gap energy have been determined (DMF: 1.59, NMP: 1.62, DMAC: 1.63 and s- state: 1.93 eV) by the following equation ($E_g=1240/\lambda_{max}$) and using cut off charge transfer absorption (Figure 4.1) band with

the wavelengths of (DMF: 779, NMP: 765 and DMAC: 760 nm) and at s-state: 642 nm. Consequently the HOMO energy level of DMF, NMP and DMAC were calculated -5.66, -.5.63, -5.70 and -6.17 eV respectively.

5.9 Thermal Properties of the Compounds

Using DSC (differential-scanning calorimetry) under nitrogen atmosphere and TGA under oxygen atmosphere (thermo-gravimetric analysis) by the heating range of 10 °C per minuet the thermal properties of the synthesized compounds have been studied.

The DSC thermal analysis of TPDI (Figure 4.88) has not shown any melting point or glass-transition by heating up to 440 °C. Checking TGA thermo-gram has shown the first 5 % weight loss at 335 °C and the main one took place between 440-650 °C which was 50 % of the initial sample heating process was run up to 950 °C and 50 % char yield was gained. The results reveal high thermal stability of the compound.

Likewise the measurements of TCPDI have been done as can be seen in (Figure 4.89) DSC thermo-gram has not shown any specific transition instead in TGA the first weight loss has been observed at 305 °C around 4 % and the major weight loss started at 501-700 °C which gave 98% weight loss and 2 % char yield.

In DSC thermo-gram of TAPDI (Figure 4.90-a) no specific transition has been observed, in TGA thermo-gram the first mass loss was detected at 330°C with the mass loss of 3 %, and the second mass loss (22 %) was monitored at 450 °C and 4.2 % has been found as the final char yield.

In BPY-PDA (Figure 4.91) DSC measurement like other two compounds did not show melting or glass-transition point, in TGA graph at 357°C, 4 % weight loss was observed and at 497-677 °C, 98.7 % of the sample was loss and gave 1.3 % char yield. Similar to bay-substituted one the DSC result of BPY-PPDI (Figure 4.92) has not shown any special transition but TGA thermogram demonstrates high stability of the compound after imidization the first weight loss had been observed at 332 °C at which 11 % of the compound was lost and the major loss was at 530-940 °C at which 53 % weight loss was gained with char yield of 47%.

In TGA thermogram of BTC-PDA (Figure 4.93) at 303 °C, 3 % weight loss has been observed and the major loss was at 472-716 °C at which 98.4 % of the sample was lost with 1.6 % char yield, DSC graph like other compounds has not shown any melting –point or glass-transition point.

For BTC-TCPDI (Figure 4.94) single weight loss has been observed between 340 to718 °C at which 97.7 % of the sample was lost with 2.3 % char yield. In BTC-APDI (Figure 4.95) the TGA graph has shown 96.6 % weight loss between 296°C to 601 °C with char yield of 3.4 %. DSC graphs of both BTC-TCPDI and BTC-APDI have not contained transition peaks like (melting-point or glass-transition point).

Chapter 6

CONCLUSION

In the present study, Three different perylene diimide which two of them were symmetrical (**TPDI** and **TCPDI**) and one was highly soluble asymmetrical (**APDI**) with donor-acceptor-donor (DAD systems) building block have been synthesized, in order to change the photophysical and photochemical properties of the diimides, 1,7-symmetrically substituted perylenebis (dicarboximide) dyes (**BTC-TCPDI**, **BPY-PPDI** and **BTC-APDI**) with electron donating groups have been synthesized in good amount of product under mild conditions, to achieve this purpose, at first brominated PDA or shortly (Br-PDA) was prepared in accordance with the literature procedure and then modification of perylene core at bay position was done by using different alcoholic substituents. And in the end the synthesis was completed by functionalisation of imide positions. The products have been purified and optical, thermal and electrochemical properties of them were measured and characterized carefully. It is worthy to mention that in spectroscopic studies of the compounds a wide absorption bands have been observed which were somehow expanded to near infrared region (NIR) with H-bond possibility at bay or imides positions which could enhance the self-assembly of the molecules. In most of the above mentioned synthetic compounds (**TCPDI**, **APDI**, **BTC-TCPDI**, **BTC-PDA**, **BTC-APDI**) the reactions are done by using thiazolium hydrochloride (Vitamin B_1) as an electron donating group either at imide or bay positions, based on literature it was reported that the resonance energy-transfers generally takes place over distances similar to

most biological macromolecules i.e. ranging from 10 to 100A˚, The energy transfer rate is extremely dependent on how close are the gaps between excited and ground states of donor-acceptor system. Since vitamineB_1 is one of the crucial biological molecules and a vital nutritional compound in the human diet with water solubility it has been used as a substituent for modification of perylene properties in the current research. It has been expected that using these synthesized compounds can be a great method for studying conformation and activity of biological molecules such as DNA, protein etc., which play an important role in maintenance of human-body healthiness.

REFERENCES

[1] Lindsey, J. S. (1991). Self-assembly in synthetic routes to molecular devices. Biological principles and chemical perspectives. *New Journal of Chemistry,* 15, 153-180.

[2] Whitesides, G. M., Mathias, J. P., & Seto C. T. (1991). Molecular Self-Assembly and Nanochemistry: A Chemical Strategy for the Synthesis of Nanostructures *Science*, 254, 1312-1319.

[3] Lehn, J. M. (1995). *Supramolecular Chemistry Concepts and Perspectives* VCH: New York.

[4] Philp, D., & Stoddart, J. F. (1996). Self-Assembly in Natural and Unnatural Systems. *Angewandte Chemie International Edition,* 35, 1154-1196.

[5] Batten, S. R., & Robson, R. (1998). Interpenetrating Nets: Ordered, Periodic Entanglement *Angewandte Chemie International Edition*, 37, 1460-1494.

[6] Reinhoudt, D. N., Stoddart, J. F., & Ungaro, R. (1998). Supramolecular Science Where it is and where it is going. *Chemistry–A European Journal*, *4*(8), 1349-1351.

[7] Mendoza, D. (1998). Self-Assembling Cavities: Present and Future *Chemistry A European journal,* 4, 1373-1377.

[8] Rebek, J. (1990). Molecular Recognition with Model Systems *Angewandte Chemie International Edition*, 29, 245-255.

[9] Vögtle, F. (1991). *Suparmolecular Chemistry*. John VCH: New York

[10] Pauling, L. (1940). *The Nature of the Chemical Bond and the Structure of Molecules and Crystals. An Interaction to Modern Structural Chemistry.* Oxford University Press, London.

[11] Atkin, P. (1989). *General Chemistry*, Scientific American Books, New York.

[12] Dhotel, A., Chen, Z., Delbreilh, L., Youssef, B., Saiter, J. M., & Tan L. (2013). Molecular motions in functional self-assembled nanostructures. *International Journal of Molecular Sciences*, 14, 2303-2333.

[13] Desiraju G. R. (2011). Reflections on the hydrogen bond in crystal engineering. *Crystal Growth & Design*, 11, 896-898.

[14] Głowacki, E. D., Irimia-Vladu, M., Bauer, S., & Sariciftci, N. S. (2013). Hydrogen-bonds in molecular solids–from biological systems to organic electronics. *Journal of Materials Chemistry B*, 1(31), 3742-3753.

[15] Waters, M. L. (2002). Aromatic interactions in model systems. *Current opinion in chemical biology*, *6*(6), 736-741.

[16] Tybrandt, K., Larsson, K. C., Kurup, S., Simon, D. T., Kjäll, P., Isaksson, J., & Berggren, M. (2009). Translating electronic currents to precise acetylcholine–induced neuronal signaling using an organic electrophoretic delivery device. *Advanced materials*, *21*(44), 4442-4446.

[17] Würthner, F. (2004). Perylene bisimide dyes as versatile building blocks for functional supramolecular architectures. *Chemical communications*, (14), 1564-1579.

[18] Avlasevich, Y., Li, C., & Müllen, K. (2010). Synthesis and applications of core-enlarged perylene dyes. *Journal of Materials Chemistry*, *20*(19), 3814-3826.

[19] Würthner, F., Thalacker, C., Diele, S., & Tschierske, C. (2001). Fluorescent J-type aggregates and thermotropic columnar mesophases of perylene bisimide dyes. *Chemistry–A European Journal*, *7*(10), 2245-2253.

[20] Chen, Z., Debije, M. G., Debaerdemaeker, T., Osswald, P., & Würthner, F. (2004). Tetrachloro-substituted perylene bisimide dyes as promising n-type organic semiconductors: studies on structural, electrochemical and charge transport properties. *ChemPhysChem*, *5*(1), 137-140.

[21] Dubey, R. K., Efimov, A., & Lemmetyinen, H. (2010). 1, 7-And 1, 6-regioisomers of diphenoxy and dipyrrolidinyl substituted perylene diimides: Synthesis, separation, characterization, and comparison of electrochemical and optical properties. *Chemistry of Materials*, *23*(3), 778-788.

[22] Böhm, A., Arms, H., Henning, G., Blaschka, P., & AG, B. (1997). German Pat. DE 19547209 A1, 1997. In *Chem. Abstr*(Vol. 127, p. 96569g).

[23] Qian, H., Liu, C., Wang, Z., & Zhu, D. (2006). S-heterocyclic annelated perylene bisimide: synthesis and co-crystal with pyrene. *Chemical Communications*, (44), 4587-4589.

[24] Li, Y., Li, Y., Li, J., Li, C., Liu, X., Yuan, M., & Wang, S. (2006). Synthesis, Characterization, and Self-Assembly of Nitrogen-Containing Heterocoronenetetracarboxylic Acid Diimide Analogues: Photocyclization of N-Heterocycle-Substituted Perylene Bisimides. *Chemistry–A European Journal*, *12*(32), 8378-8385.

[25] Langhals, H., & Kirner, S. (2000). Novel fluorescent dyes by the extension of the core of perylenetetracarboxylic bisimides. *European Journal of Organic Chemistry*, *2000*(2), 365-380.

[26] Alibert-Fouet, S., Seguy, I., Bobo, J. F., Destruel, P., & Bock, H. (2007). Liquid-Crystalline and Electron-Deficient Coronene Oligocarboxylic Esters and Imides by Twofold Benzogenic Diels–Alder Reactions on Perylenes. *Chemistry–A European Journal*, *13*(6), 1746-1753.

[27] Rohr, U., Schlichting, P., Böhm, A., Gross, M., Meerholz, K., Bräuchle, C., & Müllen, K. (1998). Liquid crystalline coronene derivatives with extraordinary fluorescence properties. *Angewandte Chemie International Edition*, *37*(10), 1434-1437.

[28] Bhattar, S. L., Kolekar, G. B., & Patil, S. R. (2008). Fluorescence resonance energy transfer between perylene and riboflavin in micellar solution and analytical application on determination of vitamin B_2. *Journal of Luminescence, 128*(3), 306-310.

[29] Balzani, V. (1990). Supramolecular photochemistry. *Pure and Applied Chemistry*, *62*(6), 1099-1102.

[30] Balzani, V., Moggi, L., & Scandola, F. (1987). Towards a supramolecular photochemistry: assembly of molecular components to obtain photochemical molecular devices. In *Supramolecular Photochemistry* (pp. 1-28). Springer, Dordrecht.

[31] Mattay, J., & Griesbeck, A. (Eds.). (2008). *photochemical key steps in organic synthesis: an experimental course book*. John Wiley & Sons.

[32] Carey, F. A., & Sundberg, R. J. (2007). *Advanced organic chemistry: part A: structure and mechanisms*. Springer Science & Business Media.

[33] Turro, N. J. (1991). *Modern molecular photochemistry*. University science books.

[34] Gilbert, A., & Baggott, J. E. (1991). *Essentials of molecular photochemistry*. CRC.

[35] Klessinger, M., & Michl, J. (1995). *Excited states and photochemistry of organic molecules*. Wiley-VCH.

[36] Jaffé, H. H., & Orchin, M. (1962). Theory and applications of ultraviolet spectroscopy.

[37] Turro, N. J. (1991). *Modern molecular photochemistry*. University science books.

[38] Valeur, B., & Berberan-Santos, M. N. (2012). *Molecular fluorescence: principles and applications*. John Wiley & Sons.

[39] Rettig, W. (1994). Photoinduced charge separation via twisted intramolecular charge transfer states. In *Electron Transfer I* (pp. 253-299). Springer, Berlin, Heidelberg.

[40] Chibisov, A. K., Slavnova, T. D., & Görner, H. (2004). Dimerization kinetics of thiacarbocyanine dyes by photochemically induced concentration jump. *Chemical physics letters*, *386*(4-6), 301-306.

[41] Miljanic, S., Cimerman, Z., Frkanec, L., & Zinic, M. (2002). Lipophilic derivative of rhodamine 19: characterization and spectroscopic properties. *Analytica Chimica Acta*, *468*(1), 13-25.

[42] Mchedlov-Petrosyan, N. O., & Kholin, Y. V. (2004). Aggregation of rhodamine B in water. *Russian journal of applied chemistry*, *77*(3), 414-422.

[43] Micheau, J. C., Zakharova, G. V., & Chibisov, A. K. (2004). Reversible aggregation, precipitation and re-dissolution of rhodamine 6G in aqueous sodium dodecyl sulfate. *Physical Chemistry Chemical Physics*, *6*(9), 2420-2425.

[44] Antonov, L., Gergov, G., Petrov, V., Kubista, M., & Nygren, J. (1999). UV–Vis spectroscopic and chemometric study on the aggregation of ionic dyes in water. *Talanta*, *49*(1), 99-106.

[45] Ghasemi, J., Niazi, A., Westman, G., & Kubista, M. (2004). Thermodynamic characterization of the dimerization equilibrium of an asymmetric dye by spectral titration and chemometric analysis. *Talanta*, *62*(4), 835-841.

[46] Evans III, L., & Patonay, G. (1999). Effects of organic and aqueous solvents on the electronic absorption and fluorescence of chloroaluminum (III) tetrasulphonated naphthalocyanine. *Talanta*, *48*(4), 933-942.

[47] Su, G. J., Yin, S. X., Wan, L. J., Zhao, J. C., & Bai, C. L. (2004). Dimerization of three xanthene dyes on Au (III) surface. *Surface science*, *551*(3), 204-212.

[48] Burdett, B. C. (1983). *Aggregation of Dyes in Studies in Physical and Theoretical Chemistry*, vol. 2.

[49] Taguchi, T., Hirayama, S., & Okamoto, M. (1994). New spectroscopic evidence for molecular aggregates of rhodamine 6G in aqueous solution at high pressure. *Chemical physics letters*, *231*(4-6), 561-568.

[50] Goftar, M. K., Moradi, K., & Kor, N. M. (2014). Spectroscopic studies on aggregation phenomena of dyes. *European Journal of Experimental Biology*, *4*(2), 72-81.

[51] Spano, F. C., & Siddiqui, S. (1999). Exciton–vibrational coupling in pinwheel aggregates of π-conjugated molecules. *Chemical physics letters*, *314*(5-6), 481-487.

[52] Borsenberger, P. M., & Weiss, D. S. (1993). *Organic photoreceptors for imaging systems* (Vol. 39). New York: Dekker.

[53] Jelley, E. E. (1936). Spectral absorption and fluorescence of dyes in the molecular state. *Nature*, *138*(3502), 1009.

[54] Nyanhongo, G. S., Steiner, W., & Gübitz, G. M. (Eds.). (2011). *Biofunctionalization of polymers and their applications* (Vol. 125). Springer Science & Business Media.

[55] Pasaogullari, N., Icil, H., & Demuth, M. (2006). Symmetrical and unsymmetrical perylene diimides: Their synthesis, photophysical and electrochemical properties. *Dyes and Pigments*, *69*(3), 118-127.

[56] Würthner, F., Stepanenko, V., Chen, Z., Saha-Möller, C. R., Kocher, N., & Stalke, D. (2004). Preparation and characterization of regioisomerically pure 1, 7-disubstituted perylene bisimide dyes. *The Journal of organic chemistry*, *69*(23), 7933-7939.

[57] Koyuncu, S., Kus, M., Demic, S., Kaya, İ., Ozdemir, E., & Icli, S. (2008). Electrochemical and optical properties of novel donor-acceptor thiophene-perylene-thiophene polymers. *Journal of Polymer Science Part A: Polymer Chemistry*, *46*(6), 1974-1989.

[58] Yuney, K., & Icil, H. (2007). Synthesis, photochemical, and electrochemical properties of naphthalene-1,4,5,8-tetracarboxylic acid-bis-(N,N′-bis-(2,2,4(2,4, 4)-trimethylhexylpolyimide)) and poly (N,N′-bis-(2,2,4(2,4,4)-trimethyl-6-aminohexyl)3,4,9,10-perylenetetracarboxdiimide). *European polymer journal*, *43*(6), 2308-2320.

[59] Gonzalez, E., Provazi, K., Campos, B., Espinosa, D., Bernardes, A., Tenorio, J., & Montereali, M. (2001). *Electrochemical Methods. Fundamentals and Applications*, New York, J.

[60] Leonat, L., Sbarcea, G., & Branzoi, I. V. (2013). Cyclic voltammetry for energy levels estimation of organic materials. *UPB Sci Bull Ser B*, 75, 111-118.

[61] Williams, A. T. R., Winfield, S. A., & Miller, J. N. (1983). Relative fluorescence quantum yields using a computer-controlled luminescence spectrometer. *Analyst*, 108(1290), 1067-1071.

[62] Icil, H., & Icli, S. (1997). Synthesis and properties of a new photostable polymer Perylene-3,4,9,10-tetracarboxylicacid-bis-(N,N′-dodecylpolyimide). *Journal of Polymer Science Part A: Polymer Chemistry*, 35(11), 2137-2142.

[63] B Bodapati, J. B., & Icil, H. (2011). A new tunable light-emitting and π-stacked hexa-ethyleneglycol naphthalene-bisimide oligomer: synthesis, photophysics and electrochemical properties. *Photochemical & Photobiological Sciences*, 10(8), 1283-1293.

[64] Amiralaei, S., Uzun, D., & Icil, H. (2008). Chiral substituent containing perylene monoanhydride monoimide and its highly soluble symmetrical diimide: synthesis, photophysics and electrochemistry from dilute solution to solid state. *Photochemical & Photobiological Sciences*, 7(8), 936-947.

[65] Ice, H., Icli, S., & SAYIL, C. (1998). Synthesis and Properties of a New Photostable Soluble Perylene Dye: N,N'-Di-(1-Dehydroabietyl) Perylene-3,4,9,10-Bis (Dicarboximide). *Spectroscopy letters*, *31*(8), 1643-1647.